Isotropically Conductive Adhesive Filled with Silver Metalised Polymer Spheres

By Shiwani Jain

A Doctoral Thesis

Submitted in partial fulfilment of the requirements

for the award of

Doctor of Philosophy of Loughborough University

Feburary 2016

ABSTRACT

Isotropic conductive adhesives (ICAs) have a growing range of applications in electronics packaging and have recently emerged as an important material in photo-voltaic module interconnections, particularly for thin-film and other non-silicon technologies where soldering processes are often unsuitable due to the nature of the metallisation or the limited maximum temperature the assembly can be exposed to. ICAs typically comprise of a high volume fraction of solid metallic flakes, usually silver, in an adhesive matrix because of its highly conductive oxide however, this thesis will focus on adhesives containing a large volume fraction of silver coated/metalised mono-sized polymer spheres (Ag-MPS). Incorporating silver coated mono-sized polymer spheres is anticipated to deliver specific advantages such as a significant reduction in the required silver content, improvement of the overall mechanical properties and flexibility to tune the properties of the filler according to the application compared with conventional flake filled adhesives.

In this research advancements in the understanding of Ag-MPS filled ICAs, both through theory and experiments, have been made. Analytical models to predict an individual Ag-MPS resistance and Ag-MPS filled ICA resistance have been developed. The experiments based on the flat punch nanoindentation technique have been conducted to determine individual Ag-MPS resistances. The theoretical and experimental studies establish Ag-MPS diameter, coating resistivity, coating thickness, contact radius, and contact geometry as the main contributors towards the resistance of an Ag-MPS filled ICAs. These studies showed that Ag-MPS resistance decreases with increasing coating thickness and contact radius but increases with increasing coating resistivity. The experiments have also been conducted to investigate the effect of Ag-MPS volume fraction, diameter, coating thickness, curing conditions and shrinkage (affecting contact radius) on ICA conductivity and comparisons are made with flake filled and commercial ICAs. The results showed that ICA conductivity increases with increasing volume fraction and coating thickness but decreases with diameter. More importantly the results showed that conductivities similar to those of flake filled ICAs, including those commercially available, can be obtained using 70% less silver. The results show that, Ag content can be reduced further to just 7% with use of larger 30μm Ag-MPS but with a lower resulting conductivity. Thus for applications where very high

conductivity is not required larger Ag-MPS may offer even greater potential cost benefits, which is something flake filled ICAs cannot offer. This is a significant achievement which can allow tuning of ICA formulations according to the demands of the application, which is not possible with the use of silver flakes as there is only a limited range of silver flake volume fractions that will yield useful levels of conductivity.

ACKNOWLEDGEMENTS

During the time of my PhD study, there have been many people involved to varying extent. I gratefully acknowledge their contributions to my PhD research.

I would like to express my deepest thanks to my main supervisor Mr. David C. Whalley for his continual support, patient guidance and encouragement throughout this PhD research. His constructive feedback have been of great importance for the success of my PhD study. I would also sincerely thank my co-supervisor Prof. Changqing Liu for his valuable support throughout this work.

I would also like to thank team at Conpart As, Norway especially Dr. Keith Redford and Ms. C. B Nilsen for producing Ag-MPS for testing. I would especially like to thank Dr. Michael Cottrill, Dr. Helge Kristiansen, Mr. Tore Helland, for their continual guidance and valuable discussions. Their inputs have been very important in developing conductivity models and designing experiments. I would also like to thank Mr. Erik Kalland for his valuable suggestions on choosing epoxy matrix and Mr. Anders Ombustvedt for encouragement.

I would also like to extend my gratitude to all the technical staff in the Wolfson School who helped me during my research, but in particular to Mr. Andy Sandaver for his assistance and useful discussions during sample characterisation, Mr. Jagpal Singh for his training and valuable discussions during thickness and volume measurements and Mr. Dave Britton for his support on stencils preparation. I would also like to thank Dr. Keith Yendall and Dr. Geoffry West in Materials department for their training and assistance during sample characterisation using FEG-SEM and FIB.

I would like to thank Mr. Erik Foss and Mr. Junjie Zhu from IFE Norway, Dr. Jianying He from NTNU, Trondhiem, Norway and Dr. Ralph Gottschalg, Dr. Tom Betts and Xiaofeng Wu from CREST, Loughborough University, UK, for providing access to their facilities, assistance on experiments and time for discussions.

This work is co-sponsored by Mosaic Solution As, Norway and Loughborough University, UK. I am also grateful for the financial and technical support provided by the Wolfson School and Mosaic Solutions As, Norway. I am also grateful to our research coordinator Ms. Jo Mason for her support and help during the difficult time.

I would also like to thank Dr. Hoang-Vu Nguyen from Vestfold University College, Norway for the collaborative work on electrical characterisation of individual Ag-MPS as presented in Chapter 5 and Ms. Susanne Helland for sharing her experimental results used in Chapter 6.

Finally, but most importantly, I would thank my husband, my parents, my in-laws and my friends for their love and encouragement. Without their understanding and full support, I would not have accomplished this research.

DEDICATIONS

To My Husband and My Mother-in-Law:

Thank you for your patience, understanding and support.

CONTENTS

LIST OF FIGURES

LIST OF TABLES

NOMENCLATURE

a	Area of contact spot
A_a	Apparent contact area
A_b	Actual contact area
ACA	Anisotropic conductive adhesive
Ag	Silver
Ag-MPS	Silver coated polymer spheres
Al	Aluminium
Au	Gold
A_{vr}	Average cross-sectional area
BGA	Ball grid array
Bi	Bismuth
cc	Cubic centimeter
CCD	charged coupled device
CTE	Co-efficient of thermal expansion
Cu	Copper
C.V.	Co-efficient of variance
d	Depth of deformation
e^-	Electronic charge
E	Young's modulus
ECA	Electrically conductive adhesive
EL	Electroluminescence
EMF	Electromotive force
EMI	Electromagnetic interference
E_s	Elastic modulus of sphere
EU	European Union
EVA	Ethylene-vinyl-acetate
EWT	Emitter wrap through
E^*	Effective elastic modulus
F	Applied load
FE	Finite element
FEGSEM	Field emission gun scanning electron microscopy
FF	Fill factor
FFI	Norwegian Defence Research Establishment, Norway
FR4	Flame retardant 4
FS-34	Silver flakes purchased from Johnson Matthey, UK
FWR	Four wire resistance
HCP	Hexagonal close packing
h_d	Height of deformed sphere
H_2O	Water molecule

I	Current
ICA	Isotropically conductive adhesive
IC	Integrated circuit
I_D	Diode current
IFE	Institute for Energy Technology, Norway
I_{in}	Current entering the MPS
I_L	Photo generated current
I_{MP}	Current at the maximum power point
In	Indium
I_o	Saturation current of the diode
I_{out}	Current leaving the MPS
I/O	Input/Output
IR	Infrared
I_{SC}	Short circuit current
I_{SH}	shunt current
I-V	Current -Voltage
k	Boltzmann constant
l_d	Length of deformed sphere
l_F	Length of filler
L	Distance between the voltage probes
LCD	Liquid crystal display
LED	Light emitting diode
M	Non-noble metal
Manf.	Manufacturer
MEMS	Micro-electro-mechanical systems
Mo	Molybdenum
MPa	Mega Pascal
MPS	Metallised polymer spheres
MWT	Metallisation-wrap-through
n	Valency
N	Diode ideality factor
N/A	Not applicable
NCA	Non-conductive adhesive
n.d.	No date
Ni	Nickel
O_2	Oxygen
OH^-	Hydroxyl ion
Pb	Lead
$Pb(OH)_2$	Amorphous
Pd	Palladium
PCB	Printed circuit board

PET	Polyethylene terephthalate
P_{IN}	Input electrical power
P_{MAX}	Maximum power
PMMA	Polymethylmethacrylate
P_{OUT}	Output electrical power
PP	Plating process
PPy	Polypyrrole
Pt	Platinum
PTFE	Polytetrafluoroethylene
PV	Photovoltaic
q	Elementary charge
r	Radius of MPS
r_c	Contact radius
R_{cell}	PV cell internal resistances
RCP	Random close packing
R_{cr}	Contact resistance
$R_{CR(Ag,\ ICA)}$	Contact resistance between the Ag metallisation and ICA
$R_{CR(Al,\ ICA)}$	Contact resistances between Al metallisation on the back of cell and ICA
$R_{CR(Cu,ICA)}$	Contact resistances between Cu of front and back contacts and ICA
R_{csr}	Constriction resistance
$R_{Cu\text{-}Track}$	Cu track resistance
r_f	Radius of flake
RFID	Radio Frequency Identification Device
RH	Relative humidity
R_{hs}	Resistance of half spherical shell
R_{ICA}	Resistance of ICA
R_{mps}	Resistance of MPS
RoHS	Restrictions of hazardous substances
rpm	Rounds per minute
R_{ps}	Contact resistance between particle and substrate
R_{pt}	Contact resistance between particle and flat punch
R_S	Series resistance
R_{SH}	Shunt resistance
R_{si}	Resistance of the portion of the substrate between the current source connection on the substrate and the particle
R_{sv}	Resistance of portion of the substrate between voltage measurement connection on the substrate and the particle
R_t	Tunneling resistance
R_{tv}	Resistance of the portion of the flat punch between the voltage measurement connection on the punch and the bottom surface of the punch

s	Second
S	Siemens
Sb	Antimony
SC	Simple cubic
SEM	Scanning electron microscope
Si	Silicon
S_a	Surface Area
Sn	Tin
Sn-Pb	Tin-lead
t	Thickness of printed ICA stripe
T	Cell temperature
t_c	Coating thickness
TC	Temperature cycling
TCR	Temperature coefficient of resistance
t_i	Thickness of insulating film
t_f	Thickness of flake
T_g	Glass transition temperature
TWR	Three wire resistance
V	Voltage
V	Volt
V_{MP}	Voltage at the maximum power point
V_{OC}	Open circuit voltage
vol%	Volume fraction percentage
w	Width of ICA strip
WEEE	Waste electrical and electronics equipment
wt%	Weight percentage
Zn	Zinc
σ_{ICA}	Conductivity of ICA
θ_c	Contact angle
α_{Filler}	CTE of filler
°C	Degree centigrade
δ	Delta
Ø	Diameter
ε	Dielectric constant of insulating film
η	Efficiency
ϕ_{meff}	Effective maximum packing fraction of filler
ϕ_{max}	Maximum packing fraction of filler
ϕ_c	Percolation threshold
v_s	Poisson's ratio of the spheres
η_r	Relative viscosity of a suspension
ρ_{ICA}	Resistivity of ICA

ρ_m	Resistivity of metal
Θ	Rise in temperature
ΔT	Temperature change
α	Temperature coefficient of resistivity
λ	Thermal conductivity of metal
ρ_t	Tunnel resistivity
ϕ_f	Volume fraction of filler
ϕ_{Filler}	Volume of the filler
$\Delta\phi_{Filler}$	Volume change of the filler
$\Delta\phi_{ICA}$	Volume change of the ICA sample
ϕ_{ICA}	Volume of the ICA sample
ϕ_{Matrix}	Volume of the matrix
$\Delta\phi_{Matrix}$	Volume change of the matrix
ϕ_{sat}	Volume fraction at saturated conductivity
Φ	Work function of metal

CHAPTER 1

RESEARCH AIMS AND OBJECTIVES

This chapter identifies general problems related to interconnection materials in electronics and photovoltaic (PV) applications. Based on the identified problems, the research aims and objectives are defined. An overview of the thesis is also presented in this chapter.

1.1 Identification of Problems Related to the Interconnections in Electronics and Photovoltaic (PV) Applications

1.1.1 Interconnections in Electronics

Microelectronic devices such as Integrated Circuits (ICs) form the basis of all modern electronic products. ICs are integrated with other active or passive devices/components to make a complete electronic product. A typical electronic product life cycle starts with designing a circuit diagram integrating ICs and other electronic devices/components. After designing the circuit, the components are physically laid out and interconnected using an interconnection material such as copper on a printed circuit board. Such methods of interconnecting ICs and components to form an electronic product are described as electronic packaging. Electronic packaging converts the topology of a circuit diagram into a physical product that can be produced at an acceptable cost. The selection of an optimal packaging technology to produce an electronic product is guided by a multitude of factors, such as, its (Halbo et al. 1995):

- Performance specifications;
- Operating environment;
- Required reliability and life-time;
- Required Size;

- Production volume;
- Need for reparability; and
- Cost.

Typically electronic systems are made up of several layers or levels of packaging, and each level of packaging has distinctive types of interconnection associated with it (Halbo et al. 1995; Tummala 2000 a; Gilleo 2002; Greig 2007). A three-level packaging hierarchy is illustrated in Figure 1.1.

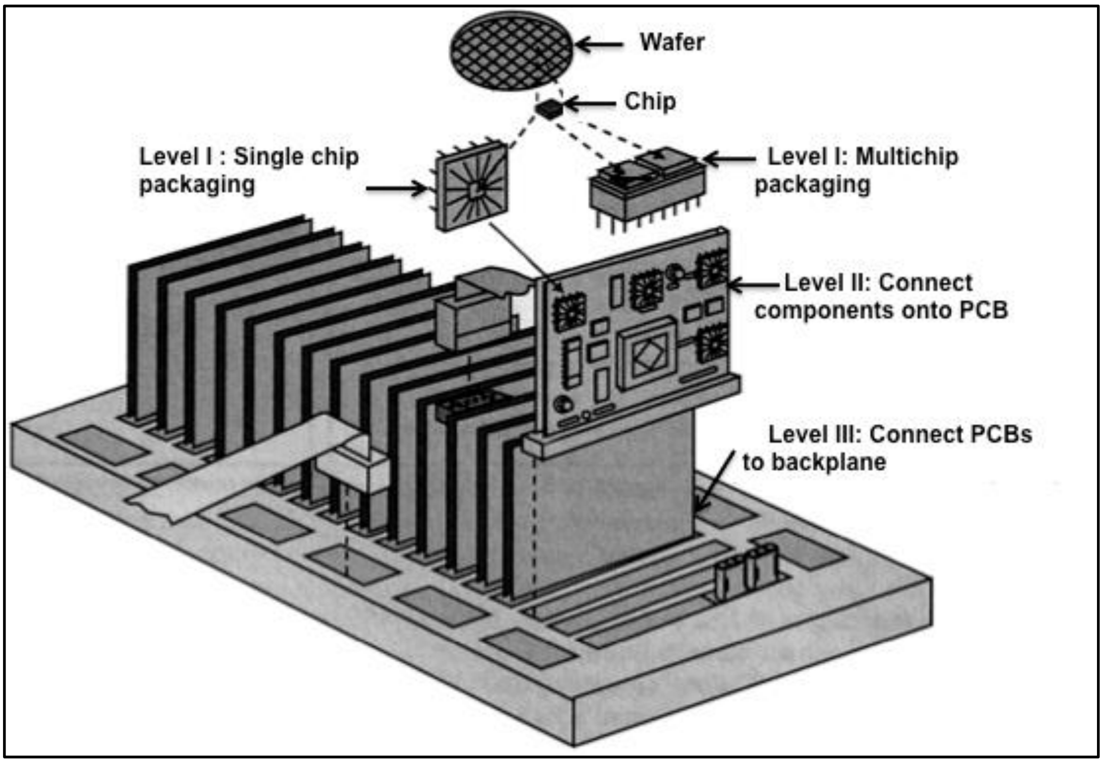

Figure 1.1 A three-level packaging hierarchy after (Tummala 2000 a)

i) Level I: In this level the Input/Output (I/O) pads on the IC are connected to the lead frame, which has been fabricated to a specific shape in order to make it ready for interconnection to the next level of packaging. In this level the interconnections are generally accomplished by wire bonding, flip-chip bonding, or tape automated bonding (TAB). In wire bonding and standard TAB, the die/chip is mounted face up i.e. the chip's un-patterned rear surface is directly bonded to the package lead frame face up using wires. In flip chip packaging, conductive bumps are formed on the die/chip surface and the bumped die/chip is then flipped over and placed face down, with the bumps connecting to the lead frame. Figure 1.2 illustrates wire bonding, TAB and flip chip technology used in making level I interconnections. Flip chip bonding has become widely adopted by the industry due to the technology's advantage in size, performance, flexibility, reliability and cost over other packaging methods. In the case illustrated a silicon wafer is diced and the individual dies are assembled onto either a lead frame or a multichip module.

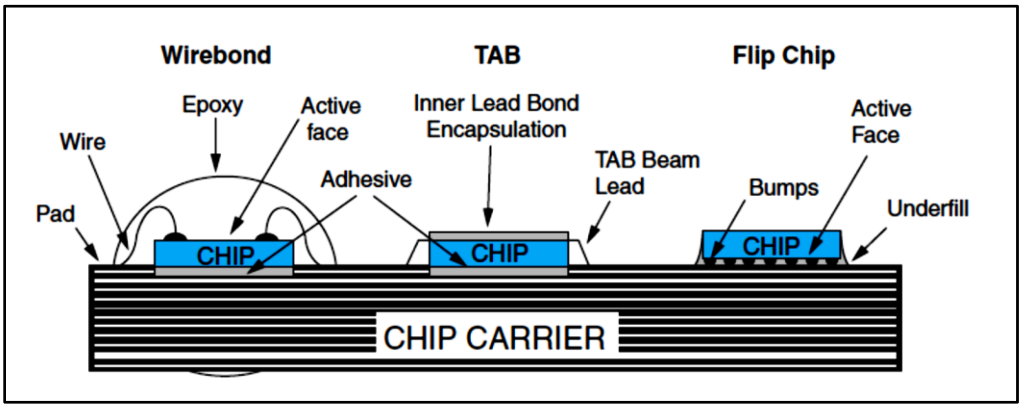

Figure 1.2 Illustrating wire bonding, TAB and flip chip interconnection techniques (Tummala 2000)

ii) Level II: In this level packaged components are assembled onto an interconnecting substrate such as Printed Circuit Board (PCB).

iii) Level III: In this level the printed circuit boards are connected to a backplane to form a module. At this level, connections are usually separable as opposed to the normally permanent connections at earlier levels.

Some levels may be skipped and there may be more levels depending on the system complexity and the types of packaging used (Whalley 1988; Tummala 2000 a). To connect different electronic components within a level and different levels of packaging for power, ground, and signal transmission suitable interconnection materials are required. The selection of such interconnection materials is based on the type of packaging technology used and the properties of the material in relation to expected operating conditions. The important properties identified include (Halbo et al. 1995; Gilleo 2002):

- Electrical properties, such as conductivity and contact resistance;

- Mechanical properties, such as flexural strength and hardness;

- Thermal properties, such as coefficient of thermal expansion and thermal conductivity;
- Adhesion properties, such as adhesive strength; and
- Rheological properties, such as viscosity and flow behaviour.

Apart from these properties, compatibility with components and surface finishes, ability to be produced in different shapes, ease of rework, reliability during the lifetime of the product, availability, cost and (more recently) their environmental impact also play a considerable role in the selection of an interconnection material.

1.1.2 Interconnections in Photovoltaic Modules

Photovoltaics are a growing sector among the various renewable energy sources (Gelman 2012). To become a viable option in the market PV modules have to be reliable and closer in price to consumer electricity without government subsidies (Szlufcik et al. 2005). Individual photovoltaic cells generate limited power and must be tied together electrically, to form modules and arrays, in order to produce electricity for most applications. For this, cells are joined to one another in series until their individual power contributions add to the required value. Therefore connecting cells to form modules and modules to form arrays is an extremely important aspect of PV technology (Hersch et al. 1982). Photovoltaic modules can be subdivided into three principle categories i.e. crystalline - silicon (Si) wafer based modules, thin film modules and organic photovoltaic modules. The vast majority of today's commercially available photovoltaic modules are based on crystalline-Si solar cells although thin film and organic photovoltaic modules are also growing their market share particularly in niche applications (Wiese et al. 2010). The two main assembly techniques currently used for the interconnection of crystalline Si solar cells into modules are (Wiese et al. 2012):

1) ***Tab String Assembly***. This is the traditional interconnection technique used to connect PV cells. The cells connected using this assembly are called H-Pattern cells. In tab string assembly the cells are usually interconnected to each other by copper ribbons (called strings), which connect the front side of one cell to the back side contact of the next cell (Klengel et al. 2011) as shown in Figure 1.3 (a). Most currently produced photovoltaic modules are manufactured using this

traditional tab string process, however it has some disadvantages. To reduce material costs the cells have been made thinner and bigger but for increased efficiency cells requires thicker and/or wider tabs for interconnection (Spath et al. 2008). These wider tabs result in more shadowing of Si and thicker tabs result in a stiffer interconnection, leading to more thermo-mechanical damage during module manufacture and operation (Kerschaver et al. 2006); and

2) ***Back Contact Assembly***: In order to avoid shadowing effects on the front side, and reduce thermo-mechanical damage during module manufacture and operation, different concepts for putting most of the interconnect structure on the backside of the solar cells have been developed (Jong et al. 2005; Kerschaver et al. 2006). The two main types of cell developed with all the contacts at the back are metallisation-wrap-through (MWT) cells and the emitter wrap through (EWT) cells, both of which can use a flexible printed circuit board to interconnect individual solar cells (Gee et al. 1997; Eikelboom et al. 2001). Figure 1.3 (b) illustrates the concept of back contact assembly using MWT cells. These back contact cells offer several benefits over conventional cells H-pattern cells such as (Gee et al. 1997; Spath et al. 2008): compatible processing with thin and long cells; lower shading losses as less metal is needed on the cell side facing the sun; lower series resistance as the contact can be expanded over the complete cell area; a higher module packing density as there are no tabs passing between the cells meaning that the cells can be placed closer together in the module thereby increasing the effective module area which helps improve efficiency; and reduced silver consumption as less metallisation to carry current is required on the front surface of these cells.

In both of the assembly techniques mentioned above the connections have to provide good conductivity and reliability for long periods (normally 20–25 years) despite seeing large temperature variations and other climatic stresses (Hersch et al. 1982; Eikelboom et al. 2002). This indicates that the performance and reliability of PV modules depends significantly on the quality and reliability of the interconnections that are used in the assembly of PV modules. This is also evident from a study conducted on PV module warranty claims made by the customers of a major PV module manufacturing company, BP Solar. The study was carried out on conventional polycrystalline silicon PV modules. The study showed that over the period from 1994 to 2002, 0.13% (approximately 2600) of their PV modules failed and were returned under warranty from a total of two million modules in the field. Failure analysis of the PV modules returned under warranty showed a high percentage (40.7%) of the field failures were due to breaking of cells or interconnections (Wohlgemuth 2003). A summary of the various causes of failure for these PV modules is shown in Table 1.1.

The above sections discussed the importance of the interconnections, and the prerequisites of the interconnection material. The next section will discuss the primary interconnection materials used in electronics and PV applications.

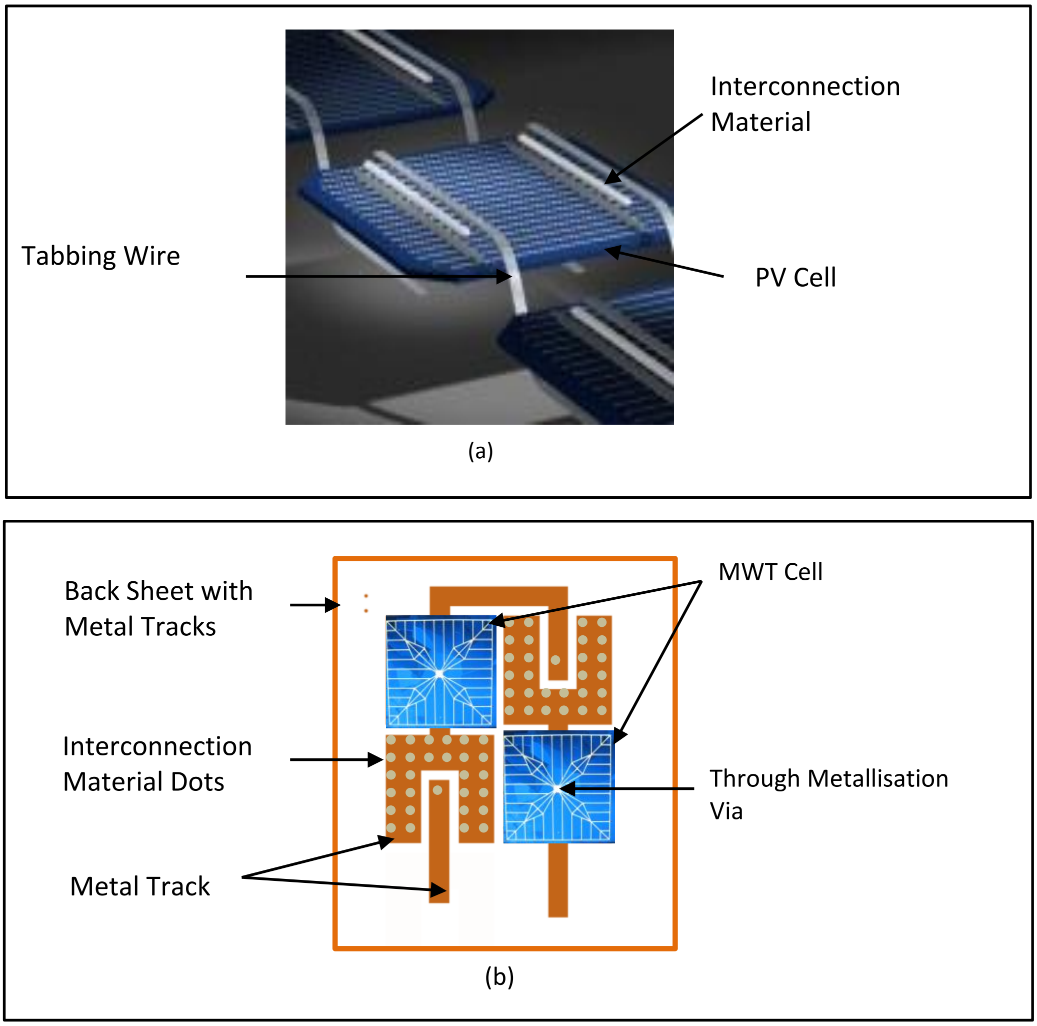

Figure 1.3 Interconnection in (a) traditional tab string assembly (Henkel 2013) (b) back contact assembly with MWT cell

Table 1.1 Types of field failures observed in PV modules (Wohlgemuth 2003)

Types of Failure	% of Total Failures
Corrosion	45.3
Cell or Interconnect Break	40.7
Output Lead Problem	3.9
Junction Box Problem	3.6
Delamination	3.4
Overheated wires, diodes or terminal strip	1.5
Mechanical Damage	1.4
Defective Bypass Diodes	0.2

1.1.3 Tin Lead Solder (Sn-Pb): A Primary Interconnection Material in Electronic and PV Applications

Within the scope of microelectronics and electronics applications and PV modules made using crystalline Si, Sn-Pb eutectic solder has historically been used as a primary interconnection material for making permanent interconnections (Ulrich et al. 2006; Schwertheim et al. 2008). The main advantages of Sn-Pb solders are (Gilleo 2002):

- Their low volume resistivity (~10^{-5} Ωcm) and high mechanical strength (28-40 MPa);
- Their good wetting and compatibility with most of the surface finishes;
- Their malleability i.e. ease to be produced into various shapes such as wires, powder or spheres;
- Their availability in paste form;
- Their self-alignment and easily reworkable property;
- The abundance of both the constituent materials, tin and lead; and
- Their low cost.

Despite these advantages of Sn-Pb, it has several disadvantages including:

- ***High Temperature Processing:*** It has a melting point of 183°C. Thermally sensitive components and substrates such as glass or polyester flex, which are used in low cost consumer electronic products are not able to withstand this high reflow temperatures (Li et al. 2006). In PV, high temperature processing induces large thermal stresses in the cells (Wiese et al. 2010). Further, as crystalline silicon PV cells reduce in thickness the residual stresses due to soldering processes become more significant. During the lifecycle of a PV module, stresses induced in the cells and the interconnections at the time of manufacture can result in micro-cracking of the PV cell. This decreases PV module efficiency and ultimately results in a failure (Schwertheim et al. 2008; Spath et al. 2008). Therefore, it is important to keep the process temperature for interconnection as low as possible to reduce the induced residual stresses and hence increase the reliability of PV modules. Further, high processing temperatures make solders incompatible with the plastic substrates used in PV modules containing thin film and organic solar cells (Matsunaga et al. 2009);

- ***Complex Processing:*** It generally requires use of flux and often flux cleaning solvents (Morris et al. 2007);
- ***Thermal Fatigue Failure***: It is susceptible to thermo-mechanical fatigue under temperature cycling conditions, which eventually leads to the solder joint cracking (Gilleo 2002); and
- ***Environmental Impact:*** The lead used in Sn-Pb solder is a toxic substance. When ingested, even small quantities of Pb can lead to damage to the brain, nervous system, liver and kidneys. A large proportion of electronic products have historically not been recycled and ended up in landfills which can led to lead accumulation in water sources and can affect the biosphere. For this reason WEEE & Restrictions of Hazardous Substances (RoHS) directives of the European Union (EU) have forced the elimination of lead from most of the electronic products (RoHS 2008). Therefore, great efforts have been made to develop lead-free and environmentally sound interconnect bonding technologies as an alternative to conventional Sn-Pb solders.

1.1.4 Alternative to Lead Based Solder for Electronic and PV Interconnections

One alternative to lead based solders is isotropically conductive adhesives (ICAs). ICA mainly consists of adhesive matrix (usually epoxy resin) and metallic filler. ICAs have high metallic loading usually 25 – 35 vol% of silver flakes. This high metal loading is to provide better electric conduction (Morris 1999; Yi. Li et al. 2010). ICAs conduct electricity equally in all directions like solder. ICAs are already used in various niche applications e.g. die-attach, flip-chip bonding (Li et al. 2006; Yi. Li et al. 2010). Recently, silver flake based ICAs have also been examined as an interconnection material in PV modules (Eikelboom et al. 2002; Schonecker et al. 2002; Bultman et al. 2003; Jong et al. 2005; Schwertheim et al. 2008; Spath et al. 2008; Bremaud 2009). ICAs offer several advantages over solder. These include:

- ***Less Environmental Impact:*** Use of ICA eliminate Pb and the flux associated with normal soldering processes. Silver (Ag) and the epoxies used in ICAs are less toxic than Pb, but they are not completely environmentally friendly. Silver, particularly in its nano form, is harmful to lower aquatic and marine life i.e. the base of the aquatic food chain (Luoma 2008) and unreacted epoxies when in direct contact with skin can cause skin allergies (Christensen et al. 2000);

- ***Low Temperature Processing***: ICAs have low processing temperatures, typically in the range of 100-150°C or sometimes less. Such low process temperatures induce low stresses in the components and substrates and enable the use of heat-sensitive and low-cost components and flexible substrates such as plastics (Kang et al. 1998; F.M.Coughlan 2006). For PV applications the ICA processing temperature can be matched well with the temperature required for module lamination, thus providing the possibility of accomplishing lamination and interconnection in a single step (Bultman et al. 2003; Spath et al. 2008). This makes the module assembly easier and faster, and reduces the thermal stresses a PV cells has to undergo (Eikelboom et al. 2002); and

- ***Simpler Processing***: ICAs do not require flux or cleaning, unlike normal soldering processes, thereby offering simple processing with fewer processing steps and reduces processing cost (Morris et al. 2007).

However, ICAs are still in their infancy in comparison with the mature soldering technology and have some limitations. These include:

- ***Low Electrical Conductivity***: ICAs have lower electrical conductivity than lead based solders, with typical volume resistivities a factor of two higher than solders (Puttlitz et al. 2004; Li et al. 2010). To obtain high electrical conductivity, conductive adhesives typically require a high metallic loading (usually of silver) of around 25 - 35 vol%. Apart from cost, a major drawback of this high loading is poor mechanical strength (Morris et al. 2007). High loadings also result in high viscosity of the adhesive which affects their processability (Li et al. 1998);

- ***Application:*** Unlike solders ICAs do not self-align and high accuracy is therefore required to mount small components (Boyle et al. 1992a; Morris et al. 2005);

- ***Rework:*** ICAs are difficult to rework;

- ***Short Pot Life:*** ICAs typically have a short pot life, and once fully formulated they therefore require very low temperature storage;

- ***Lower Reliability***: Another limitation of ICAs is that they may exhibit poor electrical and mechanical reliability i.e. an unstable contact resistance and poor impact performance after high humidity exposure and/or temperature and mechanical cycling/shock cycling (Kudtarkar et al. 2002); and

- ***High Cost:*** The cost of silver flake filled ICAs is high i.e. £5780/kg (Epotek 2012) compared to £100 - £190/kg for solder paste (Farnell 2014). Further, less noble metallisations such as Sn or Sn/Pb, Cu, Ni or Al used with Sn-Pb are cheap and abundant and are widely used in electronic and in PV module interconnections. ICAs show poor reliability on these metallisations (Jagt 1998; Eikelboom et al. 2002), and replacing them with expensive Ag, Au, Ag/Pt, Au/Ni or Ag/Pd metallisations to enable reliable ICA interconnections makes the use of ICAs even less favourable in these applications.

Thus it shows that for ICAs to gain widespread acceptance as a solder replacement in electronics and PV applications, there is a need to both reduce their cost and improve electrical and mechanical reliability after high humidity exposure, temperature and mechanical cycling/shock cycling (Mir et al. 2008; Spath et al. 2008; Nguyen 2012). Such ICAs would also be applicable in other products, such as heated windscreens for motor vehicles and body area network (BAN) applications.

1.2 One Approach to Simultaneously Improve Reliability and Reduce Cost of an ICA

One of the causes of poor ICA reliability is the thermo-mechanical mismatch between the metal particles and the adhesive matrix. During thermal or mechanical loading of the silver-epoxy composite, this will cause significant internal stress and potentially micro-cracking at the interface between the two materials. To improve the reliability and at the same time reduce the cost of an ICA Gakkestad et al. (2010), Nguyen (2012) and Kristiansen et al. (2013) have recently proposed the use of mono-sized silver coated polymer spheres instead of solid silver flakes/particles as a conductive filler. A cross-section view of silver coated polymer sphere is shown in Figure 1.4.

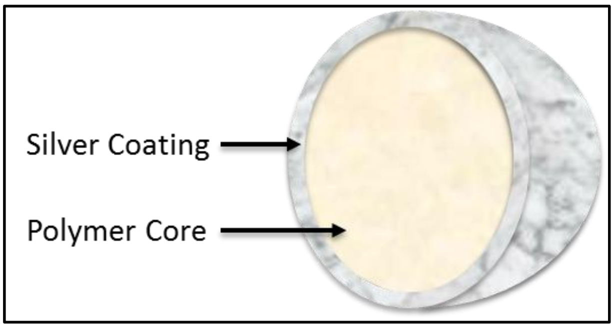

Figure 1.4 A cross-sectional view of a silver coated polymer sphere

The following benefits of this approach were anticipated:

- With a thin silver coating compared to the size of the polymer spheres the mechanical properties of the more flexible polymer core will dominate, providing better absorption of mechanical stresses;
- With the elastic modulus and thermal expansion coefficient of the polymer core better matching the surrounding adhesive matrix, the stresses under cyclic

thermal and mechanical loads will be reduced, improving adhesive reliability under thermal and mechanical stresses;

- The density of the filler will be close to that of the polymer matrix helping reduce filler sedimentation;
- Due to the symmetric filler particle shape it may offer better conductivity in the direction (z-axis) perpendicular to the plane (x-y plane) of printing;
- Substantial reduction in metal content in the ICA as compared with traditional silver flaked filled ICAs, thus reducing the usage of precious metal and potentially resulting in a significant cost reduction;
- The spherical shape and deformable nature of the Metalised Polymer Sphere (MPS) will help reduce the viscosity compared to the same volume fraction of solid flakes/particles; and
- The use of a mono-sized and symmetric filler shape, will allow the effect of various parameters such as MPS core material, size and coating thickness on the conductivity of an ICA to be readily investigated. Such investigation will give more opportunity to tune the size and properties of the core (to control mechanical properties) and the thickness of coating (to control electrical conductivity) according to the application requirement.

Gakkestad et al. (2010) have also shown that MEMS (Micro-Electro-Mechanical Systems) test structures directly mounted to the fuse of medium caliber ammunition using conductive adhesives based on uniformly sized silver coated polymer spheres performed well (with less than 15% change in the contact resistance for their test structures) after being subjecting to rapid temperature cycling (according to MIL-STD 883G method 1010.8 test condition B (-55°C to 125°C)). Further, they have shown that these test structures successfully passed a 60,000g acceleration firing test (with 31 out of 36 contact resistances changing less than 15%). In addition, the collaborating partners, have carried out rheological and mechanical studies on ICAs filled with mono-sized silver coated polymer spheres. They have shown that the mechanical shear strength of ICAs filled with silver coated polymer spheres (29 MPa) is similar to that of lead based solders (28–40 MPa) and have a rheology suitable for screen and stencil printing up to 50 vol% of filler (Nguyen et al. 2010).

The mono-sized silver coated polymer spheres are referred to Ag-MPS or MPS and corresponding ICAs are referred to as novel ICAs in the context of this thesis.

1.3 Research Aims

The above discussion shows that reliable ICAs with a rheology suitable for stencil and screen printing and with greatly reduced metal content can be obtained using Ag-MPS as the conductive filler, however based an earlier theoretical study by Morris (1999) anticipated some concerns related to the use of metallised polymer spheres in an ICA that warranted further investigation. These are, the anticipated higher percolation threshold and lower system conductance compared to traditional ICAs loaded with flakes/particles. Kristiansen et al. (2013) have investigated the bulk conductivity of such novel ICAs using 6, 10, 15 and 20µm Ag-MPS with different coating thicknesses. However, details of the conduction mechanisms in the MPS filled ICAs have not been thoroughly studied yet. The effect of MPS volume fraction, MPS size/size distribution and metal coating thickness on the electrical performance of ICAs is less well understood. Additionally, where solid metallic particles/flakes are used as the filler, the resistances of the individual particles are a very small part of the overall material resistance (Li et al. 1997; Lu et al. 1999). However, for metal-coated polymer spheres the thickness and morphology of the metallisation could be expected to have a significant influence on the conductivity of an individual MPS as the bulk of the conductor particle is comprised of a highly insulating polymer. These limits and the effects of the coating thickness and morphology on the electrical performance of the MPS, and hence on an ICA, are still to be investigated. Thus in the wake of the mentioned concerns and their being no available data on the electrical performance of MPS and MPS filled ICAs, it is concluded that there is a need for a detailed study to investigate the electrical performance of these novel ICAs. Based on this conclusion the main aims of this research are defined as being:

- to develop a low cost and highly reliable ICA using mono-sized Ag-MPS as the conductive filler; and

- to investigate the underlying conduction mechanisms which will mainly govern the electrical performance of an Ag-MPS and the Ag-MPS filled ICAs.

1.4 Research Objectives

To achieve the above-defined aims the following objectives have been established:

- To critically review the literature to gain an understanding of the factors that can affect the performance of an ICA and identify the merits and demerits of using mono-sized metal coated polymer spheres in an ICA in place of silver flakes;

- To establish the feasibility of using mono-sized metal coated polymer spheres in ICAs in place of silver flakes by benchmarking novel ICAs against a traditional silver flake filled ICA;

- To develop a theoretical model to gain an understanding of the effect of different factors such as MPS diameter (Ø), coating thickness and morphology, on the electrical performance of an MPS;

- To develop a theoretical model to gain an understanding of the effect of different factors such as MPS volume fraction, diameter (Ø), coating thickness and morphology, curing conditions, and curing shrinkage of the epoxy resin on the electrical performance of an ICA filled with MPS;

- To experimentally verify the findings of the theoretical models on the electrical performance of MPS and the novel ICAs; and

- Based on the theoretical model and the experimental findings to establish a link between the electrical properties and different factors such as MPS volume fraction, size, coating thickness and morphology, curing conditions, epoxy shrinkage, which will help design MPS and ICAs with tailored properties for specific applications.

In summary, the focus of the research reported in this thesis is to gain knowledge of the parameters affecting the electrical performance of MPS and MPS based ICAs to allow the design of MPS and ICAs with properties tailored for specific applications. This research was supported by Mosaic Solutions AS, Norway, who were also supporting parallel research activities at Vestfold University College, Norway and NTNU, Trondheim, Norway, with whom collaboration has taken place as part of this thesis work. The mechanical strength and the rheology of the Ag-MPS based ICAs have been studied by the collaborating partners at Vestfold (Nguyen et al. 2010; 2011; 2012; 2013).

1.5 Thesis Structure

Based on the research objectives, the structure of the thesis was established and is presented in Figure 1.5. A brief summary of the chapters is provided below.

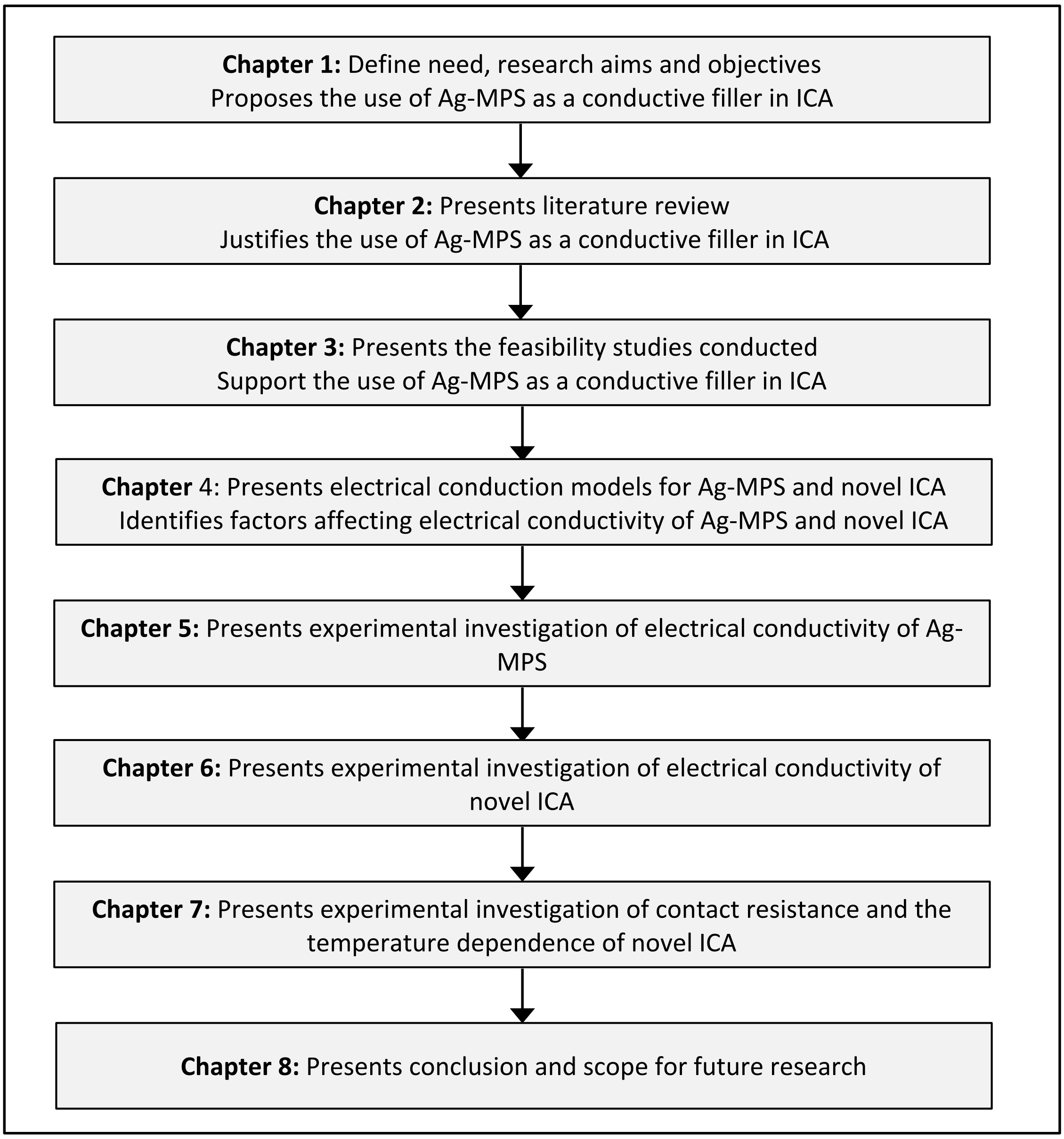

Figure 1.5 Overview of the research reported in the thesis

- *Chapter 1: Research Aims and Objectives*

  This chapter presents the aims and objectives of the research. This includes problems which have been identified in interconnections for electronics and the photovoltaic applications. A solution to the identified problems is presented and based on that, the aims and objectives of this research are defined. This chapter proposes the use of silver-coated polymer spheres as a conductive filler to formulate novel ICAs.

- *Chapter 2: Literature Review*

  This chapter introduces electrically conductive adhesives (ECAs) in general and then concentrates on ICAs with a focus on the properties of their constituents, their benefits and limitations. To support the use of mono-sized silver-coated polymer spheres as conductive fillers in novel ICAs, a literature review of the presently employed fillers and their properties is also presented in this chapter. This review leads to the conclusion that there is an opportunity to replace silver flakes in ICAs to improve their mechanical properties while reducing the silver content and hence the cost. This therefore, justifies the reason to use the mono-sized silver-coated spherical polymer particles as a conductive filler to formulate improved novel ICAs.

- *Chapter 3: Feasibility Study – Use of Silver Metalised Polymer Spheres as Conductive Filler in ICA*

  This chapter presents initial studies to investigate the feasibility of using Ag-MPS as a conductive filler in an ICA addressing the concerns mentioned earlier in Section 1.3. This chapter also benchmarks the Ag-MPS filled ICAs against a traditional flake filled ICA highlighting the relative benefits of using the Ag-MPS filled ICA. However, a case study on the use of Ag-MPS filled ICAs in a novel PV module assembly application is presented in Appendix D.

- *Chapter 4: Theoretical Model of Electrical Conductivity of ICAs Filled with Silver Metalised Polymer Spheres*

  This chapter gives a detailed insight into the conduction mechanisms within the novel ICAs. The chapter reviews models for conduction in traditional ICAs and in single metal-coated polymer spheres and identifies a need for a conduction model for the novel ICAs. The chapter identifies the important factors which would be expected to affect the electrical resistance of novel ICAs. The chapter then proposed a novel model to predict both the resistance of the individual Ag-MPS and of the novel ICAs containing them.

- *Chapter 5: Experimental Investigation of the Conductivity of Individual Silver Metalised Polymer Spheres*

  To validate the model developed in Chapter 4, this chapter presents an experimental investigation of single Ag-MPS resistance. This has been achieved by use of a special configuration of nanoindentation instrument to simultaneously measure both the resistance and deformation of single Ag-MPS. Comparing the theoretical and experimental results this chapter summaries the main factors which can affect the resistance of an Ag-MPS.

- *Chapter 6: Factors Affecting Conductivity of ICAs Filled with Silver Metalised Polymer Spheres*

  This chapter investigates the effect of MPS volume fraction, diameter, Ag coating thickness and morphology, polymer matrix type, curing conditions and adhesive shrinkage on the resistance of novel ICA. This chapters also links the experimental results with the theoretical models.

- *Chapter 7: Other Electrical Measurements*

  This chapter presents an investigation of the effect of the MPS volume fraction, size and coating thickness on the contact resistance of Ag-MPS filled ICAs and compares it with those for silver flake filled ICAs. This chapter also presents an investigation of the temperature dependence of resistance in order to gain an insight into the conduction mechanisms occurring within Ag-MPS filled ICAs.

- *Chapter 8: Conclusions and Recommendations for Future Work*

  This chapter summarises the major conclusions and outlines potential areas of future work.

A case study showing suitability of MPS filled ICAs for a PV application is presented in Appendix D.

1.6 Concluding Remarks

Various problems related to the interconnection materials used in electronics and in photovoltaic industry have been presented in this chapter. For the identified problems, a solution is proposed and, based on this proposed solution the thesis aims are identified. The main aim of this research is to use mono-sized silver-coated polymer spheres as a conductive filler to formulate novel ICAs. Based on the identified research aims, the objectives of this research have been presented in this chapter. The next chapter presents an introduction to the use of ICAs in interconnections.

CHAPTER 2

LITERATURE REVIEW

Chapter 1 proposes the use of mono-sized Ag coated polymer spheres as a conductive filler within isotropically conductive adhesives. The proposed concept is believed to overcome some of the limitations of traditional flake filled adhesives. Isotropically conductive adhesives are a class of electrically conductive adhesive. This chapter firstly presents a brief literature review on the various types of electrically conductive adhesives and then reviews in more detail isotropically conductive adhesives.

2.1 Electrically Conductive Adhesives

Electrically conductive adhesives (ECAs) are composed of a polymeric binder or matrix (such as, an epoxy, a silicone, or a polyimide) and a conductive filler material (usually a metal such as silver, gold, nickel or copper, or carbon may be used where high conductivity is not required). The polymeric binder mainly provides mechanical properties such as adhesion, mechanical strength and impact strength, whereas the conductive filler provides electrical conductivity (Boyle et al. 1992a; Morris et al. 2005; Morris et al. 2007; Yi. Li et al. 2010). The use of ECAs in electronic applications commenced in 1966 (Epotek n.d.) however their use has been limited to niche applications such as in die attach, liquid crystal displays (LCDs), smart card applications, flip–chip assembly, chip scale packaging (Licari et al. 2005; Rabilloud et al. 2005). Recently the possibility of using ECAs for other interconnection applications has been explored increasingly because of (i) the environmental issues surrounding the use of lead in solders; and (ii) the requirements for ultra-fine pitch connections (Zwolinski et al. 1996; Kang et al. 1998; Morris et al. 2005; Morris et al. 2007).

ECAs can be classified into two types. These are:

- Anisotropic conductive adhesives (ACAs), which conduct only through the thickness of a thin layer (often described as being along the z-axis where the x and y axes are in the plane of the film); and
- Isotropic conductive adhesives (ICAs), which conduct approximately equally in all the three orthogonal directions.

There is another class of adhesives called non-conductive adhesives (NCAs), which do not contain any metallic filler for conductivity, but can provide a method for holding two conductive surfaces in electrical contact.

A brief description of these three types of adhesive is presented in the following sections.

2.2 Anisotropic Conductive Adhesive (ACA)

ACA are typically used in applications where it is difficult to apply adhesives separately to features with very small dimensions e.g. the ultra-fine pitch interconnections of LCD displays. Conductivity only through the film thickness is achieved by inclusion of a low volume fraction loading of conductive filler particles within a polymer matrix. The loading is usually maintained between 5 to 10 vol% (Williams et al. 1993). ACAs are generally spread over the whole interconnection area as shown in Figure 2.1, and the electrical connections are formed where the conductive particles are locked in between the component and the substrate bond pads during the simultaneous application of heat and pressure (Dou et al. 2004; Chen et al. 2011).

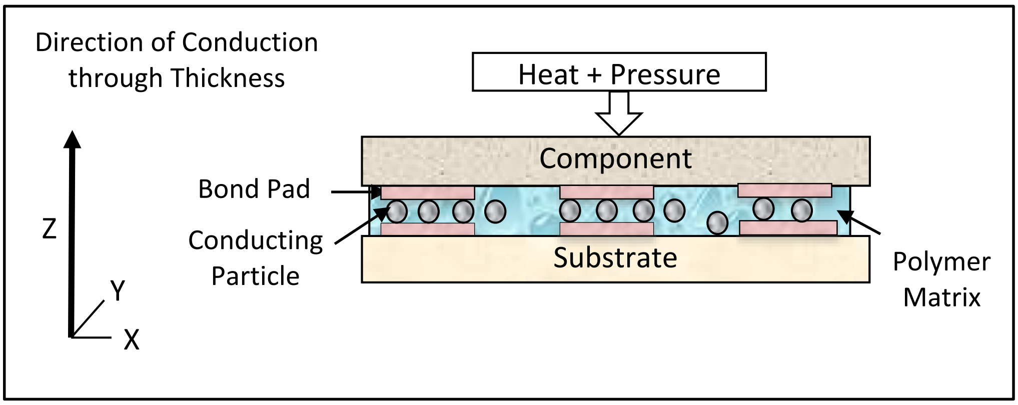

Figure 2.1 Schematic illustration of traditional ACA interconnection

ACAs typically use spherical shaped filler particles instead of the flakes which are generally used in isotropic conductive adhesives as they provide a lower percolation probability for the same metal content (Williams et al. 1993). The spherical filler can be hard solid spheres such as nickel, silver, or gold spheres or with a deformable core such as a metal-coated polymer microsphere. Solid spheres can have advantage e.g. penetrating oxide films however, in many applications metal-coated polymer microspheres have been preferred over solid conducting fillers, as hard solid spheres do not deform to an adequate degree and only touch component and substrate at a small number of points whereas metal-coated polymer microspheres can be flattened during bonding (Yim et al. 2006). The flattening increases the effective contact area at the joint interface enhancing the electrical conductivity of the bond. In addition, use of metal-coated polymer microspheres also help to reduce problems due to poor coplanarity of bond pads and thermal expansion mismatches (Dou 2007). The most popular conductive fillers for ACA applications are polymer microspheres (3µm to 10µm) plated with nickel and then a thin layer of gold (Gilleo et al. 2002; Dou et al. 2004; Li et al. 2010). Nowadays, ACAs are widely used in both LCD displays and for chip scale package and flip chip attachment for a wide range of products (Morris et al. 1999; Morris et al. 2007; Li et al. 2010).

2.3 Isotropic Conductive Adhesive (ICA)

ICAs consist of a conductive filler (usually silver flakes) in a polymer matrix at a loading of 25 to 35 vol%. This high loading ensures conductivity in all directions. The flakes tend to orient parallel to the horizontal plane and hence lower the percolation threshold in the x and y directions (Lu et al. 1998; Morris 1999; Su 2006). Figure 2.2

illustrates a typical ICA assembly. A more detailed review of ICAs is presented in Section 2.6

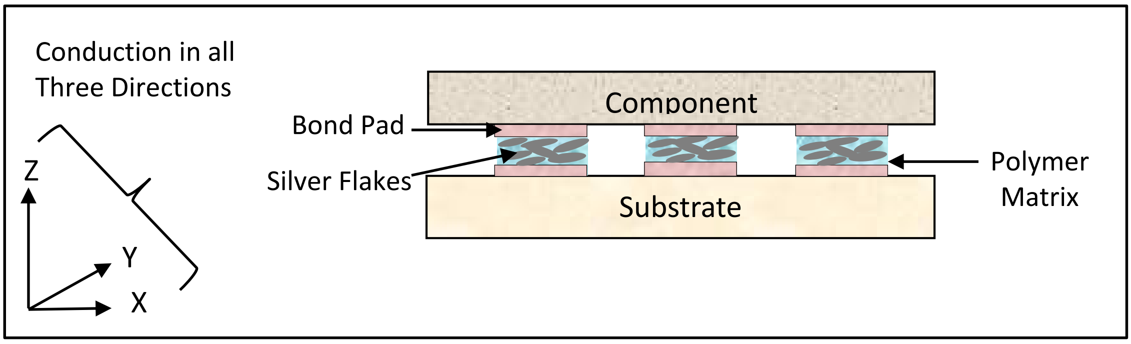

Figure 2.2 Schematic illustration of traditional ICA interconnection

2.4 Non Conductive Adhesive (NCA)

NCAs consists of a polymer matrix without any conductive filler particles. Without the presence of any conductive filler particles, the electrical connection or conductivity is achieved by sealing the nanoscale rough structures of the component and substrate bond pads together under both heat and pressure (Suhir et al. 2007; Yi. Li et al. 2010), as shown in Figure 2.3, which results in only a small number of contact spots forming. This allows the electric current to flow between the two pads. Conductive joints made with non-conductive adhesives avoid short circuiting and the pitch of NCA joints is limited only by the pitch pattern of the bond pad, providing a solution for ultra-fine pitch interconnections (Ito et al. 1998; Usui et al. 1999; Lohokare et al. 2006; Chuang et al. 2009; Yi Li et al. 2010).

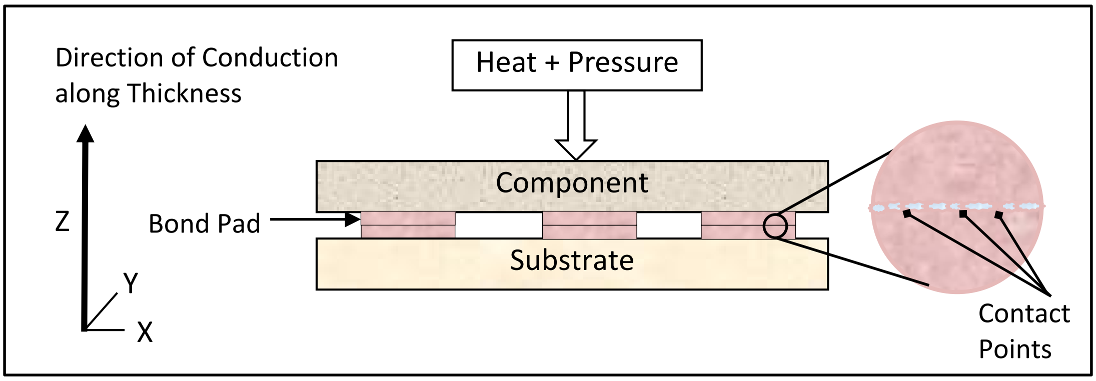

Figure 2.3: Schematic illustration of NCA interconnection

Recently NCAs have found applications in the manufacturing of LCDs, LED (light emitting diode) array modules, smart cards and RFIDs (radio frequency identification devices) (Yi Li et al. 2010). Since electrical conductivity is achieved through physical/mechanical contact and no metallurgical joints are formed, they requires high bonding pressures. It also has limited electrical conductance and current-carrying capability as well as electrical instability at high temperatures (Li et al. 2007; Yu et al. 2007; Finkenzeller 2010).

2.5 Adhesive/Polymer Matrix

The adhesive matrix for an ECA is required to have:

- Good adhesion to different surfaces and ability to withstand mechanical stresses;
- Suitable rheology to accommodate the required amount of filler while retaining processability;
- Low temperature curing;
- High thermal stability;
- High purity i.e. contains low levels of ionic contaminants;
- Low moisture absorption;
- Low outgassing during cure; and
- No environmentally or occupationally harmful ingredients.

The adhesive matrices used for ECA formulations are commonly classified as either thermoplastic or thermosetting depending on whether their molecular structures after the bonding process are linear or cross-linked (Rabilloud et al. 2005). Thermoplastic polymers are typically linear long chain molecules made up of smaller repeating units. The linear chains may be straight or branched but they do not have inter-chain cross-links, as shown in Figure 2.4. Thermoplastic adhesives soften, melt and flow when heated above their operating temperature which limits their in service performance (Licari et al. 2005; Petrie 2006).

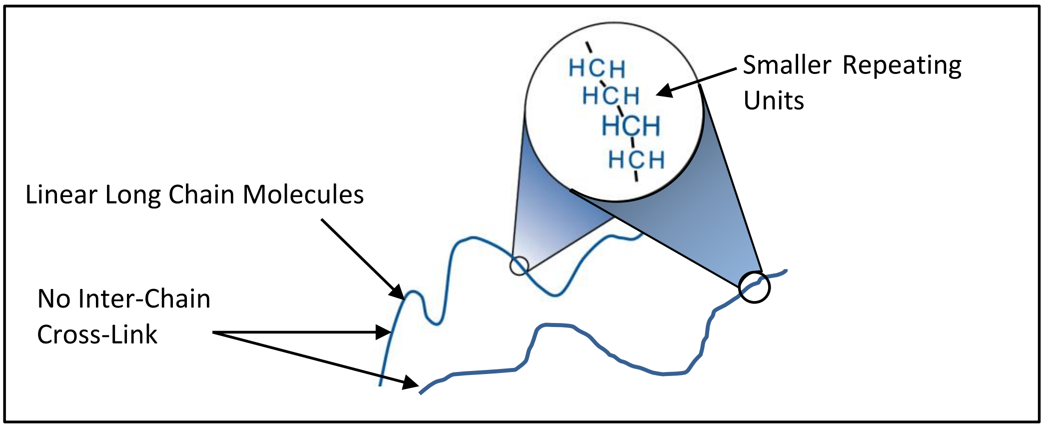

Figure 2.4 Illustration of thermoplastic polymer (after Epotek (2011))

On the other hand thermosetting polymers contain cross-linked polymer chains. This crosslinking locks the chains together restricting their chain movement, as shown in Figure 2.5. Thermosets are usually preferred over thermoplastics because (i) the cross-linked structure resists deformation and gives greater mechanical stability at high temperature (Gilleo et al. 2002; Petrie 2006); (ii) they have excellent adhesive strength, good chemical and corrosion resistance; and have low cost. The main disadvantages with the use of thermosetting polymers are that (i) they do not offer easy rework as they have cross-linked structures and therefore do not melt on reheating once cured; (ii) they have a moderate-to-high tendency to absorb moisture which has been shown to reduce their long-term reliability (Gilleo et al. 2002).

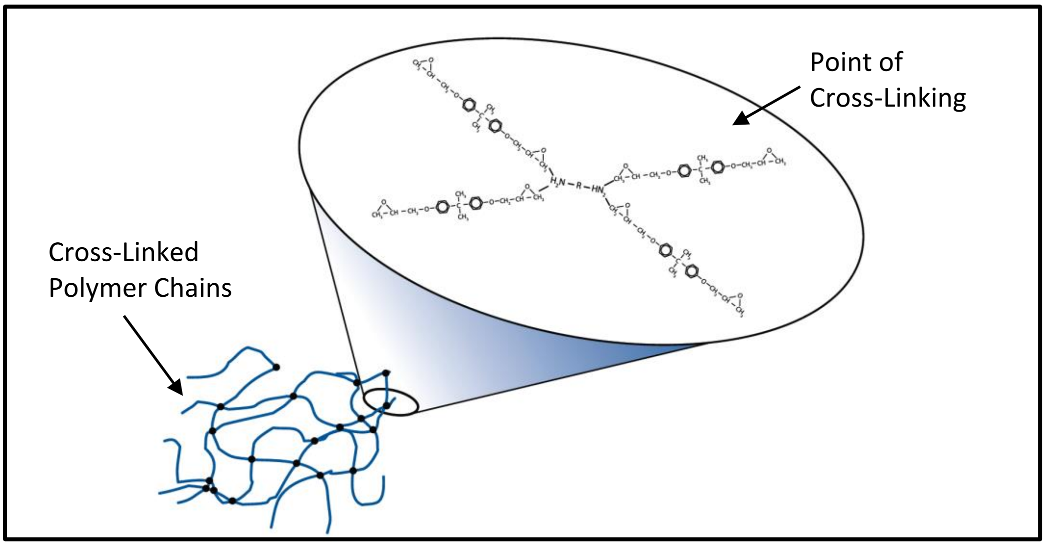

Figure 2. 5 Illustration of thermosetting polymer (after Epotek (2011))

The common adhesive/polymer matrices with their advantages and disadvantages are described below (Cognard 2005; Licari et al. 2005; Petrie 2006):

- Elastomers: cure at room temperature; have excellent adhesion to many substrates; are extremely flexible; and have superior thermal resistance. However, they have poor cohesive strength and some may be swelled by non-polar solvents.

- Polyurethanes: are extremely tough; have high impact and cohesive strength; good resistance to solvents and abrasion, however have limited high temperature use and primer may be needed for adhesion to some substrates.

- Cyanoacrylates: cure rapidly at room temperature, have excellent adhesion to most substrates and are available in wide range of viscosities. However they have poor peel strength, poor durability on glass, poor solvent resistance, low temperature resistance, and may stress crack some plastics.

- Hot melts: have high adhesion to plastics, and are available in a wide variety of formulations such as polyamide, polyolefin and reactive polyurethanes. However, they require a heated dispensing point, have poor adhesion on metals and are sensitive to moisture.

- Acrylics and acrylates: have room temperature cure that can be accelerated with heat, high peel and impact strength, and good environmental resistance. However, activator may contain solvents and requires controlled dispensing process, and may have strong odor. Mainly used to bond heat-sensitive electronic devices in 5-30 seconds at room temperature in niche optoelectronics and medical applications.

- Epoxies: have high adhesion to many substrates, good toughness, superior environmental resistance, low temperature cure schedules that can be accelerated with heat, and are available in wide variety of formulations. However, they have long cure and fixture times, can absorb water, have high amounts of chloride and other ions if not purified well, and present a risk of outgassing if not cured fully.

Among these mentioned adhesive matrices the most commonly used matrix for ICA formulation are epoxies because of their adhesion to most of the substrates, superior adhesive strength and good mechanical performance under high thermo-mechanical stresses (Licari et al. 2005). Usually commercially available epoxy resins used for ICA formulations are based on the diglycidylethers of bisphenol-A, bisphenol-F or other phenolic compounds such as epoxy phenol novolac, whose properties can be altered and tailored for specific applications through the choice of different hardeners, catalysts, fillers, and other additives (Petrie 2006).

2.6 Isotropic Conductive Adhesives - A Review

ICAs consist of a polymeric/adhesive matrix combined with conductive fillers, as shown in Figure 2.2. The polymer matrix provides bond strength and withstands mechanical stresses whereas the conductive filler is mainly responsible for the conductivity although the type and amount of filler also affects mechanical strength and rheology and there is some evidence that the matrix may contribute to the conductivity (Cognard 1991). The main focus of this research is on the electrical performance of Ag-MPS filled ICAs therefore a more detailed discussion on factors affecting conductivity and of the conductive fillers used in ICAs is presented below.

2.6.1 Percolation Threshold and ICA Conductivity

The conductive filler particles can only provide electrical conductivity through chains of contact between them. At a lower volume fraction of filler particles the resistivity of an ICA is very high i.e. the material behaves as an insulator because the conductive particles are isolated within the polymer matrix, as shown in Figure 2.6.

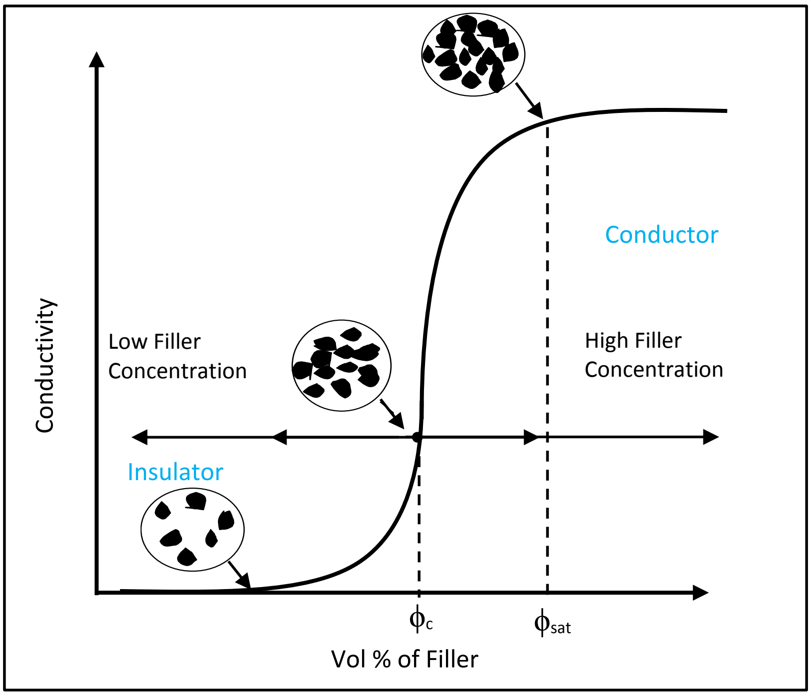

Figure 2.6 Change of conductivity of ICAs based on percolation theory (after Morris et al. (2007))

Conduction occurs only when the volume fraction of filler is more than a certain value, called the percolation threshold (ϕ_c). At this volume fraction sufficient particles are in contact to form initial conductive pathways between the electrodes i.e. at the percolation threshold, at least one chain, forms a conductive path between the measuring electrodes (Li et al. 1995; Morris et al. 2007). As formation of conductive path is a stochastic process, therefore for the same filler and matrix systems different percolation thresholds could be obtained (Ruschau et al. 1992a; Ruschau et al. 1992b). On further increasing the volume fraction of filler, the number of chains increases and the conductivity of adhesive increases (Li et al. 1997). It is believed that a point is reached where most of the conductive particles contact their neighbours to form a three-dimensional network and the conductivity then increases only slightly with any further increase in the filler concentration. This point is called ϕ_{sat} as shown in Figure 2.6 (Morris 1999).

The percolation threshold (ϕ_c) and the conductivity of an ICA has been found to depend upon the filler geometry/shape, size, size distribution and on sample dimensions (Edward 2008). Non-spherical fillers have been found to have lower percolation thresholds and higher conductivities (Ruschau et al. 1992b; Li et al. 1997; Morris 1999; Su 2006). This is because spherical fillers tend to pack much more densely whereas non-spherical filler normally show a greater tendency for bridging, which enables connectivity at lower volume fractions, leading to their lower packing densities and hence their lower percolation threshold and higher conductivities. The bridging become especially significant when fibre or flake fillers are used (Ruschau et al. 1992a; Li et al. 1997). However, it has been found that with the use of such irregular shaped fillers, the viscosity of the system rises more rapidly with filler content, which can reduce the ease of processing (Morris 1999; Petrie 2008; Licari et al. 2011). The effect of the filler on viscosity of an ICA is important factor to be taken into consideration when selecting the filler as it can affect printing or dispensing (Edward 2008). The relative viscosity for suspensions of non-spherical (irregular shaped) particles was given by Krieger et al. (1959) as:

$$\boldsymbol{\eta_r = \frac{\eta}{\eta_m} = \left(1 - \frac{\phi_f}{\phi_{meff}}\right)^{-2}} \qquad \mathbf{2.1}$$

where η_r is the relative viscosity of a suspension;

η the steady-state viscosity of a suspension with particles (Pa.s);

η_m is the viscosity of the suspending medium without particles (Pa.s);

ϕ_f is the volume fraction of filler; and

ϕ_{meff} is the effective maximum packing fraction of filler above which no flow is possible.

For non-spherical fillers with length to diameter ratios (L/D) between 6 to 27, ϕ_{meff} varies between 0.44 to 0.18, whereas for mono-sized spheres (L/D = 1), $\phi_{meff} = \phi_{max} = 0.63$ (Kitano et al. 1981). Equation 2.1 shows that for a given volume fraction of filler, the relative viscosity increases with increasing aspect ratio (non-sphericity) of the particles, thus mono-sized spheres offers lower relative viscosities than flakes for similar volume fraction. Furthermore, deformable spheres have been found to result in lower relative viscosities than solid spheres (Genovese 2012).

In addition, flakes have a tendency to become oriented parallel to the adhered surfaces during application processes and under the influence of gravity. This results in a better conductivity in the plane of the substrate compared to conductivity normal to this plane. This can be beneficial for printed conductors but for bonding applications, where electrical conductivity is required perpendicular to the bond line, this type of orientation can reduce conductivity and be a disadvantage (Morris et al. 2007).

Ruschau et al. (1992a) and Li et al. (1997) found that the percolation threshold for an ICA depends on the measurement geometry. They also found that the resistivity across thickness differed from the resistivity through the thickness. Ruschau et al. postulated that the important variables that determine the degree of anisotropy in conduction are the geometry factor, G (= area of contact electrode / distance between electrodes) and Γ (= particle size / the smallest sample dimension). As G and Γ increased, the percolation probabilities increased/decreased from bulk samples of the same composite. Li et al. showed that as the sample thickness increases to ten times the particle size percolation become independent of the thickness (Li et al. 1997).

Ruschau et al. (1992a), Li et al. (1997) and (Su 2006) have shown that for the same filler shape, smaller filler particles offer a lower percolation threshold and lower resistivity as compared to larger fillers. Ruschau et al. identified the reason for this lower percolation threshold for smaller particles as their lower packing density. This decrease in packing density for smaller particles was attributed to an increase in surface area, lower particle mass, and therefore the greater significance of weak short-range forces leading to agglomeration. These short-range forces include electrostatic fields and surface adsorption of moisture and other wetting liquids. They have also shown that fillers with a larger particle size distribution offer lower percolation thresholds and lower resistivity compared to mono-sized fillers as particles with a larger size distribution pack less densely than particles with a narrow size distribution. Further, fillers with a wider size distribution has been found to reduce the viscosity. This is mainly because for a wider particle size distribution, the smaller particles may occupy spaces between the larger particles such that the maximum packing fraction ϕ_{meff} thereby decreasing the relative viscosity (Genovese 2012). However, increasing the effective packing fraction will increase the amount of filler and may have an adverse effect on mechanical strength (Ogunjimi et al. 1992b; Morris et al. 2007).

2.6.2 Conductive Fillers

The above section showed that the electrical conductivity of an ICA depends on the fillers' quantity, aspect ratio and size/size distribution. The electrical conductivity and chemical stability of the filler surface has also been found to be an important factor in choosing the type of filler (Edward 2008; Lewis et al. 2008). As adsorption of organic molecules and formation of oxide films on the conductive filler surface may impede/obstruct passage of electrons across contact points they will affect the conductivity of an ICA. The conductive filler that have typically been used to formulate ICAs are silver, gold, copper, nickel, carbon. The resistivities of metal fillers and their corresponding ICAs are given in Table 2.1. Though, the ICA resistivity will also depend on the shape and volume fraction of metal. The following sections will discuss these filler types (and their advantages/disadvantages).

Table 2.1 Resistivities of bulk metal and corresponding ICA

	Volume Resistivity (Ω cm)			
	Cu	**Ni**	**Ag**	**Au**
Bulk Metal (Hyperphysics)	1.68×10^{-6}	7.0×10^{-6}	1.59×10^{-6}	2.2×10^{-6}
ICA	10^{-4} (Qi et al. 2012)	5×10^{-3} (Masterbond 2013)	10^{-5} -10^{-4} (Morris et al. 2007)	10^{-3} (Henkel 2009)

2.6.2.1 Silver Fillers

Silver is the most commonly used filler in commercial ICAs because unlike most metals it has a highly conductive oxide and therefore offers good resistance stability throughout the life of an ICA. It also has the highest electrical and thermal conductivity at room temperature among all metals and thus produces highly conductive ICAs. It is highly malleable and ductile and can be formed into a wide range of filler shapes and sizes for boosting conductivity (Gilleo et al. 2002). However, there are some disadvantages associated with the use of silver as the conductive filler in an ICA. The most significant are that:

(i) Silver is a precious metal, having a much higher cost compared to for example copper (Cu) and nickel (Ni) as can be seen in Table 2.2. This increases the cost of silver filled ICAs compared to copper and nickel filled ICAs; and

Table 2.2 Cost comparison of bulk metals (Metalprices 2012)

Metal	**Cu**	**Ni**	**Ag**	**Au**
Cost (£/kg)	4.8	17	347	24905
Cost (£/m^3)	42,912	151,436	3,640,030	481,164,600

(ii) With prolonged exposure of ICA to heat and moisture, silver ions can leach out of the filled resin and redeposit elsewhere in the circuit (Morris et al. 2001; Y. Shirai 2001), a phenomenon called silver migration. This may cause short circuits in applications with very fine pitch interconnection. Alloying silver with Sn has also been seen to reduce the silver migration. (Shirai et al. 2001).

(iii) Silver, particularly in its nano form, is harmful to lower aquatic and marine life and thus its use has environmental implications (Luoma 2008; Morris 2008).

Thus to reduce the cost and environmental effect, there is a need to reduce the amount of silver used in ICAs.

2.6.2.2 Gold Filler

Gold (Au) has good room temperature electrical and thermal conductivity, as can be seen in Table 2.1 and has no issue of migration after prolonged exposure to heat and moisture. It is also the most non-reactive metal and does not corrode or oxidise. However, it is very expensive as can be seen in Table 2.2 and as a result of this it has only been used in limited applications. It is typically only used where silver migration poses a serious risks or where long-term reliability in severe thermal and aggressive environments is required, such as in military, aerospace and medical applications where its cost can be readily justified (Rabilloud et al. 2005; Liu et al. 2011).

2.6.2.3 Nickel Filler

Nickel, in spite of its lower cost as compared to silver (as can be seen in Table 2.2) and the resistance of its ions to migration under prolonged exposure to heat and moisture, is still not preferred as filler over silver because nickel has lower electrical conductivity than silver as can be seen in Table 2.1 (Lu et al. 1999; Sancaktar et al. 2011). Nickel forms resistive oxide, is hard and has poor malleability which makes it difficult to process into filler particles of optimal size and shape to boost conductivity (Gilleo et al.

2002). Moreover, Nickel is classified as a class 2B carcinogen (possible carcinogen for humans) and is related to skin sensitisation and allergies so is not a desirable choice although it is used in ACAs (e.g. as 3µm solid spheres or plated on polymers).

2.6.2.4 Copper Filler

Copper offers high electrical and thermal conductivities, comparable to silver and with no issue of ion migration even after prolonged exposure to heat and moisture, at a comparatively lower cost than silver and gold. However, oxidises rapidly to form an oxide which is an electrical insulator resulting in poor resistance stability (Yim et al. 2007; Qi et al. 2012). For example, a copper-filled epoxy showed an increase in resistivity by a factor of 100 or more after 24 hours in air at moderate temperatures (Gilleo et al. 2002). This, in spite of its good properties limits the use of copper as a filler to applications where it is not exposed to air. Various approaches have been investigated for surface treatment and oxidation prevention of copper fillers. These approaches includes, (i) using copper-based conductive adhesives with antioxidants (Yim et al. 2007), (ii) coating copper powder with self-assembled monolayers (SAM) (Qi et al. 2012) and (iii) coating copper flakes and powder with silver (Zhang et al. 2010). However, these coatings were found to lose their effectiveness when exposed to the curing condition of ICAs and still show increased volume resistivity on aging, especially under high-temperature and humidity conditions.

2.6.2.5 Carbon Filler

Carbon fillers have low conductivity and has been used as conductive fillers. Hermann et al. (2009) used carbon nanotubes for low temperature flip chip connections. Wu et al. (2007) tested ICAs filled with carbon nanotubes and silver coated carbon nano tubes and the electrical resistivities achieved were 3.62 x $10^{-3}\Omega$cm and 2.2 x $10^{-4}\Omega$cm respectively, and the highest shear strength achieved was 19.6 MPa. Although these results show low resistivity and good shear strength, no investigation of the contact resistance has been reported.

2.6.2.6 Silver Coated Polymer Particles (Irregular Shaped):

Krupa et al. (2007) used silver coated polyamide particles (irregular shaped) as filler and reported low electrical resistivity (~$10^{-3}\Omega$cm) at around 33 vol% of filler. They also reported that both the shear strength and the peel strength to aluminium substrate increased on increasing filler content. However, the reliability of the formulated adhesive was not investigated after humidity and temperature cycling or mechanical loading.

2.6.2.7 Silver Coated Mono-Sized Polymer Spheres:

Mono-sized silver coated polymer particles have recently been studied as a filler in ICAs with promising initial results from electrical, mechanical, rheological and reliability studies (Gakkestad et al. 2010; Nguyen 2012; Kristiansen et al. 2013). They also offer many potential benefits as discussed in Section 1.2. However, their anticipated higher percolation threshold and lower electrical resistivity is a matter of concern and needs investigation.

2.7 Limitation of ICAs

ICAs have tended to only be used in niche applications such as die attach, small passive chip attachment in automotive and aero electronics, RFID, chip on board and to bond heat sensitive components to low cost substrates, such as polyester or glass. Recently ICAs have been identified as a potential interconnection material in inorganic thin film and organic thin film PV cells and potential replacement material to solders for connecting solar cells using very thin Si wafers where standard soldering techniques induces more stress in the module during assembly process, such as metallisation wrap through cells and emitter wrap through cells.

As discussed in Section 1.1.4 the main limitations which are impeding widespread use of ICAs are its poor long term reliability, i.e. unstable contact resistance and poor impact performance after exposure to high humidity and temperature, and mechanical cycling/shock. Thus to gain widespread acceptance as a solder replacement in electronics and PV applications, there is a need to both reduce their cost and improve electrical and mechanical reliability after exposure to high humidity and temperature and mechanical cycling/shock. The following sections will discuss these limitations and measures that might have been taken to overcome them.

2.7.1 Cost of ICA

The cost of silver filled ICAs are currently around £5780/kg (Epotek 2012), about 30 times that of Sn-Pb solders, which is around £110 - £190/kg (Farnell 2014). However, these materials are used by volume not weight. Since the density of Sn-Pb eutectic solder is 8.4 g/cc and the density of ICA is around 3.00 g/cc (depending on the amount of silver used), an ICA joint would require around one third of the weight of material as compared to Sn-Pb joint. Moreover, ICA also requires a thinner deposit as compared to solder pastes since solder losses 50% vol but only 10% mass during reflow and the adhesive loses less than 10% volume during cure (Gilleo et al. 2002). Thus, it could be argued that in costing the technology the material cost on a gram for gram basis is not a valid comparison and that the total system cost be must be evaluated i.e. after checking the material costs, the amount of material used must be estimated and the assembly process including process temperature, no need to clean assemblies, processing time, pot life, inspection technique, rework costs, and assembly yield must be considered. Depending on the processes involved in assembling a product, the higher material cost may be an insignificant part of the total system cost.

Further, the cost of bulk silver is only £347/kg (Metalprices 2012) whereas the cost of silver flakes is around £2400/kg (Matthey 2012) and cost of silver filled ICA is £5780/kg (Epotek 2012), which is nearly sixteen times the cost of bulk silver (£347). This shows that in addition to the price of silver, the processes involved in the processing bulk silver into flakes and then to formulate adhesives contribute more towards the overall costs of an ICA. These processes may include manufacturing, storage, handling and support services. Thus to reduce the overall cost of an ICA there is a need to look at the individual cost contribution of different processes.

The cost of ICAs have been reduced by using the low cost fillers such as Cu, Ni flakes/particles and carbon as shown in Table 2.2 but these ICAs have limited reliability and applicability as discussed in Sections 2.6.2.3 and 2.6.2.4.

2.7.2 Reliability of ICA

The key factors leading to poor reliability of an ICA have been identified as (Morris et al. 2001) (i) the absorption of moisture by the polymer matrix; (ii) the galvanic corrosion of the bonding surfaces; (iii) damage due to thermo-mechanical stresses; and

(iv) void formation. The following sections discuss how these factors affect the reliability of an ICA and what measures have been made to limit their affect.

2.7.2.1 Absorption of Moisture by the Polymer Matrix

All of the polymer matrices used in ICAs absorb moisture to some extent which affects their electrical and mechanical properties. If the absorbed or environmental moisture level is high, the electrical and mechanical performance of an ICA degrades rapidly. Moisture absorption affects the ICA joint by (i) altering adhesive properties (Boyle 1992b); and (ii) corrosion (oxidation or hydration) of the filler or bonding surfaces (Morris et al. 2001; Xu et al. 2003).

Boyle (1992) studied the effect of moisture absorption on the mechanical and electrical performance of epoxy based conductive adhesives. Boyle proposed that conductive channels containing negative charge exists in the metal epoxy interphase. Where the interphase is defined as the region within the epoxy where its structure is affected by the proximity to the metal. These channels contribute to both conduction and adhesion. Existence of these channels was previously confirmed by (Cognard 1991). Water ingress at the interphase reduces the electric field strength, and thus the adhesion force and the charge density in the channels leading to poor adhesion and reduced conduction.

Frisk et al. (2012) studied the reliability of fourteen commercial ICAs under humid conditions. These ICAs were used to attach zero ohm resistors with Sn/Ni terminations onto FR-4 test boards with a Sn/Ni over Cu finish. Under test conditions of 10°C to 65ºC at 85-90%RH for 200 cycles (with each cycle lasting 4 hrs) all of the ICAs failed except two (one polyimide based and one with a composition not disclosed) which survived the tests without significant changes in resistance. The failure of the ICA joints was found to be either delamination between the resistor and ICA or between the copper tracks and ICA or corrosion of the nickel coating on the copper tracks leading to poor contact resistance stability. Liu et al. (2011) investigated the effect of moisture absorption on adhesive bonds to a non-noble (Sn37Pb) metallization. They found that after 1000hrs of aging, under 85°C/85% RH conditions, moisture penetrated to the Sn37Pb surface and hydrated it, resulting in the formation of amorphous $Pb(OH)_2$. $Pb(OH)_2$ is an insulating compound that has a powdery structure which resulted in the deterioration of both electrical and mechanical properties of the ICA joint. Xu et al. (2003) also investigated the effect of moisture on both Cu and Au/Ni plated Cu substrates. During moisture conditioning for 1200 hrs at 85°C/100% RH they found that the ICA joints on the Cu substrates failed faster (by 120 hrs) as compared to Au/Ni coated Cu substrate (by 1200 hrs).

One method to reduce the effect of moisture and help improve the reliability of the joint is the use of higher electric potential (EP) metal finishes such as Ag, silver-palladium (Ag/Pd) or Gold (Au) however, use of Ag, Pd and Au lead to an increase in the cost (Yamashita et al. 2001). Modifying the polymer matrix to absorb less moisture is another method of improving reliability in humid conditions. Goobich et al. (1982), Barrie et al. (1985) and Shaw et al. (1994) replaced some hydrogen atoms within the epoxy matrix by halogen atoms. However, they found that the resulting polymers are rigid and highly cross-linked systems forming brittle adhesives with relatively low peel and impact strengths. In another study, Liong et al. (2005) used a thermoplastic polymer with low moisture absorption (0.28 wt%), called polyarylene ether and blended it with coupling agents. The coupling agents reduced the moisture absorption and showed improved adhesion strength and stable contact resistance to an Au/Ni substrate. However, they found that it is necessary to optimize the concentration of coupling agent for different surface finishes. Li et al. (2006) added polycyanate thermoset to a thermoplastic elastomer. This modified cyanateoster-based ICA yielded a toughened and flexible composite with low moisture absorption. This modified ICA also provided a solution to the phenomenon known as popcorn cracking. Popcorn cracking occurs in large and thin plastic component packages, when rapid heating causes moisture absorbed within the polymer turn to steam building up pressure inside the component and causing the package to crack (Gilleo 2002).

Another method evaluated to increase the reliability of ICA interconnections in humid environments was the use of protective coatings to cover a whole device or “glob top” material to cover only the attached component. The aim of these materials is to protect the attachment from humidity and corrosion. Frisk et al. (2012) used glob top materials to improve the reliability of ICA joints under cycling between 10°C to 65ºC at 85-90% RH. For the poorer reliability ICAs tested the glob top was found to increase the reliability. On the other hand, for ICAs with better reliability the effect was reversed.

Thus their use should be carefully considered including selection of an optimal glob top material.

2.7.2.2 Galvanic Corrosion of the Bonding Surfaces

Galvanic corrosion has been found to be one of the main causes of increased contact resistance and poor mechanical performance of ICA joints especially on non-noble surfaces (Jagt 1998; Tong et al. 1999; Shimada et al. 2000; Yim et al. 2007; Zhang et al. 2010; Liu et al. 2011). Typically in corrosion of ICA interconnections, a metal (usually the silver filler) with a higher electrochemical potential acts as the cathode and a metallisation (such as Sn, Cu, Ni, or Sn-Pb layers on the substrate or component) with a lower electrochemical potential acts as the anode. Table 2.3 lists the electrochemical potentials of some typical metals used in ICA interconnections.

Table 2.3 Electrochemical potential of some typical metals used in ICA interconnection

Metal	Au	Pt	Ag	Cu	Pb	Sn	Ni
Electrochemical Potential (V)	+ 1.50	+1.20	+ 0.80	+ 0.34	- 0.13	- 0.14	- 0.24

During the corrosion process the following reactions occur at the anode and cathode (Li et al. 2006):

Reaction at anode: $$\boldsymbol{M - ne^{-} = M^{n+}} \qquad 2.\,2$$

Reaction at cathode: $$\boldsymbol{2H_2O + O_2 + 4e^{-} = 4OH^{-}} \qquad 2.\,3$$

where M is the lower EP metal;

n is its valency;

e^- is the electronic charge;

H_2O is a water molecule;

O_2 is an oxygen molecule; and

OH^- is a hydroxyl ion.

The lower EP metal ions M^{n+} released from the substrate combine with OH^- ions to form a layer of metal hydroxide, which can be further oxidized to form a metal oxide layer. For most metals these layers are highly electrically insulating increasing the contact resistance. From Equations 2.2 and 2.3 it can be seen that the presence of water, oxygen, an electrolyte and at least two dissimilar metals (metals with a significant difference in electrochemical potential) are necessary to initiate galvanic corrosion.

Lu et al. (2000) studied the contacts made onto Sn/Pb surfaces using different ICAs. The ICAs were formulated using different epoxy resins, but the same hardener and catalyst. They also had similar properties, but different moisture absorption capacities. After aging tests (85°C/85%RH) they found that the ICA joints containing the resin with the higher moisture absorption corroded faster than those with the lower moisture absorption. In another study, Zwolinski et al. (1996) showed that ions present in the polymer matrix form electrolyte upon moisture intake. This electrolyte, when in contact with less-noble metals will initiate galvanic corrosion. In another study on the reliability of ICA interconnections in PV modules, Eikelboom et al. (2002) and Knauss et al. (n.d.) found that interconnections made between non-noble metals (aluminium plated silicon substrates and copper tabs) had a more than 15% increase in their contact resistance after aging tests (200 temperature cycles from –40°C to +80°C and 2500hrs of damp/heat storage at 85°C/85%RH) as compared to interconnections involving only silver (silver-plated substrates and silver plated tabs). This increase is contact resistance was the result of corrosion of the interconnecting surfaces. In another study Lu et al. (1999) also observed a large increase in contact resistance after 500hrs of ageing under 85°C/85%RH with the use of Ni, Sn, and Sn/Pb as compared to Ag, Au, and platinum (Pt). They further investigated the use of similar metals (for example nickel filled ICA to join nickel surfaces or silver filled ICA to join silver surfaces) and showed they had more stable contact resistances as compared to the use of dissimilar metals (such as nickel filled ICA to join silver surfaces or silver filled ICA to join nickel surfaces) after 5000hrs of aging at 85°C/85%RH. These studies show that to improve contact resistance stability, galvanic corrosion should be minimised. They also indicate that use of a polymer matrix with low moisture absorption, noble metallisation on the bonding surfaces and resins with high purity (low levels of ionic contaminants) can help reduce galvanic corrosion (Petrie 2006). One of the approaches to formulate an ICA with more stable contact resistance is to select epoxy and hardener combinations which can provide ICAs with as low as possible moisture absorption.

In addition, the use of additives such as (i) corrosion inhibitors which are chemicals that adsorb on metal surfaces and act as a passivation barrier layer between the metal and the environment by forming an inert film; (ii) oxygen scavengers which remove oxygen by reacting with any dissolved oxygen in the aqueous solution and thus consuming oxygen diffusing into ICA joints have been shown to improve contact resistance stability (Tong et al. (1999); Lu et al. (2000)). Tong et al. and Daoqiang et al. studied the effect of both, corrosion inhibitors and oxygen scavengers on Sn-Pb surfaces under 85°C/85%RH aging. However, they found that oxygen scavengers could only delay the corrosion process by up to about 100hrs but do not solve the corrosion problem completely. With continuing aging the oxygen scavenger within the ICA becomes depleted and oxygen may then diffuse to the interfaces and accelerate the corrosion process. They found that the corrosion inhibitors were more effective than the oxygen scavengers, however the effectiveness of the corrosion inhibitors is highly specific to the types of contact surfaces, and with the use of appropriate corrosion inhibitors, highly stabilized contact resistance were achieved.

2.7.2.3 Damage Due to Mechanical Stress

During the life time of an ICA it may be subjected to cyclic temperature changes which may be “slow” or “fast”. Typical epoxy resins have high (80 - 200 x 10^{-6}/°C) (Epotek 2013) coefficients of thermal expansion (CTE) as compared to silver (19 x 10^{-6}/°C) (Hyperphysics 2014). This means that temperature changes will cause stress at the material interfaces. These stress variations over the lifetime of an ICA may initiate cracking, leading to poor impact performance of adhesive joints. The elastic modulus of silver (70 GPa) is roughly 20 times higher than that of typical epoxy resins (below T_g) (Petrie 2006). During mechanical loading of the silver-epoxy composite, this will cause significant stress at the interface between the two materials. The damage due to these thermo-mechanical stresses induced during the life time of a product leads to micro-cracking and potentially failure of ICA joints (Ogunjimi et al. 1992a; Morris 2006).

Ogunjimi et al. (1992b) investigated stresses induced during curing. They bonded silicon die to alumina substrates using either a fully imidised polyimide or an epoxy.

They used epoxies with both low and high glass transition temperatures (T_g). They found that a higher level of stress (110MPa) was induced for the high T_g epoxy because of its higher processing temperature and high modulus of elasticity. Further, in their simulation studies Ogunjimi et al. found that the presence of inclusions and voids in the ICA led to an increase in stress, and that cracks in the polymer matrix were likely to propagate along the interface between the filler and polymer matrix thus high filler concentrations may promote crack growth. Bjorneklett et al. (1993) investigated the thermo-mechanical stresses induced in large silicon chips bonded to rigid substrates during curing and thermal cycling. The joint studied was made of 8 x 8 mm silicon die, bonded to three different substrates with different CTE (Aluminium (Al) > Cu > molybdenum (Mo)), using three different ICAs with both different curing temperatures and different T_gs. The stress induced was measured using integrated piezoresistive strain gauges on test chips. After temperature cycling from 10°C to 150°C the stress was found to be different between different adhesives. Larger stresses were found in the joints that have adherends with a larger CTE mismatch and which were cured at a higher temperature. Further, the effect of temperature cycling (resulting in stress cycling which strongly depends on the mismatch in thermal expansion) was investigated by measuring the thermal resistance between chip and substrate. An increasing thermal resistance was found with delamination of die or crack propagation in the adhesive.

Zwolinski et al. (1996) studied the reliability of twenty five commercially available ICAs by mounting 44 input/output plastic leaded chip carriers on to PCB boards using these ICAs and subjecting them to drop tests. They found that none of the adhesives was able to pass the six drop tests. Adhesive joints show fracture at the lead adhesive interface after one drop while complete separation of plastic leaded chip carriers from the board was seen after 2–3 drops. Su (2006) studied the effect of stress generated by the relative displacements between component and substrate on the performance of ICA joint by applying cyclic compressive/tensile stresses and found that the samples under tensile strain failed faster (after 735 cycles) as compared to those under compressive stress (after 2000 cycles). Su also found that all failures were electrical conduction failures rather than mechanical (loss of adhesion or cracks). Su attributed this to the combined effect of deformation of the matrix and the accumulation of mechanical stress at the interface between the insulating polymer and the flakes due to cyclic displacements between component and substrate. This mechanism leads to debonding of silver flakes from the adhesive (observed in scanning electron microscope images of the ICAs) which leads to electrical failure of the adhesive joint before any major cracking is evident.

Many approaches have been studied to improve the impact performance of ICA materials. One approach was to decrease the filler loading to improve the impact strength. However, this will lead to a decrease in electrical performance (Morris et al. 2007; Mir et al. 2008). Another approach is to improve the energy-dissipating capability of the ICA materials, and Vons et al. (1998), Shuangyan et al. (2003) and Rao et al. (2004) reported that by use of a flexible polymeric material with high loss factor and low Young's modulus, the impact energy can be effectively dissipated. The ICA they formulated passed the drop test. However, to design materials with high energy dissipation capability requires selection of polymers with T_g below room temperature. The resulting lower T_g, elastic modulus and strength and higher CTE, limit the use of such ICA materials in many applications (Licari et al. 2005). Kotthaus et al. (1997) showed that by using the porous Ag instead of Ag flakes strain before failure can be improved by a factor of two however the resistivity increased to $\sim 10^{-2}\Omega$cm instead of typical values of $\sim 10^{-4}\Omega$cm. To reduce the local stress at the interface between the polymer matrix and the conductive particle, Mir et al. (2010) incorporated electrically conducting polymer (polypyrrole particles) into an epoxy matrix to form an ICA, without using solid metal particles. The ICA with 15 wt% polypyrrole particles showed good impact performance under drop tests, high mechanical lap shear strength, and sufficiently low moisture absorption. However, the electrical resistivity of this ICA with polypyrrole particles was very high (in the range of 10^3 Ωcm) compared with traditional ICAs. In order to reduce damage due to stress Gakkestad et al. (2010) and Nguyen (2012) replaced the solid Ag flakes/particles with Ag-MPS. This allowed the CTE and the elastic modulus of the conductive particles to be much better matched to those of the adhesive matrix as compared to solid Ag particles. Gakkestad et al. showed that the ICAs filled with Ag-MPS successfully passed a 60 000 g acceleration firing test demonstrating their excellent impact performance. Nguyen et al. showed ICAs filled with Ag-MPS have higher cohesive strength compared to commercial silver flake filled ones. However, the electrical performance of these ICAs is yet to be investigated in detail.

2.7.2.4 Void Formation

Another mechanism that has been found to be responsible for poor reliability is the formation of voids during processing or due to formation of intermetallic compounds during humidity and temperature cycling (Ogunjimi et al. 1992a; Licari et al. 2005). In their simulation studies Ogunjimi et al. (1992a) found that the presence of inclusions and voids in an ICA can locally raise the stress and can therefore lead to greater risk of cracking of the bond. Adhesives are typically rejected if voids exceed 15% of the interconnection area, but in some applications, like windscreens and PV modules, any visible voids are not acceptable as they affect the appearance. Voids in the ICA joint during processing could be formed due to (i) poor wetting of adhered surfaces; (ii) trapping of air during mixing process of ICA; and (iii) evaporation of highly volatile components from ICA during curing.

Formation of voids due to the formation of intermetallic compounds after humidity and temperature cycling when using Sn-Pb metallisation has also been reported (Yamashita et al. 2005; Yamashita et al. 2006). Yamashita et al. (2005) and (2006) investigated the interface between ICAs and Sn-Pb plated Cu electrodes after temperature cycling. Their element mapping analysis showed the apparent diffusion of Sn into the Ag filler particles. This results in large Kirkendall voids in the Sn-Pb plating layer, which decreases the true bonding area of the ICA joint and thus degrades both electrical and mechanical properties. These authors also pointed out that the diffusion constant of Sn in Ag_3Sn (6.37×10^{-12} m^2/s) is even higher than that of Sn in Ag and the formation of Ag_3Sn cannot hinder the Kirkendall diffusion of Sn.

Formation of voids during processing can be reduced by optimizing mixing and surface preparation processes; improving the wetting of the polymer matrix; and using ICA with low outgassing and no solvents (Petrie 2006).

2.8 Focus of the Thesis and Novelty of the Proposed Research

Gakkestad et al. (2010) and Nguyen (2012) investigated a novel idea i.e. to use Ag-MPS as the conductive filler in ICAs. This was driven by the belief that it would improve the mechanical performance of ICA materials and at the same time reduce their cost. In preliminary tests, ICAs based on uniformly sized Ag-MPS showed positive results when exposed to temperature cycling and mechanical stress tests

(Gakkestad et al. 2010). Further, Nguyen et al. (2010), (2011) and (2013) extensively studied the rheological and the mechanical aspects of the use of Ag-MPS in ICA, and based on their rheological and mechanical characterisations, had proved the feasibility of using Ag-MPS as a conductive filler in an ICA. However, some concerns have been raised by (Morris 1999) on the use of metallised polymer spheres (MPS) in an ICA. These are the higher percolation threshold and lower system conductance compared to ICAs loaded with traditional flakes/particles. Further, the electrical performance and details of the conduction mechanism of ICAs using MPS have not been thoroughly studied yet. The effect of MPS volume fraction on electrical conductivity is less well understood, as are the effects of MPS size/size distribution and metal coating thickness on the electrical performance of ICAs. Additionally, where solid metallic particles/flakes are used as the filler, the resistance of the individual particles is likely to be a small part of the overall material resistance. However, for a MPS the thickness and morphology of the metallisation could be expected to have a significant influence on conductivity as the bulk of the conductor particle is comprised of a highly insulating polymer. These limits and the effects of the particle morphology on the electrical performance of the ICA are still to be investigated.

In view of the mentioned concerns and lack of available data on the electrical performance of use of Ag-MPS as the conductive filler in ICAs, it is concluded that there is a need for a detailed study to investigate the electrical performance of the ICAs filled with Ag-MPS. Thus the focus of the research reported in this thesis is to investigate the parameters affecting the electrical performance of Ag-MPS and Ag-MPS based ICAs.

In addition to improving the mechanical performance of ICA it is anticipated that the proposed concept will help reduce the amount of silver used in ICAs by up to 93%, i.e. 93% of the cost contribution of the silver towards ICA would be reduced. When using only a few kg of ICA this may not be a large reduction but if widely adopted in PV applications where few tonnes of the material is used, it may offer potential cost savings. Further, reduced silver content will reduce the environmental impact of ICAs.

2.9 Concluding Remarks

This chapter has reviewed various filler materials used within ICAs and has shown that on performance grounds gold can compete with silver. This chapter also reviews various approaches being adopted by different research groups to improve ICA reliability. This chapter identifies the use of Ag-MPS in ICA as a promising concept. The use of Ag-MPS will help reduce the amount of silver used in ICA, and hence it's cost and environmental impact. Section 2.8 highlights a lack of research on the electrical performance of ICAs filled with Ag-MPS and identifies the need to investigate the electrical behaviour of these ICAs. Next, Chapter 3 will present in detail a feasibility study of Ag-MPS based ICAs.

CHAPTER 3

FEASIBILTY STUDY - USE OF SILVER METALISED POLYMER SPHERES AS CONDUCTIVE FILLER IN ICA

This research aims at replacing the commonly used solid silver flake/particle ICA filler with Ag-MPS. The use of Ag-MPS offers several potential benefits such as a significant reduction in the required silver content and improvement of the overall mechanical properties. Furthermore, it also offers more flexibility to tune the properties of the filler according to the application. Despite these benefits, the use of spherical shaped fillers has not generally been considered to be advantageous in ICAs because of the following concerns (Morris 1999):

(i) the higher percolation threshold, as compared to traditional flake fillers; and

(ii) the absence of the higher in plane conductivity observed when flakes become oriented.

The higher percolation threshold, which means a higher volume fraction of the filler is required to get adequate conductivity, will lead to a high viscosity, which can result in poor quality stencil/screen printing or dispensing of adhesives. In addition, a higher volume fraction of filler (i.e. a low volume fraction of the adhesive matrix) may also result in an ICA with low mechanical strength.

Further, for the widespread acceptance of Ag-MPS ICAs in the market, they must be capable of achieving either similar or enhanced electrical performance as compared to the commercially available silver flake filled ICAs. In the first experimental phase of this research, initial experimental studies were carried out to benchmark the electrical conductivity of Ag-MPS filled ICAs against a commercially available silver flaked filled ICA. The rheology and mechanical strength of Ag-MPS filled ICAs was investigated by the collaborating partners. Their studies investigated the effect of Ag-MPS volume fraction on printability and mechanical behaviour in comparison with commercially available silver flake filled ICA. The aim of the experimental studies presented in this chapter was to further verify if Ag-MPS volume fractions imparting desirable conductivity lying within the limit suitable for stencil printing as determined by (Nguyen et al. 2010) and hence to check the effect of higher the percolation threshold for spheres on processability of ICAs. Details of these initial experiments are presented in this chapter.

3.1 Experimental Investigation to Benchmark Ag-MPS Filled ICAs against Silver Flake Filled ICAs

3.1.1 Aims

i) To determine and compare the percolation threshold and electrical conductivity of ICAs formulated using Ag-MPS and silver flakes.

ii) To benchmark the formulated Ag-MPS filled ICAs against a commercially available silver flake filled ICA.

iii) To investigate the viability of a significant reduction in silver content with the use of Ag-MPS as a conductive filler.

3.1.2 Materials Used

In this study, Ag-MPS of two different diameters (4.8µm and 30µm) and silver flake fillers were used. The Ag-MPS fillers were produced and supplied by Conpart AS, Norway while silver flake fillers were purchased from Johnson Matthey, UK. Conpart initially supplied 30µm Ag-MPS and its density was measured using a Pycnometer, (details of the experiment are given in Appendix A). The same instrument was then purchased by Conpart and subsequent filler material was supplied with its density already measured. For silver flakes, the bulk density of Ag was used as they lose only 0.6% of the weight when heated to 600°C (Matthey 2010). The main specifications of the filler materials used are given below in Table 3.1. The nomenclature used for Ag-MPS (in Table 3.1) is defined based on its size, thickness and plating process, while for silver flakes the standard manufacturer product name is used. The Ag-MPS size is given in terms of average core diameter which has a typical co-efficient of variance (C.V.) of approximately 3%. The coefficient of variance is the ratio of the standard deviation to the mean. The polymer particles used were produced using the patented Ugelstad, two-step seeded polymerization method owned by Invitrogen Corporation Dynal. Using this method polymer particles with such an extremely narrow size distribution (almost identical sizes) and a wide variety of chemical composition can be synthesized (Redford 2010). The possibility to tailor mechanical properties as well as the narrow size distribution has been the main motivation to extending the Ugelstad technology into ICA applications through metallizing the polymer particles. The silver was deposited onto the polymer spheres by electroless-plating however, the details of the method used for plating were not disclosed by the manufacturer. Moreover, the plating process details are not critical as the focus of this research is not to design particles. However, for comparison purposes, it is important to know if the specimens were produced using the same plating process or not. The same process, referred to as process 'A' in this case was used to prepare both specimens 4.8_15A and 30_13A.

Table 3.1 Specifications of the fillers used

Filler Type	Core Type	Nomenclature Used	Size (µm)	Ag Coating Thickness (µm)	Plating Process	Density (g/cc)
Ag-MPS	Highly cross linked methacrylate	4.8_15A	4.8	0.15 ± 5%	A	2.50 ± 5%
Ag-MPS	Slightly cross linked methacrylate	30_13A	30	0.13 ± 5%	A	1.44 ± 5%
Silver Flake (Matthey 2010)	N/A	FS-34	D_{90} 7.3[a] D_{50} 2.5[b] D_{10} 1.0[c]	N/A	-	10.5

Note:

[a] : D_{90} 7.3 corresponds to 90% of the flakes are below 7.3µm

[b] : D_{50} 2.5 corresponds to 50% of the flakes are below 2.5µm

[c] : D_{10} 1.0 corresponds to 10% of the flakes are below 1.0µm

SEM images in Figure 3.1 show the spherical shape and a narrow size distribution of the Ag-MPS and the much wider size distribution of the silver flakes. The fillers listed in Table 3.1 were mixed with a two component epoxy matrix, Epo-Tek 353ND, purchased from Epo-Tek, UK to formulate ICAs. The formulated ICAs were also benchmarked against a widely used, two component, silver flake filled commercial ICA (Epo-Tek H20E) purchased from Epo-Tek, UK. Not all the constituents of 353ND and H20E are disclosed by the manufacturer in their material safety datasheets, but the constituents that are disclosed are given in Table 3.2. The amount of silver used in Epo-Tek H20E is also not specified in the manufacturer's data sheet and is therefore estimated (to be 31 vol%) from a technical article published by Epo-Tek (Brassell et al. n.d.).

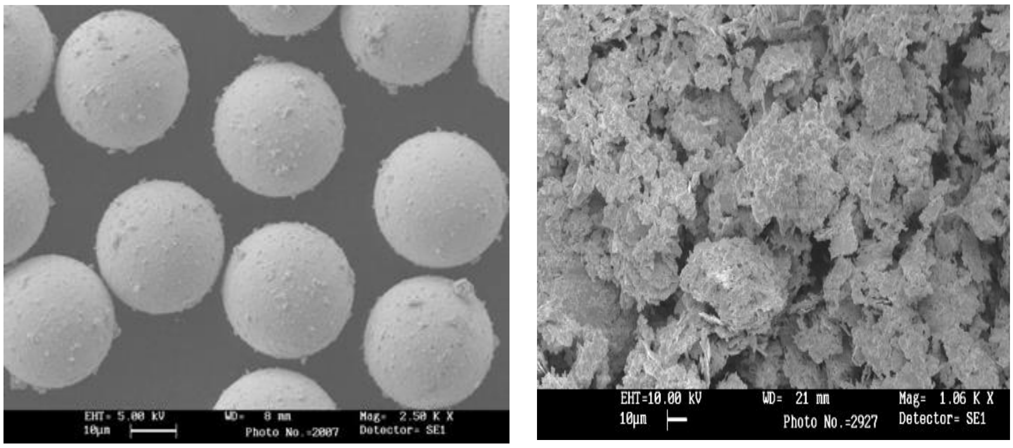

(a) (b)

Figure 3.1 SEM micrographs showing (a) 30µm Ag-MPS with a narrow size distribution, and (b) FS-34 silver flakes with a wide size distribution

Table 3.2 Specifications of the adhesive matrix used (Epotek 2010c; Epotek 2010d)

Epoxy	**Resin (Part A)**	**Curing Agent (Part B)**	**Conductive Filler**	**Manuf. Recommended Curing Profile**
Epo-Tek 353ND	Epoxy phenol novolac and Polar activator	Imidazole and Imidazole blend	N/A	150°C/1min 120°C/5min 100°C/10min 80°C/30min
Epo-Tek H20E	Epoxy phenol novolac	Substituted imidazole and Reactive diluent	Silver flakes and particles included in part A and B	175°C/45 sec 150°C/5min 120°C/15min 80°C/3hrs

The formulated ICAs were tested by printing onto specially designed PCBs supplied by Mosaic Solutions AS, as shown in Figure 3.2. These PCBs were manufactured on FR-4 laminate material with a standard Cu/Ni/Au surface finish. Contact tracks on these PCBs are connected to probe pads for making resistance measurements.

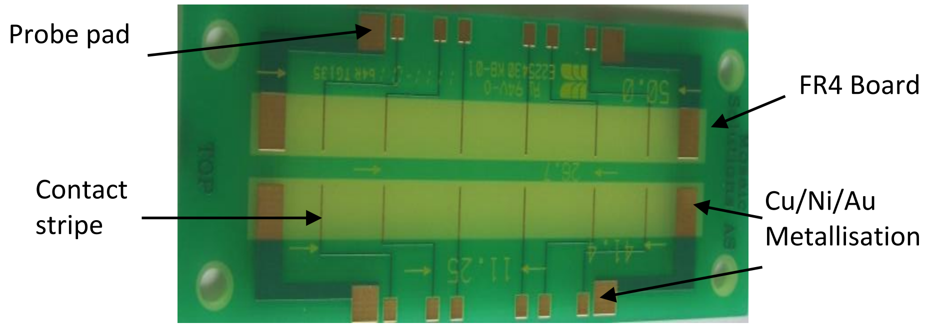

Figure 3.2 Specially designed PCB for resistance measurements

3.1.3 Equipment Used

A digital weighing balance of 1mg resolution was used for weighing filler and resin. A Flack Tek Speed Mixer, DAC 150 FVZ-K from Hauschild, Germany, was used for mixing the materials. This mixer works on the dual asymmetric centrifuge principle i.e., by spinning a high speed mixing arm in one direction and the basket in the opposite direction as shown in Figure 3.3.

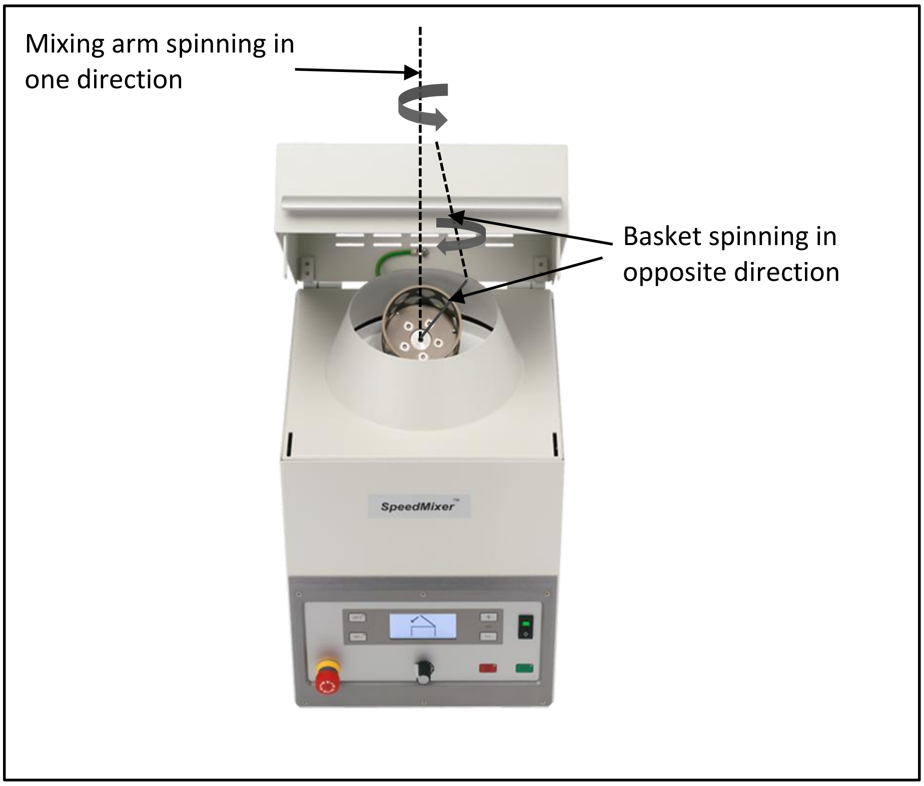

Figure 3.3 Speed Mixer™ DAC 150 FVZ-K

A 90 µm thick laser cut plastic stencil with 2 mm x 58 mm apertures was used to print prepared ICAs onto the PCB boards. A JEM 310 single zone convective reflow oven was then used to cure the samples and a DataPaq data logger was used to continuously monitor the time/temperature profile within the oven. The resistance of cured samples was measured using a Keithley 580 micro Ohm-meter.

3.1.4 Methodology

3.1.4.1 ICA Preparation

The percolation threshold of randomly packed mono-sized spheres has been reported to be around 27 vol% (Zallen 1998). Therefore, a volume fraction of 20%, which is lower than this reported percolation threshold, was used as the initial filler volume fraction for the silver coated polymer spheres to ensure the onset of conduction was not missed. The percolation threshold for flakes has been predicted to be lower than that of mono-sized spherical particles (Morris 1999). Therefore a volume fraction of 12% was selected as the initial filler volume fraction for silver flakes to again ensure the onset of conduction was not missed.

To prepare ICAs with these initial volume fractions, firstly the required amount of conductive filler and epoxy matrix was calculated using their density values. The epoxy matrix parts A and B hardener were mixed to the ratio10:1 by weight, as specified in the manufacture's datasheet. The calculated amount of conductive filler and epoxy matrix was then mixed using Flack Tek Speed Mixer to form the ICAs samples. As listed in Table 3.1 there is a ±5% uncertainty in the density values of the Ag-MPS which may lead to a ±5% error in the volume fraction calculations. The mixing parameters (i.e., mixing speed of 2000 rpm and mixing time of one minute) were kept same for all the ICAs formulated to ensure consistency throughout the experiment. After preparing ICAs with the initial volume fractions, the loading of filler was then increased in increments of 2 - 4 vol% to detect the percolation threshold. After each filler addition the adhesive was remixed. This process was repeated until the point was reached where printing of the adhesive was difficult. The commercial silver filled ICA, Epo-Tek H20E, was formulated by mixing part A and part B in the ratio of 1:1 by weight, as recommended by the manufacturer (Epotek 2010a) using the same mixing parameters.

3.1.4.2 ICA Printing

Thin stripes of the formulated ICAs were then printed onto the test PCBs using the stencil and a razor blade. The printing process is illustrated in Figure 3.4. Several factors are known to affect printing (Kay et al. 2012) these include the stencil material, aperture dimensions and roughness, printing medium rheology, printing parameters and environment, stencil framing and alignment and the properties of the substrate to be printed onto. However, as the main aim of the study was to investigate the electrical behaviour of novel ICAs, the effect of these parameters on print quality was not investigated. However, for widespread acceptance of these ICAs as an interconnection material the effect of parameters on printing requires investigation which will need to be addressed in future studies.

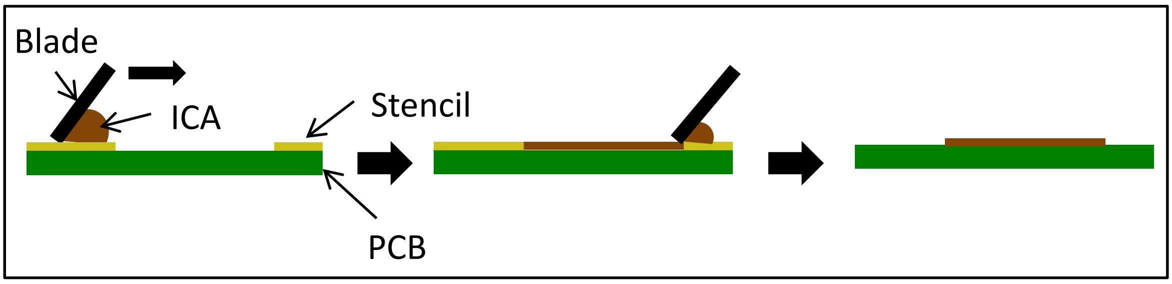

Figure 3.4 Schematic of the stencil printing process

3.1.4.3 ICA Curing

The focus of this research is to investigate the suitability of MPS filled ICAs for applications such as PV module assembly. In PV manufacturing it would be preferable if the lamination of modules and curing of ICAs could be done together in a single step. Thus ICAs having a curing schedule the same as that of typical EVAs used for lamination are preferred. Most of the EVAs used in PV lamination have a curing temperature of around 150°C. Therefore, the printed samples were cured for fifteen minutes at a target temperature of 150°C. The time (15 min) to cure at 150°C was purposely kept higher than recommended by the manufacturer (1 min) as specified in Table 3.2. Using differential scanning calorimetry Cai (2012) showed 99% cure for novel ICA (30µm Ag-MPS in 353ND) at 150°C for 15 min. The samples were then cooled to approximately 100°C before removal from the oven. The temperature profile during curing is shown in Figure 3.5. This figure also shows that the temperature in the oven reaches 150°C in around three minutes and then over shoots to 166°C, while the temperature inside an ICA sample reaches 150°C in around nine minutes and over shoots to159°C.

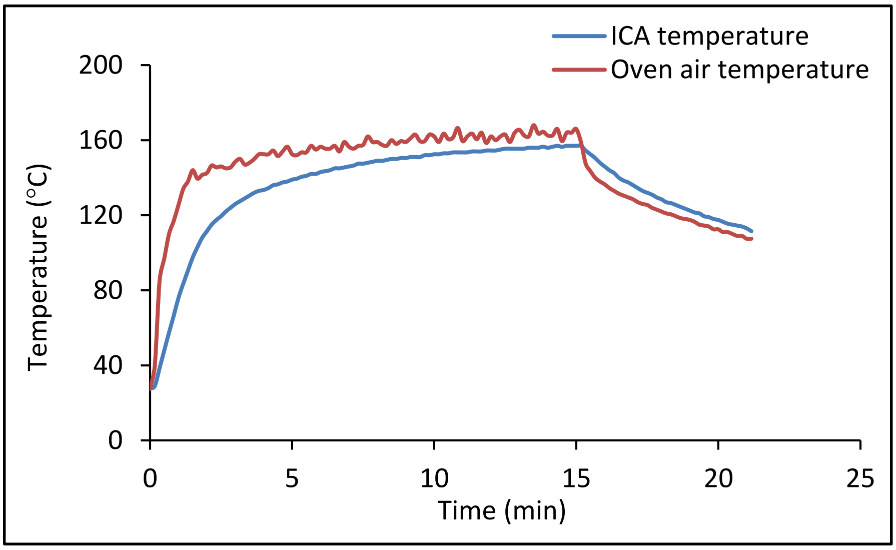

Figure 3.5 Temperature profile during curing

3.1.4.4 Conductivity Measurements

Conductivity measurements of the printed ICAs were made in accordance with the ASTM standard D2739 “Standard Test Method for Volume Resistivity of Conductive Adhesives" (ASTM 2004). The micro-ohmmeter was used to carry out four-wire resistance (FWR) measurements. The main advantage of FWR measurement is that it eliminates any contact test lead resistances and only the bulk resistance of the sample is measured. In this measurement technique, current was supplied to the outer pair of probe pads on the PCB and the potential difference was measured between an inner pair of probe pads, as shown in Figure 3.6. For each of the ICA volume fractions formulated, resistance measurements on six stripes on PCB substrates were carried out.

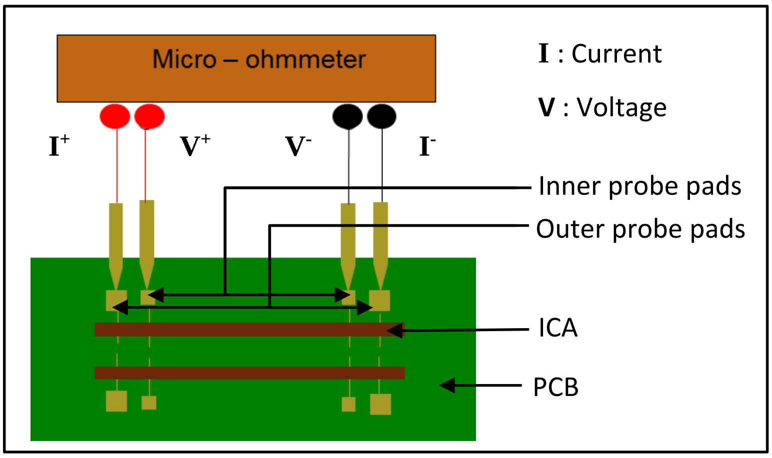

Figure 3.6 Schematic of the four probe resistance measurements

Once the resistance measurements were made, the volume resistivity, ρ_{ICA}, of each printed trace was calculated using:

$$\boldsymbol{\rho_{ICA}\ (\Omega\ cm) = R_{ICA}.\frac{w.t}{L}} \tag{3.1}$$

where, R_{ICA} is the measured resistance of the ICA trace (Ω);

w is the width of the ICA trace (m);

t is the thickness of ICA trace (m); and

L is the distance between the voltage probes (m).

The width of the stencil opening was taken as the width of the printed ICA trace and thickness of the stencil used for printing was used as the thickness of the printed trace in the resistivity calculations. As the infinite resistivity could not be plotted the calculated resistivity ρ_{ICA} was then converted to conductivity σ_{ICA} using the formula given below:

$$\boldsymbol{\sigma_{ICA}\ \left((\Omega\ cm)^{-1}\right) = \frac{1}{\rho_{ICA}}} \tag{3.2}$$

Variation of the resistance during the curing of one sample of each adhesive was also monitored for the maximum volume fraction of filler, as shown in Figure 3.7. A sixty channel Agilent 34970A Data Acquisition with Agilent 34901A module was used to record the resistances and oven temperature variations. Both measurements of resistance and temperature variations were in situ measured simultaneously and when making FWR measurements data acquisition system automatically compensates for thermal EMFs. Polyethylene terephthalate (PET) insulated wires, which can withstand temperatures up to 180°C, were used to connect the ICA samples to the Agilent 34901A module.

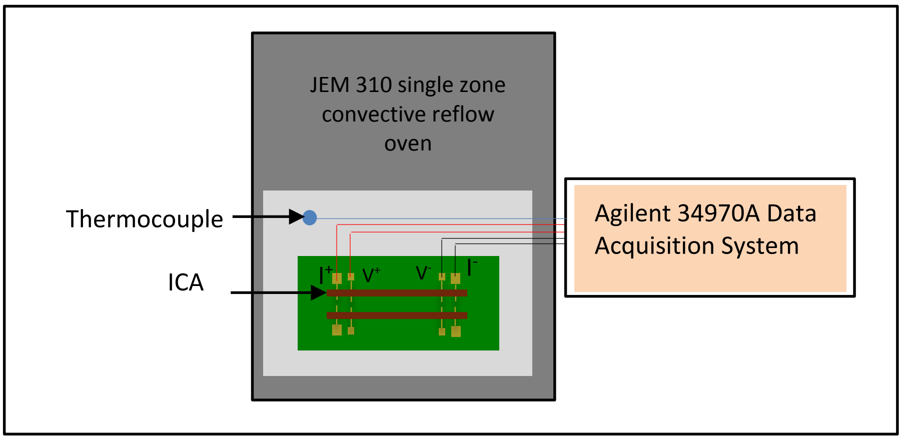

Figure 3.7 Schematic of resistance measurement during curing of an ICA

3.2 Results and Discussions

Figure 3.8 shows the averaged results from the resistance measurements plotted on log scale, together with standard deviation error bars vs volume fraction, for all three formulated ICAs. The hollow rectangles are shown for volume fractions where only two to four samples, out of the six formulated samples were conducting. It can be seen in Figure 3.8 that at low volume fractions, high resistance values with large standard deviations are obtained, whereas at higher volume fractions much lower resistance values and with small standard deviations are obtained. The reason for this greater variation at low volume fractions could be the smaller variable number of end to end conduction paths**.** However at high volume fractions there exists a multitude of different similar pathways, hence low and more repeatable resistance values are obtained.

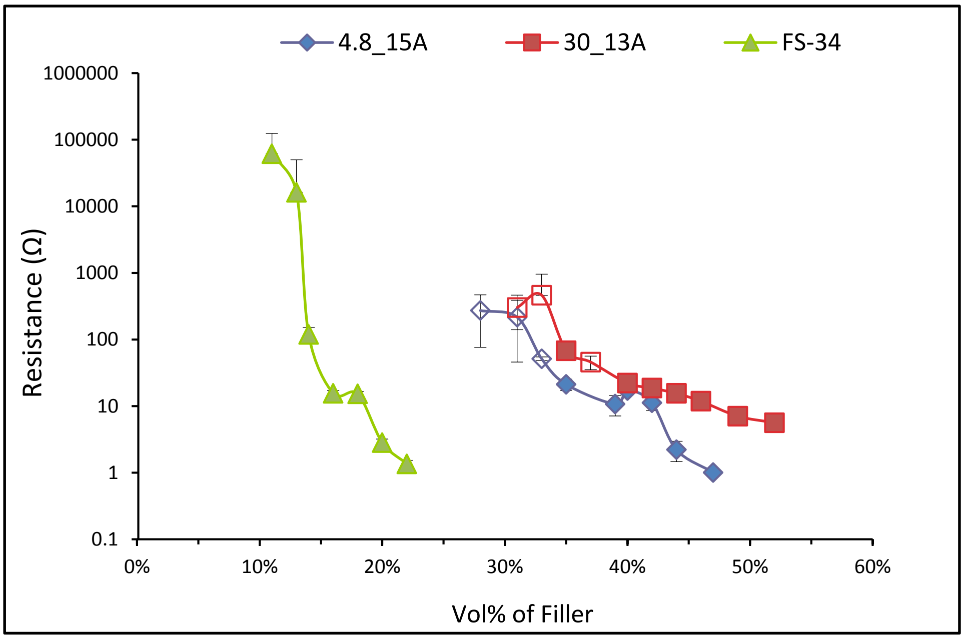

Figure 3.8 Log resistance vs volume fraction curve for all three formulated ICAs together with one standard deviation error bars

For some samples the track dimensions were measured using the contact gauge of a Talysurf CLI 2000 (by Talysurf Hobson) where a diamond stylus was traversed at three positions along length of each trace and the readings averaged. Figure 3.9 (a) and (b) illustrates cross-section profiles of these ICA samples which contained 30 and 40 vol% of 4.8 µm MPS. Table 3.3 gives the means of the measured peak thickness and width values. The thickness and width of the ICA samples is not same as that of the stencil opening they were printed through, as can be seen in Table 3.3. Similar patterns were observed for other ICAs samples printed at these volume fractions. Thus calculating the resistivity assuming the same value of width and thickness for all the samples may affect the accuracy of the results and could be another cause of variation in the resistance values.

Table 3.3 Mean Thickness and width for samples of ICA 4.8_15A at 30 and 40 vol%

Volume Fraction (vol%)	Stencil Thickness (µm)	Mean Thickness (µm)	Stencil Aperture Width (µm)	Mean Width (µm)
30	90	141	2113	3335
40	90	150	2113	2260

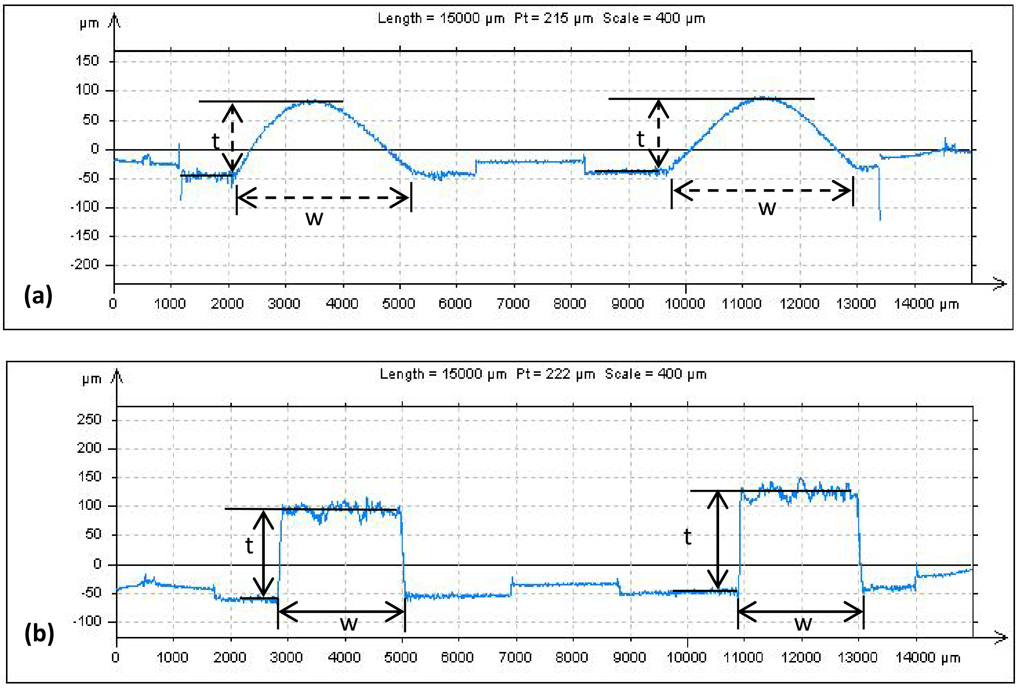

Figure 3.9 Thickness profiles for cured ICA 4.8_15A at (a) 30 vol% and (b) 40 vol%

3.2.1 Percolation Threshold

Figure 3.10 illustrates the percolation curves obtained by plotting the average conductivity against the volume fraction of filler for all the ICAs (A plot of conductivity against volume fraction of silver for these ICAs is presented in Figure 3.15). According to percolation theory, the percolation threshold for conducting systems, such as ICAs, is defined as the point at which a sharp phase transition from totally non-conducting to conducting occurs (Zallen 1998). However, it is difficult to find the exact percolation threshold due to experimental variations in the sample preparation and other experimental conditions (Ruschau et al. 1992a; Ruschau et al.

1992b; Zallen 1998). Figure 3.10 (b) shows the percolation threshold values observed for the formulated ICAs. It can be seen from Figure 3.10 (b) that for the ICAs formulated using silver flakes the non-conducting to conducting transition first occurs at 11 vol% of filler but they again become non-conducting at 13%, then again becoming conductive at 14 vol% and remain conducting thereafter, therefore the percolation threshold is taken as 14 vol%.

At 28 and 31 vol% the percolation threshold values obtained for the Ag-MPS materials are in close proximity to the empirical value of 27 vol% for random close packed structures made using mono-sized spheres obtained by (Zallen 1998). It can be seen from Figure 3.10(b) that the percolation threshold for the silver flakes is considerably lower compared to that for Ag-MPS, which is probably because of a combination of their (i) higher surface area values; (ii) alignment in the conduction direction; and (iii) wide size distribution. Table 3.4 compares the volume and surface

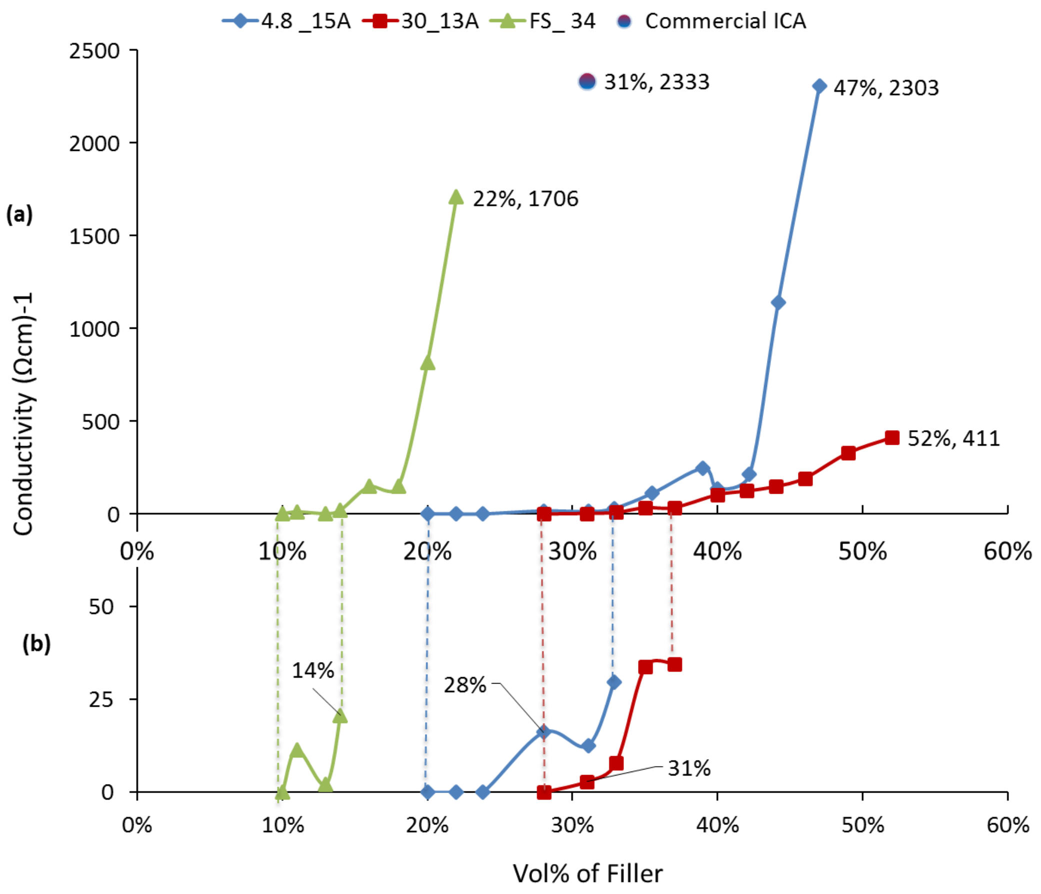

Figure 3.10 Conductivity vs volume fraction curves for Ag-MPS and silver flakes (a) showing full range of conduction and (b) enlarged view at low volume fractions to show the percolation threshold (ϕ_c)

area for the Ag-MPS and silver flakes used in this study. It shows that the smaller 4.8μm Ag-MPS and silver flakes have higher surface area to volume ratio as compared to 30μm Ag-MPS. In calculating the volume and surface area of the flakes the thickness of the flakes is taken equal to particle size as thickness values were not provided in the manufacturer's datasheet (Matthey 2010). In addition, the percolation curves shown in Figure 3.10(b) also shows lower percolation threshold (ϕ_c) for 4.8μm as compared to 30μm MPS. This could be due to larger surface area to volume ratio for .8μm as compared to 30μm MPS.

Table 3.4 Volume and surface areas for the Ag-MPS and silver flakes used

Filler Type	Radius (μm)	Thickness (μm)	Volume (μm^3)	Surface Area (μm^2)	Surface Area/ Volume (μm^{-1})
Sphere	15	-	14137	2827	0.19
	2.4	-	53	66	1.25
Silver Flake	0.5 - 3.5	1.0 – 7.0	1.04 - 359	7.85 - 384	7.5 - 1.07

Furthermore, horizontal alignment and wide size distribution of the silver flake was observed in the SEM image, as shown in Figure 3.11. This may boost flake connectivity in the "XY" plane, thereby initiating in-plane conduction at a lower volume fraction of flakes (Ruschau et al. 1992b). This may be an advantage if the ICA is used to create printed tracks, as here, but when used as an adhesive this orientation of flakes may reduce through thickness, conductivity. The MPS filled materials are not expected to display this anisotropy of conductivity.

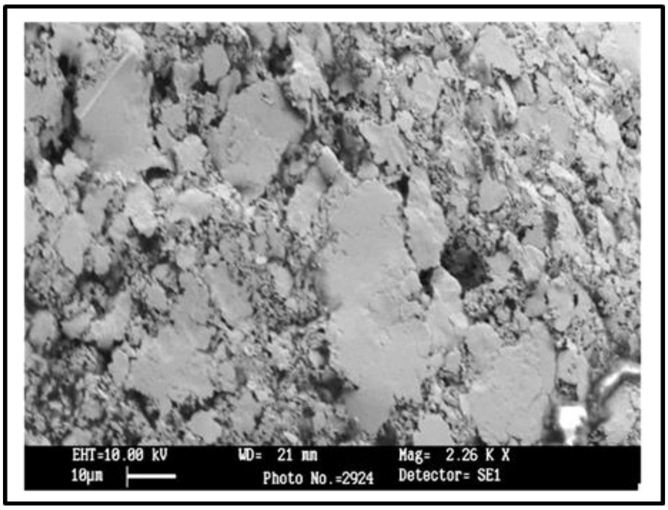

Figure 3.11 SEM image of the top surface of commercial silver flake filled ICA

3.2.2 Electrical Conductivity

Further observations made from the Figure 3.10 are given below in Table 3.5. It can be seen from Table 3.5 that electrical conductivity close to that of a commercial silver flake filled ICAs was achieved with the use of 4.8µm MPS but with a higher volume fraction. This higher volume fraction may have a negative impact on the printability and the mechanical strength of the ICA. However, according to Genovese (2012) high concentrations of deformable spheres can accommodate each other at rest and squeeze past each other during flow, increasing ϕ_{meff} than for flakes or solid mono-sized spheres and reducing η_r in Equation 2.1 resulting in a lower viscosity. Further, previous studies conducted on the rheology of the Ag-MPS filled ICAs demonstrated (i) good aperture filling during stencil printing and (ii) mechanical strength similar to that of a commercial flake filled ICA at as high as 50 vol% of Ag-MPS (Nguyen et al. 2010; 2011; 2013). This shows that the processability and mechanical strength are not major concerns for ICAs loaded with as high as 50 vol% of Ag-MPS. However, if rheology modifiers such as SiO_2 (silica) are used, the printing may be difficult at 50% (Redei 2014).

Table 3.5 Maximum observed conductivity of formulated ICAs

ICA	Maximum Observed Conductivity $(\Omega cm)^{-1}$	Vol% of Filler at Maximum Conductivity
With 4.8µm Ag-MPS	2302	47%
With 30µm Ag-MPS	411	52%
With FS-34 Silver Flakes	1706	22%
Commercial ICA with Silver Flakes	2333	31% (Brassell et al. n.d.)

Table 3.5 also shows that the conductivity of an ICA formulated using silver flakes is lower than that with 4.8µm Ag-MPS. This may be because the silver flakes used in the study are coated with surfactants to reduce the tendency for clustering or agglomeration, whereas the Ag-MPS used are not coated with any surfactants. The presence of surfactants on the surface of flakes may increase the contact resistance between silver flakes and could therefore be a cause of their lower conductivity. Furthermore, Table 3.6 also shows that the conductivity of the ICA formulated using silver flakes is lower than that of the commercial ICA, H20E, filled with silver flakes. The lower volume fraction of silver in the ICA formulated compared with the

commercial ICA could be one reason for their lower conductivity. Another reason could be that 353ND and H20E contain same resin but in different quantities, further the curing agents is also different in both these matrices, some of the constituents of the commercial ICA and 353ND are not listed in the material safety data sheet (as given in Table 3.2). Therefore due to different curing agents, these matrices will have different curing reactions. H20E contains a reactive diluent, the presence of a reactive diluent generally leads to a faster rate of cure and a higher crosslink density than without one. Thus different curing agent and presence of a reactive diluent may impart different shrinkages to H20E than 353ND thus different conductivities (Klosterman et al. 1998; Lu et al. 1999). The effect of shrinkage of epoxy matrix on the conductivity of the ICA is further investigated in Chapter 6. Figure 3.10 shows a steeper rise in the conductivity of the ICA containing 4.8µm Ag-MPS and silver flakes as compared to 30µm Ag-MPS. The reason may be that as the volume fraction of filler is increased beyond the percolation threshold the number of parallel paths increases more in 4.8µm Ag-MPS and silver flakes filled ICAs as compared to 30µm Ag-MPS because of the smaller size of 4.8µm Ag-MPS and silver flakes.

The resistances of all the four ICAs during cure were monitored and its variation with temperature is plotted in Figure 3.12. The volume fractions used in this experiment were the ones showing maximum conductivity. The plots in Figure 3.12 show that before cure the commercial ICA, H20E, has relatively very high resistance as compared to all other ICAs formulated using 335ND.

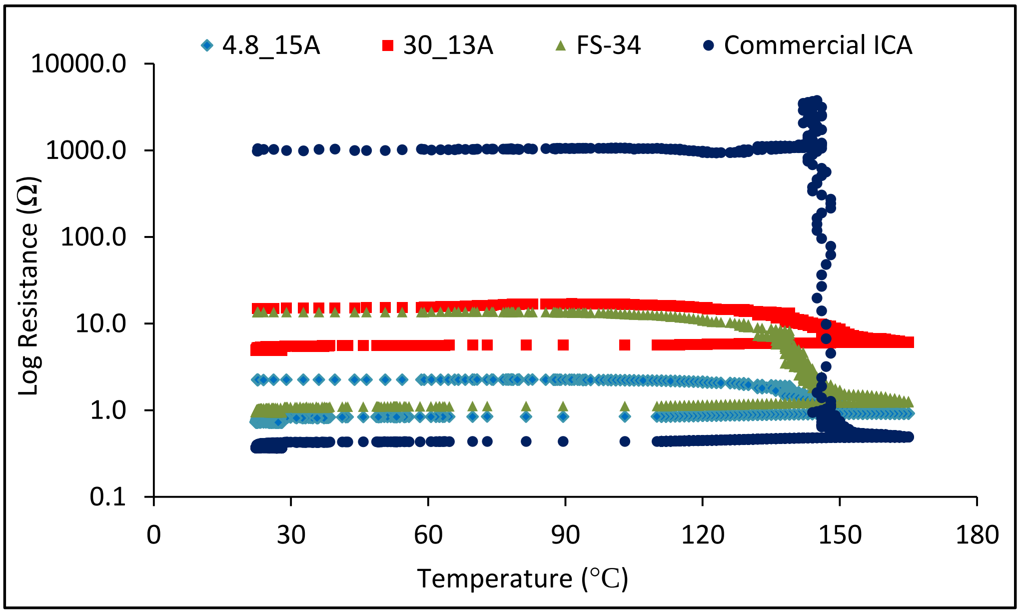

Figure 3.12 The variation of the resistance with temperature during thermal cure

As the temperature is raised above room temperature the resistance of all the ICAs remain nearly constant until 100°C, after 100°C the resistance of ICAs made using 353ND starts decreasing but the decrease in resistance is small with further increase in temperature. As the temperature is increased beyond 135°C the decrease in resistance increases and this decrease in resistance continues till 150°C. In an adhesive matrix, cure begins with the formation and growth of the linear polymer chains and as the cure proceeds these chains begin to branch and then crosslink, forming a cross-linked network. The transformation from a viscous liquid to an elastic gel marks the first appearance of the cross-linked network and is called gelation. The formation of elastic gel does not inhibit the curing process. On further curing this elastic gel converts to a glass state this is called vitrification. This marks the end of cure. The initial decrease in resistance around 100°C can be associated with conductive filler packing on heating i.e. as the adhesive viscosity falls on heating it is squeezed from intra filler spaces lowering the resistance. The large decrease in resistance after 135°C can be explained that as temperatures increases more chains get cross-linked and the adhesive transforms from a viscous liquid to an elastic gel forcing the filler together. The subsequent decrease in resistance can be associated with the transformation of elastic gel to a glassy state called vitrification where on further development of cure, larger force on the particles act, forcing them further closer. Any solvent if present in the adhesive matrix may evaporate during curing. This may also the affect ICA conductivity. However, different trend is seen in the case of H20E. During the curing of H20E the resistance suddenly increases at around 140°C and then decreases drastically. This indicate the presence a constituent which either decomposes on heating at around 145°C or initiates rapid cure at around 140°C. The decomposition of this constituent or rapid curing may be one of the reason for better final conductivity of the commercial ICA than other ICAs. This observation needs further detailed investigation and is out of scope of the present study.

Further, ICA samples at volume fractions close to percolation threshold have been found to bleed. Pictures of uncured and cured ICA samples are shown in Figures 3.13 and 3.14 respectively. Comparison of these images shows bleeding of adhesives below 40 vol% of filler. The bleeding makes the width and thickness of the cured sample non-uniform along the whole length of the printed trace. If the spreading/bleeding of the resin displaces the filler particles with it then it would affect the long range particle to particle connectivity and may increase the percolation threshold and reduce the conductivity.

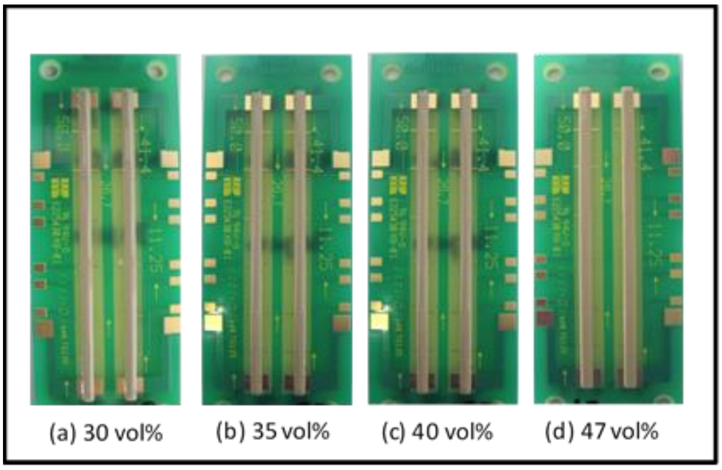

Figure 3.13 Uncured 4.8µm Ag-MPS filled ICA at different volume fractions

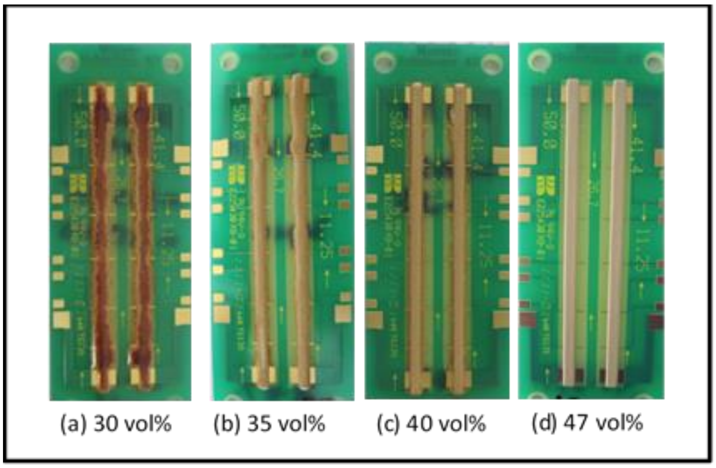

Figure 3.14 Cured 4.8µm Ag-MPS filled ICA at different volume fractions

On the other hand, if bleeding/spreading adhesive does not displaces the filler particles with it, instead the particles come closer upon curing then the resin bleed/spread may increase the effective volume fraction of the particle in the adhesive increasing the particle to particle connectivity thus lowering the percolation threshold and increasing the overall conductivity. However, effect of bleeding on particle displacement within adhesive and thus on conductivity needs detailed investigation and is out of scope of the present study. Moreover, it can be observed from the Figure 3.14 the resin do not bleed on the Cu/Ni/Au metallisations even at volume fractions below 40 vol%. The reason could be that the adhesive made larger contact angle with gold compared to FR4 substrate. Thus choosing the suitable substrate which makes larger contact angle with the adhesive matrix the bleeding may be controlled (Petrie 2006).

3.2.3 Silver Content

The Ag-MPS with thin silver coating compared to solid silver flakes/ particles are anticipated to reduce the amount of silver used to manufacture ICAs. However, there was a concern that reducing the amount of silver may affect the conductivity (Morris 1999). The effect of reduced silver amount on the ICA conductivity is presented in this section. Figure 3.15 plots the average values of conductivity for the formulated ICAs against the volume fraction of silver within them and compares them with commercial ICA.

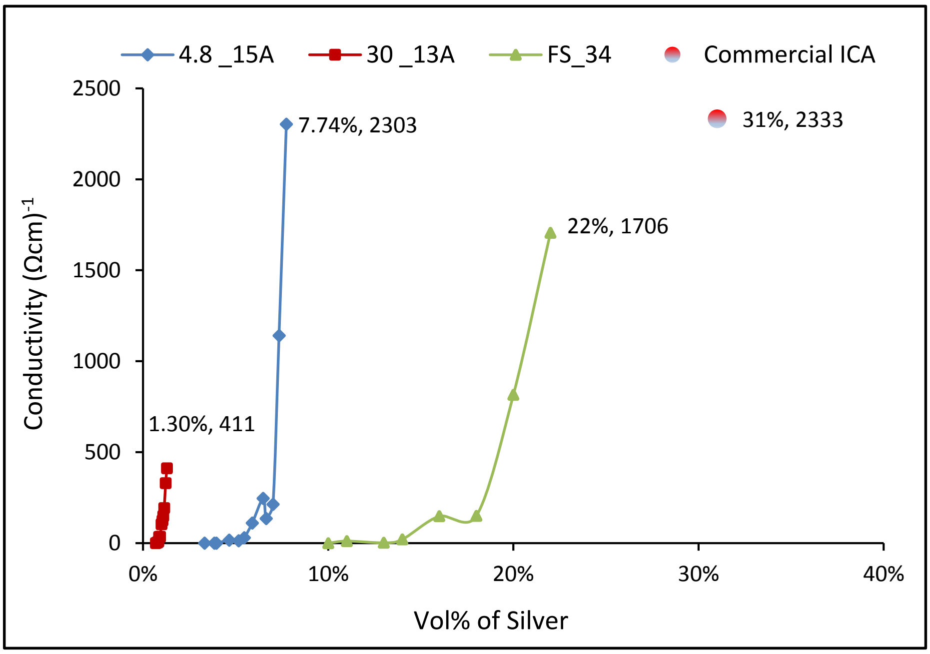

Figure 3.15 Conductivity vs volume fraction of silver

Figure 3.15 shows that for a similar value of electrical conductivity, the 4.8µm MPS filler has significantly lower silver content (approximately 7.74 vol%) as compared to the commercial flake filled ICAs (31 vol%). This is a less than 75% reduction of the silver content, hence offering potential cost benefits. Additionally, it can also be observed that moderate conductivity value of up to 411 $(\Omega cm)^{-1}$ can be achieved with significantly lower amounts of silver (< 2 vol%), in the case of the 30µm MPS filler. On the other hand, for such low amounts of silver, both silver flake and 4.8µm MPS filled ICAs are non-conducting. Thus, 30µm Ag-MPS can offer even greater potential cost benefits for applications where high conductivity is not a requirement.

3.3 Concluding Remarks

The experimental investigation reported in this chapter has showed promising results for the use of Ag-MPS as a conductive filler in ICAs. The results demonstrated that high conductivity values, comparable with commercially available ICAs, can be obtained by the use of Ag coated polymer spheres as conductive filler, but with a greatly reduced Ag content.

The results also indicate that for a similar Ag coating thickness a higher conductivity can be achieved with a smaller diameter MPS. However the effect of thickness of MPS metallisation on conductivity needs further investigation. Further, the results show that the silver content in the larger MPS ICA is less than that in the smaller MPS, therefore for applications where very high conductivity is not required larger MPS may offer even greater potential cost benefits.

The results provide a strong indication that Ag-MPS will be suitable for the production of robust and low cost ICAs following their optimization. Thus a more detailed insight into their conduction behaviour both by theoretical and empirical methods is required. The next chapter presents a theoretical study of the electrical conductivity of ICAs made using Ag-MPS to gain insight into the effect of various parameters such as MPS size, coating thickness, properties of the polymer matrix, and the manufacturing process conditions.

CHAPTER 4

THEORETICAL MODEL OF ELECTRICAL CONDUCTIVITY OF ICAs FILLED WITH SILVER METALLISED POLYMER SPHERES

The feasibility study presented in Chapter 3 showed that, for equivalent conductivity, a significant reduction in the required silver content can be achieved if Ag-MPS are used as the filler in ICAs instead of conventional solid silver flakes/particles. The study also showed that it is the higher volume fractions of Ag-MPS which provide the maximum benefits. However, the results presented in Chapter 3 are not sufficient to support the replacement of the silver flakes by Ag-MPS. To enable commercial use, optimisation of ICAs made using Ag-MPS is necessary. This requires a more detailed insight into the conduction behaviour of ICAs made using these spheres, both by theoretical and empirical methods. This chapter presents a theoretical study carried out to gain an understanding of various parameters which affect the conduction in ICAs filled with a high volume fraction of Ag-MPS. The Ag-MPS used are hereafter referred to as simply MPS or particles in this thesis.

4.1 Factors Affecting Electrical Conduction in ICAs

Electrical conduction in an ICA is a result of the formation of continuous linkages of conductive filler particles, i.e. percolation. The main factors which determine the resulting conductivity of an ICA are: (i) the volume fraction of filler particles; (ii) particle-to-particle conductivity; and (iii) conductivity within the individual particles. These three factors are discussed below in more detail.

4.1.1 Volume Fraction of Filler Particles

The volume fraction of filler particles plays a very important role in determining the electrical conductivity of ICAs. In this study the filler used is mono-sized Ag-MPS instead of silver flakes and the percolation curves shown in Figure 4.1 demonstrate the effect of volume fraction of Ag-MPS on ICA conductivity. These curves are based on the experimental data presented in Chapter 3 and can be divided into three main regions, as identified in Figure 4.1.

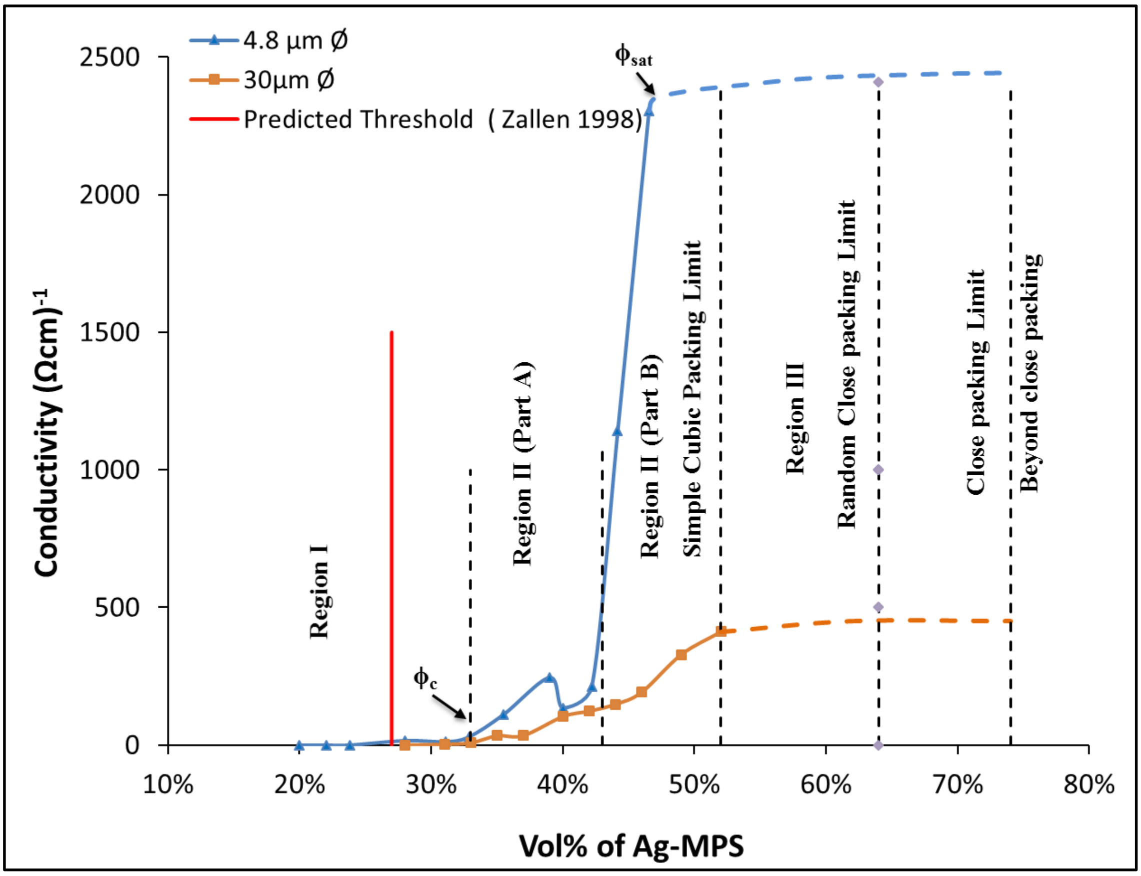

Figure 4.1 Percolation curves for the Ag-MPS filled ICAs used in the feasibility study

(i) *Region I (0 vol% - 31 vol%)*: This region is below the percolation threshold (ϕ_c), and is where negligible conductivity is observed. This non-conducting behaviour is due to the low packing density resulting in a small probability of forming continuous chains of particle-to-particle contact;

(ii) *Region II (31 vol% - 52 vol%)*: This region is above the percolation threshold, but below the conductivity saturation point (ϕ_{sat}). The conductivity saturation point is described as a point on the percolation curve beyond which negligible further increase in conductivity occurs with increasing filler volume fraction. This region can be further divided into two parts, Part A and part B;

Region II Part A (31 vol% - 43 vol%): Low but gradually increasing conductivity is observed in this region. This shows that there is still a significantly low probability of formation of continuous chains of particle-to-particle contact with increase in packing density/volume fraction. This low probability results in formation of only a small number of complete conductive paths between ends of the sample, lower the length of the sample and hence explains the low conductivity in this region;

Region II Part B (43 vol% - 52 vol%): In this region conductivity increases rapidly with relatively small increases of volume fraction. This shows that the probability of formation of continuous chains of particle-to-particle contact increases substantially in this region with relatively small increases in packing density/volume fraction resulting in increased numbers of conductive paths. It has been shown that the desired levels of high conductivity can be achieved in this region with volume fraction values which are less than the upper limit for processability of the ICAs (Nguyen et al. 2010; Nguyen et al. 2013). This volume fraction range also results in good mechanical strength (Nguyen et al. 2010; Nguyen et al. 2011). However, in the case of flake filled ICAs desired levels of conductivity can be achieved with volume fractions of only 25 – 35 vol% (Li et al. 1995); and

(iii) *Region III (52 vol% and beyond):* This is the region above the conductivity saturation point. In this region processing of the ICA becomes difficult due to very high viscosity and as a result of this ICA samples could not be mixed. Based on typical percolation curves, only a very small increase in conductivity would occur with further increases in volume fraction within this region (Morris 1999; Morris et al. 2007). This is shown by extending the experimental percolation curves by dotted lines in Figure 4.1.

(iv) The negligible change in the number of conductive paths for any further increase in packing density/volume fraction of filler explains the negligible change in conductivity in this region.

It is evident from the above discussion that, for a given volume fraction of Ag-MPS, the ICA conductivity depends upon the number of conductive paths which in turn will depend upon the packing arrangement of the filler particles. Significant packing arrangements for spherical particles are (i) simple cubic packing (SC), (ii) hexagonal close packing (HCP) and (iii) random close packing (RCP) as shown in Figure 4.2 (a), (b) and (c) respectively. The grey coloured circles in Figure 4.2 corresponds to the first/base layer. The blue coloured, hollow circles corresponds to the place where second/subsequent layers could be placed. In SC packing, the spheres in the subsequent layers are placed exactly above the spheres in the first layer as shown in Figure 4.2 (a). It is the least dense ordered packing arrangement where each particle has a coordination number of six i.e. has six nearest neighbours, and results in a volume fraction of 52%.

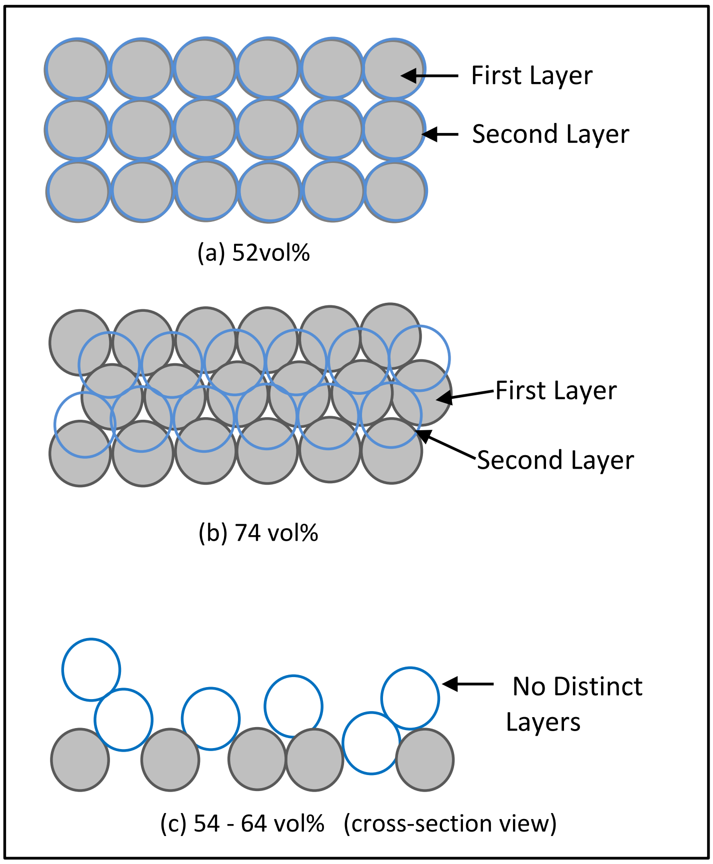

Figure 4.2 Illustrating (a) simple cubic (b) hexagonal and (c) random, close packing arrangement.

In HCP, the spheres in the subsequent layers are placed above the voids in the preceding layer as shown in Figure 4.2 (b). HCP are the densest possible arrangement of spheres and have a coordination number of twelve. This packing is achieved at a volume fraction value of 74%. In RCP, there will not be any defined layers and spheres can be placed anywhere as shown in Figure 4.2 (c). Random close packing has coordination numbers between 5.3 to 6 and a packing density between 56 and 64 vol% (Scott et al. 1969; He et al. 1999). Further as the volume fraction of filler in an ICA is increased above percolation threshold which is ϕ_c, the probability during shearing flow of collisions and hydrodynamic interactions between filler particles rapidly increases (Stickel et al. 2005). This leads to an increase in the viscosity (Krieger et al. 1959;

Genovese 2012). The viscosity of ICAs filled with Ag-MPS can be determined by considering them as dense mono disperse suspensions (Nguyen et al. 2010; 2013). At low volume fractions the relative viscosity of such mono disperse suspensions can be described by the theoretical equation of Einstein (1906) as:

$$\boldsymbol{\eta_r = \frac{\eta}{\eta_m} = 1 + [\eta]\phi_{Filler}} \qquad \mathbf{4.1}$$

where η_r is the relative viscosity of a suspension; η the steady-state viscosity of a suspension with particle volume fraction; η_m is the viscosity of the suspending medium without particles; $[\eta]$ is the intrinsic viscosity of particles and for uncharged monosized spheres it is 2.5, and ϕ_{Filler} is the volume of filler. However, at higher volume fractions, particle crowding produce hydrodynamic interactions as well as increasing probability of collision between particles, resulting in significant positive deviations from Equation 4.1. One of the most useful expressions that can be used to describe the relative viscosity at higher volume fractions of filler is the semi-empirical equation of Krieger et al. (1959):

$$\boldsymbol{\eta_r = \frac{\eta}{\eta_m} = \left(1 - \frac{\phi_{Filler}}{\phi_{max}}\right)^{-[\eta]\phi_{max}}} \qquad \mathbf{4.2}$$

where ϕ_{max} is the maximum packing fraction of particles, above which no flow is possible. As filler concentration approaches the level corresponding to a dense packing of particles in HCP (ϕ_{max} = *74 vol%),* there is no longer sufficient fluid to lubricate the relative motion of particles, and the viscosity rises to infinity. At this point the suspension shows a shear yield stress. However, ϕ_{max} is usually lower than this theoretical maximum. In equation 4.2, ϕ_{max} is taken to be 64 vol% because the arrangement of spheres in suspensions generally follows random close packing as discussed in several review papers (Krieger et al. 1959; Woods et al. 1970; Choi et al. 1986; Stickel et al. 2005; Genovese 2012). Further, during processing, for the adhesive to flow the particle layers must slide over each other. As the volume fraction increases from 64% it must imply an increase in order (crystallinity) with perhaps regions of HCP which make adhesive flow and processing above 64% increasingly difficult. Using Krieger and Dougherty's equation Nguyen et al. (2010) and (2013) found that the upper limit for processability of ICAs filled with MPS are in the range of 45 - 55 vol% as their measured data fits very well with Krieger and Dougherty's equation over the entire range of volume fractions. From Figure 4.1, volume fractions of 45 - 55 vol% have also been identified as being sufficient to generate desirable conductivity. Therefore, volume fractions of Ag-MPS that are of key importance lie in this range of 45 to 55 vol%, which implies a very loose random packing arrangement.

4.1.2 Particle-to-Particle Conductivity

Particle-to-particle conduction typically starts during the curing process and results in a sharp increase of ICA conductivity (Klosterman et al. 1998; Lu et al. 1999; Su 2006). It is believed that during the curing process, shrinkage of polymer matrix helps the filler particles to come into contact with each other. Some filler particles are also believed to have a (non- conduction) coating of surfactant film, which may dissolve in the resin above certain temperature (Lu et al. 1998; Lu et al. 2000). Particle-to-particle conduction can be a result of (i) a direct physical contact, or (ii) indirect physical contact with the presence of a very thin insulting film between them, or (iii) a combination of both. Particle-to-particle conductivity can therefore be described in terms of contact resistance, R_{cr}, and can be written as:

$$\boldsymbol{R_{cr} = R_{csr} + R_t} \qquad \mathbf{4.3}$$

where, R_{csr} is the constriction resistance (Ω) which accounts for direct physical contact and R_t is the tunneling resistance (Ω) which accounts for indirect physical contact. These two components of R_{cr} will be discussed in the following two sections.

4.1.2.1 Constriction Resistance

Most surfaces are rough at the microscopic level, with projections, called “asperities” and such projections remain even with excellent plating or polishing process. When two metal surfaces come in contact with each other, initially they touch only at a few of these asperity points. However, when an external load is applied, these asperity contact points become enlarged into small areas and new contact spots also emerge. These load bearing asperity contact areas and spots, cover only a very small portion of the apparent contact area as shown in Figure 4.3. These load bearing areas and spots are called the actual contact area A_b, whereas the whole covered area is called the apparent contact area, A_a. Therefore, electrical current flowing between the two particles is constricted within these actual contact areas instead of flowing through the entire nominal contact surface. The constriction resistance is the resistance offered by these actual contact areas to the flow of current. However, it is very difficult to measure the actual contact area and therefore in theoretical calculations apparent contact area is typically used.

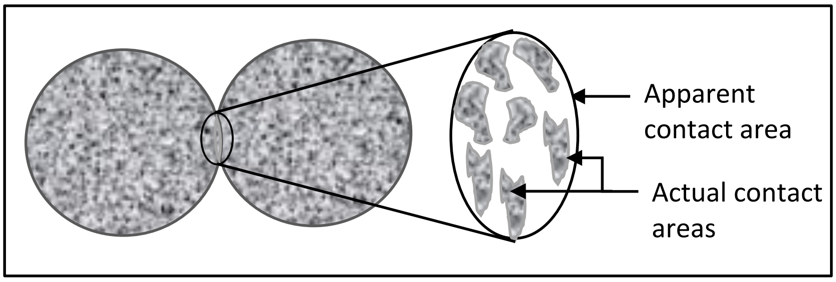

Figure 4.3 Physical contact between two particles showing apparent contact area and actual contact area

Holm's stationary electrical contact theory is widely used to calculate constriction resistances (Holm 1967; Li et al. 1995; Lu et al. 1999; Su et al. 2004; Dou 2007):

$$R_{csr} = \frac{\rho_{m1} + \rho_{m2}}{4r_c} \qquad 4.4$$

where ρ_{m1} and ρ_{m2} are the electrical resistivities of the two contacting surfaces (Ωm); and r_c, is the contact radius (m).

If the contacting surfaces are of the same material then $\rho_{m1}=\rho_{m2}=\rho_m$ and the constriction resistance can be re written as:

$$R_{csr} = \frac{\rho_m}{2r_c} \qquad 4.5$$

where the contact radius, r_c, of contact between two spheres has been estimated using Hertz's equations. The Hertz's equations calculates the contact radius between the two bodies/spheres by assuming them to be semi-infinite half-spaces and that deformations are small (i.e. behaviour is linear elastic) and have been successfully used to model the contact of small and elastic deformations in electronic interconnections (Holm 1967; Johnson 1987; Chin et al. 2004). Liu et al. (1998) have shown that for two contacting spheres with small and elastic deformations up to 10% of the sphere diameter, the Hertz's equations are valid. In the case of ICAs, where the compressive force on the neighboring particles is applied by the shrinkage of the polymeric matrix because of the curing process and thermal contraction during cooling from curing temperature, the particle deformation can safely be assumed to be less than 10% of the diameter, thus

Hertz's equations have been used here to estimate the particle-to-particle contact radius. For two, nominally spherical bodies in contact the Hertz's equations give the contact radius as a function of the normal contact force, the radii of curvature of both bodies and their elastic properties. If two homogenous spheres of radii *r* (Ø/2) can be assumed to be semi-infinite half-spaces with $r_c << r$ and with small and linear elastic deformations then the Hertzian relationship for the contact radius is (Johnson 1987):

$$\boldsymbol{r_c^3 = \frac{3FR_{eff}}{4E^*}} \qquad \mathbf{4.6}$$

where, *F* is the normal force applied between the contacting spherical particles (N);

E^* is the effective elastic modulus of the contacting spherical particles (Pa); and

R_{eff} is the effective radius of the contacting spherical particles (m).

E^* and R_{eff} are further defined as:

$$\boldsymbol{R_{eff} = \frac{r}{2}} \qquad \mathbf{4.7}$$

$$\boldsymbol{\frac{1}{E^*} = \frac{2(1-v_s^2)}{E_s}} \qquad \mathbf{4.8}$$

where, E_s is the elastic modulus of the contacting spherical particles (Pa); and

v_s is their Poisson's ratio.

In the case of ICAs, the normal force is induced due to shrinkage of the polymer matrix. Polymer matrices with higher shrinkage will therefore induce a larger normal force, which will increase the contact radius. Therefore, a polymer matrix with higher shrinkage will offer less constriction resistance and could therefore be expected to be preferred for the formulation of ICAs. An experimental study of the effect of volume shrinkage on conductivity is presented in Chapter 6.

A large contact area is desirable as it offers lower constriction resistance. It can be seen from equations 4.6, 4.7 and 4.8 that a larger contact area between particles can be achieved by selecting particles with (i) large diameter, (ii) smaller elastic modulus, and

(iii) smaller Poisson's ratio. In the case of solid metallic particles/flakes, the elastic properties (such as elastic modulus and Poisson’s ratio) are the same for all sizes of filler particle, but in the case of the silver coated polymer spheres their elastic properties may vary due to changes in the properties of the core material, size of sphere and coating thickness. He et al. (2009 a) investigated the effect of core material on the mechanical properties of polymer spheres and found that the Elastic modulus increases with increasing the crosslink density. Thus polymer spheres with a lightly cross-linked polymer core may be preferred over a highly cross-linked polymer. In another study He et al. (2008) found that, for the same polymer core, spheres with a smaller diameter were stiffer than larger spheres. Thus a larger diameter MPS may offer a lower modulus and therefore may be preferable to smaller ones. Another study conducted by He et al. (2009 b) showed that coating thickness, when it was less than 3% of the polymer core radius, had only a small effect on the mechanical properties of nickel-coated polymer spheres. In the case of silver coated polymer spheres, the effect of the coating thickness may be even lesser than for nickel as silver has a much lower modulus (83 GPa) than nickel (200 GPa). However, further investigation is required to determine the effect of silver coating thickness on the elastic modulus and Poisson’s ratio of Ag-MPS.

4.1.2.2 Tunneling Resistance

When the conducting particles are in close proximity but are not in direct metal to metal contact with neighbouring particles because of the presence of a very thin insulating film between the particles, conduction may take place by electrons penetrating this thin film, which is called tunnelling (Simmons 1963; Hill 1967). These films may be oxides or surfactants present on the particle surface, additives within the adhesive matrix for rheology control, adhesive matrix not squeezed out during curing or air trapped in between the particles. The resistance of these films can be described as a tunnelling resistance, R_t, which for very thin insulating films, i.e. less than approximately 1.5 nm, can be written as (Johnson 1987):

$$\boldsymbol{R_t = \rho_t/\pi r_c{}^2} \qquad \mathbf{4.9}$$

where ρ_t is the resistance per unit area although referred to as tunneling resistivity and is given by :

$$\boldsymbol{\rho_t = 5 \times 10^{-23} A^2 exp[AB/(1 + AB)]} \qquad \mathbf{4.10}$$

where

$$\boldsymbol{A = 7.32 \times 10^{5}(t_i - 7.2/\Phi)} \qquad \mathbf{4.11}$$

$$\boldsymbol{B = 1.265 \times 10^{-6}(\Phi - 10/t_i\varepsilon)^{-1/2}} \qquad \mathbf{4.12}$$

Φ = work function of the metal (eV);

t_i = thickness of the insulating film (m); and

ε = dielectric constant of the insulating film.

Equations 4.9 to 4.12 show that the tunnel resistivity depends on the thickness, dielectric constant, $\boldsymbol{\varepsilon}$, and work function, Φ, (a measure of minimum energy needed to remove a conduction electron) of the insulating film. The silver flakes used in ICAs are usually coated with surfactants to reduce the tendency for clustering/agglomeration, however the Ag-MPS used in this study are not coated with any surfactants thus any thin insulating films could be adhesive additives e.g. organic solvents, hardeners, metal catalysts or SiO2 for rheology control, epoxy matrix not squeezed out during adhesive cure, or air trapped in between particles.

For a given material, the parameters $\boldsymbol{\varepsilon}$ and Φ don’t change, while the film thickness t_i becomes smaller when the contact pressure is increased. In the case of ICAs the contact pressure is exerted by shrinkage of the adhesive matrix during curing thus an adhesive matrix with high shrinkage will again be preferred. The curing profile also affects the shrinkage of the ICA (Lu et al. 2000; Su 2006).

4.1.3 Conductivity within a Single Particle

In conventional silver flake filled ICAs, the conductivity of the flakes can be considered to be equivalent to the bulk conductivity of silver (Li et al. 1995; Li et al. 1997; Lu et al. 1999). However, in the case of ICAs formulated with silver coated polymer spheres fillers, the filler conductivity is less than that of bulk silver. This is because the silver coating only accounts for a small proportion of the volume of the filler particles compared to the highly insulating polymer core. Therefore, the thickness and morphology of the silver coating is expected to have a significant influence on the filler particle conductivity. Metal coated polymer spheres (especially Nickel (Ni) and Gold

(Au) coated) are already widely used in ACA applications (Dou et al. 2004). However, both heat and pressure are simultaneously applied to ensure the formation of electrical connections in ACAs which significantly deforms the MPS. The deformation of MPS in ACA assembly is illustrated in Figure 4.4. Williams et al. (1993), Hu et al. (1997) and Shi et al. (1999) presented models to calculate the resistance of an individual solid metal particle in an ACA assembly. Unfortunately, their models are not applicable to the metal-coated polymer spheres used in the present study. Määttänen (2003) first presented an analytical model to calculate the resistance of a single metal-coated polymer sphere, R_{mps}. Määttänen calculated the resistance as a function of the degree of deformation and coating thickness by treating the MPS as a series of metal rings of thickness t_c around the polymer particle. When external pressure is applied an MPS is deformed by depth d to height h_d as shown in Figure 4.4.

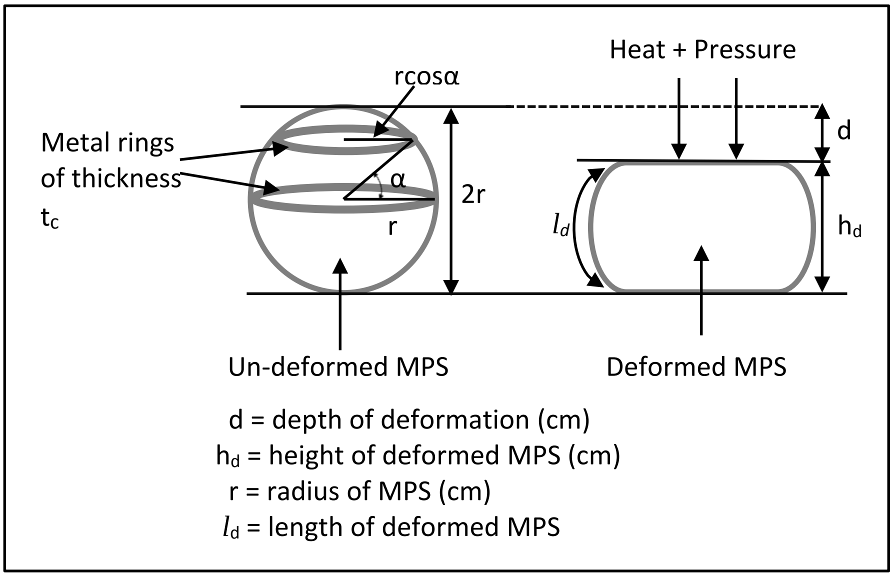

d = depth of deformation (cm)
h_d = height of deformed MPS (cm)
r = radius of MPS (cm)
l_d = length of deformed MPS

Figure 4.4 Deformation of MPS in ACA application

Määttänen calculated the average cross-sectional area, A_{vr}, of the thin metal rings around the polymer particle and the length, l_d, of the MPS as a function of deformed height h_d as:

$$\frac{1}{A_{vr}} = \frac{2}{\pi^2 h_d t_c} \ln \tan\left[\frac{\pi}{4}\left(1 + \frac{h_d}{2r}\right)\right] \tag{4.13}$$

$$l_d = \frac{\pi h_d}{2} \tag{4.14}$$

Assuming that the average cross sectional area through which the current passes is the average area of the thin metal rings around the polymer particle, he calculated the MPS resistance as:

$$\boldsymbol{R_{mps}} = \frac{(\boldsymbol{Resistivity\ of\ metal\ coating}) * (\boldsymbol{Length\ of\ deformed\ MPS})}{\boldsymbol{Average\ cross{-}sectional\ area\ of\ metal\ rings}} \qquad \textbf{4.15}$$

Combining equations 4.13 and 4.14 in equation 4.15 gives:

$$\boldsymbol{R_{mps}} = \frac{\boldsymbol{\rho_m}}{\boldsymbol{\pi . t_c}} \boldsymbol{ln\, tan}\left[\frac{\boldsymbol{\pi}}{\mathbf{4}}\left(\mathbf{1} + \frac{\boldsymbol{h_d}}{\mathbf{2}\boldsymbol{r}}\right)\right] \qquad \textbf{4.16}$$

where ρ_m is the resistivity of metal coating.

By also assuming that the MPS metallisation is made up of metal rings of thickness t_c around the polymer particle Dou et al. (2003) derived another model to calculate the MPS resistance. They also obtained the particle resistance function based on the degree of deformation and coating thickness. However, their particle resistance function was more difficult to integrate, and required numerical solution.

However, in the case of ICAs, the degree of deformation would be negligible as compared to ACAs. This is because no external pressure is applied and deformation is due to any adhesive shrinkage upon curing. In this study resistance model of a single MPS for ICA applications is developed in terms of on contact radius instead of the degree of deformation of the sphere and is presented in the next section.

4.1.3.1 Conductivity Model of a Single Metalised Polymer Sphere

In this model the MPS is considered as a spherical shell of radius r and coating thickness t_c , made up of annular rings of radius $r\sin\theta$ and length $rd\theta$, as shown in Figure 4.5. The following assumptions are made in this model;

(i) The metal coating is smooth and homogenous; and

(ii) Current flows uniformly in the metal coating parallel to the surface from one pole to the other.

The resistance of each annular ring can be calculated using Ohm’s law and then integrated to calculate the resistance of whole MPS. The resistance contribution, *dR,* of a ring is given by:

$$\boldsymbol{dR = \frac{\rho_m . r d\theta}{2\pi . r sin\theta . t_c}} \qquad \mathbf{4.17}$$

where ρ_m is the metal coating resistivity (Ωm); and $2\pi r sin\theta t_c$ is the cross-sectional area of this annular ring (m^2).

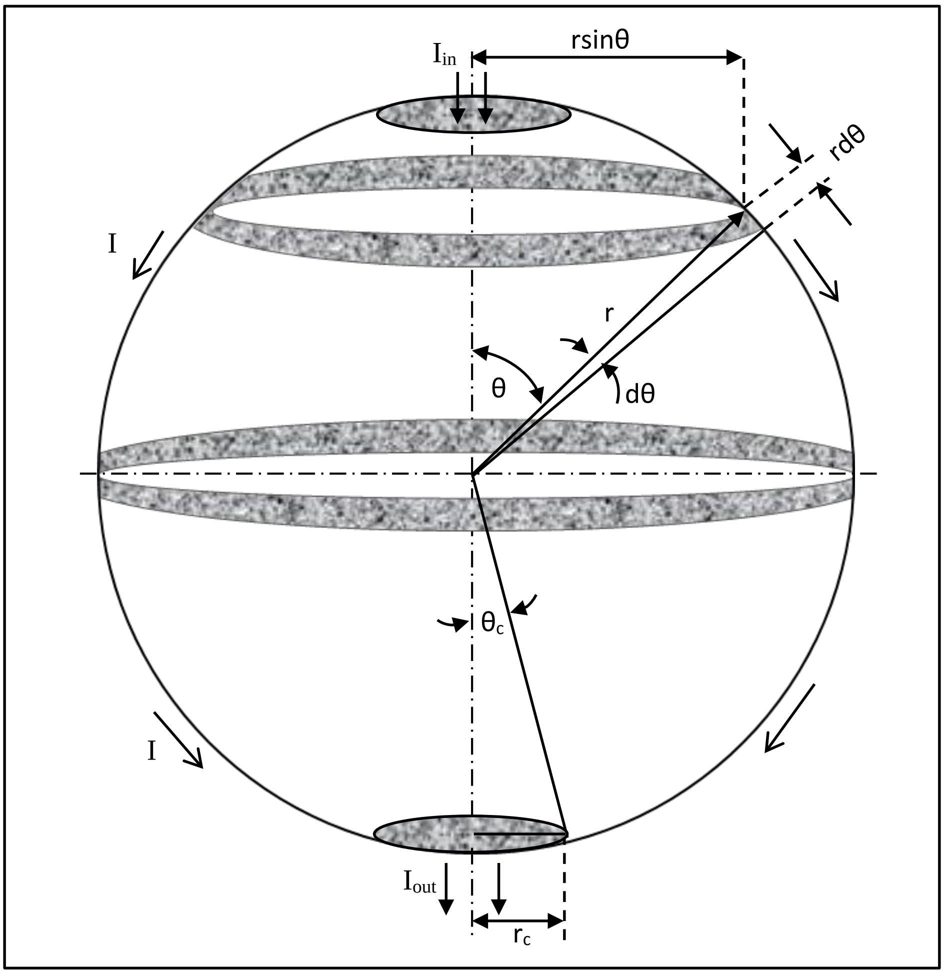

Figure 4.5 Metal coated polymer sphere shown as made up of small annular rings (for clarity only two rings are shown)

As the geometry is symmetrical the resistance of a half spherical shell is calculated, which is then multiplied by two to calculate the total resistance. The resistance R_{hs} of the half spherical shell can be obtained by integrating Equation 4.17 between θ values of 0 and π/2.

$$\boldsymbol{R_{hs} = \int_{\theta=0}^{\theta=\pi/2} \frac{\rho_m . r d\theta}{2\pi . r sin\theta . t_c} = \frac{\rho_m}{2\pi . t_c} \int_{\theta=0}^{\theta=\pi/2} \frac{d\theta}{sin\theta}} \qquad \mathbf{4.18}$$

In general:

$$\int_{\theta_1}^{\theta_2}\frac{d\theta}{\sin\theta}=\left\{\ln\left[\tan\frac{\theta_2}{2}\right]-\ln\left[\tan\frac{\theta_1}{2}\right]\right\} \qquad 4.19$$

Therefore equation 4.18 can be restated as:

$$R_{hs}=\frac{\rho_m}{2\pi.t_c}\left\{\ln\left[\tan\frac{\theta_2}{2}\right]-\ln\left[\tan\frac{\theta_1}{2}\right]\right\}_{\theta_1=0}^{\theta_2=\pi/2} \qquad 4.20$$

$$R_{hs}=\frac{\rho_m}{2\pi.t_c}\left\{\ln\left[\tan\frac{\pi}{4}\right]-\ln[\tan 0]\right\} \qquad 4.21$$

$$R_{hs}=\frac{\rho_m}{2\pi.t_c}\{\ln[1]-\ln[0]\}=\infty \qquad 4.22$$

It can be seen from equations 4.18 and 4.22 that at the poles i.e. when θ = 0, the area of annular rings becomes zero and the resistance of the half spherical shells become infinite. This is because the model effectively assumes that the particle contact area is an infinitesimal. In reality the current will not flow through a point but through an area of contact between two particles. Assuming a small contact area between adjacent particles, a small value of θ_1 is taken instead of zero, where this angle of contact $\theta_c = \sin^{-1}(r_c/r)$ and r_c is the contact radius as shown in Figure 4.5. The resistance R_{hs} of the half spherical shell can now be calculated by integrating equation 4.18 from $\theta_1 = \theta_c$ to $\theta_2 = \pi/2$:

$$R_{hs}=\frac{\rho_m}{2\pi.t_c}\left\{\ln\left[\tan\frac{\theta_2}{2}\right]-\ln\left[\tan\frac{\theta_1}{2}\right]\right\}_{\theta_1=\theta_c}^{\theta_2=\pi/2} \qquad 4.23$$

$$R_{hs}=\frac{\rho_m}{2\pi.t_c}\left\{\ln\left[\tan\frac{\pi}{4}\right]-\ln\left[\tan\frac{\theta_c}{2}\right]\right\} \qquad 4.24$$

i.e.:

$$R_{hs}=\frac{\rho_m}{2\pi.t_c}\left\{\ln(1)-\ln\left[\tan\frac{\sin^{-1}(r_c/r)}{2}\right]\right\} \qquad 4.25$$

which as *ln* (1)= 0 reduces to:

$$R_{hs}=\frac{\rho_m}{2\pi.t_c}\left\{-\ln\left[\tan\frac{\sin^{-1}(r_c/r)}{2}\right]\right\} \qquad 4.26$$

For small angle, sinθ ≈ θ so equation 4.26 reduces to:

$$\boldsymbol{R_{hs}} = \frac{\boldsymbol{\rho_m}}{\boldsymbol{2\pi.t_c}} \left\{-\boldsymbol{ln}\left[\boldsymbol{tan}\frac{\boldsymbol{r_c}}{\text{Ø}}\right]\right\} \qquad \mathbf{4.27}$$

And as the resistance of the whole MPS, R_{mps}, is twice the resistance of a half spherical shell:

$$\boldsymbol{R_{mps}} = \frac{\boldsymbol{\rho_m}}{\boldsymbol{\pi.t_c}} \left\{-\boldsymbol{ln}\left[\boldsymbol{tan}\frac{\boldsymbol{r_c}}{\text{Ø}}\right]\right\} \qquad \mathbf{4.28}$$

Equation 4.28 shows that the resistance of a metal coated polymer sphere depends on the (i) metal coating resistivity, (ii) metal coating thickness, (iii) contact radius, and (iv) MPS diameter (Ø). Figure 4.6 plots the variation of R_{mps} for different metallic coatings, MPS Ø and coating thickness, as a function of contact radius. Figure 4.6 (a) plots the variation of resistance of a 4.8µm MPS when coated with 120nm of the noble metals silver and gold. Figure 4.6 (a) shows that the silver coated MPS has lower resistance as compared to one gold coated, however gold has other advantages such as it does not oxidise and its ions are less susceptible to migration. Figure 4.6 (b) plots the variation of the MPS resistance with diameter and coated with 100nm of Ag. It shows that as the MPS diameter increase its resistance increase. Figure 4.6 (c) plots the variation in resistance of a 4.8µm MPS coated with Ag of different thickness. It shows that as the thickness of the Ag increases the resistance decreases. All of the plots in Figure 4.6 show that resistance decreases with increasing contact radius. It can be further observed from Equation 4.5 that contact radius depends upon the stiffness of the polymer core and the normal force between adjacent MPS (due to shrinkage). Thus a MPS with a soft core are preferred. Therefore, experiments were carried out to investigate the effect of coating material, MPS Ø, coating thickness, contact radius, polymer core material and applied normal force on MPS conductivity. The details of these experiments are presented in Chapter 5.

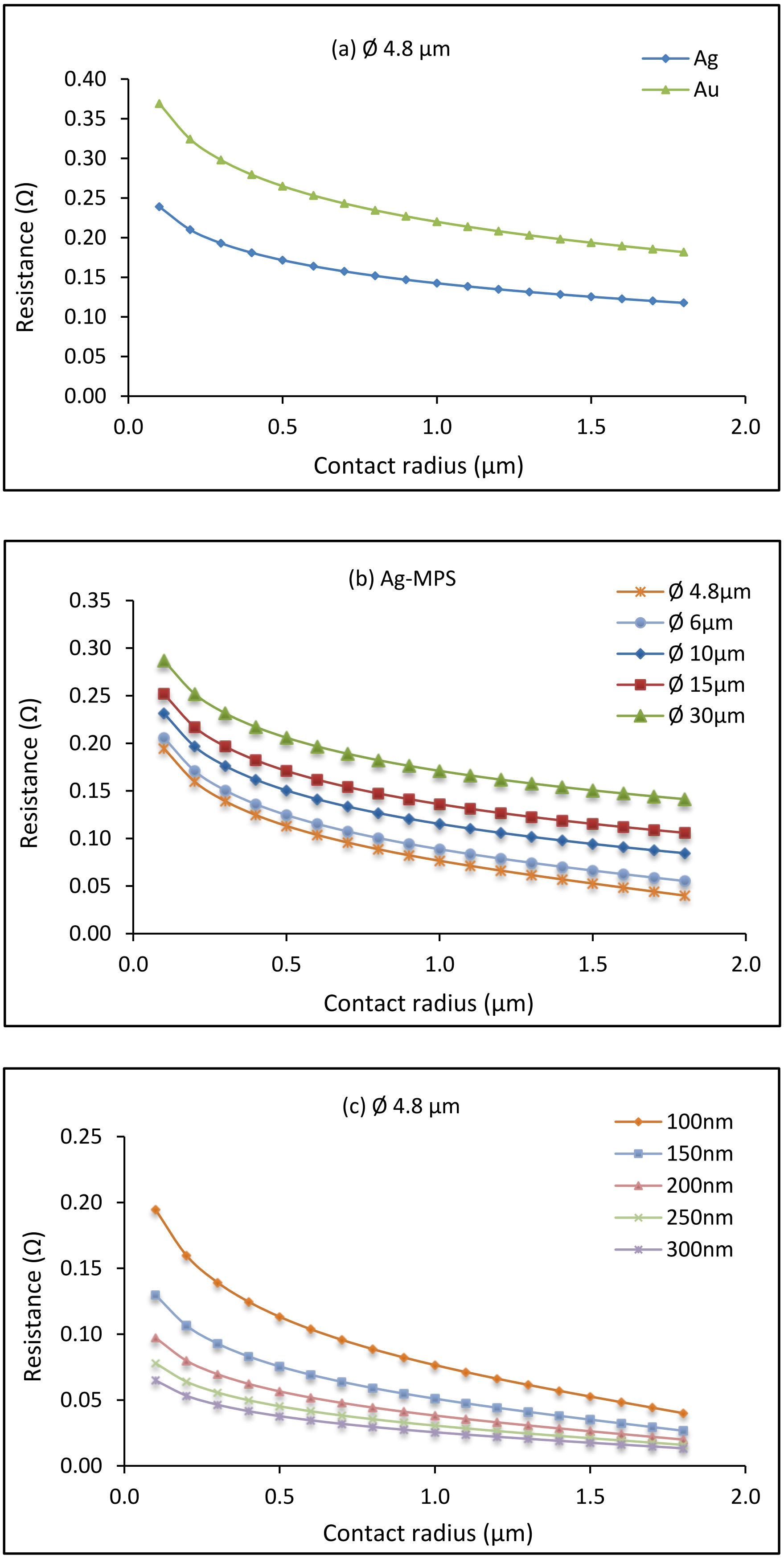

Figure 4.6 Variation of R_{mps} with (a) different metallic coatings, (b) MPS diameter (Ø) and (c) coating thickness

4.2 Conductivity Model for an ICA formulated with Metalised Polymer Spheres

The main aim of this research has been to investigate and optimise the parameters which effect the conductivity of ICAs formulated with Ag-MPS. Therefore, it is important to develop an ICA conductivity model. As discussed in Section 4.1, the conductivity of an ICA depends upon the volume fraction of filler, particle-to-particle conductivity and conductivity within a single particle. Conductivity models based on both a random distribution and regular distributions are discussed below. ICAs contain random arrangements of particles as it is not possible to achieve a volume fraction where regular arrangements (hexagonal or simple) of filler particles occur but models of random arrangements requires long calculation times due to solving complex iterative equations. Although, models based on a regular distribution of filler particles cannot be used to accurately predict the resistivity of a real ICA sample, such models will provide a lower bound on the resistivity and will help to establish optimum combination of values for design parameters such as MPS volume fractions, diameter and metal coating thickness.

Resistivity models based on random packing have been investigated and developed to predict the resistivity of a block of ICA (Li et al. 1995; 1997; Su et al. 2004). Li et al. (1995) first made a model in two dimensions which was later extended (1997) to three dimensions while Su et al. made a model only in three dimensions. A brief description of these models is presented below:

The models of both Li et al. and Su et al. are simulations based on algorithms to generate random sites to place filler particles within a space between two electrodes, such that the particles must not impinge upon the space occupied by another particle or of the electrodes. After the placement of particles, the algorithm identifies whether there are any conductive pathways between the two electrodes. For each identified conductive pathway, the algorithm gives a common pathway identification number and counts the number of particles in that pathway. If any two sites at the opposite ends of the electrodes have the same identification number, the sample is determined to percolate in the direction perpendicular to the electrodes. The particle at each site in the pathway is considered as a resistor together with associated contact resistances. The overall resistivity of the ICA block is then calculated by the program which solves

Kirchoff’s current equation at each site, by iteration and finite difference methods. These models has some limitations associated with them including:

(i) As the models are simulation based, generation of random sites and solving complex iterative equations associated with random packaging takes a long time and hence resistivity calculations also take a long time;

(ii) Investigating the effect of different parameters such as filler size, and volume fraction on the resistivity of an ICA requires multiple independent simulations to be run; and

(iii) These models do not directly lead to an equation that can quantify the effects of the various parameters which determine the resistance of an ICA. In both Li and Su’s models, numerical value of the resistivity of the filler and pre-calculated contact resistance values are used to calculate the resistance of an ICA and they do not quantify the effect of various parameters on which the resistance of the filler and contact resistance depends.

The resistance of an MPS is high compared to that of the bulk metal and depends upon various parameters as discussed in section 4.1.3.1. Further, as discussed in section 4.1.2, the contact resistance also depends upon various parameters. To establish the effect of various parameters that can affect the resistance of an ICA, an analytical model represented by an equation is needed.

Conduction through regular arrangements of filler particles, such as hexagonal and simple cubic packaging, can be readily represented by equations allowing quantification the effects of many of the parameters affecting the resistance of MPS based ICAs. These models can also overcome the above identified problem of long calculation times due to the complex iterative process associated with simulating random packaging.

As discussed in Section 4.1.1, hexagonal packing occurs at volume fractions so high that processing of an ICA would be impossible. Therefore, an analytical model based on the simple cubic arrangement is more suited to explaining conduction within ICAs and is presented below.

In a simple cubic model layers of particles are stacked parallel to each other as shown in Figure 4.7. A conductive path is formed when a continuous chain of contact between particles is established between the two electrodes. Each conductive pathway comprises of a series of resistances formed due to the combination of particle-to-particle resistance and resistance offered by the particle itself. Every particle is different from each other and, similarly so are the contact resistances between adjacent particles. Furthermore, each particle in a simple cubic packing arrangement is connected to six other particles. This variability could lead to a conductive path that is very complex to accurately evaluate. Hence, the following assumptions have been made to allow development of an ICA conduction model:

i) The volume fraction of the MPS is 52%;

ii) Each particle has the same resistance value, R_{mps} ;

iii) Particle-to-particle contact resistances are the same for all particles, R_{cr};

iv) Each particle therefore contributes equally to conduction and there are no dead ends;

v) Each particle only has two points involved in forming the conducting paths. These two points are considered to be at the opposite ends of particle; and

vi) The conductive pathways are straight chains as shown in Figure 4.7, rather than meandering randomly through the ICA volume.

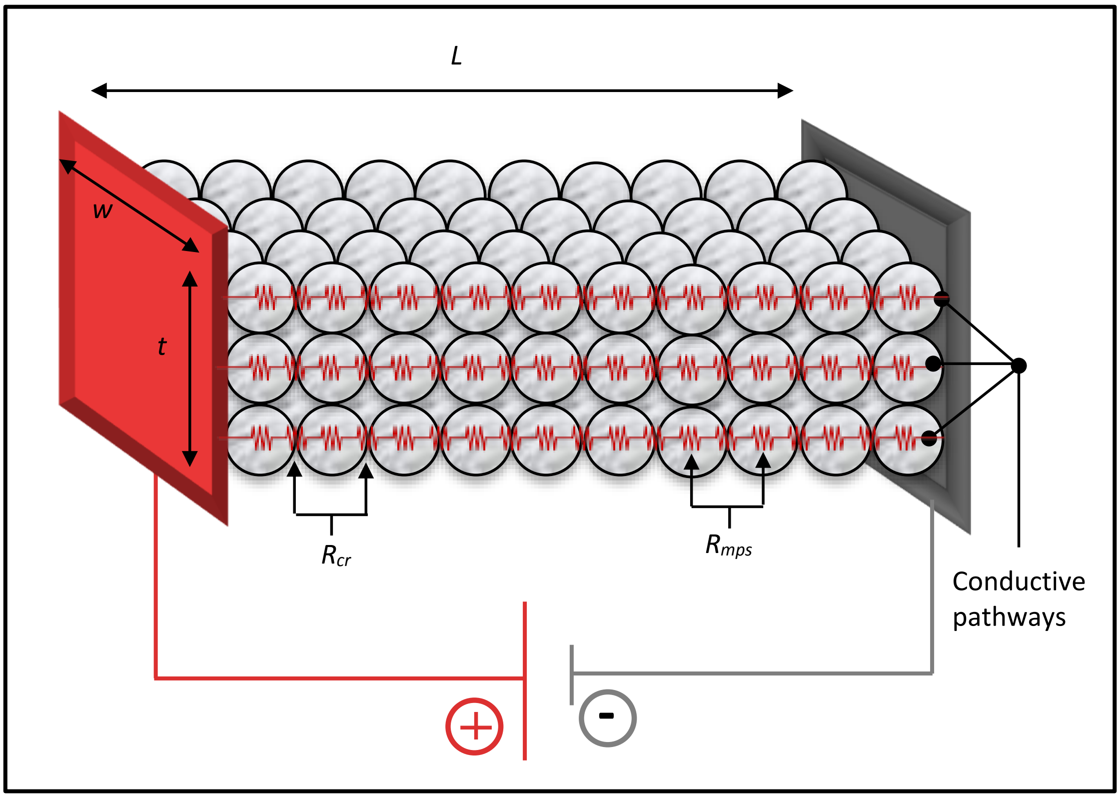

Figure 4.7 Simple cubic arrangement of filler in an ICA illustrating conductive paths (for simplicity only the paths on the front face of the ICA are shown)

Utilising these assumptions the total resistance of a volume of ICA can be given as a function of both particle resistance and particle-to-particle contact resistance, i.e. for an ICA stripe of length *L*, width *w* and thickness *t*, the total resistance can be given as;

$$R_{ICA} = \frac{R_{mps}n_L + R_{cr}(n_L - 1)}{n_w n_t} \tag{4.29}$$

where $n_L = \frac{L}{2r}$, number of MPS along the length *L*;

$n_w = \frac{w}{2r}$, number of MPS across the width w;

$n_t = \frac{t}{2r}$, number of MPS through the thickness t; and

r = MPS radius (m).

If the number of MPS along the length of the ICA volume is very large, then

$$\boldsymbol{n_L - 1 \cong n_L} \qquad \mathbf{4.30}$$

Substituting this value of n_L-1 in Equation 4.29, we get

$$\boldsymbol{R_{ICA} = \frac{(R_{mps}+R_{cr})n_L}{n_w n_t}} \qquad \mathbf{4.31}$$

Further, the ICA resistivity can be estimated by combining Equation 4.31 with Equations 4.28, 4.5 and 4.9, as:

$$\boldsymbol{R_{ICA} = \frac{\left(\frac{\rho_m}{\pi.t_c}\left\{-ln\left[tan\frac{r_c}{\emptyset}\right]\right\}+\frac{\rho_m}{2r_c}+\frac{\rho_t}{\pi r_c^2}\right)n_L}{n_w n_t}} \qquad \mathbf{4.32}$$

Which on further simplifying is:

$$\boldsymbol{R_{ICA} = \frac{\left(\frac{\rho_m}{\pi.t_c}\left\{-ln\left[tan\frac{r_c}{\emptyset}\right]\right\}+\frac{\rho_m}{2r_c}+\frac{\rho_t}{\pi r_c^2}\right)\emptyset.L}{w.t}} \qquad \mathbf{4.33}$$

And the resistivity is therefore :

$$\boldsymbol{\rho_{ICA} = \left(\frac{\rho_m}{\pi.t_c}\left\{-ln\left[tan\frac{r_c}{\emptyset}\right]\right\}+\frac{\rho_m}{2r_c}+\frac{\rho_t}{\pi r_c^2}\right)\emptyset} \qquad \mathbf{4.34}$$

Equation 4.34 shows that the resistivity of an ICA filled with Ag-MPS is directly proportional to:

(i) ***Metal coating resistivity, ρ_m.:*** In the case of an MPS, the resistivity of the metal coating can be assumed to be at least the bulk resistivity of the metal. Thus, MPS coated with a metal with lower resistivity will typically yield an ICA with lower resistance. Further, for a given metal, the resistivity of the thin metal coating will depend upon the thickness and quality of the coating. The resistivity of metal coatings on a flat substrate can usually be measured experimentally (Cui et al. 2012), however it is very difficult to measure the resistivity of the metal coating on a microsphere;

(ii) ***Tunnel resistivity, ρ_t,:*** As discussed in section 4.1.2.2 tunnel resistivity depends on the thickness, dielectric constant and work function of the insulating film. The dielectric constant and work function of the insulating film may depend on the insulating film material, however the film thickness depends upon contact pressure and becomes smaller when the contact pressure is increased. In the case of ICAs the contact pressure is exerted by shrinkage of the adhesive matrix; and

(iii) ***MPS Diameter:*** MPS with smaller diameter but for same t_c and r_c will yield an ICA with a lower resistance, but at the cost of more metal due to the greater total MPS surface area.

Equation 4.34 shows that the resistivity of an ICA filled with Ag-MPS is inversely proportional to:

(i) ***Thickness of the metal coating, t_c:*** ICAs filled with MPS having a thick silver coating will have less resistance as compared to those with a thinner coating; and

(ii) ***Contact radius, r_c, between adjacent Ag-MPS***; The contact radius between two adjacent MPS will depend upon the (i) MPS diameter, and (ii) normal force applied due to the shrinkage of the epoxy during curing.

The effect of metal coating thickness and quality, MPS diameter, and the curing profile and resulting shrinkage on the conductivity of an ICA is experimentally investigated in Chapter 6.

4.3 Concluding Remarks

In this chapter the factors effecting the conductivity of an ICA made using silver coated polymer spheres have been discussed. These factors include, the volume fraction of filler particles, the particle-to-particle contact resistance and the individual particle resistance. The model has been developed to calculate both the resistance of a single particle and resistance of an ICA. These models show that particle size, its contact radius, coating thickness, stiffness of polymer core and the normal force exerted due to shrinkage of polymer matrix during curing are expected to affect the particle-to-particle contact resistance and single particle resistance and hence the overall resistance of an ICA made using MPS.

To investigate the effect of these parameters on the electrical resistance of a single particle and on the resistance of an ICA formulated with Ag-MPS experimental studies have been carried out and are presented in Chapters 5 and 6.

CHAPTER 5

EXPERIMENTAL INVESTIGATION OF THE CONDUCTIVITY OF INDIVIDUAL SILVER METALISED POLYMER SPHERES

The theoretical model for the average resistance of a MPS network within an ICA that was presented in Chapter 4 showed that the resistance of two MPS in contact depends upon the resistivity of the metal coating, the thickness of the metal coating, the MPS diameter and the radius of contact between them. This chapter presents experiments conducted using a nano-indentation based flat punch method to experimentally investigate the effect of these parameters on MPS resistance for comparison with the theoretical model.

5.1 Testing of MPS Properties

The mechanical and electrical properties of metal-coated plastic spheres used in an ACA assembly have been studied by a number of researchers. Kristiansen et al. (2001) compressed a large number of MPS (typically in the order of 1000) between two flat silicon chips and investigated the effect of temperature on their mechanical properties. Later, Zhang et al. (2007) used the method introduced by Kristiansen et al. to investigate the elastic properties such as compression modulus and the Poisson's ratio of the MPS up to 20% deformations. In both these studies the electrical properties of the MPS were not investigated. Moreover, for investigating mechanical properties a large number of MPS (such as in an ACA assembly) were simultaneously compressed. Any size variation between the MPS can therefore affect the characterisation of MPS properties. In order to accurately characterise the properties of single MPS, compression of an individual MPS needs to be investigated.

Wang et al. (1998) characterised the mechanical properties of MPS by probing individual MPS in a cross-sectioned ACA assembly using nano-indentation technique. Nano-indention is mainly used for characterising the mechanical properties of materials at the micro and nano-scale, where a pointed tip indenter penetrates the flat material surface while the contact load and displacement are simultaneously measured using highly sensitive transducers (Vanlandingham 2003; Schuh 2006). The standard pointed nanoindentation tip is however, not suitable for testing the free standing MPS therefore Dou et al. (2006), Kwon et al. (2006) and He et al. (2007) and (2008) and Helland (2008) replaced the conventional pointed tip indenter with a flat tip indenter. Using flat tip diamond indenter Kwon et al. (2006) compressed single MPS and characterised the bonding parameters for an ACA assembly they however did not measure the electrical resistance of an individual MPS during compression. Dou et al. (2006, 2007) specially manufactured flat and conducting nano-indenter tips, and for the first time measured the electrical resistance of individual gold and nickel plated polymer spheres while applying compressive force. He et al. (2007) and (2008), and Helland (2008) used the flat punch diamond nanoindenter to investigate the hardness, compression modulus, and Poisson's ratio of individual MPS. As Dou et al. successfully measured the electrical resistance of single MPS, the methodology used by them is adapted in this research to measure the resistance of an individual Ag-MPS. Details of the experiments carried out are presented in the following sections.

5.2 Resistance Measurement Using the Nanoindentation Method

5.2.1 Aims

The main aim of this experiment is to investigate the effect of the following parameters on the electrical resistance of Ag-MPS:

i) MPS diameter;

ii) Silver coating thickness and quality/morphology (this affects the resistivity of the coating and therefore of the MPS) ; and

iii) Deformation of the MPS (from which the contact radius between two MPS is estimated).

The results will assist in optimising the design of Ag-MPS for different ICA applications and in developing improved models for their conduction.

5.2.2 Materials Used

Ag-MPS supplied by Conpart AS, Norway, with cores having two different diameters and materials were used in this study. These spheres are coated with silver layers of different thicknesses and two different types of plating processes were used. Observations of the particles under SEM, show a narrow size distribution for each type, as shown in Figure 5.1. The flakes of silver that can be seen in Figure 5.1(f) are probably silver that did not get plated on to the MPS during electroless plating. The specifications of the Ag-MPS used are given in Table 5.1.

Table 5.1 Specifications of silver coated polymer spheres

Ø (µm)	Core material	Ag Coating Thickness[1] (µm)	Plating Process	Nomenclature Used
30	Lightly cross linked methacrylate	0.13 ± 5%	A	30_13A
30	Lightly cross linked methacrylate	0.10 ± 5%	B	30_10B
30	Lightly cross linked methacrylate	0.15 ± 5%	B	30_15B
30	Lightly cross linked methacrylate	0.20 ± 5%	B	30_20B
30	Lightly cross linked methacrylate	0.25 ± 5%	B	30_25B
4.8	Highly cross linked methacrylate	0.15 ± 5%	A	4.8_15A

---

[1] Thickness is estimated by the manufacturer from the weight of the silver used in the plating process

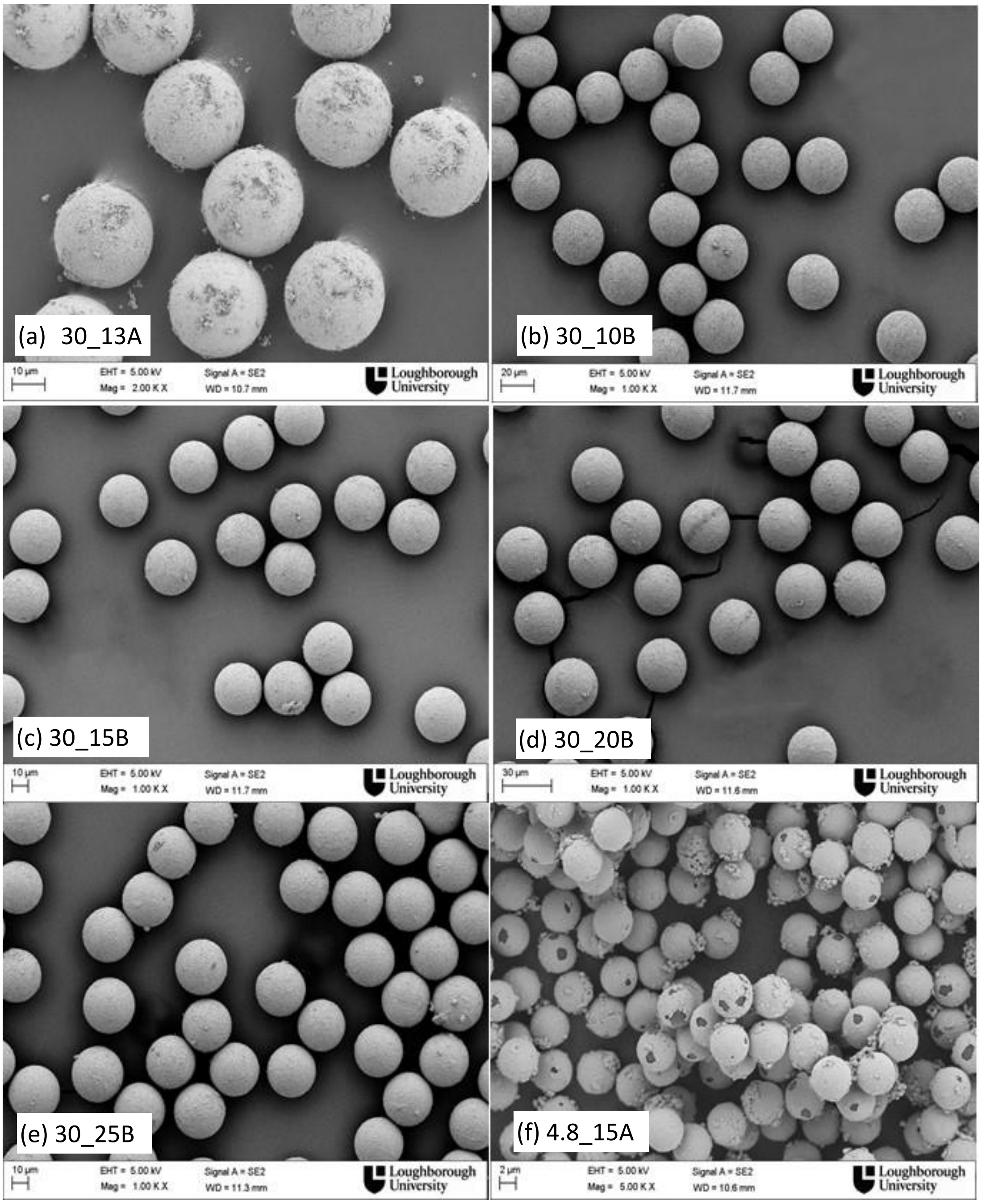

Figure 5.1 SEM images of the Ag-MPS used in the study

5.2.3 Equipment Used

5.2.3.1 *Nanoindentor*

Two Nanoindentation instruments were used in this work. A NanoTest, manufactured by Micro Materials Ltd.[2] together with a custom made flat tip indenter, as used by Dou et al. (2006, 2007), was initially used. The high resolution of 100nN of the NanoTest allowed accurate application of a very small force in the order of 100mN, and also made possible recording of the resulting deformations of less than 6μm at a resolution of 0.1nm while simultaneously measuring electrical resistance. However, the NanoTest broke down while carrying out the initial experiments and therefore another nanoindentation testing system, a TriboIndenter manufactured by the Hysitron Incorporation[3], USA was subsequently used, as shown in Figure 5.2.

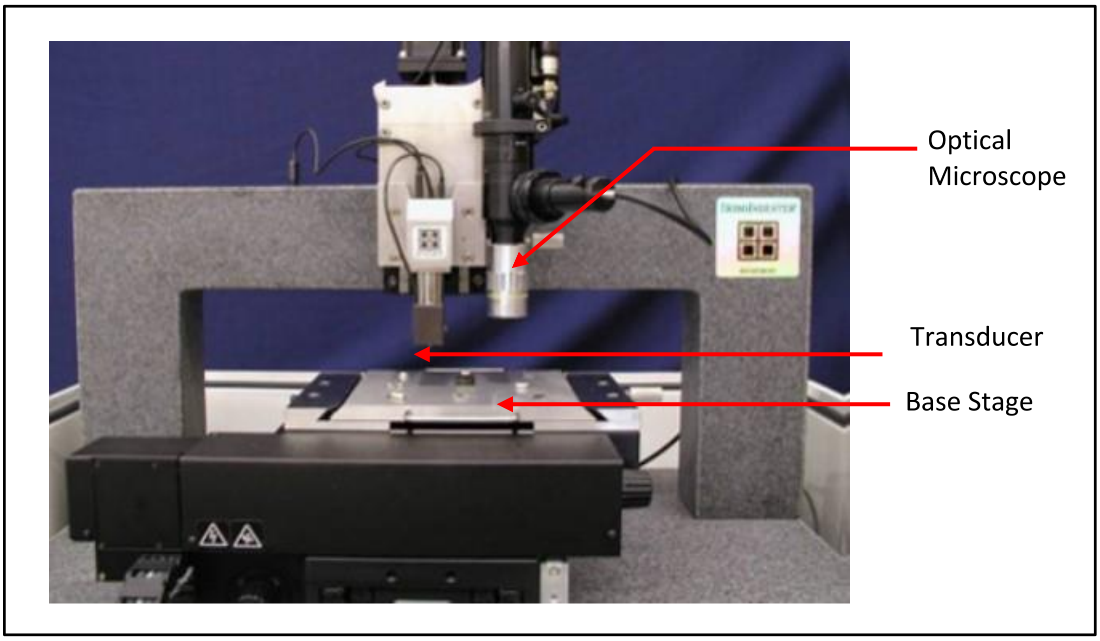

Figure 5.2 TriboIndenter® with standard stage setup

The Triboindenter uses a specially designed three-plate capacitive transducer for load and displacement measurements. The indenter tip is mounted to the central capacitor plate, which is suspended on springs and free to move in the normal direction, as shown

---

[2] http://www.micromaterials.co.uk

[3] http://www.hysitron.com

in Figure 5.3. By modulating the electrical potential applied to this centre plate with respect to the top and bottom plates an electrostatic force is created between the plates, which drives the indenter tip.

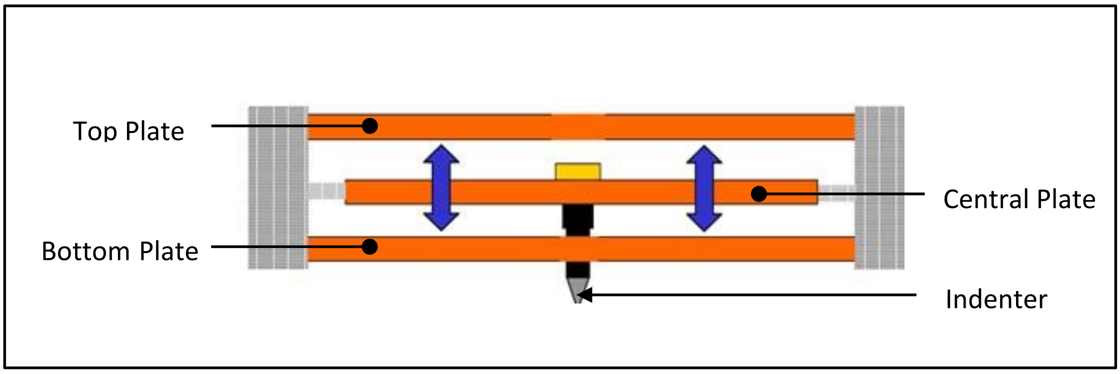

Figure 5.3 Cross-section of three-plate capacitive transducer

The force applied to the indenter tip is therefore the sum of the electrostatically applied force and the net force introduced by the deformation (displacement) of the springs. The displacement is calculated by measuring changes in the capacitances between the centre plate and the top and bottom plates. The transducer used in this study can create a maximum load of 10000μN and a maximum indentation depth of 5μm, with load and displacement resolutions of 1nN and 0.1nm, respectively. The force-deformation data were recorded using the TriboIndenter whereas resistance data was measured using a separate Keithley 2602 source meter, as there was no provision to record resistance within the TriboIndenter. The standard tips used with TriboIndenter are pointed and were therefore replaced with a specially designed flat tip, which henceforth is referred as a flat punch in the context of this thesis. A simplified schematic of the experimental setup is shown in Figure 5.4.

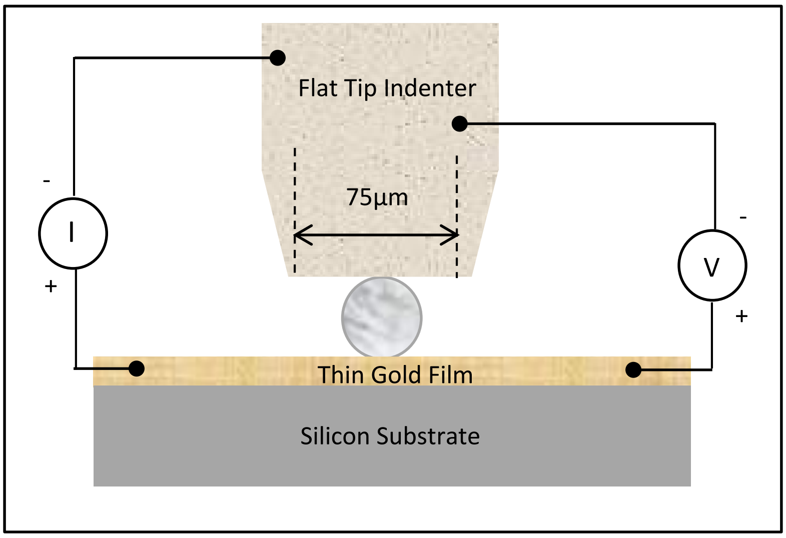

Figure 5.4 Experimental setup for the nanoindentation-based flat punch tests

5.2.3.2 *Flat Punch and Substrate*

The particles were deformed between the flat punch and a substrate mounted on the base stage of TriboIndenter as shown in Figure 5.4. The materials of the flat punch and substrate were selected such that they are significantly harder than the particles. This is to prevent any deformation of the flat punch and substrate during indentation, thus aiding accurate measurement of particle deformation. In addition to being hard, the material should also have good electrical conductivity to allow particle resistance measurement. Diamond has been used as a common material for indenter tips, because of its very high hardness. However, diamond could not be used for making the indenter tip in this study, because it is an electric insulator and is therefore not suitable for resistance measurements. As an alternative to diamond, tungsten carbide was used for making the flat punch as it is also very hard, whilst having a low resistivity of 2×10^{-6} Ωcm at 25°C. Considering the particle size and the required planarity of both flat punch head and substrate surface, the punch head tips were made circular and approximately 75µm in diameter, as shown in Figure 5.5.

Silicon wafers with a sputtered thin gold film 200 nm thick were used as the substrate. These gold coated silicon wafers were supplied by Acreo AB, Sweden. The gold film on the substrates ensured good electrical contact between the MPS and substrate and as its thickness is small compared to the diameter of the tested particles (30µm & 4.8 µm), any deformation of the gold film during particle indentation can be assumed to have a negligible effect on the results.

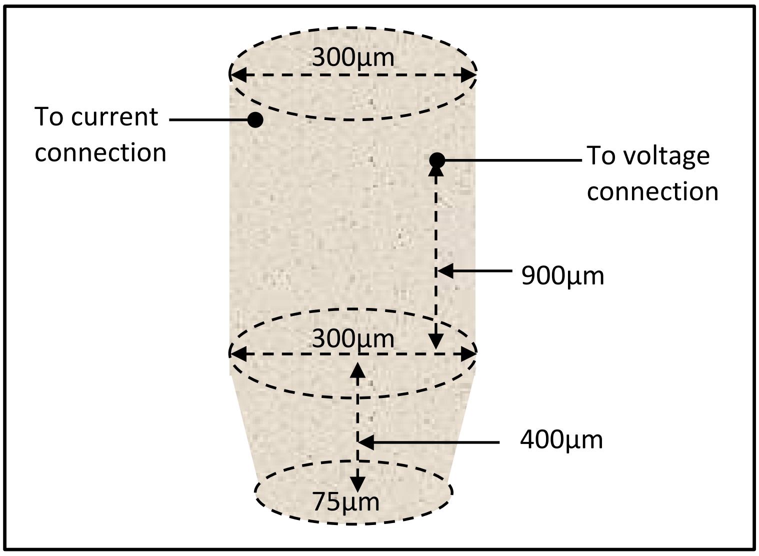

Figure 5.5 Flat punch

5.2.3.3 *Base Stage*

The base stage of the TriboIndenter has nine positions which can be used to mount samples. The centre of each sample position has a magnet mounted inside the stage to hold down the samples magnetically. Steel discs are provided to allow rapid mounting of the samples using the magnetic force. The Si substrates were glued onto the steel discs using Cyanoacrylate "instant" adhesive. The base stage has an integrated optical microscope with 10X magnification and can be used to locate a specific particle for indentation and to subsequently observe the indented particle.

5.2.3.4 *Resistance Measurement Method*

The load and deformation measurements on the Ag-MPS were recorded by the control computer within the TriboIndenter. However, it is not capable of measuring electrical resistance. Therefore a Keithley 2602 source meter was used to record the electrical resistance. The Keithley 2602 source meter has two channels and when making FWR measurements automatically compensates for thermal EMFs. Using this meter, a constant current value was applied between the flat punch and the substrate, and the resulting voltage difference was automatically recorded using Lab View software in a computer connected to the Keithley 2602 source meter through a RS-232 interface. Table 5.2 lists the range and resolution of the Keithley 2602 source meter.

Table 5.2 Resolution of the Keithley 2602 source meter for the voltage

Function	Range	Resolution
Test Current	1-10 mA	100 nA
Measured Voltage	1-10 mV	1 µV
Measured Resistance	0.1-10Ω	1 µΩ

5.2.4 Experimental Procedure

The experimental procedure can be divided into three main steps as follows: sample preparation; flat punch co-planarity check and calibration; and compression of the particle with simultaneous resistance measurement.

5.2.4.1 *Sample Preparation*

The tests require the particles to be dispersed on the substrate such that they are fixed onto the substrate, while being far enough apart that they do not interfere with the measurement of other particles. Researchers previously have tried different techniques for attaching the particles to the substrate. Dou et al. (2006,2007) induced a static charge on the substrate by rubbing it with lens cleaning paper, which helped to attach the particles onto the substrate, whereas Helland (2007) and He et al. (2007) used 96% industrial ethanol solution to disperse the particles over the substrate. However, Helland and He et al. investigated only the mechanical properties and did not investigate the electrical properties. In the present study, an open circuit was detected during the resistance measurements when the particles were dispersed using ethanol. It is believed that a thin residual layer of ethanol is the cause of the open circuit. Therefore in order to make successful electrical contact it was decided not to use any solvent to help disperse the particles and a tiny amount of dry particles was sprinkled onto the Au-coated Si substrates for the tests.

5.2.4.2 *Flat Punch Co-Planarity Check and Calibration*

A simplified schematic of the experimental set up is shown in Figure 5.4. The particles are placed on the substrate and indented between the flat punch and the silicon substrate. Planarity of the flat punch and parallelism between the punch surface and the substrate are of crucial importance to the precision of the measurement. Particularly for the smaller particles if the planarity and parallelism of the flat punch are poor, the edge of the punch might touch the substrate before compression of the particle is finished, as shown in Figure 5.6.

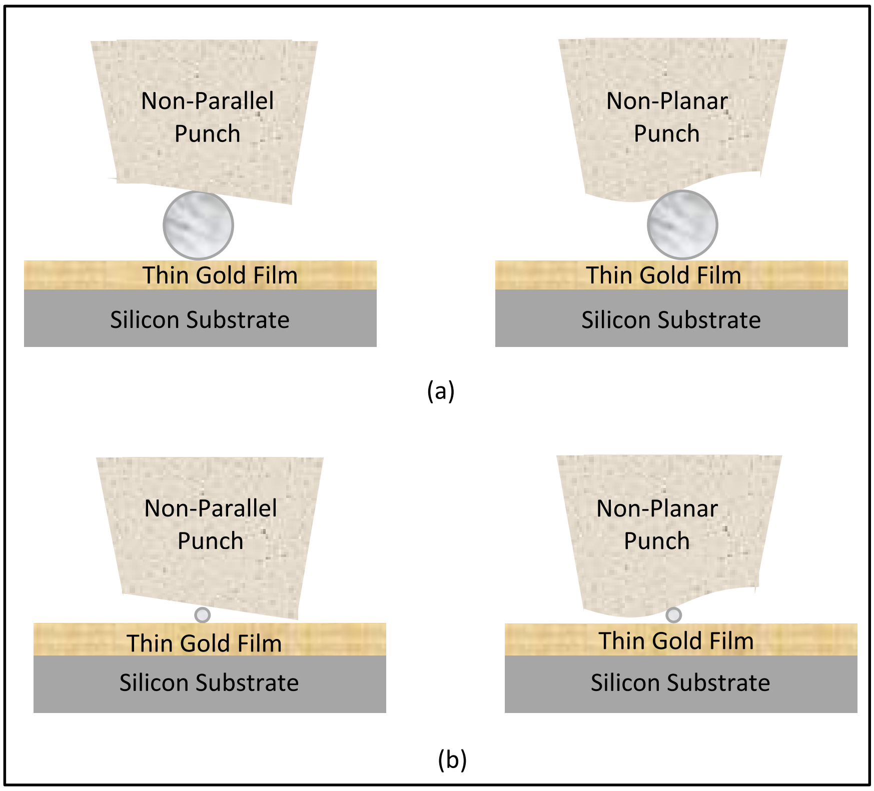

Figure 5.6 Illustration of effect of non-coplanar punches on (a) large and (b) small MPS

The primary factor influencing parallelism of the flat punch is the mechanical mounting of the tip. After carefully mounting the tip to the transducer, the parallelism of the flat punch was checked by making indents into a polished indium surface. Though the indent onto the indium surface was not exactly uniform and circular, the tip was regarded to be acceptable for the 30µm particles involved in this experiment, because the non-coplanarity of the tip was not believed sufficient to cause the effects on the measurements shown in Figure 5.6. The relative positions of the integrated optical microscope and the indenter were also calibrated using the indent on the indium. This ensures the indentation takes place at the position chosen with the optical microscope. From the mounting of the tip, the co-planarity check and the calibration to taking measurements, the TriboIndenter was operated by a highly experienced operator, Dr Jianying He.

5.2.4.3 *Compression of the Particle*

After co-planarity and calibration checks were completed, the compression of the particles was carried out using the following procedure:

i) Prior to each test, the flat punch was cleaned using cotton buds dipped in ethanol to remove external impurities. All tests were performed in air and at room temperature;

ii) Individual particles at a sufficient distance from their closest neighbour were identified using the integrated optical microscope of the TriboIndenter;

iii) Compression was performed using the load/force controlled mode of the instrument, in which the applied load/force follows a predefined profile. The loading and unloading profile used in this experiment is shown in Figure 5.7 and Table 5.3. A maximum load of 8000μN was selected due to the limit of the transducer and the fact that the MPS are not so highly deformed in an ICA as they are in an ACA;

iv) After compression the coordinates and an image of the tested particle were recorded, to make sure that the same particle was not tested twice; and

v) For each group of particles, at least four single particles were tested in order to check the repeatability of the results.

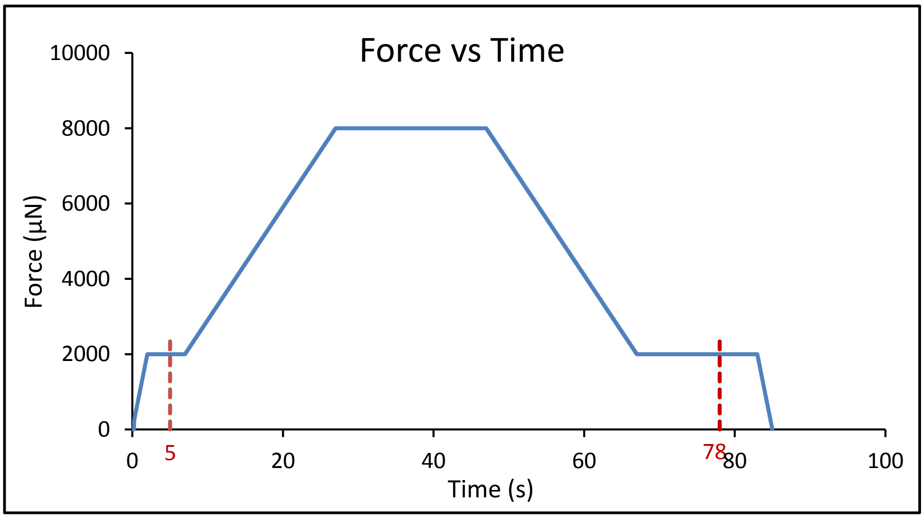

Figure 5.7 Loading and unloading profile for the compression of Ag-MPS

Table 5.3 Force and time values for loading, holding and unloading phases

		Force (µN)	Time (s)	Rate (µN/s)
Loading Profile	Loading	0 - 2000	2	1000
	Holding	2000	5	-
	Loading	2000 - 8000	20	300
Holding Profile		8000	20	-
Unloading Profile	Unloading	8000 - 2000	20	300
	Holding	2000	16	-
	Unloading	2000 - 0	2	1000

5.2.4.4 *Resistance Measurement*

During the compression of Ag-MPS, electrical resistance measurement was only conducted during a specific period, in order to prevent the tested particle from being destroyed due to sudden discharge off current when the flat punch contacts the particle if the current source was activated before contact. The resistance measurement was started after 5s when the force was being held at 2000 µN and was stopped at 78s when the force was again held at 2000 µN, as illustrated by the dotted red lines in Figure 5.7. No resistance measurements were conducted in the first loading phase i.e. between 0-2000 µN and in the last unloading phase 8000-2000µN. Therefore to reduce the experimental time, loading and unloading rates were kept higher in these two phases. For each compression, the force, deformation and resistance were recorded as functions of time. The flat punch and the Au-coated substrates were connected to the current source and voltmeter as shown in Figure 5.4. The resulting current flow and the electrical resistances involved in the measurement are shown in Figure 5.8. R_{sv} is in series with the voltmeter and thus not in the current path and could be neglected. It can be seen form Figure 5.8 that:

$$\boldsymbol{Measured\ Resistance = R_{MPS} + R_{tv} + R_{ps} + R_{pt}} \qquad 5.1$$

Therefore:

$$\boldsymbol{R_{MPS} = Measured\ Resistance - \left(R_{tv} + R_{ps} + R_{pt}\right)} \qquad 5.2$$

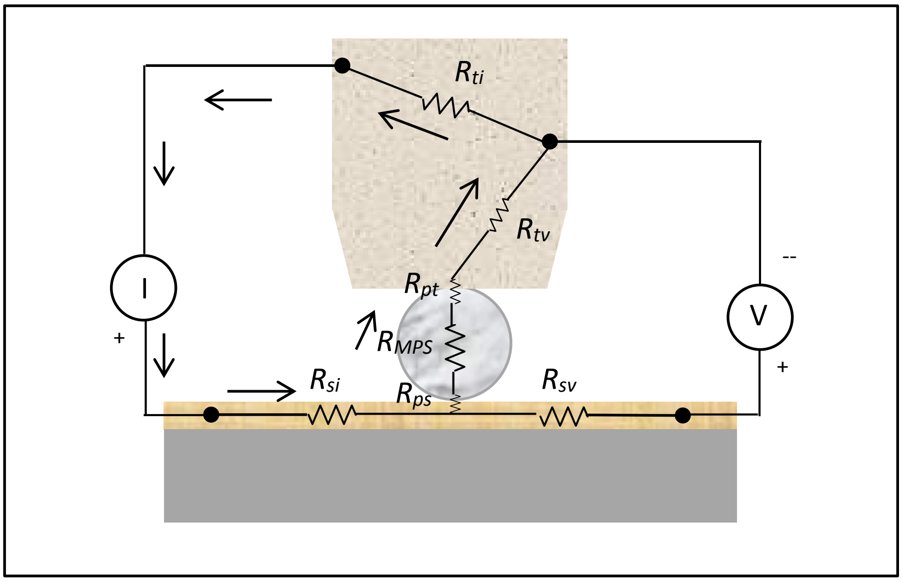

Figure 5.8 Electrical resistances included in the measurement

where R_{MPS} is the MPS resistance ;

R_{pt} is the contact resistance between particle and flat punch;

R_{ps} is the contact resistance between particle and substrate;

R_{si} is the resistance of the portion of the substrate between the current source connection on the substrate and the particle;

R_{sv} is the resistance of portion of the substrate between voltage measurement connection on the substrate and the particle;

R_{tv} is the resistance of the portion of the flat punch between the voltage measurement connection on the punch and the bottom surface of the punch; and

R_{ti} is the resistance of the portion of the flat punch between the current source and voltage measurement connections on the punch.

The portion of the flat punch imparting resistance R_{tv} can be considered to be made by joining a truncated cone and cylinder as shown in Figure 5.5. The resistance of a truncated cone made of tungsten carbide with smaller base diameter of 75µm, larger base diameter of 300µm, and height of 400µm was calculated to be 4.52mΩ. The resistance of a cylinder of tungsten carbide with diameter of 300µm and height of about

900µm was calculated to be 2.54 mΩ. Thus the total resistance R_{tv} was calculated to be 7.06 mΩ.

R_{ps} and R_{pt} were calculated using Holm (1967) and Hertz's formulae Johnson (1987) discussed in Section 4.1.2.1 as:

$$\boldsymbol{R_{ps}}(\Omega) = \frac{\boldsymbol{\rho_{Ag}} + \boldsymbol{\rho_{wc}}}{\boldsymbol{4r_c}} \tag{5.3}$$

$$\boldsymbol{R_{pt}}(\Omega) = \frac{\boldsymbol{\rho_{Ag}} + \boldsymbol{\rho_{Au}}}{\boldsymbol{4r_c}} \tag{5.4}$$

where r_c is the contact radius (m);

ρ_{Ag} is the resistivity of silver (Ωm);

ρ_{wc} is the resistivity of tungsten carbide (Ωm); and

ρ_{Au} is the resistivity of gold (Ωm);

The contact radius, r_c, can be estimated from the deformation using (Johnson 1987):

$$\boldsymbol{r_c} = \sqrt{\boldsymbol{r}\left(\frac{\boldsymbol{d}}{\boldsymbol{2}}\right)} \tag{5.5}$$

where r is the radius of the Ag-MPS (m); and

d is the depth of deformation (m).

Using the bulk resistivities of silver as 1.59 x 10^{-6} Ωcm, tungsten carbide as 2.0 x 10^{-5} Ωcm, and gold as 2.4 x 10^{-6} Ωcm (Hyperphysics 2014) and depth of deformation between 600 to 1700 nm, the sum of R_{ps} and R_{pt} is estimated to be in the range of 30.1 – 23.3 mΩ. For deformations in the range over which resistance data is available, the sum of R_{tv}, R_{ps} and R_{pt} lies therefore between 30.36 – 37.16 mΩ. This is very small in comparison to the measured resistance values of the MPS for these deformations (of the order of 0.500 - 1.1 Ω) and their contribution towards the measured resistance values can therefore be neglected.

5.3 Results and Discussion

5.3.1 Mechanical Characterisation

Deformation of all the particles under the application of force was measured and recorded by the TriboIndenter. Figure 5.9 (a), (b), (c), (d) and (e) exhibits the force-deformation curves for 30_13A, 30_10B, 30_15B, 30_20B and 30_25B respectively. For each particle type, deformation curves for three particles are shown. The plateaus in each force-deformation curve correspond to the holding segments on the loading profile, where the applied force is held at 2000µN, 8000µN and then 2000µN. Further, the average mechanical response for the five types of Ag-MPS are shown in Figure 5.10, where the average values of force and deformation for three tested particles for each batch shown in Figure 5.9 are plotted. The force deformation curves in Figure 5.9 show that the deformation increases with the applied force. The curves show larger deformations in the first loading segment (0 - 2000 µN) as compared to in the second loading segment (2000µN - 8000µN). The loading rate is also higher (1000µN/s) for the first loading segment as compared to the second loading segment (300µN/s). It can be also be seen that during the holding segments at constant load of 2000µN and 8000µN, the deformation increases. The deformation decreases on the release of load during unloading segment but after complete removal of load, non-recoverable deformations of up to 900nm were observed. Increase in deformation with increase in loading rates during the loading segment show the viscoelastic nature of the MPS. The decrease in deformation during unloading segment shows the viscoelastic nature of the MPS however, MPS do not retain its original shape on the release of load showing viscoplastic nature. The increase in the deformation with time but at a constant load during the holding segments shows that there is creep or viscoelastic creep of the MPS. Similar phenomena were observed by Dou et al. (2007) and He et al. (2008) in their studies. Solid polymers are often viscoelastic (Ward et al. 1993), and the observed viscoelastic nature of the MPS is probably due to the viscoelastic nature of the polymer core.

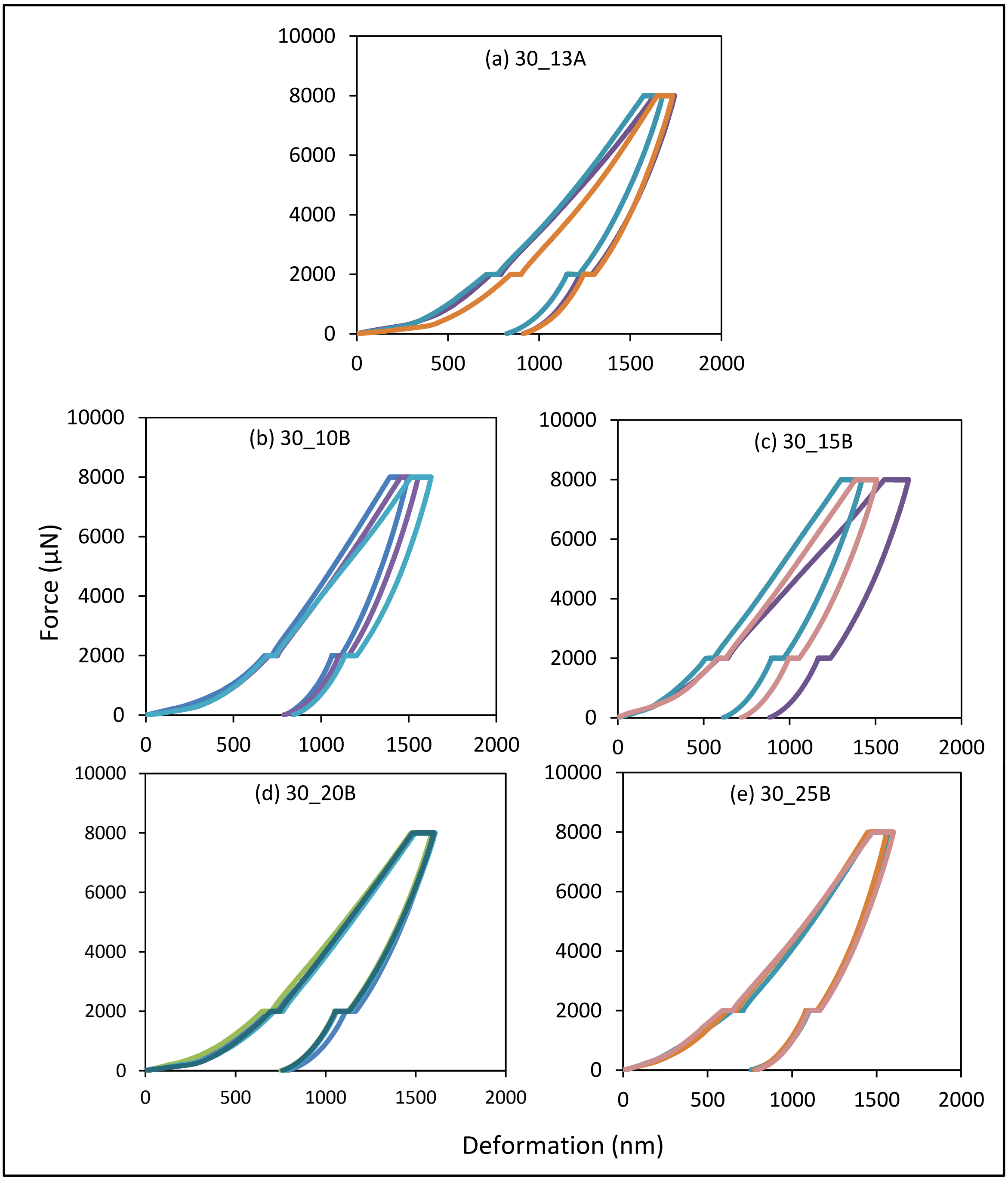

Figure 5.9 Force vs deformation curves for 30μm Ag-MPS

No evidence of the MPS being crushed during compression was obtained from the force versus deformation curves, which is unlike what Dou et al. and He et al. have observed in their studies. Dou et al. and He et al. both observed that, for larger forces, the MPS deformation increased within a few milliseconds by about 20%, for almost no recorded change in the force whereas in these tests no such abrupt increase in deformation is observed at constant force. In this study, a maximum applied load of 8000μN was applied, as compared to the 50,000μN and 10,000μN applied by Dou et al. and He et al.

respectively, such that maximum deformations of only 5 – 7% of the particle diameter observed, as can be seen in Figure 5.10 (b), are also much lower than 50% and 63% achieved by Dou et al. and He et al. respectively. The low load force used might therefore not be enough to crush the MPS.

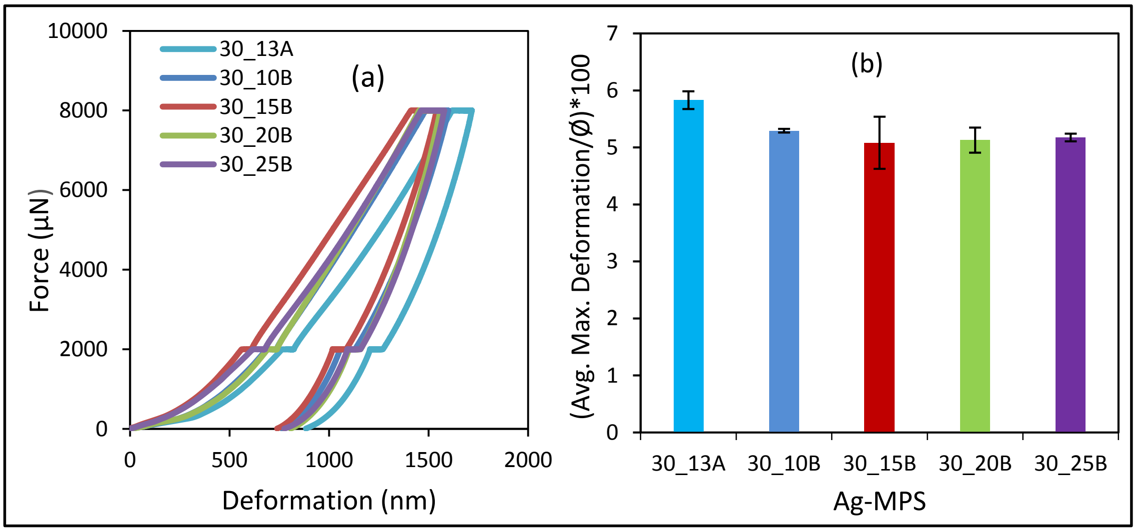

Figure 5.10 Average compression test results for different coating thickness (a) Force vs deformation curves (b) Average maximum deformation attained for 30 µm Ag-MPS at 8000µN with one standard deviation error bars

The force deformation curves in Figure 5.10 (a) show the effect of Ag coating thickness and the plating quality/morphology on the mechanical performance of the MPS. For the MPS plated using method B, there is little effect on the mechanical response with increasing coating thickness. However, slightly larger deformations are exhibited by MPS 30_13A, which were plated using method A. The silver coating on these particles is made of interlinked silver deposits grown from dispersed nucleation sites scattered across the surface of the particle where the silver can grow outwardly from the surface of the polymer as well as along the surface starting from the nucleation site (Kristiansen et al. 2013). This means that the thickness of the silver coating is not constant. Figure 5.11 shows SEM images of the different silver coatings on the 30µm Ag-MPS. These images show that the silver deposits that make up the coating of 30_13A are circular in shape and did not coalesce with each other whereas the silver deposits that make up the coating of 30_10B, 30_15B, 30_20B and 30_25B are irregular in shape and well coalesced. This lack of coalescence of the 30_13A silver deposits may reduce the coating strength, and therefore the mechanical properties of the polymer core may play

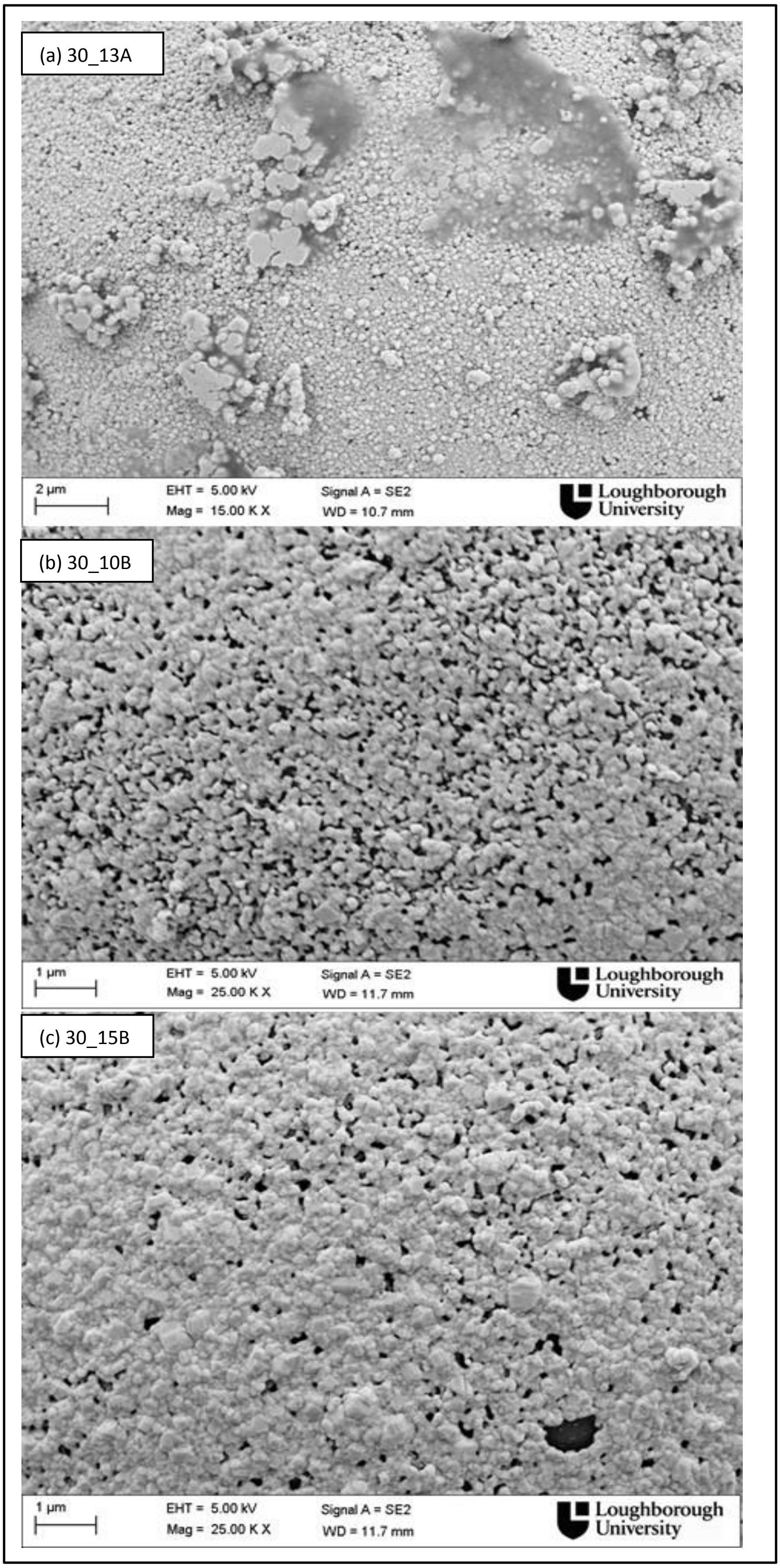

Figure 5.11 SEM images of the silver coatings on (a) 30_13A (b) 30_10B, (c) 30_15B, (d) 30_20B and (e) 30_25B (contd……..)

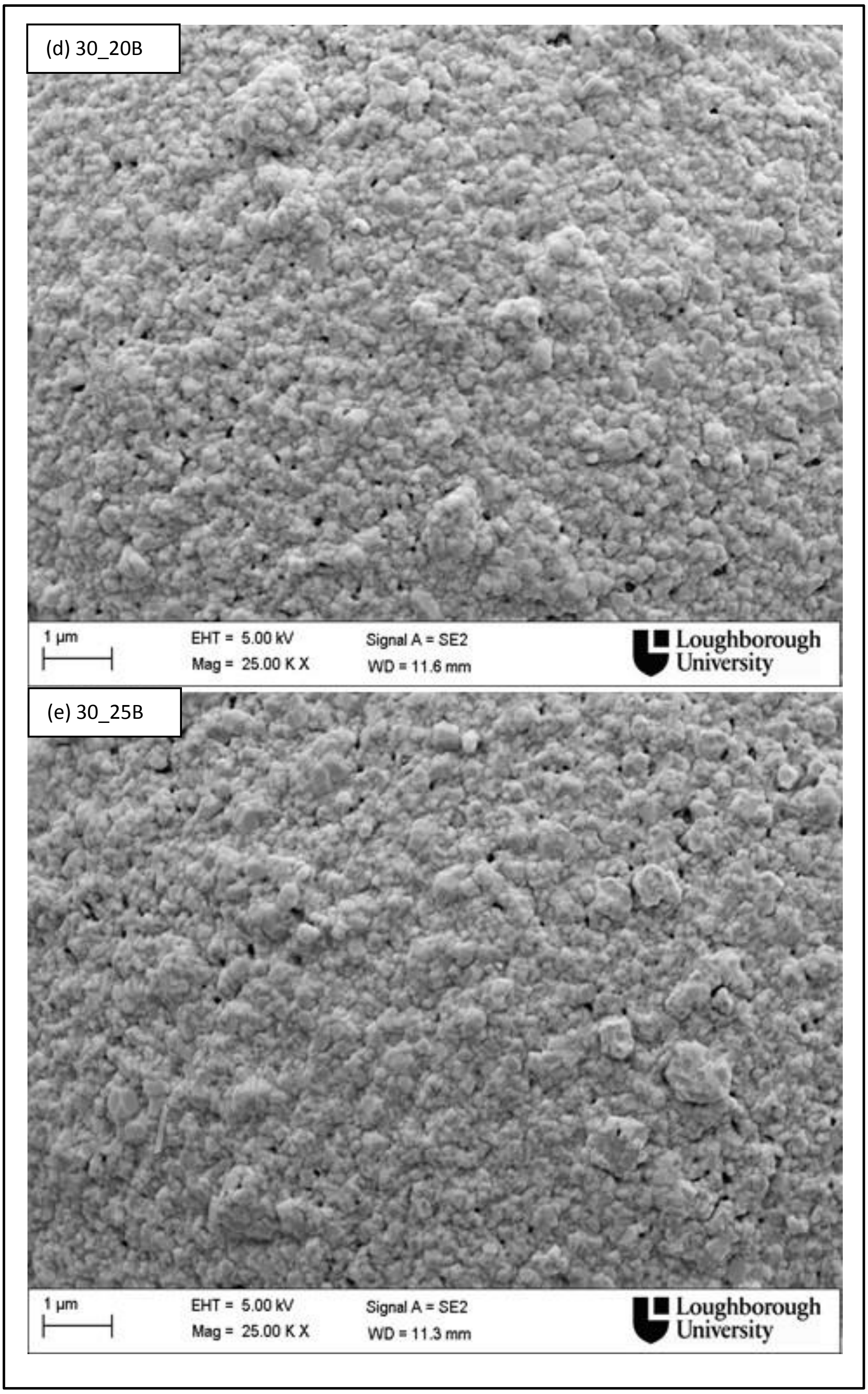

Figure 5.11 SEM images of the silver coatings on (a) 30_13A (b) 30_10B, (c) 30_15B, (d) 30_20B and (e) 30_25B

a greater part in determining the mechanical properties of these particles and this could be the reason for slightly larger deformation of these particles as compared to those coated with method B. In the present study, the electrical resistance was also simultaneously measured during the measurement of mechanical deformation of the particle. The current supplied for the electrical measurements may lead to an increase in the temperature of the contact area, due to localised heating (Holm 1967). For similar contacting surfaces the increase in temperature Θ would be (Holm 1967):

$$\boldsymbol{\Theta = \frac{U^2}{8\rho\lambda}} \qquad \textbf{5.6}$$

where ρ is the electrical resistivity of the contacting surface (Ωm) ;

λ is the thermal conductivity of the contacting surface ($Wm^{-1}K^{-1}$);

U is the voltage applied (V);

If the contacting surfaces are made of dissimilar materials then the ρ and λ of the surface with poorer electrical and thermal conductivity is used. Using the values of ρ = 0.2 x 10^{-6}Ωm and λ = 84.03 $Wm^{-1}K^{-1}$ of tungsten carbide, at the maximum voltage of 6.0 mV measured in this experiment, the rise in the temperature of the contact area would be only 0.268 K. However, the effect of the constriction area and the thickness of the conducting surfaces on the rise in the temperature would need to be determined using FE models, as was done by Oguibe et al. (1998) for gold and nickel coated ACA particles This was out of the scope of present research and could to be addressed in future studies. A previous study by Helland (2008) showed that softening of the particle occurred with localised heating. The variation in the mechanical behaviour due to local heating of the particle may cause large deformations. However this topic is beyond the scope of the present study and needs to be addressed in further studies.

Force-deformation curves for one of the much smaller 4.8_15A MPS, are compared with and an indentation directly onto the gold plated silicon substrate in Figure 5.12. The holding force was reduced to 500µN for this test. The force-deformation behaviour observed for 4.8 MPS shows that as the force is increased up to 5000µN, the deformation increases rapidly and reaches nearly 50% of the particle Ø, and all the particles tested undergo different deformation. On further increasing the load force, deformation remains constant, this suggests that at this point one end of the flat punch started indenting on the flat substrate preventing further compression of the MPS. The reason being that the non-coplanar tip, with diameter 75µm is too big for testing the 4.8µm MPS because it comes into contact with the substrate, when the force is applied during compression of the MPS as shown in Figure 5.6. However, a smaller tip suitable for both electrical and mechanical measurements was not available, and due to this and constraints on time and funds, further indentation experiments on 4.8µm MPS were not carried out. Therefore, the electrical and mechanical performance of 4.8µm MPS is not presented in this study. The effect of MPS diameter and core material on the resistance of MPS based ICAs therefore still needs to be addressed in future studies.

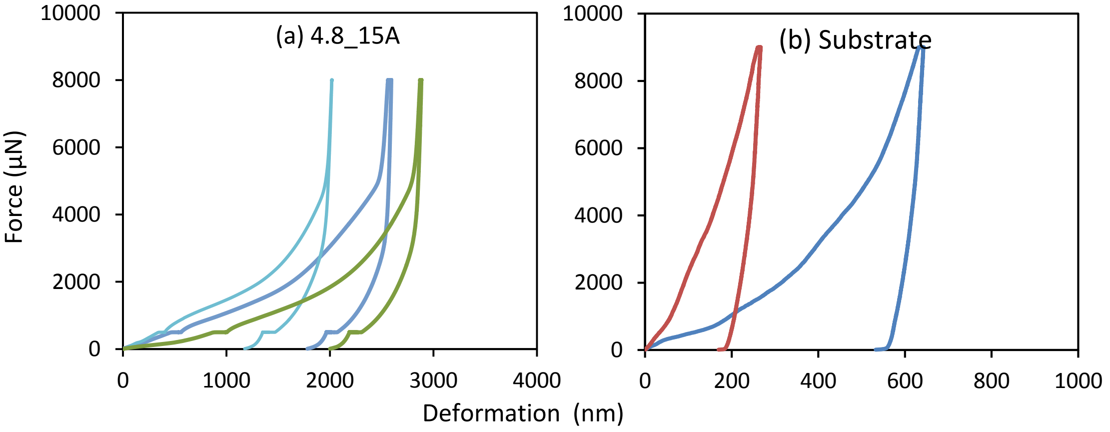

Figure 5.12 Force vs deformation curves for (a) 4.8µm Ag-MPS and (b) Au plated silicon substrate

5.3.2 Electrical Characterisation

The electrical resistance of the Ag-MPS were measured simultaneously with the force and deformation. The resistance measurement data were noisy, as can be seen in Figure 5.13, which is because of the small signal being measured. Due to the large number of data points it is not feasible to tabulate all values, but to show the scale of the signals measured, the maximum values of the voltage drop recorded at the 5mA test current are given in Table 5.4 along with the calculated resistance for this voltage. Further, due to the equipment available, the resistance data and the force-deformation data were recorded with different sampling rates. Therefore in order to correlate the particle resistance with the applied load and deformation (i) the noise had to be filtered from the resistance measurement data; and (ii) the resistance measurement data had to be matched in time to the applied load and deformation. The resistance measurement data were fitted using a non-parametric fitting tool within MATLAB software[4]. Figure 5.13 plots the fitted data and as measured data versus time. The non-parametric tool uses an algorithm which filters the noise using the weighted average method and, at the same time, extracts resistance data with the same sampling rate as the force and deformation data using spline interpolation. Figure 5.13 shows the fitted resistance values are similar to those obtained by taking a simple moving average over 30 samples and the fitted values of the resistance and the deformation follow the same trend as the measured ones. Therefore the method used to filter the noise from the measured resistance and match the sampling rates of the resistance with the deformation and force was considered acceptable and is used in this study.

Table 5.4 Max voltage and resistance values recorded for each type of MPS tested

Ag-MPS	Maximum Measured Voltage (mV)	Maximum Resistance (Ω)
30_13A	5.6	1.13
30_10B	4.2	0.85
30_15B	3.6	0.724
30_20B	2.9	0.593
30_25B	2.8	0.570

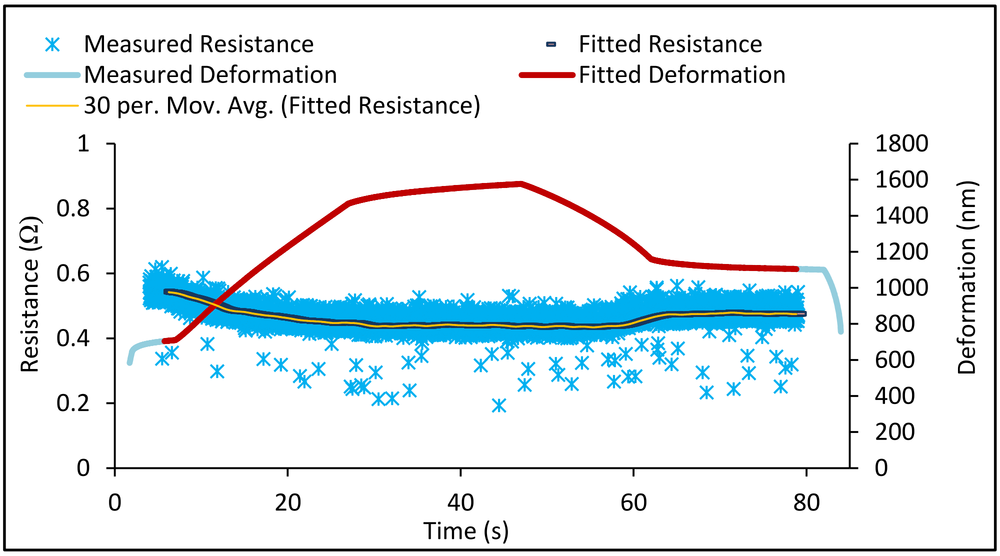

Figure 5.13 Plot showing the variation of measured resistance with deformation, and the fitted resistance and deformation with time

---

[4] The data fitting was done by the collaborative partner from Norway using MATLAB.

Figure 5.14 plots the variation of experimentally measured resistance values for each tested particle against the measured deformation. The results presented in Figure 5.14 show that as expected, the resistance decreases with increasing deformation.

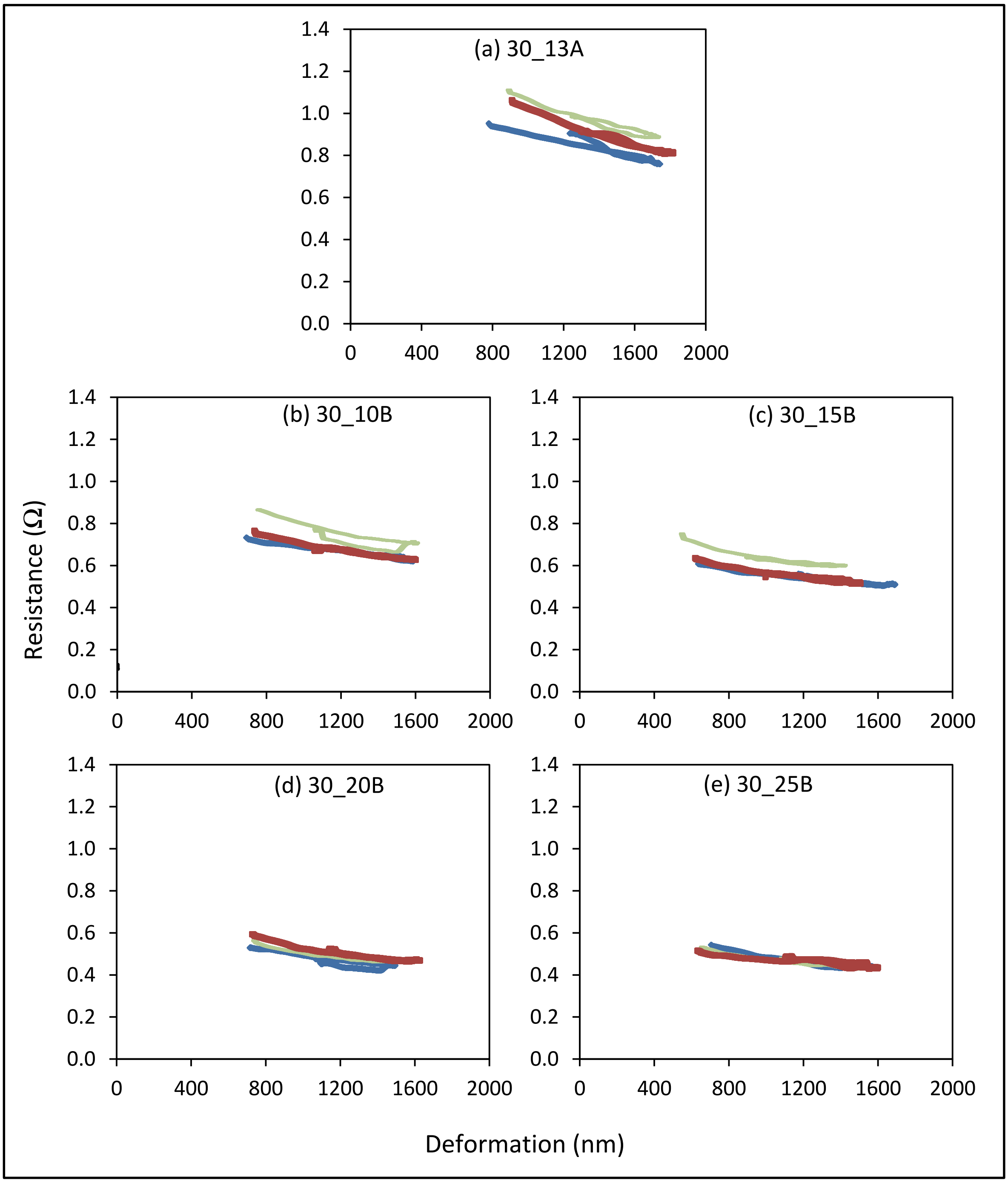

Figure 5.14 Variation of particle resistance with deformation for three samples each of (a) 30_13A (b) 30_10B, (c) 30_15B, (d) 30_20B and (e) 30_25B

The Ag-MPS used in the study have the same polymer core, but have different coating thicknesses and are coated using two different plating processes. Figures 5.14 (b) to (d) show that for the same plating process and deformation, the resistance of the Ag-MPS decreases with increasing coating thickness and as the coating thickness increases, more consistent resistance values for the three tested particles from each batch are obtained. The plots in Figure 5.14 (d) and (e) do not show a significant further reduction in the resistance values on increasing the coating thickness from 200nm to 250nm.The coating thickness for the Ag-MPS is estimated from the weight of silver used to coat the MPS, where the silver deposits/grains making up the coating are assumed to be uniform in size and perfectly coalescing with the neighbouring grains to give a continuous coating. However, in reality the silver deposits/grains making the coating are not uniform in size and at places the neighbouring deposits/grains do not coalesce thereby leaving a pore in the coating, as can be seen in SEM image in Figure 5.11. Figure 5.15 shows a FEGSEM image of a cross-section through the Ag-MPS coating at high magnification.

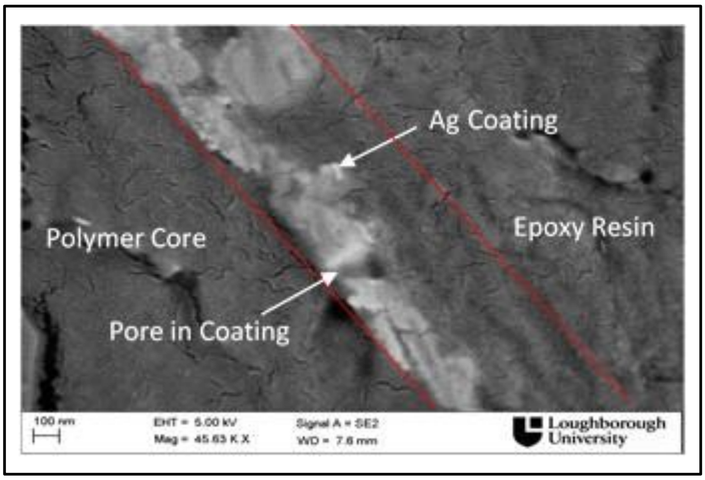

Figure 5.15 Cross-section of the Ag-MPS coating showing uneven thickness

Because of the difference in morphology between the assumed smooth and continuous coating and the actual coating, the actual thickness may differ from the estimated value. Another factor which could influence the coating thickness estimation is that all of the silver added is not used in making the coating, e.g. some of the silver take the form of a residue on the MPS surfaces, as shown in Figure 5.16 (highlighted by the red arrows). Including the amount of silver in the form of these residues in the estimate of the coating thickness leads to a higher estimated value than the actual thickness. Because of this limitation of the estimating method, there is a possibility that the difference in the coating thickness between 30_20B and 30_25B MPS is smaller than estimated and could be a reason for their similar resistance values. Further it can be observed from Figure 5.14 that although 30_13A has a thicker coating than 30_10B it exhibits higher resistance values and with comparatively large scatter. Ag-MPS 30_13A and 30_10B are coated with plating process A and B respectively which result in different coating qualities/morphologies. The observed high resistance and the large resistance scattering for 30_13A could be due to poor quality/morphology of the Ag coating. The silver deposits on 30_13A are not as dense as those on 30_10B, as can be seen in Figure 5.11 (a) and (b). Small Ag grains and the resulting many grain boundaries on 30_13A may scatter electrons, thus increasing the resistivity of the coating and hence the resistance of the particle.

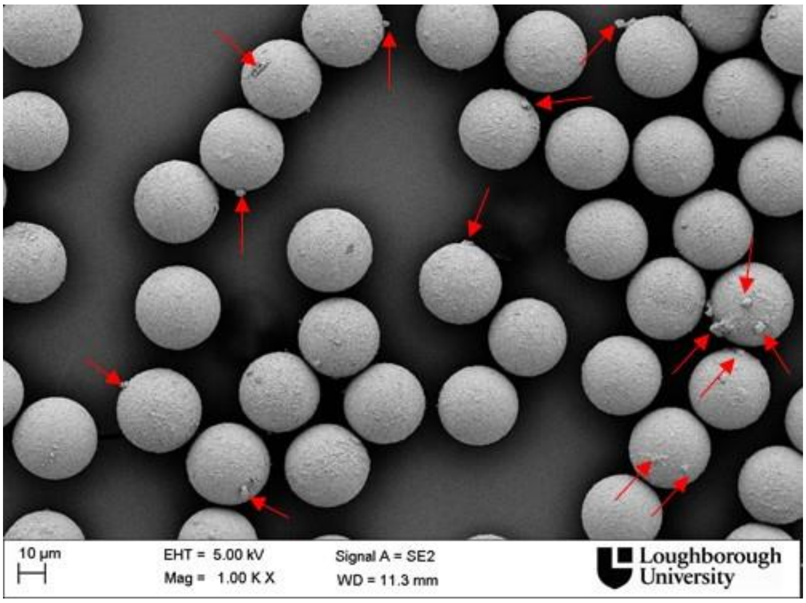

Figure 5.16 Sample showing large Ag deposits on Ag-MPS

5.4 Comparison with Theoretical Model

The resistance measurement results were compared with the theoretical model for MPS conductivity presented in Chapter 4, where the theoretical resistance values for different contact radii was calculated using Equation 4.27. To compare the resistance measurement results with the theoretical model, the contact radii were estimated from the measured deformation values using Equation 5.5. Figure 5.17 plots the variation of experimentally measured resistance and theoretically predicted resistance values for each tested particle against the normalized predicted contact radius i.e. r_c/r. As predicted by the theoretical model, Figure 5.17 shows that with the increasing contact

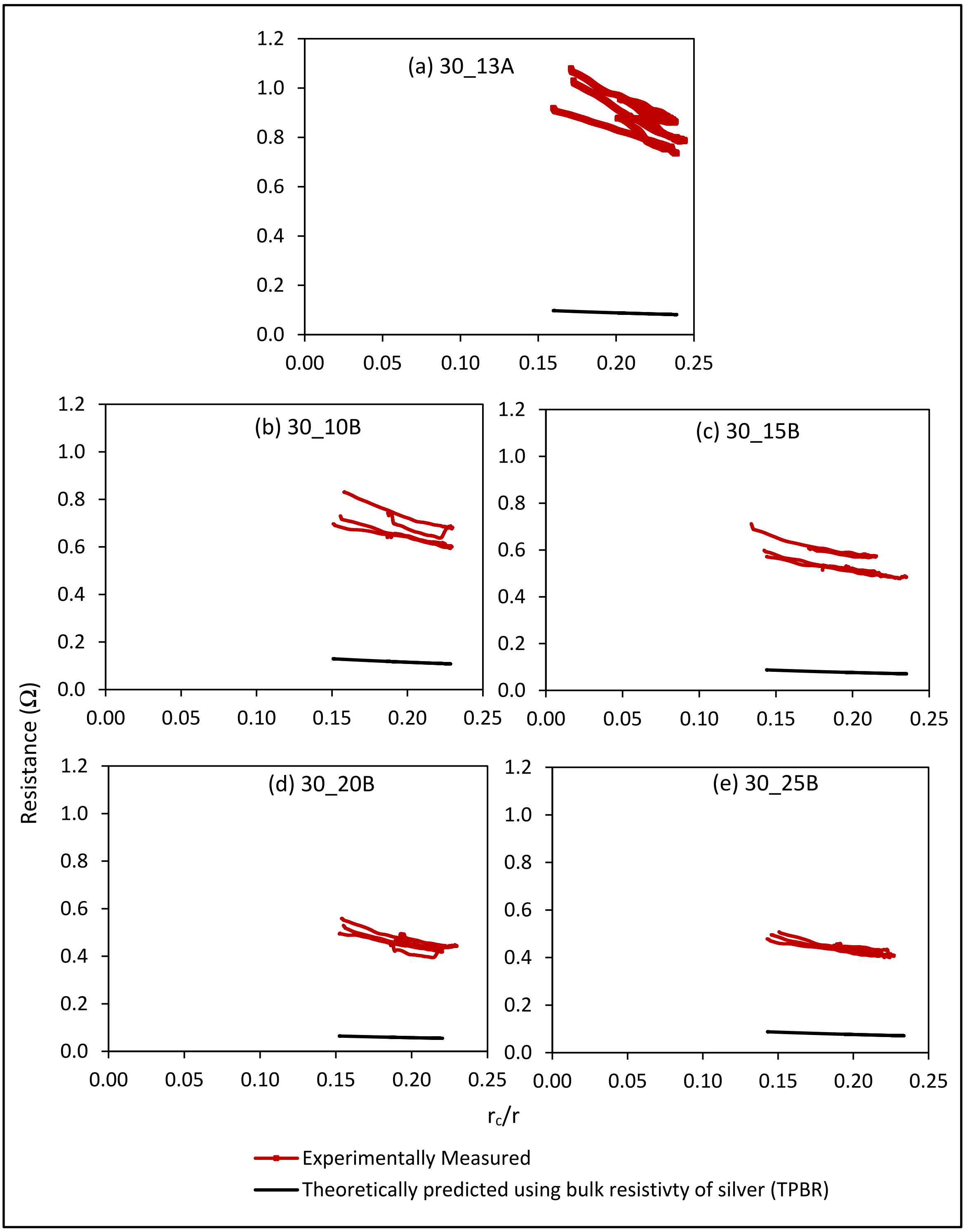

Figure 5.17 Experimental and theoretically predicted resistance vs estimated r_c/r

radius the resistance of the Ag-MPS decrease. Further, it can be seen from Figure 5.17 that, for a given contact radius, the theoretically predicted resistance of the Ag-MPS are considerably lower than those measured. For Ag-MPS that are coated with method A, the theoretically predicted resistances values are 8 - 9 times lower than the experimentally measured values. For particles coated with method B, the theoretically predicted resistances are about 4 – 5 times lower than the corresponding measured values.This difference between the measured and the theoretically predicted resistances may be due to a combination of the factors described below:

(i) In the theoretical model, the resistivity of bulk silver (1.59 x 10^{-6} Ωcm) is used to calculate the resistance of Ag-MPS, where the silver coating is assumed to be smooth and continuous. However, silver coatings are porous and nodular, with variable grain sizes as can be seen in the SEM pictures in Figure 5.11. According to a study by Sabayev et al. (2011) the resistivity of thin Ag films deposited by electroless processes depends upon the morphology of the deposited film. Sabayev et al. found that for a thickness of up to 35 - 40 nm Ag film resistivity can be much higher than for bulk material i.e. up to 11.4 x 10^{-6} Ωcm, if the film is comprised of isolated and elongated grains. This high resistance was mainly attributed to the percolation effect, where dielectric gaps separating the conducting Ag clusters restrict the electrical transport through the film. Sabayev et al. also showed that as the coating thickness increases above 30nm the isolated grains coalesce and, the effect of percolation decreases. When the film thickness reaches values larger than the electron mean free path, which is 52 nm for Ag (Kreibig et al. 1969), the resistivity of the film decreases and attains a saturated value of 2.5 x 10^{-6} Ωcm at 60 nm thickness i.e. if the thickness is increased beyond 60nm the resistivity remains same. Therefore the resistivity of Ag-coatings could be 1.57 – 7.1 times the bulk resistivity. However, all the Ag-MPS used in this study have estimated coating thicknesses above 100nm. Based on the study of Sabayev et al. if the resistivity of the Ag coating is assumed to be 2.5 x 10^{-6} Ωcm rather than 1.58 x 10^{-6} Ωcm, the predicted resistance of Ag-MPS increases, and is shown by purple lines in Figure 5.21. However, this increased film resistivity does not account for all of the observed difference between the measured and predicted resistances, as shown in Figure 5.21, and there must be other factors contributing to the difference. Furthermore, the Ag-MPS coated using process B has coalesced grains as compared to the ones coated using method A where the silver grains are isolated. Therefore the resistivity of the Ag coating coated with method A may be higher than 2.5 x 10^{-6} Ωcm (Sabayev et al.). According to Redford (2011) plating on to small spheres would differ from that onto a flat surface, even when using exactly the same plating process therefore the resistivity on a sphere could not be accurately predicted from similar coatings on a flat surface. Moreover, a study by Cui et al. (2012) showed that even for the same coating thickness, different methods will give different morphology and may have different resistivity. Cui et al. studied Cu coatings, but according to Sabayev et al. Cu coatings are more homogenous than silver coatings (because of the way they are made), and silver coatings are expected to have a more variable morphology than Cu. This shows that the nano scale nodular nature of the coating may result in increased resistivity of the coating compared to the value for bulk silver and is one of the factor contributing to the difference between the measured and predicted resistances. However, further detailed studies are required to determine accurately the resistivity of Ag coatings on micro particles to predict MPS resistance accurately, which is out of the scope of the present study. Further, gold coating on silicon may have resistivity higher than bulk gold and may affect the contact resistance. However, the resistivity of a 20nm gold film on glass has been shown to be in the range of 2.5 - 3.4 x 10^{-6} Ωcm depending upon deposition temperature (Hecht et al. 1994). It is assumed that a 200nm thick film may have a lower resistivity i.e. closer to that of gold (2. 4 x 10^{-6} Ωcm). Therefore bulk resistivity of gold is used here for calculating contact resistance.

(ii) In the theoretical model, the estimated value of the coating thickness is used to calculate the MPS resistance. As discussed in Section 5.3.2 the actual coating thickness is different from the estimated coating thickness. For example, if instead of the estimated 130nm, the average coating thickness is actually only 100 nm, then using Equation 4.27 the MPS resistance would be a factor of 1.3 higher. A sample of an ICA containing Ag-MPS was cross-sectioned in an attempt to estimate the coating thickness. However, it was difficult to measure the actual coating thickness from this cross-section because of the rough, nodular and porous nature of the coating, as shown in Figure 5.15. The difference between the actual coating thickness and the estimated coating thickness may therefore be another factor contributing to the difference between the measured and predicted resistances, but a value for this is however difficult to obtain and needs to be investigated in more detail as part of future studies.

(iii) In the measured resistance, the contribution due to the resistances R_{ps} and R_{pt} neglected. These are calculated using Equations 5.3 and 5.4, which used the apparent contact area, r_c, based on an assumption of ideally smooth contact surfaces, for both the Ag coating and the tip/substrate. In practice, all the surfaces have some degree of roughness. Figures 5.11 and 5.15 show how rough the Ag coatings are. The surfaces of the indentation tip and the Au substrate are also not perfectly flat. The contact between the Ag-MPS and the punch/substrate therefore probably consists of a number of contact spots through which the current is constricted, as shown in Figure 5.18, instead of there being a single continuous contact area i.e. the apparent contact area as is assumed in Equations 5.3 and 5.4. For such contact spots the constriction resistance will be Holm (1967):

$$\boldsymbol{R(n_s, a, l) = \frac{\rho_m}{2\pi n a} acrtg \frac{\sqrt{l^2-a^2}}{a} - 0.6\rho_m \frac{\sqrt{l^2-a^2}}{A_a}} \qquad \textbf{5.7}$$

where the contact spots are assumed to be of equal area *a,* and with an average distance between the centres of these contact areas *2l.*

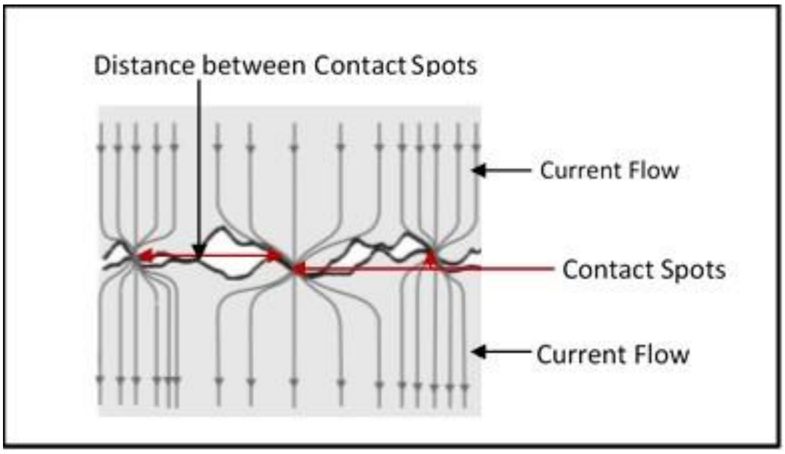

Figure 5.18 Current flow through many contact spots distributed over the apparent contact area (after (Holm 1967))

Holm (1967) predicted the variation of the normalised constriction resistance $R(n_s,a,l)/(\rho_m/4r_c)$ with the ratio l/a for different number of contact spots, n_s. Approximated values of the $R(n_s,a,l)/(\rho_m/4r_c)$ taken from Holm's graph at different l/a for different number of contact spots are given in Table 5.5. Table 5.5 shows that as the distance between the centres of the contact spots increases, the constriction resistance increases and could reach up to 5 times the constriction resistance when the contact area is considered as a single contact spot of radius r_c, but if the number of contact spots increases the constriction resistance decreases. From Figure 5.19, it appears that the number of contact points/ within in a 2µm contact radius lies between 50 - 250. For 30 µm Ag-MPS maximum contact radius at 8000µN force is estimated between 3 - 4 µm. From Figure 5.19 it also appears that in addition to being rough the surface of Ag coating is also not levelled/flat. Number of actual contact spots will depend upon the roughness and the waviness of the Ag surface.

Table 5.5 $R(n_s,a,l)/(\rho_m/4r_c)$ at different values of n_s and l/a after (Holm 1967)

No. of Contact Spots	***l/a***					
	0	**2**	**4**	**6**	**8**	**10**
5	1.0	1.4	2.4	3.4	4.4	5.4
10	1.0	1.3	2.0	2.8	3.4	4.0
50	1.0	1.2	1.4	1.8	2.1	2.4
250	1.0	1.1	1.2	1.3	1.4	1.5

Considering the waviness of the Ag coating, the number of contact spots can be assumed to be between 5 - 250 within the estimated contact area, then depending upon the value of l/a the maximum increase in constriction resistance would be up to 5.4 times over $\rho_m/4r_c$. Adding this contribution to the predicted resistance with the resistivity of Ag coatings raises the curves higher, as shown by yellow line in the Figure 5.21. However, this contribution also does not fully account for the difference and shows that there must be another factor contributing to the difference. However, it is difficult to predict the actual number of contact spots and the distance between them within any contact and it is therefore difficult to predict an actual correction factor to R_{ps} and R_{pt} based on the number of the contact spots but is it estimated to be 5.4 times.

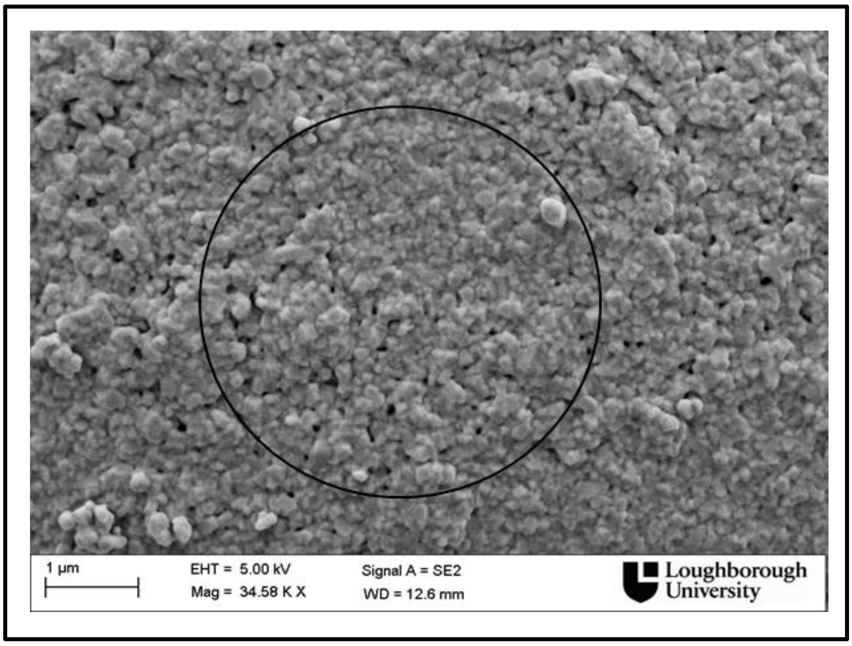

Figure 5.19 Black circle showing contact area for a 2µm contact radius on a sample of 30_20B

(iv) In addition to assuming a single apparent contact area, Equations 5.3 and 5.4 assume that the contact between MPS and flat punch/substrate is a circular contact area, as discussed in Section 4.1.2.1. The current spreading is assumed to be symmetrical into both of the contacting surfaces. However, in the case of a thin film, current lines must bend sharply at the interface and current crowding occurs in a small thickness of the film, as shown in Figure 5.20. Therefore, the constriction resistance of a contact area located in a thin film may not be accurately predicted using Equations 5.3 and 5.4.

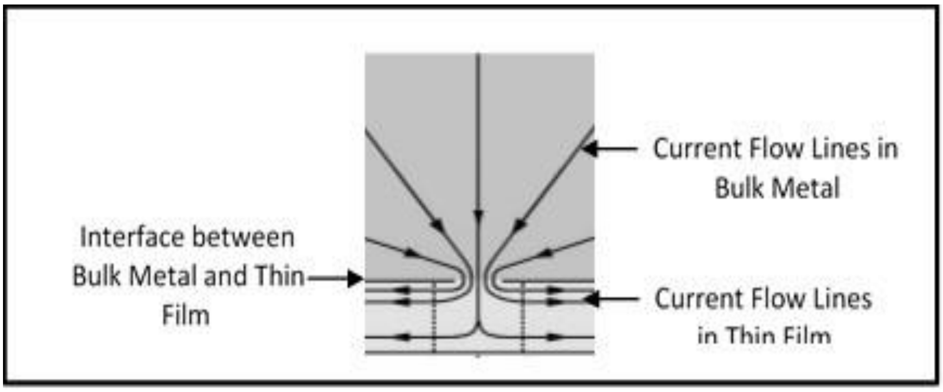

Figure 5.20 Current flow in contact between bulk metal and a thin film (after Timsit (2008))

Divigalpitiya (2008) has shown using FEA that in an ACA assembly using metal coated particles, the current flow between the coated particle and the contact pad is concentrated in a circular ring instead of a circular area, where the width of the ring is $2r_c/15$ (r_c being the outer radius of the contact ring). Divigalpitiya (2008) has shown that the constriction resistance becomes 15 times higher if the contact is ring shaped compared to a circular area. Based on Divigalpitiya's work if the constriction resistance is increased by 15 times than the sum of R_{ps} and R_{pt} calculated in Section 5.2.4.4 would increase from 23.3 mΩ - 30.1 mΩ to 349.5 mΩ - 450mΩ, adding 450mΩ to the predicted resistance value with film resistivity for 30_13A , 30_10B and 30_15B, and adding 349.5mΩ to the predicted resistance value with film resistivity for 30_20B and 30_25B the light blue curves which lies close to the experimentally obtained resistances is obtained, as shown in Figure 5.21. This then provides a credible explanation of the majority of the remaining difference between the experimental and predicted resistances, however how this value for the constriction resistance is calculated by Divigalpitiya is not clear and needs further investigation. In another study Timsit (2008) showed that the constriction resistance of a contact between a bulk solid and a thin film would differ from that calculated by Equation 5.3 and 5.4. He predicted the variation in the constriction resistance up to a value where the ratio of contact area to the coating thickness i.e. r_c/t_c is 0.5. However, in the present situation this ratio is above 10. Therefore the study by Timsit could not be used to predict R_{ps} and R_{pt}. A more detailed study is required to investigate value of R_{ps} and R_{pt} because of the bending of current flow lines and current crowding at the constriction between the flat punch/substrate and the Ag-MPS, so that the contribution of the contact resistance to the measured resistance of the MPS could be calculated. This investigation is however, outside the scope of the present study and need to be addressed in further studies perhaps using finite element analysis.

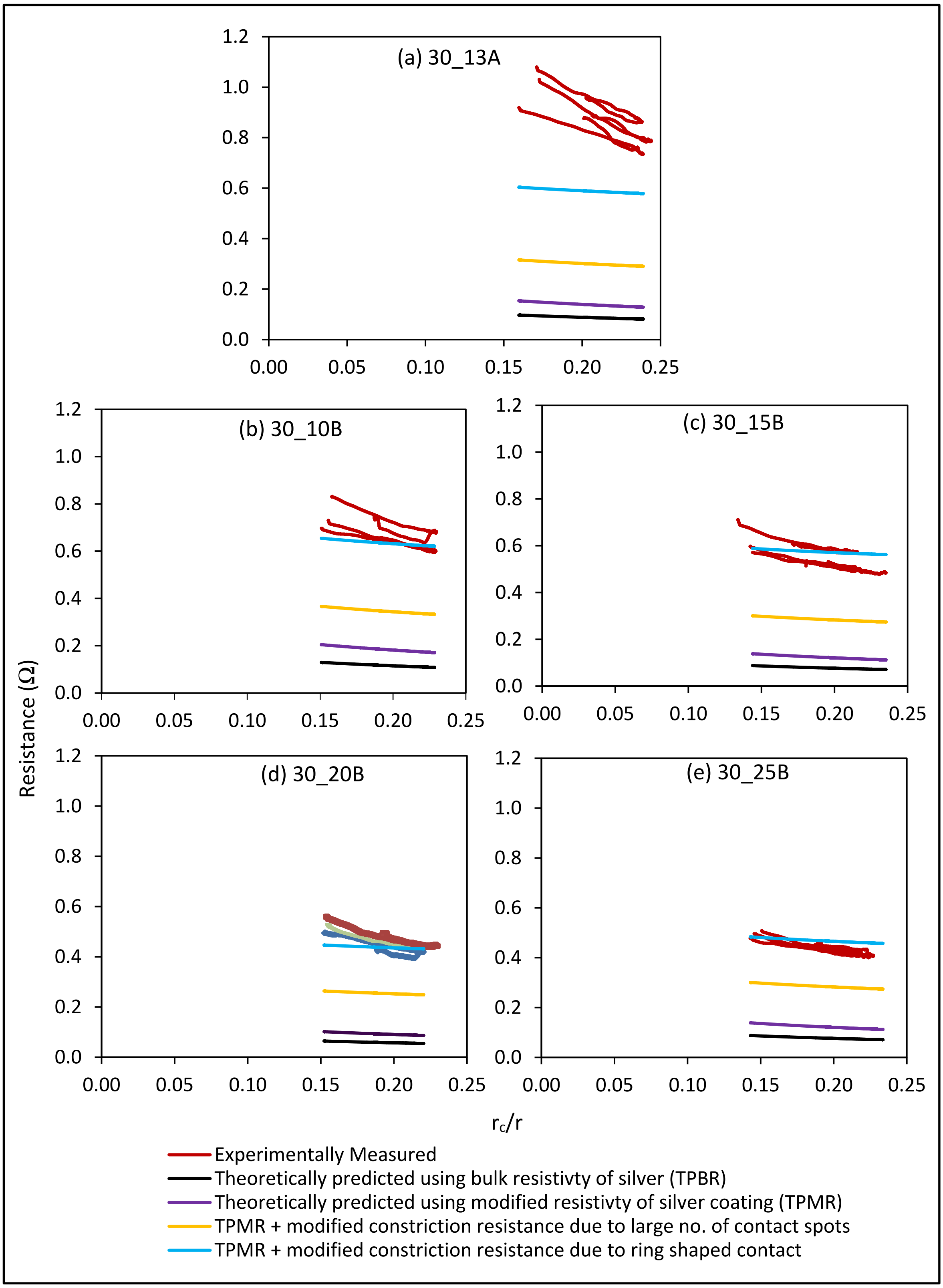

Figure 5.21 Experimental and theoretically predicted resistance with suggested modifications

(v) Furthermore, tarnish films of silver oxide (Ag_2O), with resistivity in the range of 10^{-4} Ωcm to 10^{-3} Ωcm (Reddy et al. 2014) or silver sulphide (Ag_2S) with resistivity in the range of 10^7 Ωcm to 10^{12} Ωcm (Holm 1967), may be formed on Ag surfaces at room temperature on exposure to normal atmosphere and can therefore affect silver coating resistivity and hence the contact resistance. However, Ag oxidises to Ag_2O only in the presence of ozone and Ag_2S is formed only in the presence of H_2S gas. As the concentration of H_2S is usually small in air Ag_2S films grow very slowly (because of the low rate of arrival of sulphur atoms at the surface). Both these films are soft (Ag_2S has a hardness half that of pure Ag i.e. 1.5×10^8 N/m^2) and could be easily displaced at the contact, providing relatively good conductance through metallic contact spots (Holm 1967). Moreover, the linear relationship between resistance and voltage as seen in Figure 5.22, does not indicate the presence of insulating layers, such as oxides at contact points or, if present, may have been damaged by the applied force at the contact, providing relatively good conductance through metal spots, and are therefore not expected to affect the contact resistance. Further, residues from the plating process or contamination on the flat punch and substrate can also reduce the effective contact area between particle and the tip/substrate. Any decrease in effective contact area due to such contamination will result in an increase in contact resistance between the particle and the tip/substrate. However, a study by Divigalpitiya (2008), using both finite element (FE) analysis and analytical modelling, has shown that the increase in the constrction resistance of an MPS is small, even if up to 85% of the contact surface is contaminated.

(vi) A localised increase in the temperature due to heat generated by the current flowing through the constricted surfaces can also affect the constriction resistance (Holm 1967). The resistance is increased by a factor of :

$$\left(1 + \frac{2}{3}\alpha\Theta\right) \qquad 5.8$$

where α is the temperature coefficient of resistivity (°C^{-1}) and

Θ is the rise in the temperature (°C) given by Equation 5.6

In the present case the rise in the temperature of the constricted area would be negligible, as discussed in Section 5.3.1. In addition the linear relationship between resistance and voltage over the applied current range, as seen in Figure 5.22, also do not indicate any Joule heating effect showing that heat generated at the contact points due to the current flowing through them would be negligible and thus would not lead to any significant increase in the measured constriction resistance. However, the effect of the contact area on temperature rise at contact point needs to be investigated in future studies, using FE models as was done by Oguibe et al. (1998).

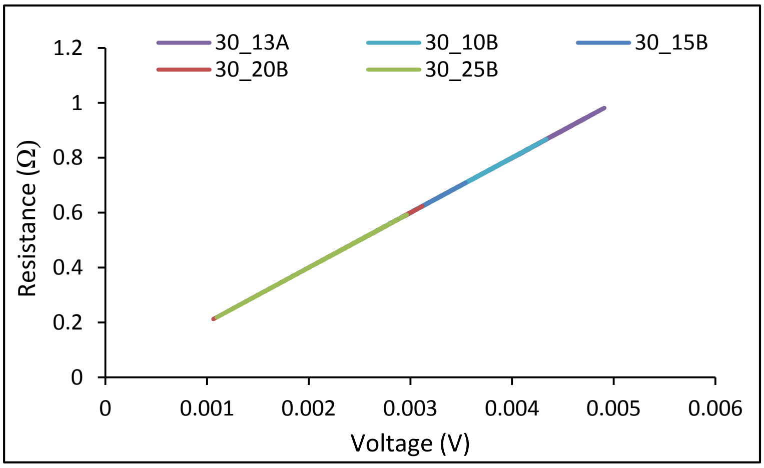

Figure 5.22 Typical resistance - voltage curve obtained for Ag-MPS tested

The comparison between the experimentally measured and theoretically predicted values have shown that many factors such as coating resistivity, difference between actual and predicted coating thickness, difference between apparent and actual contact spots, contact geometry, presence of the tarnish films on Ag and contamination of gold surfaces, and temperature increase at the contact interface can contribute to MPS and contact resistance and need to be taken into account. Among these parameters the effect of contact geometry on the constriction resistance between MPS and tip/substrate appear to be most significant and would explain the major differences between the measured and theoretically predicted values. However, accurate predictions of the contribution of each these factors is beyond the scope of this study and needs further investigation.

5.5 Concluding Remarks

This chapter has presented the results of mechanical and electrical characterisation of Ag-MPS using a nanoindentation-based flat punch method. The results show that the electrical resistance of the 30μm Ag-MPS is dependent on the thickness and quality of the Ag coating. As predicted by the theoretical model, Ag-MPS with thicker and more uniform coatings are found to have lower and more consistent resistances as compared to Ag-MPS with thinner and more porous coating. The quality of the Ag coating seems to have considerable effects on both the mechanical properties, and the electrical properties of Ag-MPS. The results presented in this chapter show that the particles showing repeatable mechanical behaviour also show more consistent electrical resistances, therefore linking the electrical resistance of the Ag-MPS to their mechanical performance. Ag-MPS, particularly with 0.20 μm and 0.25 μm, thick coatings, exhibited good properties both in terms of repeatable mechanical response, and low and consistent electrical resistance. The electrical resistance for these thicknesses was found to be similar.

The measured resistances of individual particles were compared with the theoretical model derived in Chapter 4. The theoretically predicted resistances were about 5 – 9 times lower than the measured resistances, depending on particle type, showing that additional factors not accounted for in the model have a significant effect. The discussion in Section 5.4 has shown that differences between the bulk metal and thin film resistivity, and the estimated and actual coating thickness can significantly affect the MPS resistance and need to be taken into consideration. Further, the discussion above has shown that the difference in the apparent and actual contact area, the current crowding in the bulk and the thin films, the presence of the thin insulating films on the Ag or tip/substrate surfaces are all factors which may be significant to contributing to the measured resistance and that together these factors are sufficient to explain the difference between the initial model and experiments. However, accurate predictions of the contribution of each factor discussed is beyond the scope of this study and need further investigation.

CHAPTER 6

FACTORS AFFECTING CONDUCTIVITY OF ICAs FILLED WITH SILVER METALISED POLYMER SPHERES

The model for the conductivity of ICA presented in Chapter 4 summarizes the main factors on which the conductivity of an ICA filled with MPS depends. This chapter presents an experimental investigation of the effect of these factors on conductivity.

6.1 Aims

To investigate the effect of

i) MPS diameter;

ii) coating thickness and quality/morphology; and

iii) curing conditions and shrinkage of the epoxy matrix (both which affect the resulting contact radius)

on the electrical conductivity of ICAs filled with Ag-MPS.

6.1.1 Materials Used

MPS having three different diameters, i.e. 6µm, 10µm and 30µm and with varying Ag coating thicknesses have been used. They all have a very narrow size distribution (C.V. of approx. 3%), and were produced and supplied by Mosaic Solutions AS, Norway. Three different plating processes have been used by Mosaic to coat the polymer spheres. The coating thicknesses were provided by the manufacturer with their stated margin of error in estimating the coating thickness being ± 5%. However, this coating thickness is an average estimated from the amount of silver used during the coating process. The MPS were examined in SEM before conducting the experiments and any batch of particles with poor silver coating, as shown in Appendix B, were not used. All of the particles used in this work have Ag coating, continuously covering the entire surface area of polymer sphere. Table 6.1 gives the specifications and nomenclature of the Ag-MPS used. FS34 silver flakes as used in Chapter 3 were again used for comparison.

Table 6.1 Specifications and nomenclature for the Ag-MPS used

Ag-MPS Name	PS Core diameter (µm)	Plating Process	Ag thickness (µm)	Ag Volume Fraction (%)	Density (g/cm^3)
06_10B	06	B	0.10	9.3	1.93
10_15B	10	B	0.15	8.4	1.95
10_20C	10	C	0.20	11.1	2.21
10_21D	10	D	0.21	11.6	2.26
30_10B	30	B	0.10	1.9	1.36
30_15B	30	B	0.20	2.9	1.45
30_20B	30	B	0.20	3.9	1.54
30_25B	30	B	0.22	4.9	1.64
30_20C	30	C	0.20	3.9	1.54
30_22D	30	D	0.22	4.3	1.57

Two types of polymer matrix were used, both commercially available two component epoxy systems. They are denoted as type I and type II in this study and their details are given in Table 6.2.

Table 6.2 Characteristics of epoxy systems used

	Type I	Type II
Resin	Epoxy Phenol Novolac	Bisphenol A/F
Curing Agent	Imidazole	Polyetheramine
Viscosity of Resin	High	Low
Pot Life (min)	180	480-580
Density of Resin (g/cc.)	1.20	1.18
Density of Curing Agent (g/cc.)	1.02	0.948

6.1.2 Equipment used

The same equipment used in the study described in Chapter 3 was used for conducting these experiments.

6.1.3 Methodology

The same method as used in Chapter 3 was used to the prepare samples and carry out resistance measurements. In this investigation the volume fractions of Ag-MPS used were at least 43 vol%, which is well above the percolation threshold for all of the ICAs formulated (Jain et al. 2011). The main reason for only using high volume fractions is that the variation in resistance between samples is very large near to the percolation threshold and factors other than the particle properties, such as small variations in the mixing and stencilling processes may have a significant impact. Another reason is that any commercially viable ICA is likely to require these high volume fractions to ensure consistent electrical properties, even if only moderate conductivity is required (Jain et al. 2011; Jain et al. 2013). For each type of particle listed in Table 6.1 and each volume fraction tested six ICA tracks were printed from same mix.

6.1.4 Results and Discussion

6.1.4.1 Effect of MPS size

To study the effect of MPS size on the conductivity, MPS with diameter 6µm, 10µm and 30µm, combined with the type I epoxy matrix were used. They were all coated using the same plating process, process B. The 6µm and 10µm have a 0.10µm and 0.15µm thick coating respectively and are denoted as 6_10B, and 10_15B whereas 30µm MPS with both, a 0.10µm and 0.15µm thick coating were used and are denoted as 30_10B and 30_15B. The ICAs formulated were cured at 150°C for 15 min. Figure 6.1 plots the averaged results from the resistivity measurements for ICAs formulated using these four MPS at different volume fractions, together with one standard deviation error bars. The theoretical model for conductivity in Chapter 4 gives the resistivity of an MPS filled ICA as:

$$\boldsymbol{\rho_{ICA}} = \left(\frac{\boldsymbol{\rho_m}}{\boldsymbol{\pi . t_c}}\left\{-\boldsymbol{ln}\left[\boldsymbol{tan}\frac{\boldsymbol{r_c}}{\boldsymbol{\emptyset}}\right]\right\} + \frac{\boldsymbol{\rho_m}}{\boldsymbol{2r_c}} + \frac{\boldsymbol{\rho_t}}{\boldsymbol{\pi r_c^2}}\right)\boldsymbol{\emptyset} \qquad \textbf{6.1}$$

This shows ICA resistivity increases with increasing coating resistivity ρ_m , MPS diameter, *Ø*, and contact resistance whereas decreases with increasing contact radius r_c and increasing coating thickness t_c. As predicted by model the plots in Figure 6.1 shows that ICAs made using smaller MPS, i.e. with diameters of 6µm and 10µm, have a lower resistivity than those made using larger MPS, i.e. 30µm, whereas the ICAs made using 6_10B and 10_15B have similar resistivities. The plots also shows that the difference between the resistivities of the ICAs is smaller in proportion to difference in MPS diameters. The reason for similar resistivities of 6_10B and 10_15B may be that smaller

6_10B MPS behave stiffer (He et al. 2008), and may therefore have a smaller contact radius than 10_15B for the same force applied (under similar curing conditions) which may increase resistance of 6_10B and contact resistance compared to 10_15B.

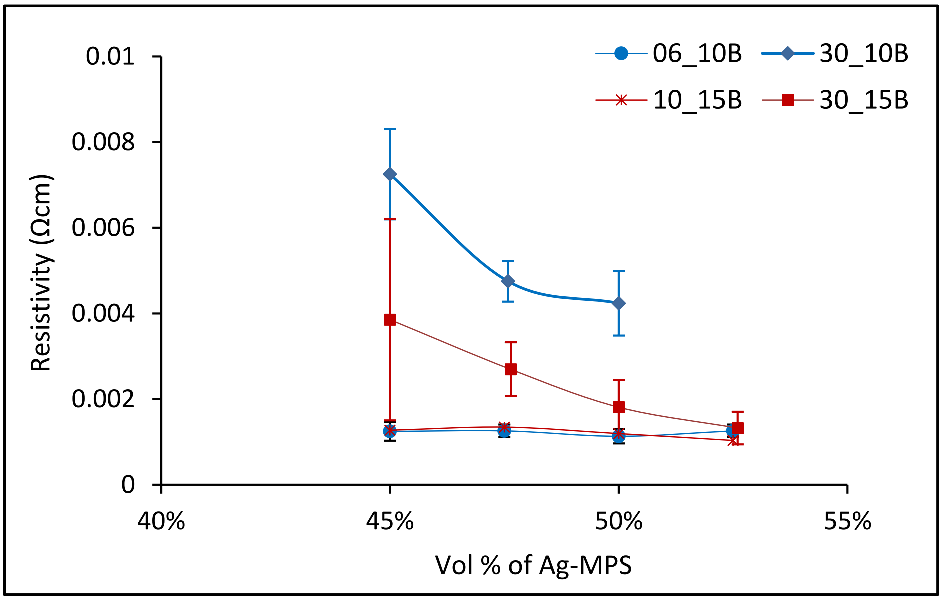

Figure 6.1 Effect of MPS size on resistivity

Additionally, when MPS diameter decreases, although there is an increase in the number of conductive pathways (which should reduce the ICA resistance), the number of particle-to-particle contacts in each pathway also increases, which increases the total of the contact resistances. Thus increased contact resistance lessens the effective reduction in resistivity due to the increase in the number of parallel paths and could be a reason for the similar resistivities of the ICAs made using 6_10B and 10_15B, and the smaller difference between the resistivities of the ICAs made using 30µm, 10µm, and 6µm MPS in proportion to their size.

It can also be seen from Table 6.1 that 10_15B uses 2.8 times and 6_10B uses 3.8 times more silver than 30_15B and they both give only a 1.8 times decrease in resistivity. This shows that although the resistivity of an ICA decreases with decreasing MPS diameter, it is not in proportion to the increase in the amount of silver used. This also shows that increasing the coating thickness on the larger MPS lowers the resistivity more in comparison to the silver increase, and therefore uses silver more efficiently offering greater environmental and cost benefits (Plots of resistivity against the quantity of silver used in Ag-MPS filled ICAs are shown in Figures 6.8 and 6.9.) Further, using larger MPS may have other benefits, i.e. for a given resistivity a larger MPS with a thicker coating will have a density closer to the resin than smaller MPS with a thinner coating thus reducing the tendency for sedimentation. This can be seen by comparing rows 2 to 5 and 9 to 11 from Tables 6.1 with rows 6 and 7 in Table 6.2. Using larger MPS, the volume fraction of the polymer core is greater compared to silver, meaning their mechanical properties will be closer to those of the polymer. Moreover, it has been shown in Chapter 5 that increasing the coating thickness on the 30µm MPS has only a minor effect on their mechanical behaviour. The next section discusses the effect of coating thickness on resistivity for 30µm MPS. The variation of the resistivity against the amount of silver is shown in Figure 6.8.

6.1.4.2 Effect of Ag Coating Thickness

To investigate the effect of coating thickness, MPS 30_10B, 30_15B, 30_20B and 30_25B were used, which all have the same core diameter and were plated using same process. All the other parameters such as adhesive matrix, curing profile and curing method were also kept identical for this investigation. Figure 6.2 shows the averaged results from the resistivity measurements for ICAs formulated at different volume fractions, together with one standard deviation error bars.

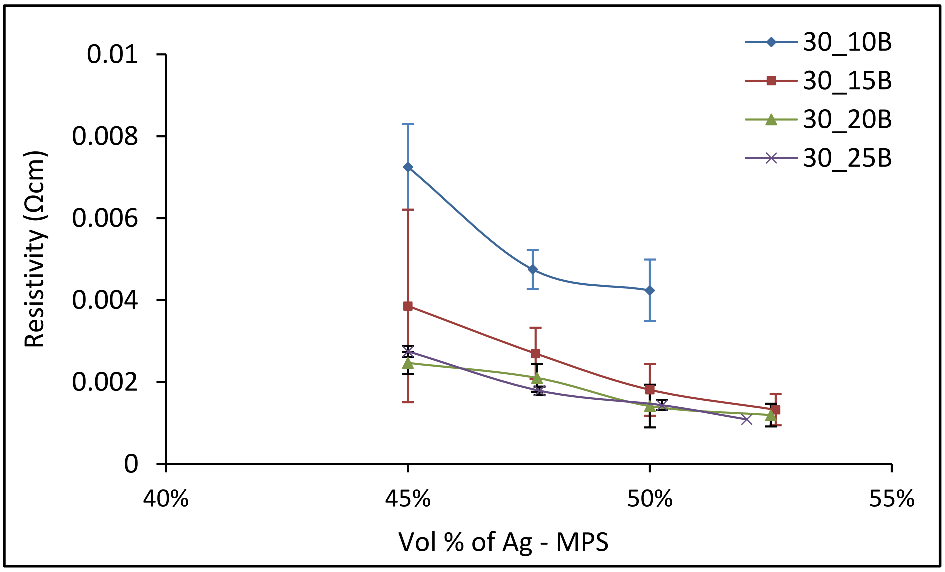

Figure 6.2 Effect of coating thickness on resistivity

It should be noted that the graph for 30_10B finishes before others in Figure 6.2. This is because a printable mixture could not be obtained for these ICAs above 50 vol%. One reason could be more porous coating on 30_10B compared to other MPS, which may increase surface roughness or trap some of the epoxy inside the pores increasing the ICA viscosity. Another reason could be accumulation of errors in calculating the volume fraction of filler as each higher volume fractions are made from adding particles to the previous mixture. The results plotted in Figure 6.2 show that (as predicted by Equation 6.1) the resistivity of the ICA decreases with increasing Ag coating thickness, although the ICAs made using 30_20B and 30_25B have nearly the same resistivities at all volume fractions. A larger variation in resistivity is observed for the ICAs made using 30_10B and 30_15B. Equation 6.1 predicts that the ICA resistance depends upon the MPS resistance and the contact resistance. The experimentally measured MPS resistance have been found to be similar for 30_20B and 30_25B, as can be seen in Figure 5.14 (d) and (e). Thus similar MPS resistance could be the reason for similar resistivities of ICAs containing 30_20B and 30_25B. Figure 6.3 plots the resistivity (log scale) calculated using ICA conductivity model developed in Chapter 4 in comparison with the measured values.

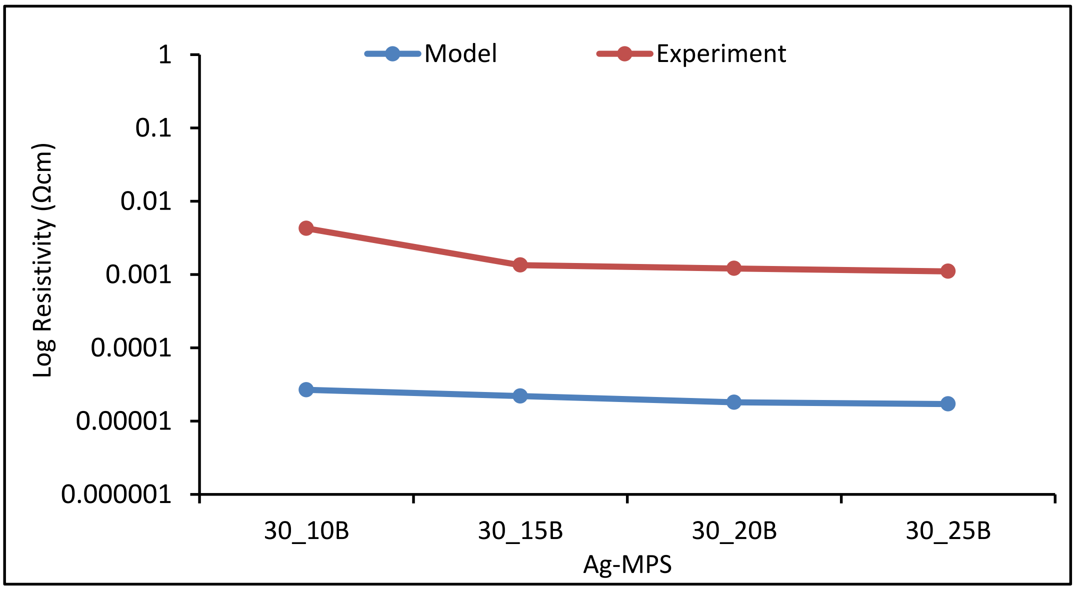

Figure 6.3 Comparison of theoretical resistivity (without contact resistances) and experimental resistivity values for ICAs containing 30µm Ag-MPS

Figure 6.3 shows that as predicted by the analytical model resistivity decrease with increasing coating thickness but, the measured values are 100 time higher than predicted. In theoretical model the resistivity was calculated using the Ag-MPS resistances as measured in the Chapter 5. However, the contact resistances were not taken into account and could be the reason for the large difference in theoretical and experimental values. This indicates the importance of the contact resistances and shows that further studies need to be conducted to successfully predict the overall resistivity.

For ICAs made using the same adhesive matrix and under the same curing conditions, the contact force is assumed to be same, however the contact radius and hence the contact resistance may vary with coating morphology. Figures 5.9 and 5.14 in Chapter 5 show a larger variation in the mechanical deformation and resistance at the same applied force, for 30_10B and 30_15B as compared to 30_20B and 30_25B. A change in the stiffness could lead to a variation in the contact radius for the same applied force due to shrinkage and may therefore result in a different contact resistance. Further, the Ag coatings on 30_10B and 30_15B are porous as compared to those on 30_20B and 30_25B, as can be seen in Figure 5.11. This porosity may lead to variations in the actual contact area and hence contact resistance. Thus a large variation in MPS resistance and contact resistance may be the reason for the large difference in resistivity between ICAs formulated using 30_10B and 30_15B. Moreover, larger variability can be seen below 48 vol%, and loose packing of the spheres at these vol% may also add to the variability in the resistivity. In addition, as discussed in Chapter 3, variability in the printed thickness of the ICAs could be another reason for the spread in measured ICA resistivity.

Further, using the values in Table 6.1 the ratio of Ag vol% on the different 30μm Ag-MPS (with increasing coating thickness) are:

$$Ag_{30\_10B} : Ag_{30\_15B} : Ag_{30\_20B} : Ag_{30\_25B} = 1 : 1.5 : 2.1 : 2.6$$

whereas the ratio of the ICA conductivities at 50 vol% from Figure 6.2 are:

$$\sigma_{30\_10B} : \sigma_{30\_15B} : \sigma_{30\_20B} : \sigma_{30\_25B} = 1 : 2.4 : 3.0 : 3.0$$

where Ag_{30_10B} , Ag_{30_15B}, Ag_{30_20B} and Ag_{30_25B} are vol% of Ag on 30_10B, 30_15B 30_20B and 30_25B respectively and σ_{30_10B}, σ_{30_15B}, σ_{30_20B} and σ_{30_25B} are the conductivities of the ICAs formulated using 30_10B, 30_15B, 30_20B, and 30_25B respectively. The ratio of Ag vol% and the conductivities is also plotted in Figure 6.4.

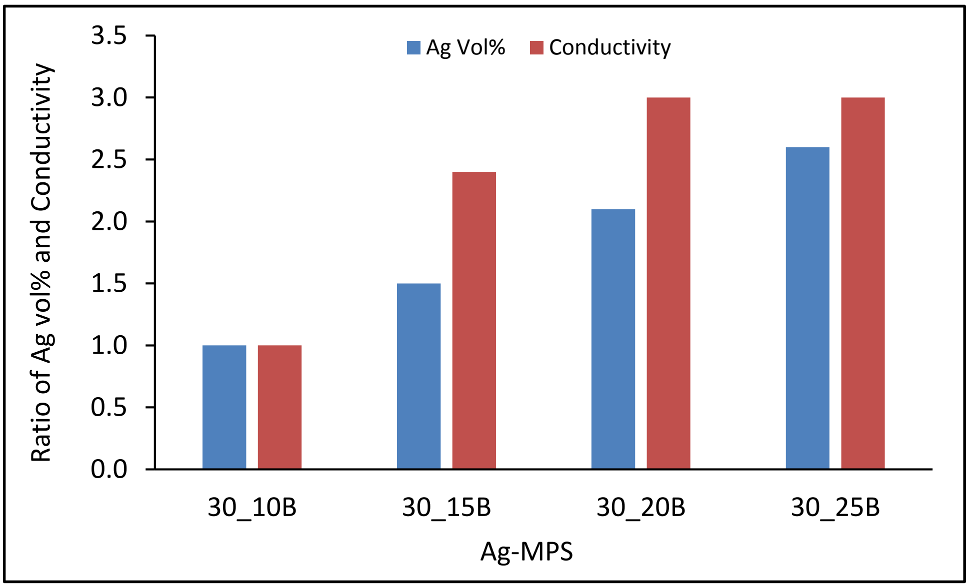

Figure 6.4 Ratio of Ag vol% and the conductivity of 30µm Ag-MPS (with increasing coating thickness)

This shows that when the Ag thickness is increased from 0.10µm to 0.15µm the conductivity of an ICA increases 2.4 times for 1.5 times increases in Ag vol% whereas when the Ag thickness is further increased from 0.10µm to 0.20µm the conductivity increases 3.0 times for a 2.1 times increase in Ag vol%. However, when the Ag thickness is further increased from 0.10µm to 0.25µm the conductivity still only increases only 3.0 times for 2.6 times increase in Ag vol%. This shows increasing thickness up to 0.20 µm results in increased conductivity but that further increasing thickness from 0.20 µm to 0.25µm, results in a negligible change in conductivity even though the Ag vol% increases by a further 25%. The reason could be similar MPS resistance for 30_20B, and 30_25B.

6.1.4.3 Effect of Plating Process and Coating Morphology

The silver plating processes for MPS are under continuous development at Mosaic, and the particles tested in this thesis have been plated with several different processes, as indicated in Table 6.1. This difference in plating process results in differences in the plating quality/morphology, as can be seen from the FEGSEM images in Figure 6.5. However, all of the particles used in this work have a continuous Ag coating over the whole MPS. To investigate the effect of plating quality arising out of the different plating processes on the ICA conductivity samples of two sizes of MPS coated using processes, B, C and D have been used, as detailed in Table 6.3.

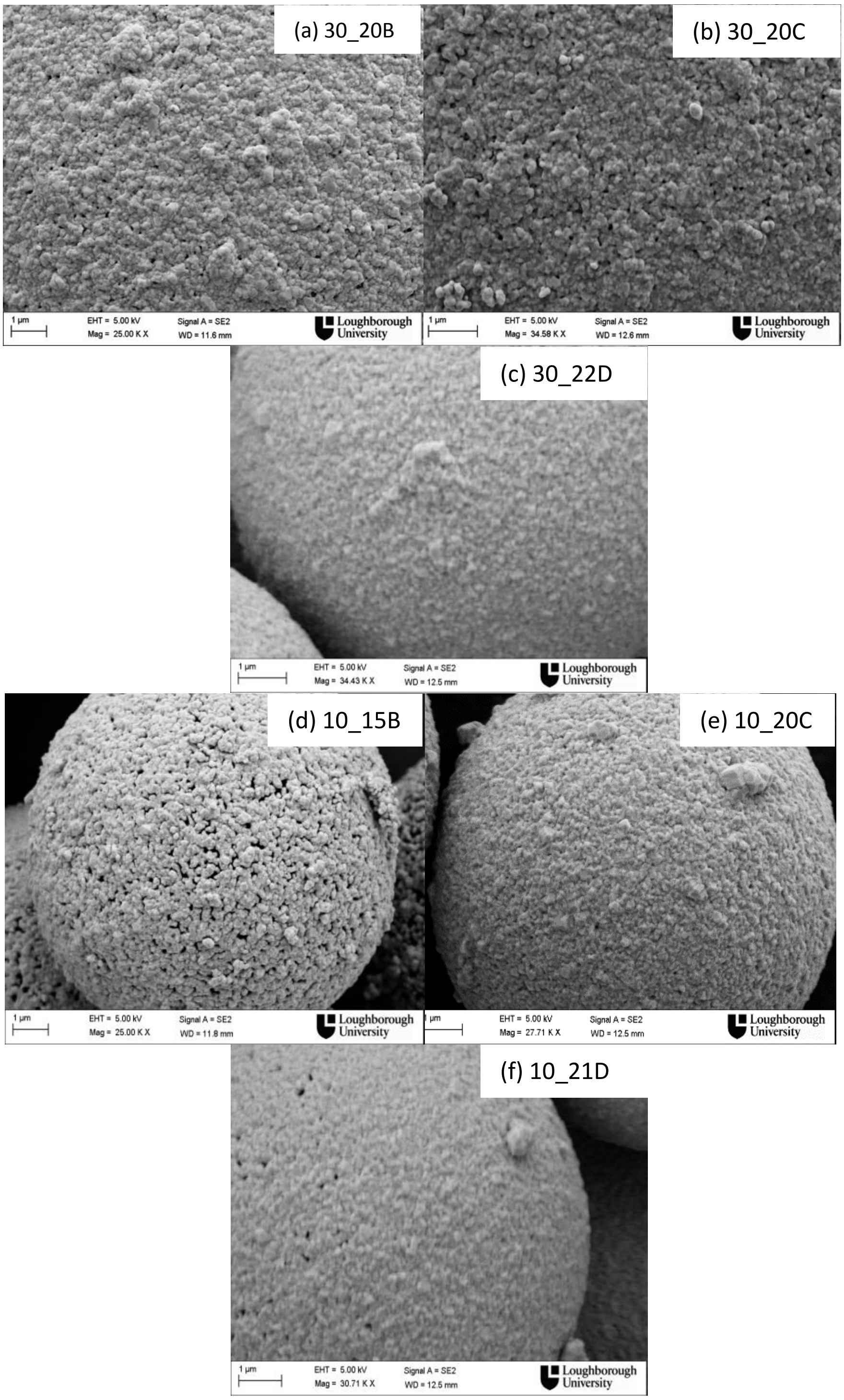

Figure 6.5 FEGSEM images of 10 and 30 µm Ag-MPS showing morphology of Ag coating due to plating process B, C and D

Table 6.3 Ag-MPS used for plating process comparison

Ag-MPS Diameter	Plating Process		
	B	C	D
10 µm	10_15B	10_20C	10_21D
30 µm	30_20B	30_20C	30_22D

To investigate the effect of coating morphology on the ICA conductivity for Ø 30µm, MPS 30_20B, 30_20C and 30_22D coated using the processes B, C and D respectively have been used. For MPS 30_20B, 30_20C, the type I resin matrix was used and the ICA was cured at 150°C for 15 minutes whereas for 30_22D, ICA samples were prepared in Norway by collaborators using the type II matrix and cured at 120°C for 30 minutes. Further, fresh samples were prepared for each vol% in Norway as compared to the procedure of further adding particles to the previously mixed vol%, as was used in the other experiments. To cure the type II samples a Termaks TS 8136 oven was used. The oven was preheated to the curing temperature and then the samples were placed in it. A Keithley 3706 System Switch/Multimeter was then used to measure the resistances. Figure 6.6 shows the averaged results from the resistivity measurements for ICAs formulated at different volume fractions, together with one standard deviation error bars

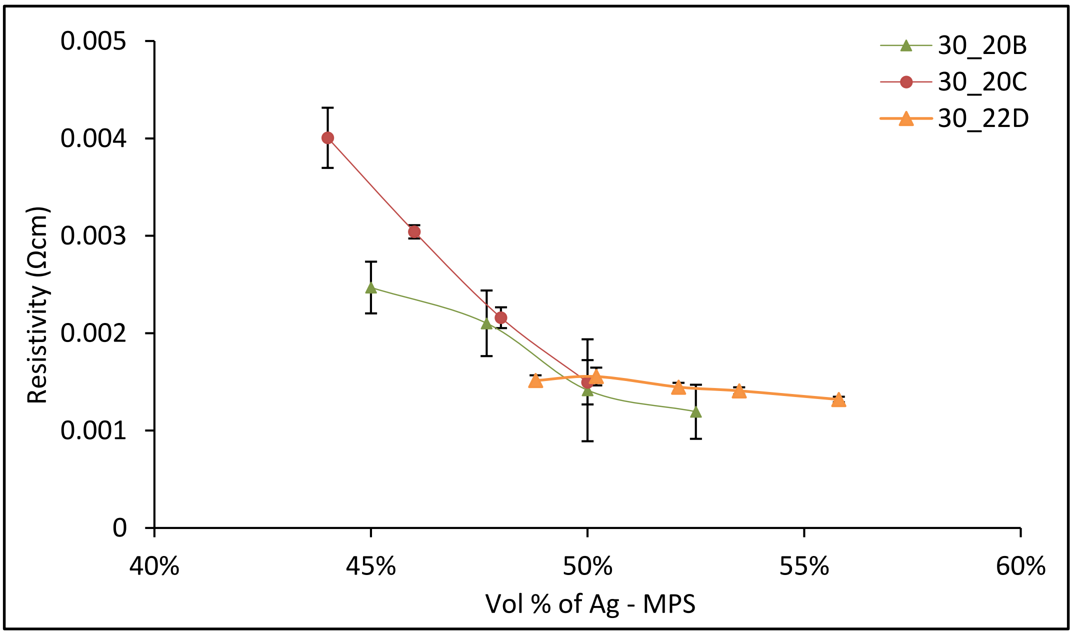

Figure 6.6 Effect of plating process B, C and D on resistivity for 30 µm Ag-MPS

Only small differences in the average resistivities for ICAs made using 30 µm MPS plated with different plating processes were observed. Above 50 vol% MPS made using plating process D produced slightly higher resistivity ICAs compared to those plated using process B and C although they have a thicker coating (0.22µm) compared to other two (0.20µm). The coating morphology on all 30 µm MPS looks similar, and apart from coating thickness and plating process the other difference is the different adhesive matrix and curing conditions. Different the adhesive matrix and curing conditions may induce different shrinkage and hence may impart different resistivity. Additionally, it can be observed that for 30_22D, ICA resistivity remains more constant with increasing vol% of filler. The reason may be that increase in the MPS vol% lead to increase in number of contact resistances which may compensate the effective decrease in resistance with increase in volume fraction of filler. Further, below 48 vol%, some difference between the average electrical resistivity of ICAs formulated using 30_20B and 30_20C can be seen, while at and above 48 vol% negligible differences can be seen. Below 48 vol% the MPS would be more loosely packed, which might be one of the causes for the differences in the resistivities of these two ICAs.

The effect of the Ag coating morphologies resulting from plating processes B, C, and D on the ICA resistivity for ICAs containing 10µm MPS has also been investigated. The Ag-MPS used were 10_15B, 10_20C and 10_21D. For 10_15B, the type I matrix was used and the ICA was cured at 150°C for 15 minute whereas for 10_20C and 10_21D, ICA samples were prepared in Norway by collaborators using the same conditions as for 30_22D described above. Figure 6.7 shows the averaged results from the resistivity measurements for ICAs formulated using 10µm MPS at different volume fractions, together with one standard deviation error bars. The results plotted in Figure 6.7 show no difference in the average resistivities of the ICA formulated with MPS 10_20C, 10_21D whereas higher average resistivities can be seen for ICAs formulated using 10_15B. Reason for the similar average resistivities of MPS 10_20C and 10_21D could be their similar coating morphologies as can be seen in Figure 6.5, and a minor difference in coating thickness whereas reason for higher average resistivities for ICAs formulated using 10_15B could be their thinner and more porous coating. Further, the ICA using 10_15B was formulated using different matrix and curing conditions compared to other two. The difference in the matrix and the curing conditions may also affect the ICA resistivity. In addition, different vol% for the ICAs using 10_15B were formed by adding the particles to the previously mixed vol%, this may affect their curing and hence final shrinkage and resistivity. However, for ICAs containing 10_20C, 10_21D fresh samples for each vol% were prepared. It should be noted that the graph for 30_20C finishes before 30_20B and 30_22D in Figure 6.6 and the graph for 10_20C finishes before 10_15B and 10_21D in Figure 6.7. This is because a printable mixture could not be obtained for these ICAs above 50 vol%. The coating has previously been shown to affect rheology when the filler concentration is above 45 vol% (Nguyen et al. 2013), though coating morphology on all 30μm Ag-MPS looks similar as can be seen in the FEGSEM images in Figure 6.5 (a) to (c), however there may be some differences in the coating morphology that could not be quantified using the FEGSEM images.

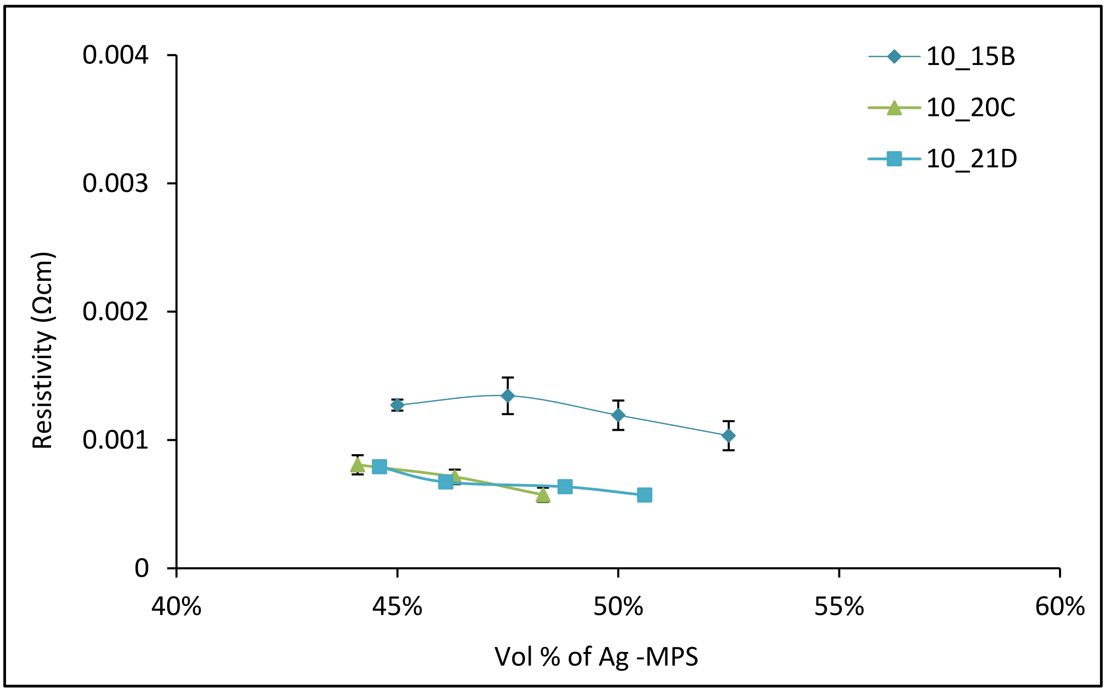

Figure 6.7 Effect of plating process on resistivity for 10 μm Ag-MPS

The results presented in this section have shown that MPS coated using different plating process B, C and D show similar resistivities when the morphology of the coating is same. In addition to the coating plating process and morphology, the adhesive matrix, curing conditions and the mixing procedure can also affect the ICA resistivity.

6.1.4.4 Effect of Silver Content

The previous sections have shown that as the amount of silver on an Ag-MPS increases, the resistivity of ICAs formulated using it decreases, however it may not be in proportion to the increase in the amount of silver. This section summarises the effect of the silver content on the ICA resistivity. Figure 6.8 shows the averaged results from the resistivity measurements for all of the ICAs formulated in this study. The volume fraction of silver is calculated corresponding to the volume fraction of Ag-MPS used. Figure 6.8 also compares the resistivity of the ICA samples at similar volume fraction of silver and with the bulk Ag resistivity at those volume fractions of silver. Figure 6.9 compares the averaged resistivity for these ICAs at the vol% of silver corresponding to a 50 vol% of Ag-MPS. The main reason for only highlighting 50 vol% is that the variation in resistance between samples is small at this vol% and all formulations had attained minimum resistivity by this vol%, while some MPS could not be processed at higher vol%.

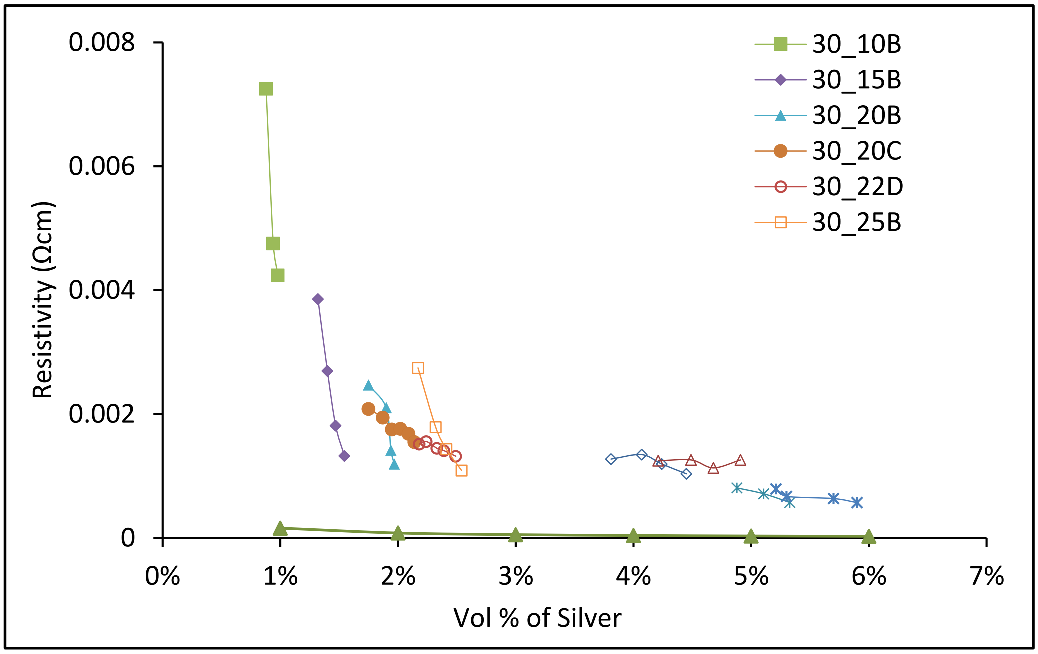

Figure 6.8 Resistivity vs silver content for all samples and bulk Ag

It is apparent from Figures 6.8 and 6.9 that as the amount of silver in the ICAs increases the resistivity decreases. Figure 6.8 shows that for a small increase in vol% of silver comparatively large reductions in ICA resistivity can be obtained with 30 µm Ag-MPS whereas for larger increases in vol% of silver, the ICA resistivity remains nearly constant when using 6 and 10µm Ag-MPS. This indicate that if the rheology of the matrix could be modified to accommodate a greater vol% of 30µm Ag-MPS, lower resistivities comparable to that obtained with 6 and 10µm Ag-MPS, could be obtained but at a lower vol% of silver. It can also be noted that the smaller spheres utilise considerably more silver than the larger 30µm spheres to provide only slightly lower resistivity i.e. they did not give a decrease in resistivity proportional to the rise in the silver content showing that the larger spheres with a thick silver coating use the silver more efficiently.

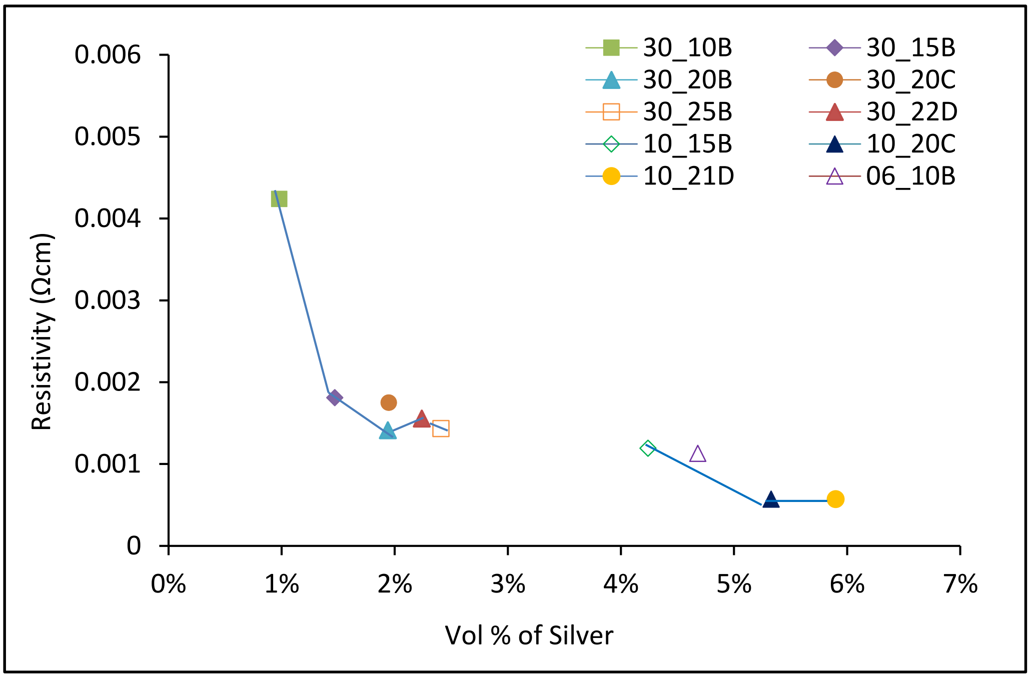

Figure 6.9 Resistivity vs silver content corresponding to 50 vol% of Ag-MPS

This should offer lower cost where the very lowest resistivity is not needed. In addition to cost benefits, when less Ag is used the vol% of polymer in the ICA increases, and thus the mechanical properties of the polymers may dominate than the metal. Moreover, Ag-MPS with less Ag have lower densities, more similar to the epoxy matrix which will help reduce the effect of sedimentation during storage. Figure 6.8 also show that the more thickly coated spheres uses more silver to provide a lower resistivity ICA as compared to spheres with a thinner coating. However, if the Ag-MPS size is kept constant, not much difference in the resistivity values for ICAs formulated using Ag-MPS with 0.20µm and thicker coatings has been observed i.e. 10_15B and 30_15B have higher resistivities but all of the other 10µm and 30µm MPS having coating thickness equal to 0.20µm or above have similar resistivities. Further, ICA formulated with 10_15B uses less silver than with 06_10B but show lower resistivity. All these examples show that apart from the silver content the quality of the MPS coating also plays an important part in determining the conductivity to an ICA. The Figure 6.8 also shows that the resistivity of the Ag-MPS filled ICAs is higher than the bulk Ag resistivity for the same amount of Ag used. This shows that the silver is not very efficiently used in these MPS to obtain lower resistivity. The reasons for this higher resistivity of ICAs compared to same vol % of bulk Ag could be (i) the contact resistance between MPS; and (ii) morphology of Ag coating on MPS. As the coating is made up of coalescing of the large number of Ag grains. This may lead to increase in Ag coating resistivity and hence the ICA resistivity.

6.1.4.5 Effect of Curing Conditions and Polymer Matrix

The effect of two different types of epoxy matrix and two curing profiles, i.e. 120°C for 30 minutes and 150°C for 15 minutes, was been investigated. In this investigation the time taken to cure the ICAs at 120°C and 150°C was purposely kept higher than recommended by the manufacturer for these temperatures. Thus it is assumed that for the curing schedules used, the epoxy was fully cured. As noted earlier the epoxies used are denoted as type I and type II. Both of the epoxies do not contain any viscosity reducing additives, solvents or diluents but type II less viscous. For this investigation the 30μm MPS, 30_20C was used. Figure 6.10 shows the averaged results from the resistivity measurements at different volume fractions, together with one standard deviation bars for the ICAs formulated. Figure 6.10 shows that the ICAs made with the type II adhesive matrix offer a lower average resistivity for up to 50 vol% of spheres, as compared to the type I adhesive. This indicates that the type of adhesive matrix in addition to the particles may also affect ICA electrical properties.

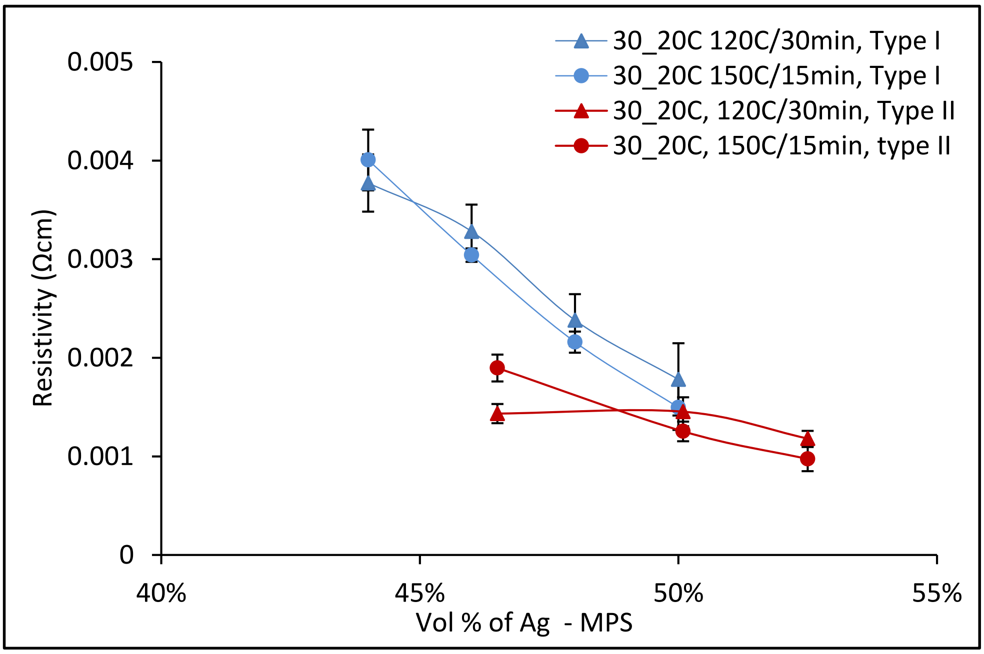

Figure 6.10 Effect of curing condition and adhesive matrix on resistivity

In addition, it has been observed that for the type II adhesive, a homogeneous and printable mixture can be obtained for up to 53 vol% of filler, whereas using type I adhesive it is difficult to get a homogenous mixture above 50 vol%. Further, from Figure 6.10 the average resistivity values are found to be lower for the ICA cured at 150°C for 15 minute than for ICA cured at 120°C for 30 minute, however the difference is quite small.

One factor anticipated to contribute to the effect of polymer matrix and curing profile on the resistivity of ICAs formulated in this investigation, is the resulting shrinkage (Kohinata et al. 2014) and a detailed investigation of this was carried out, as presented in the section below. It is well known that different thermosetting polymer matrices shrink by different amount (Lu et al. 2000), and that curing conditions can affect this shrinkage (Petrie 2006; Edward 2008). The type and volume fraction of filler can also affect the actual (observed) shrinkage of an ICA. The effect of polymer matrix, curing conditions and volume fraction of filler on the shrinkage of ICAs filled with Ag-MPS is presented in the following section.

6.2 Volume Shrinkage

Lu et al. (2000) proved that intimate contact between conductive filler particles caused by shrinkage during curing was the main mechanism for establishment of conductivity in isotropic conductive adhesives (ICAs). They investigated the changes in dimension (i.e. cure shrinkage) of three different ICA formulations (whose resins had different cure shrinkages) filled with an uncoated Ag powder and correlated them with establishment of conductivity. From this study, they concluded that (i) conductive adhesives achieved high conductivity only when enough cure shrinkage was achieved; and (ii) ICAs with higher cure shrinkage showed higher conductivity. In another study Su (2006) also established that ICAs formulated using resins with higher cure shrinkage showed higher conductivity. Therefore it is important to understand the effect of ICA shrinkage on the conductivity of Ag-MPS filled ICAs.

Lu et al. (2000) used a thermo-mechanical analyser (TMA) to measure dimensional changes in an ICA paste during curing. In the setup used by Lu the dimensional changes with temperature in the vertical direction were measured by TMA, however a small change/expansion in the lateral direction, because of flow of the ICA during curing, was not measured. Thus, this method was not considered suitable to measure changes in volume accurately during curing. On the other hand, Su (2006) used measurements based on Archimedes' principle to establish the shrinkage of an epoxy during cure. In this experiment a small amount of unfilled epoxy was placed on a thin polytetrafluoroethylene (PTFE) film, and the epoxy together with the film was immersed in a beaker filled with mineral oil. The mineral oil was then heated on a hot plate to 150°C. The apparent weight of the epoxy resin in air, and in oil before and during the curing was measured by attaching the PTFE film to a digital balance by a thin string. The volume shrinkage of the epoxy resin was calculated by measuring the change in the buoyancy force for the epoxy in the oil. However, in this experiment the epoxy was in direct contact with mineral oil during curing, and chemical interactions between the epoxy and mineral oil may have affected the epoxy shrinkage and was not taken into account in shrinkage calculations. Thus the method adopted by Su may not be suitable for measuring changes in ICA paste volume accurately during cure. Therefore, a new method which can measure the change in volume of an ICA paste accurately after curing is needed.

In this study a non-contact measurement technique using an Alicona InfiniteFocus, IFM G4 (IFM), was used to measure the change in volume due to cure shrinkage. This system is based on the focus variation principle, which combines the small depth of focus of an optical system with vertical scanning. By analysing the variation of focus for each surface point during the scanning process the height of each point is obtained. In addition to the height information, the device also provides true colour information for each measurement point, which is registered to the height data. Another important aspect in the context of measurement is that the system is able to measure very steep surface flanks of 80° (Danzl et al. 2009). With this technique changes in volume can be accurately measured based on dimensional changes both in the vertical and lateral direction. The details of these experiments are given below.

6.2.1 Materials

ICAs formulated with different combinations of filler, matrix and curing conditions, to test the effect of filler volume fraction, filler type, matrix type and curing conditions on the ICA shrinkage are described in Table 6.4.

Table 6.4 ICAs used for volume shrinkage measurement

Filler	Polymer matrix	Vol % of Filler	Curing Temp, Time	
30_20B	Type I	40, 47, 50, 52	150°C, 15 min	
30_20C	Type I	44	150°C, 15 min	120°C, 30 min
30_20C	Type II	46, 50, 52	120°C, 30 min	150°C, 15 min
FS34	Type I	21	150°C, 15 min	
FS34	Type II	21, 23	120°C, 30 min	150°C, 15 min
H20E	-------------	31	120°C, 30 min	150°C ,15 min

To formulate these ICAs the same method as described in Chapter 3 was used. Highly specular and transparent surfaces are very difficult for the IFM to capture the high data from the images of the object. This can result in certain data points of the image not being properly recorded. Thus to capture a full set of data points in the image, objects with opaque surfaces and with a small degree of roughness are required. However, if the object surface is too rough the peaks and valleys in the surface can also interfere with the measurement. Therefore, steel plates polished to an optimal smoothness (such that it does not affect the volume measurement) were used as the substrates onto which ICAs were printed.

6.2.2 Equipment Used

Figure 6.11 shows the IFM used to measure the volume of the printed ICA. This system can be equipped with objectives of different magnification ranging from 2.5X to 100X. A fixture was used to hold the steel substrates, ensuring that they did not move on the base stage.

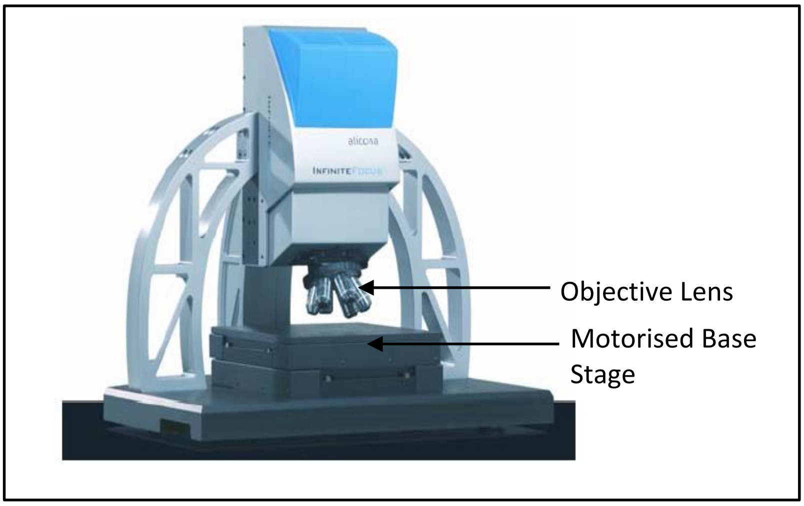

Figure 6.11 Alicona InfiniteFocus laboratory system

6.2.3 Methodology

6.2.3.1 Sample preparation

To prepare samples for volume measurement, small circular dots of the formulated ICAs were printed onto steel substrates using a 90 μm thick plastic stencil with a 1.25mm diameter opening.

6.2.3.2 Volume Measurement

The following procedure was used for the volume measurements:

(i) The sample was mounted onto the fixture;

(ii) A position on the motorised base stage of the IFM was selected and marked;

(iii) The fixture holding the sample was placed on the marked position on the motorised base stage. For all measurements the same position was used to place the fixture. This was to make the procedure consistent for every measurement and reduce the probability of error in the measurements due to set up of the equipment;

(iv) The sample was then illuminated with white light to obtain a dense 3D surface representation of the object in the form of a 3D dataset. In this case, the objective lens with 5X magnification was used from the interchangeable objectives to both provide illumination and obtain the 3D dataset. It has a field of view of 2.8 mm x 2.2 mm approximately. An in plane resolution of 7.36 μm and a vertical resolution of 552 nm were selected. At this resolution the system was able to measure the volume to a resolution of 3.0 x 10^{-8} mm^3 combined with high speed;

(v) After acquiring the 3D dataset, volume calculations were performed. To measure volume, a specific area of the image is selected on the volume measurement screen. Great care was taken to select the same area for both cured and uncured samples for a given ICA. The red rectangles in Figure 6.12 show examples of area selection on the volume measurement screen where the same area was selected for both cured and uncured samples; and

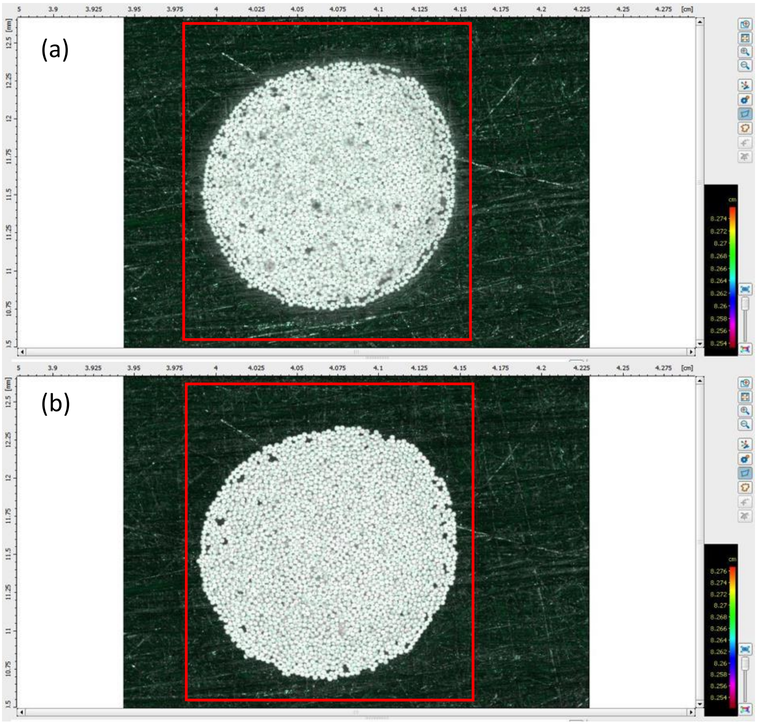

Figure 6.12 Volume measurement screen showing area selected for volume measurements (a) uncured ICA formulated with 30_20C Ag-MPS in type I epoxy matrix (b) same ICA cured at 150°C for 15min

(vi) Before conducting the volume measurements, it is important to calculate the number of samples required that are statistically significant. In this study to establish the 99% confidence level, the sample size was calculated using the formula (Moore 2004) :

$$\textit{Sample Size} = \frac{\textit{Standard deviation x } Z_{\alpha/2}}{\textit{Margin of error}} \qquad \textbf{6.2}$$

where $Z_{\alpha/2}$ is the critical value of the standard normal distribution. For a 99% confidence level, $Z_{\alpha/2}$ is 2.56 and the margin of error is 0.01. To obtain data to calculate the standard deviation five datasets were recorded for the same sample using steps (iii) and (iv), where the sample was removed from the IFM and replaced between each measurement. Then for each dataset ten volume calculations were performed using step (v). From these measurements the standard deviation was calculated to be 0.000652 (see Appendix 2). For a 99% confidence level and the measured standard deviation, Equation 6.2 gave the sample size to be less than 1, therefore in the following experiments only one sample per volume measurement was used and five volume measurements were taken for each, both before and after curing of the ICA samples. The averages of these five measurements were then used for the volume shrinkage calculations. Volume shrinkage is calculated as:

$$\%\,\boldsymbol{Volume\ Change} = \frac{\boldsymbol{Vol\ of\ cured\ ICA - Vol\ of\ uncured\ ICA}}{\boldsymbol{Vol\ of\ uncured\ ICA}}\ \boldsymbol{x\ 100\%} \qquad \mathbf{6.3}$$

A negative volume change corresponds to volumetric shrinkage upon curing.

6.3 Results and Discussion

Both the unfilled resin and hardener system and the ICAs containing a volume fraction of filler near to the percolation threshold have shiny surfaces. As discussed above, a full set of 3D data points representing the surface could not be recorded from such shiny surfaces, thus volume measurements on these samples could not be made. At volume fractions of Ag-MPS above 40%, the ICA surface texture becomes matte and volume measurements were successfully completed. The averaged volume measurements of the uncured and cured ICA samples together with one standard deviation error bars, for the different volume fractions of 30_20B MPS in type I epoxy are plotted in Figure 6.13 (a) and the corresponding % volume changes calculated using Equation 6.3 are plotted in Figure 6.13 (b). These ICAs were all cured at 150°C for 15 minutes.

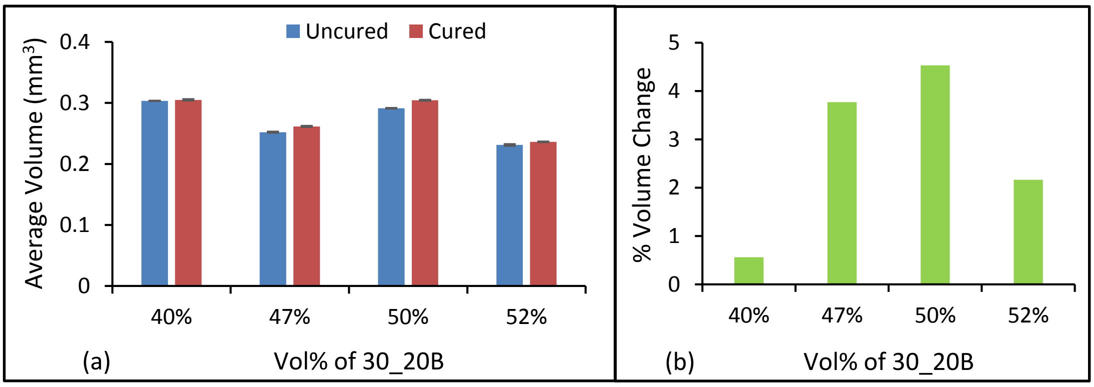

Figure 6.13 (a) Average volume of cured and uncured ICA at different vol% of 30_20B and (b) % volume change

The results plotted in Figure 6.13 all show an increase in volume, i.e. volumetric expansion following curing. This is an unexpected behaviour compared to traditional ICAs, where only volume shrinkage during curing has been reported in the literature. This is an important observation, as it may have a significant effect on the conductivity of ICAs formulated with Ag-MPS, as it will effectively increase their volume fraction and may force the neighbouring MPS into contact enhancing the contact area and reducing the contact resistance. For the 40 vol% sample the volume change is very small, close to the standard deviation, but for the other samples the volume change is well above one standard deviation (can be seen in Appendix 2). The results plotted in Figure 6.13 shows that the volume expansion increases up to 50 vol% of Ag-MPS but decreases for 52%, a non-consistent trend in volume expansion with increasing volume fraction of MPS.

The curing process can be divided into three steps: (i) heating to the curing temperature; (ii) maintaining this temperature for a specific period of time; and (iii) cooling back to room temperature. When the ICAs are heated for cure, the polymer core of the Ag-MPS, Ag coating and the epoxy resin, begin to expand. However, when the curing temperature is reached, the epoxy begin to shrink with the onset of curing, whereas the polymer core of the Ag-MPS and Ag coating is still expanding. The Ag-coating will expand less compared to the polymer core. Moreover, the polymer core is made of an amorphous polymer (Redford 2011), and typically such polymers have a thermal expansion much higher above T_g than below T_g (Brown 1999; Petrie 2006). Thus during curing process both Ag-MPS and epoxy matrix are under continuous volumetric stress that is generated because of the epoxy matrix shrinkage and relative expansions of polymer core, Ag coating and the epoxy matrix. When the temperature is maintained constant for some time, during that period of time the epoxy gets fully cured and the shrinkage of the epoxy due to crosslinking attains a constant value, but both the epoxy and Ag-MPS can still be expanding due to constant supply of thermal energy, however the expansion of epoxy will be very small compared to in uncured state. When the ICA is cooled to room temperature both the Ag-MPS and the epoxy begin to shrink. Thus, the total volume change will depend upon the thermal expansion, elastic modulus of the polymer core, Ag coating and epoxy, and the epoxy shrinkage.

Rule of mixtures which assumes that the volume change of a composite as the combination of the volume change of the filler and the matrix in relation to their proportions can give the volume change of an Ag-MPS filled ICA as:

$$\frac{\Delta\phi_{ICA}}{\phi_{ICA}} = \left(\frac{\Delta\phi_{Filler}}{\phi_{Filler}}\right)(\boldsymbol{vol.fraction\ filler}) + \frac{\Delta\phi_{Matrix}}{\phi_{Matrix}}(\boldsymbol{vol.fraction\ Matrix}) \quad \mathbf{6.4}$$

where $\Delta\phi_{ICA}$ and ϕ_{ICA} are the volume change and volume of the ICA sample , respectively (m^3) ;

ϕ_{Filler}, ϕ_{Matrix} are the volume of the filler and matrix respectively

$\Delta\phi_{Filler}$, $\Delta\phi_{Matrix}$ are the volume change of the filler and matrix respectively.

The volume change of filler upon increase in temperature can be written as:

$$\frac{\Delta\phi_{Filler}}{\phi_{Filler}} = (\alpha_{Filler}\Delta T) \qquad \textbf{6.5}$$

where α_{Filler} CTE of filler (m/m/°C); and

ΔT is temperature change (°C);

The matrix volume can be assumed to be shrunk by 3.6 % as obtained by (Redford et al. 2012) for cure schedule 100°C for 20 min, though for higher cure temperature it may shrink more. The filler 30_20B is largely made of polymethylmethacrylate (PMMA) with only 3.9% of silver (as stated in Table 6.1) in the form of plating, also the expansion of PMMA is more than silver, and the lower expansion of silver may also oppose the expansion of the PMMA. Therefore using α_{Filler} equal to CTE of PMMA as 70-77 x 10^{-6}/°C (Goodfellow 2014) in Equation 6.5, to calculate filler volume change, would give the value for maximum possible volume expansion due to filler. The relative elastic moduli of PMMA, Ag coating and epoxy, under the shrinkage stress may also oppose the expansion of the polymer core. Using these above specified values for volume change of filler and resin, the ICA volume change at all the volume fraction of 30_20B Ag-MPS tested, were calculated using Equation 6.4 and is listed in Table 6.5.

Table 6.5 Measured and predicted values of ICA volume change when filled with Ag-MPS

	40%	**47%**	**50%**	**52%**
Measured Volume Change	0.0020	0.0095	0.0132	0.005
Predicted Volume Change (using Equation 6.3)	-0.0182	-0.0156	-0.0144	-0.0135

The results presented in Table 6.5 predicts that volume ICA would decrease upon curing. However, measurements show increase in volume. Moreover, in this experiment the observed volume change is not consistent. The reason for this variation could be the presence of an additional element, such as air trapped between the Ag-MPS, which expanded during curing. This air might have got trapped between the Ag-MPS during processing i.e. mixing and printing. A large number of air bubbles can also be seen in the FEGSEM image of the small section of an ICA sample (containing 50% of 30_20B) as shown in Figure 6.14. From Figure 6.14 the relative area taken by trapped air was calculated to be approx. 8.5 % using ImageJ software[1]. In this the relative air bubbles were calculated as a ratio of the dark grey/black to grey pixels which corresponded with the fraction of air bubbles over the total surface.

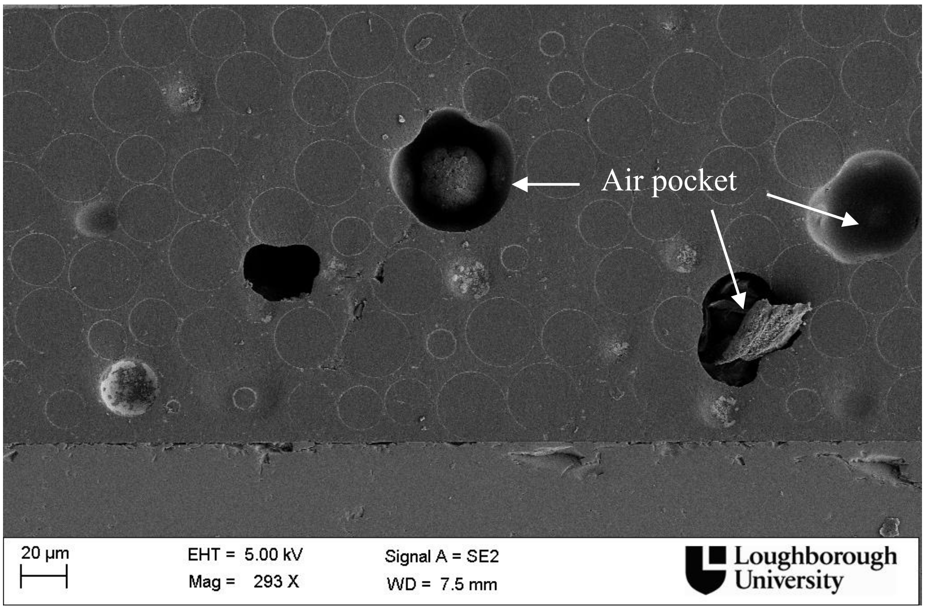

Figure 6.14 FEGSEM image of a cross-sectioned ICA sample filled with 50 vol% of 30_20B, showing trapped air

Assuming % area of trapped air is equal to the volume %, the resulting volume expansion during curing was estimated using the volumetric expansion of air between room temperature and cure, i.e. 4.9%. An estimated volume expansion of approx. 4.5% was obtained for ICA containing 50% of 30_20B as can be seen in Figure 6.13(b). The used FEGSEM image however, represent only a small section of a sample, there may be areas having less concentration of bubbles in the sample thus this calculation provides an estimate of max bubble density. As the proportion of trapped air would vary from

---

[1] The percentage of trapped air using ImageJ software was calculated by A. Thanos

sample to sample this may also explain the observed variation in volume expansion probably from sample to sample.

Further, to check whether the apparent volumetric expansion is because of trapped air, an uncured adhesive sample was placed under vacuum to expel the trapped air. This was done using a Medline Scientific OV-11 vacuum oven. However, when the pressure in the chamber was decreased below atmospheric pressure, the ICA sample started to foam up. The reason may be, as the pressure is lowered below atmospheric pressure, the air trapped boiled from the ICA and was pumped off, and when the pressure is lowered to the vapour pressure of the constituents of either resin system or MPS, they will also begin to boil off. This pumping out of the air or the constituents of the resin, when the pressure is lowered below their vapour pressures could be a reason for the foaming of the ICA. However, the material safety datasheet does not list all the constituents of the resin due to its propriety nature, thus it is difficult to verify the exact component causing the foam. But as the pressure is lower than the air pressure it could be that the air trapped inside the ICA samples is causing the ICA to foam. Table 6.6 lists the results of volume measurements on the ICA samples which were subjected to vacuum. The results show that after vacuum treatment at 50 mm of Hg, the volume of the uncured ICA filled with Ag-MPS reduced however, this reduction is small (0.5%) and within the uncertainty of the measurement, moreover when this sample was cured its volume still increased by 1.6%.

Table 6.6 Volume of the Ag-MPS filled ICA sample before and after vacuum treatment

	47 vol% Ag-MPS		
	Average Volume (mm^3)	**Standard Deviation**	**% Volume Change**
Uncured Before Vacuum Treatment	0.3477	0.0007	------
Uncured and Vacuum Treated	0.3459	0.0010	- 0.5
Cured and Vacuum Treated	0.3536	0.0006	+1.6

Another option to expel any trapped air, would have been to use a centrifuge. However, the only centrifuge available required around 2 gm of adhesive for testing. As this amount of Ag-MPS filled ICA was not available, the centrifuge test was not carried out.

To further check if the observed volume expansion is because of the specific filler used i.e., 30_20B, or for the specific batch of resin, a volume shrinkage investigation was carried out on ICAs formulated with different fillers i.e. 30_20C and solid silver flakes. To further investigate the effect of the epoxy matrix and curing schedule, volume shrinkage of ICAs formulated with both types of epoxy matrix i.e., type I and type II were also carried out and compared with commercial ICA. The advantage of carrying out investigation with solid silver flakes is that its volume expansion would be negligible as compared to Ag-MPS and the actual volume change of the ICA system could be better assessed. The ICA samples investigated were cured at two curing schedules i.e. 150°C for 15 minutes and 120°C for 30 minutes. Appendix C, Section C.1 tabulates the results of the volume shrinkage measurements carried out in this chapter. Figures 6.15 (a) shows the average volume of the uncured and the uncured ICA formulated using 21 vol% of solid silver flakes in type I adhesive and cured at 150°C for 15 minutes and Figure 6.15 (b) shows the corresponding % volume change. Figures 6.16 (a) shows the average volume of the uncured and the uncured ICA formulated using different vol% of solid silver flakes in type II adhesive and cured at different curing conditions, and Figure 6.16 (b) shows the corresponding % volume change.

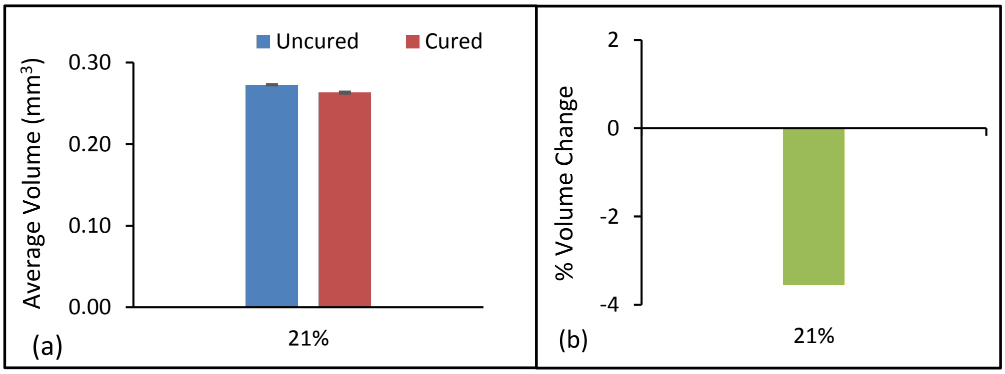

Figure 6.15 (a) Average volume of a cured and uncured ICA sample formulated using solid silver flakes in type I polymer matrix and (b) % volume change

Figures 6.15 and 6.16 show that for ICAs formulated with silver flakes:

(i) Volume shrinkage decreases with increasing volume fraction of filler. ICAs filled with 21 vol% of silver flakes show higher shrinkage than ICAs filled with 23 vol%.

(ii) Volume shrinkage increases with increasing curing temperature. ICAs cured at 150°C for 15 min showed higher shrinkage as compared to ICAs cured at 120°C for 30 min. However, it has been observed that for lower volume fractions of silver flakes the effect of curing temperature on volume shrinkage is more prominent as compared to a higher volume fraction.

(iii) For the same curing profile, ICAs made with the type II adhesive matrix exhibit more shrinkage (15.9 %) than those made with type I (3.5%).

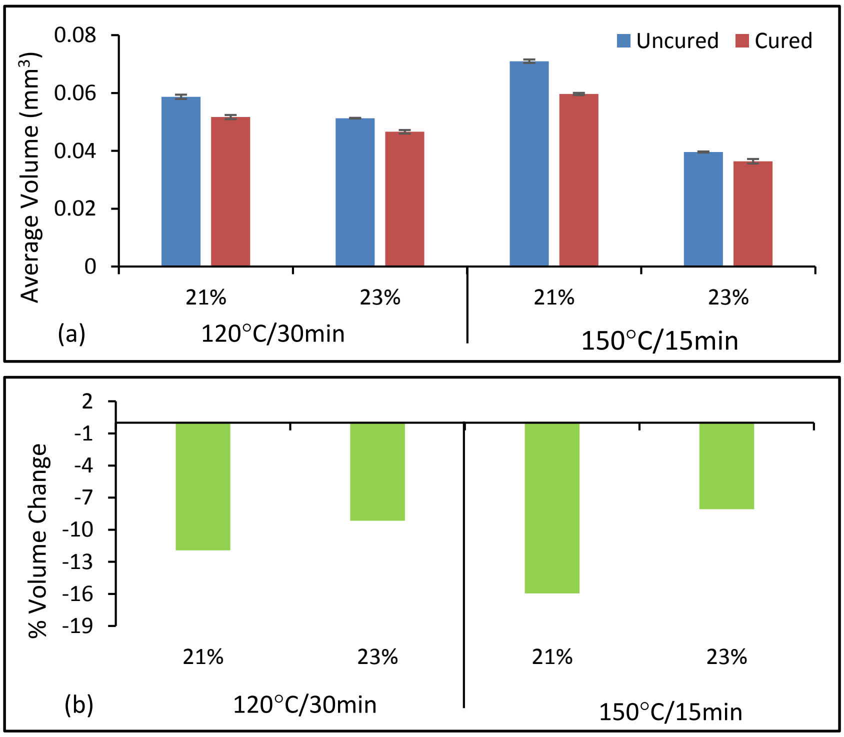

Figure 6.16 (a) Average volume of a cured and uncured ICA sample formulated using solid silver flakes in type II polymer matrix and (b) % volume change

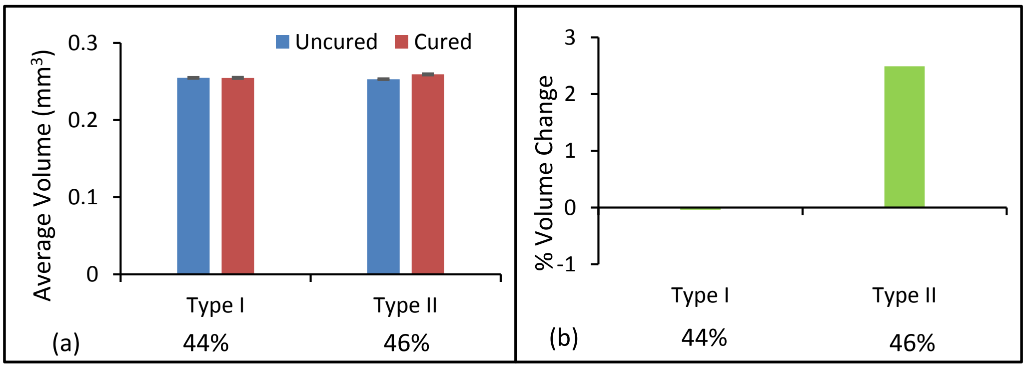

Figure 6.17 (a) Average volume of a cured and uncured ICA sample formulated using 30_20C in type I and II polymer matrix (b) % volume change

Figure 6.17 (a) shows the average volumes of the uncured and cured ICAs formulated using different vol% of 30_20C in type I and type II adhesive and cured at 150°C for 15 minutes while Figure 6.17 (b) shows the corresponding % volume change. Figure 6.18 (a) shows the average volume of the uncured and cured ICAs formulated using different vol% of 30_20C in type II adhesive and cured at different conditions, and Figure 6.18 (b) shows the corresponding % volume change.

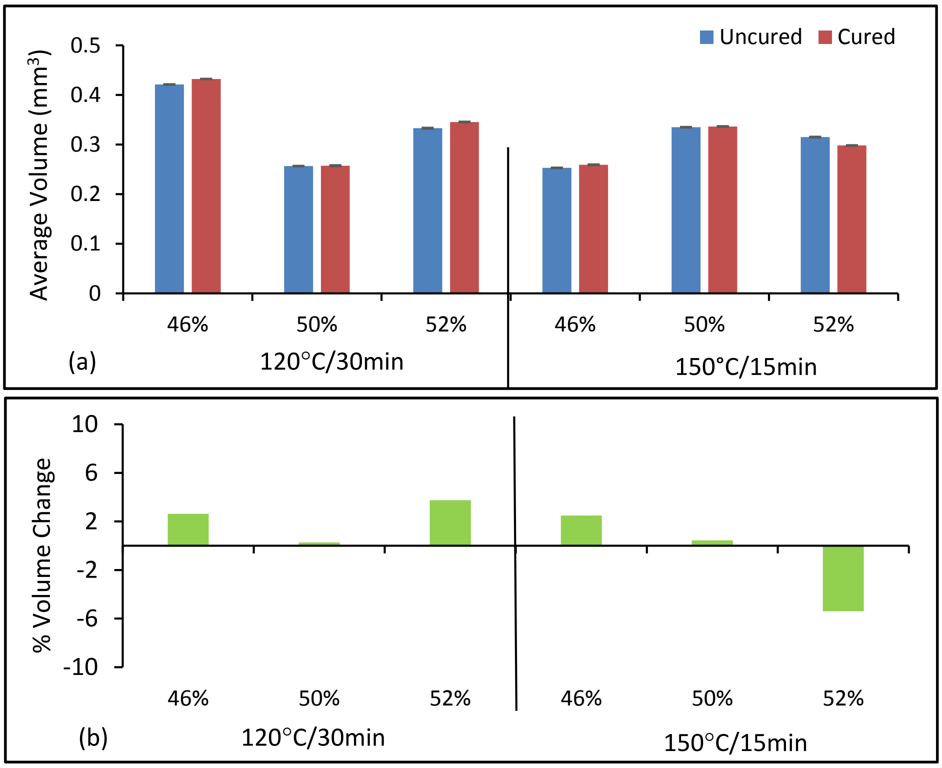

Figure 6.18 (a) Average volume of a cured and uncured ICA sample at different vol% of 30_20C in type II polymer matrix (b) % volume change

It can be seen from Figures 6.17 and 6.18 that:

(i) The ICA made using type II adhesive with 52 vol% of Ag-MPS showed volumetric shrinkage when cured at 150°C for 15 min whereas all other ICAs expanded upon curing,

(ii) Changes in volume do not follow a consistent trend with volume fraction of Ag-MPS or curing conditions.

The change in volume upon curing for H20E was also measured. Figure 6.19(a) shows the average volume of the uncured and the cured H20E at different curing conditions, and Figure 6.19 (b) shows the corresponding % volume change. It can be seen from

Figure 6.19 that H20E shrinks during curing. The decrease in volume was more for the sample cured at 150°C for 15 min compared to that cured at 120°C for 30 min. Figure 6.20 summarises all the results plotted in Figure 6.15 to 6.19 on one graph, it can be seen from Figure 6.20 that H20E shrinks more than all other ICAs tested. The composition of the type II matrix is different from both type I and from the matrix in H20E and thus H20E would expected to have different shrinkage. Type I and H20E contain a similar resin but in different quantities, further the quantity of the hardener is also different in both these matrices, thus due to different chemical components these matrices will have different curing reactions imparting different shrinkage. Moreover, it has been identified in Chapter 3 that H20E increases in conductivity suddenly at around 145°C. This could either be due to a surfactant on the flakes or due to a component of H20E, which increases shrinkage to enhance conductivity. Thus using a component which will enhance the shrinkage may enhance the conductivity (Lu et al. 2000).

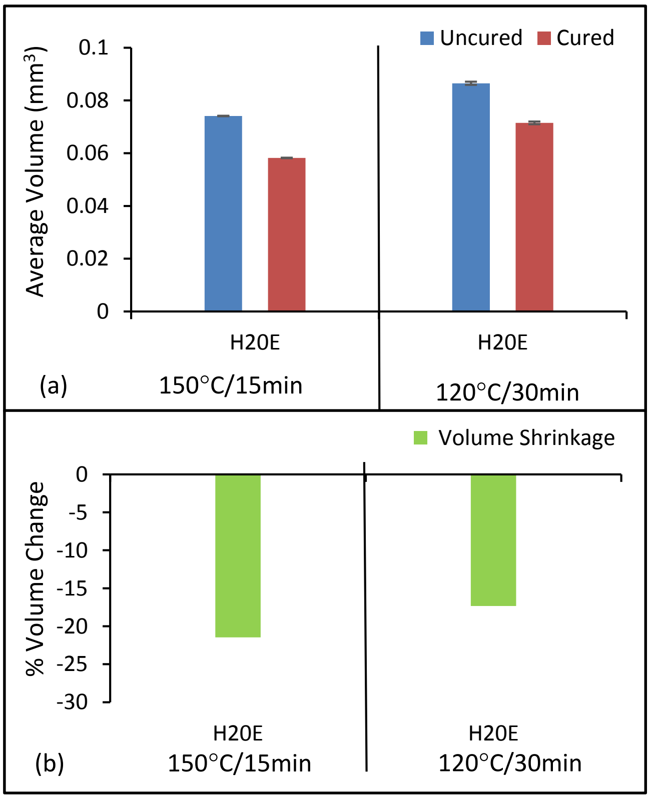

Figure 6.19 (a) Average volume of a cured and uncured H20E (b) % volume change

The volume measurements for silver flake filled ICAs show that the shrinkage depends upon volume fraction of filler, the curing conditions, and the type of epoxy matrix. However, the volume measurements on Ag-MPS filled ICA do not show any consistent trend for the dependence of shrinkage on filler volume fraction, curing conditions and

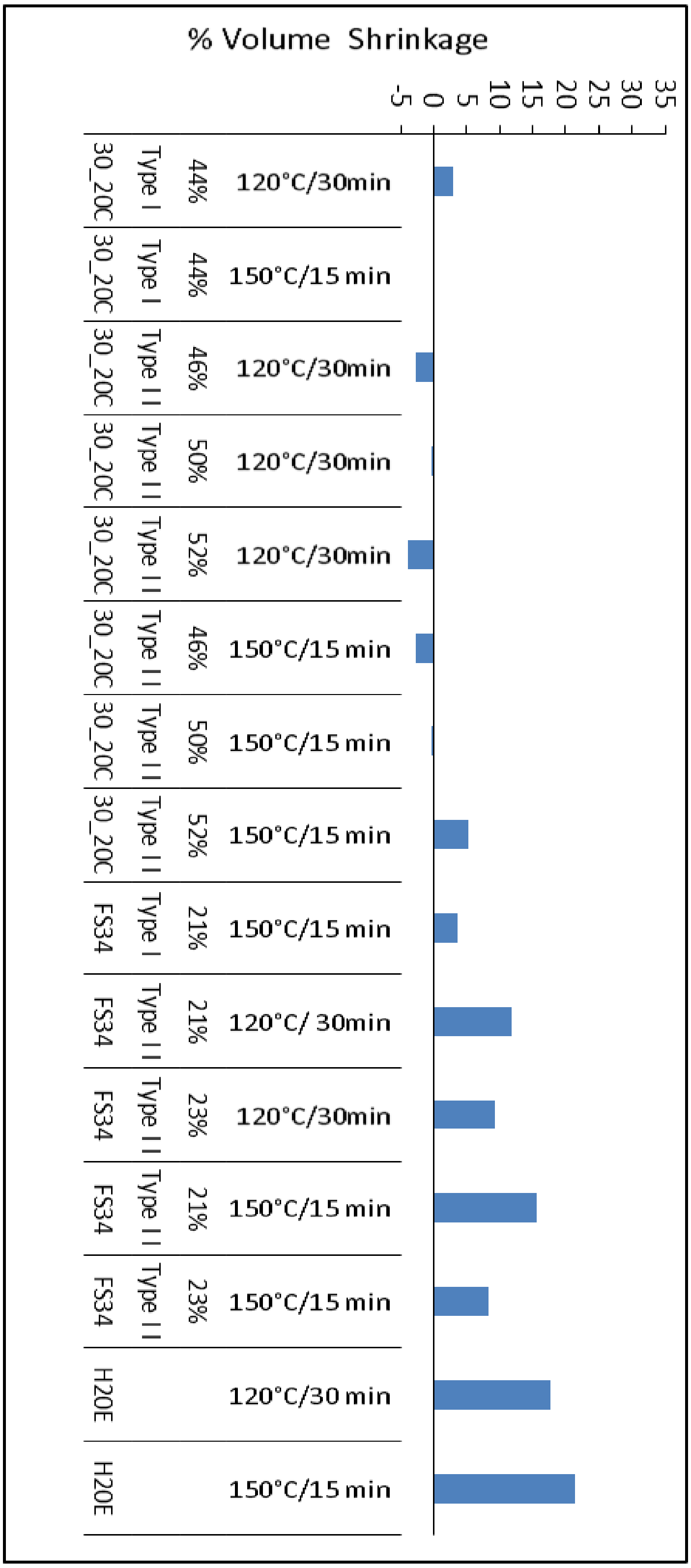

Figure 6.20 Summarises volume shrinkage of 30_20C, FS34 filled ICAs and H20E

the type of epoxy matrix. Further, the comparison of the volume measurements for silver flakes and Ag-MPS show that for same polymer matrix and curing conditions ICAs formulated with the silver flakes shrinks whereas the majority of the samples of

ICAs made using Ag-MPS expand. The observed shrinkage for flake filled ICAs indicates that both polymer matrices (type I and type II) do shrink on curing, and the observed volume expansion for the majority of ICAs formulated using Ag-MPS must therefore be because of factors such as (i) air trapped in the adhesive; (ii) expansion of the polymer core of the Ag-MPS; (iii) outgassing from MPS. However, it is difficult to quantify the effect of each factor and further detailed studies are required. The different volume changes for the silver flakes and Ag-MPS may indicate that ICAs containing Ag-MPS more readily traps air compared to silver flake filled ICAs. The silver flakes used were coated with surfactant to prevent aggregation and to aid their uniform dispersion, however the surface of the Ag-MPS is rough/porous and is not coated with any surfactants, and additionally the dry powder of Ag-MPS have been seen to aggregate into small clusters. The air can get trapped in these clusters and if not expelled on mixing then its expansion upon curing may affect the ICA volume shrinkage.

Another investigation of the volume expansion of ICAs filled with Ag-MPS after curing was carried out by Redford et al. (2012). Redford et al. used the same formulations of ICAs as used herein however, they measured the change in volume by measuring the density change, using a Pycnometer. They also observed volume expansion for Ag-MPS filled adhesive and volume shrinkage for neat adhesive. They also used a centrifuge to expel the air from the samples however, they found that it caused separation of the adhesive and the filler, and when the ICA was taken out from the centrifuge and remixed for printing, air again got trapped inside the ICA. The similar results obtained by Redford et al. using a different measurement method, increase confidence in the accuracy of the measurement methods used in this study, but still do not resolve the issue of the root cause of expansion during cure.

To establish the relationship between contact area, conductivity and the particle contact forces due to shrinkage for Ag-MPS filled ICAs and the effect of various factors such as volume fraction of Ag-MPS, curing profile and the type of matrix on shrinkage, further studies are needed which are beyond the scope of this thesis.

6.4 Concluding Remarks

The experimental results presented in this chapter go some way towards validating the conductivity model for ICA filled with MPS presented in Chapter 4. As predicted by the theoretical model the experimental results show that the conductivity of the Ag-MPS filled ICA increased with decreasing MPS diameter, increasing metal coating thickness and improved the coating morphology. However, the results also show that the smaller MPS do not give the increased conductivity in proportion to the extra silver they use. Further, the results show that the conductivity increases considerably with coating thickness up to 0.20µm but become nearly constant for a further increase in coating thickness where the morphology of the coating appears the same. The results show that larger MPS with a 0.20µm coating can offer greater benefits both in terms of cost and mechanical properties.

The results show that curing schedule and type of the epoxy matrix also affect the conductivity of the Ag-MPS filled ICA, but not to a large extent. Volume shrinkage was seen for only a few MPS containing samples whereas volume expansion was observed for most samples. Further studies need to be conducted to validate the effect of the contact area and the shrinkage force on the conductivity, however these are out of the scope of the present thesis.

The main aim of the study presented in this thesis is to investigate the electrical performance of ICAs filled with Ag-MPS. The electrical performance of an interconnection material is a combination of the volume resistivity (bulk material resistivity) and the contact resistance (interface resistance) to the conductors bonded to. The volume resistivity and the effect of various factors on volume resistivity received preliminary investigation in Chapter 3 and more detailed study in the present chapter. However, the effect of these factors on the contact resistance of Ag-MPS filled ICAs also needs investigation and is the focus of the next chapter. Further, studies on temperature dependence of resistivity of composite material has been shown to provide an insight the conduction mechanism of heterogeneous materials (Nicodemo et al. 1978). As the focus of this study is also to understand the conduction mechanism in an Ag-MPS filled ICA, thus experiments were conducted to investigate the dependence of the resistivity on temperature and the results will also be presented in the next chapter.

CHAPTER 7

OTHER ELECTRICAL MEASUREMENTS

Chapters 3 and 6 presented the effect of MPS volume fraction, diameter, Ag coating thickness, matrix type and curing conditions on ICA bulk resistivity, however how these factors affect the contact resistance between the ICA and the component or substrate terminations is also important. This chapter presents an investigation into the effect of these factors on ICA contact resistance. As discussed in Chapter 4, electrical conduction in an ICA takes place through contacting metallic filler particles, thus current encounters metallic resistance offered by the particles and the constriction and tunnelling resistances offered by the contacts. The effects of temperature on metallic resistance are different from those on constriction and tunnelling. Thus the variation of ICA resistance with temperature may give some insight into the conduction mechanisms within ICAs and an investigation of this is also presented in this chapter.

7.1 Contact Resistance Measurement for ICAs

The measurement method used for the previously presented resistance results (FWR) is designed to eliminate any contact resistances from the measurements. The contact resistance was measured by combining the existing FWR results from the samples described in Chapters 3 and 6 with a three wire resistance (TWR) measurements on the same samples. Figure 7.1 show a schematic of the TWR measurement method. In this method, one pair of the current and the voltage probes were placed on the same probe pad, so that the contact resistance between the adhesive stripe and the contact track joining to the probe pad, where current and voltage probes were placed together, was also included in the resistance measurement. The contact resistance between the adhesive and the track connected to the pad with the current and voltage probes was then calculated as:

$$\boldsymbol{Contact\ resistance = TWR - FWR} \qquad \mathbf{7.1}$$

In this experiment the contact resistance was measured to the gold PCB metallisation. The use of the same samples for FWR and TWR has enabled a comparison of volume resistivity/bulk resistance with contact resistance. For each sample, contact resistance measurements on both left and right contacts on each ICA stripe were made. In the TWR measurements the resistance of the small length of contact trace between contact with the ICA and the inner probe pad, where both the current and voltage probes are placed is also included. The estimated resistance of this track is ~ 0.0079 Ω, (details of calculation are given in Appendix C, Section C.2) and is subtracted from the measured contact resistance values.

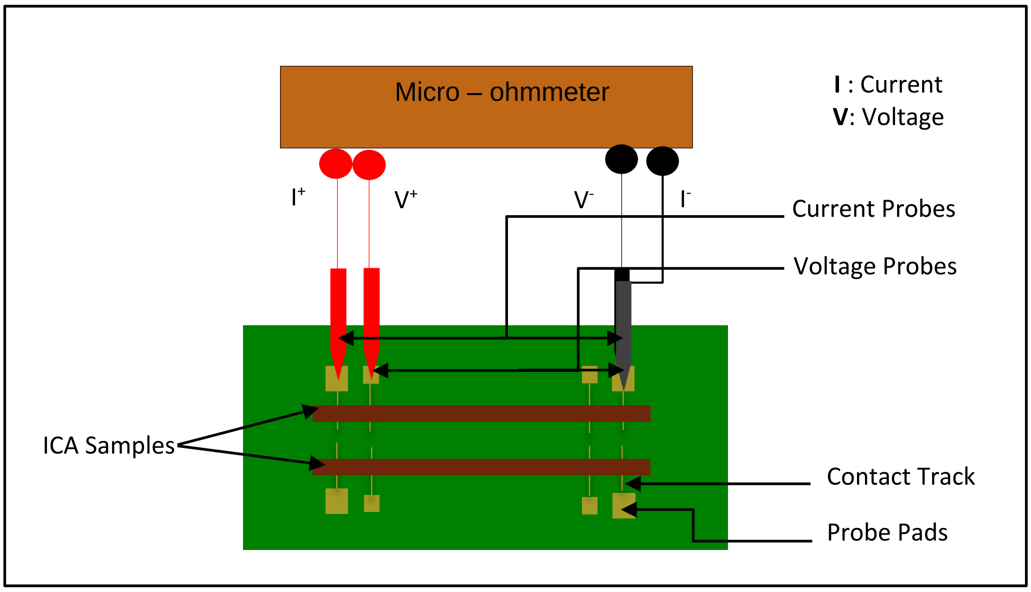

Figure 7.1 Schematic of three wire resistance measurement

7.2 Results and Discussion

The results of the contact resistance measurements are plotted in Figures 7.2, 7.3 and 7.4, with one standard deviation error bars, where each contact resistance value corresponds to the arithmetic mean of eight to twelve measurements. To investigate the effect of filler shape, the contact resistances of the Ag-MPS filled ICAs are also compared with the contact resistances of both the commercial (H20E) and FS-34 flake filled ICAs. The following sections discuss the results obtained.

7.2.1 Effect of Shape of Filler, MPS Diameter and Volume Fraction

Figure 7.2 presents the variation of contact resistance with the MPS diameter and volume fraction and type of filler. It presents the contact resistance values for ICAs made using the 4.8_15A, 06_10B and 30_13A, Ag-MPS and silver flakes all within the type I polymer matrix and cured at 150°C for 15mins. It also presents the contact resistance values for H20E. The results of contact resistance measurements were also compared with the volume resistivities of these ICAs and are presented in Appendix C, Section C.2.

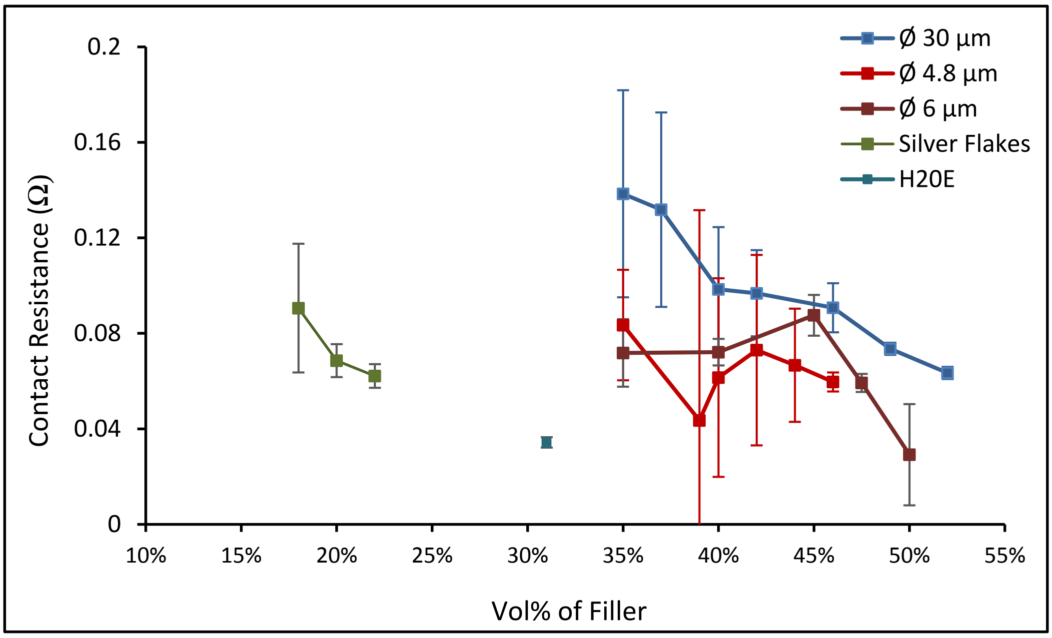

Figure 7.2 Contact resistance variation with filler volume fraction, size and type

These results show a general trend of the contact resistances decreasing with increasing vol% of filler, however at lower volume fractions large variability in the contact resistance for all ICAs can be observed. The results presented in Figure 7.2 also show that at low vol% the contact resistances of the ICAs tend to decrease with decreasing MPS diameter, however at the larger vol% not much variation in the contact resistances with MPS diameter was seen i.e. at the highest volume fraction all of the MPS gave the same contact resistance of around 0.058Ω. There is some variation in the Ag coating thickness between these MPS. At lower vol% ICAs filled with 06_10B show lower average contact resistance than those containing 4.8_15A. As these volume fractions are close to the percolation threshold, large variations in particle distribution may be the reason for this inconsistency. These results show that at high volume fractions, MPS diameter and Ag coating thickness do not have a significant effect on the contact resistance of an ICA. On the other hand it can be observed from Chapters 3 and 6 that MPS diameters and coating thickness do have a significant effect on the volume resistivity of an ICA. Detailed resistivity and contact resistance results for the samples tested in this chapter are tabulated in Appendix C.

The contact resistance at the interface between a conducting track and an ICA will depend upon the number of contact points and on the contact areas of these contact points. A large number of contact points would give more parallel paths for current to flow and would decrease the contact resistance as would larger contact areas. The contact area for each of the Au plated tracks with the ICA samples is 0.4mm^2 (2 mm length x 0.2mm width). Assuming the distribution of MPS in an ICA to be homogeneous, the number of MPS that could be accommodated on the track for different volume fractions investigated is given in Table 7.1. Smaller MPS can have more contact points than larger MPS as can be seen from Table 7.1, which could be expected to result in a decrease in the contact resistance unless their contact areas are smaller.

Table 7.1 Number of MPS that can be accommodated within the track contact area for a given vol%

Filler	Theoretical i.e. at (74%)	MPS volume fraction					
		35%	40%	42%	44%	46%	50%
4.8_15A	14719	6962	7956	8354	8752	9150	9945
6_10B	9804	4637	5299	5564	5829	6094	6624
30_13A	413	195	223	234	245	256	279

Figure 7.2 also compares the contact resistance values of Ag-MPS filled ICAs to silver flake filled and commercial ICAs. It shows that the Ag-MPS filled ICAs have contact resistances similar to the silver flake filled ICA using the same resin but higher than the commercial ICA used. The lower contact resistance of the commercial ICA might be due to (i) the higher vol% of silver flakes/particles in it; (ii) its larger volumetric shrinkage as seen in Chapter 6, which may press the filler more towards the contact track and enhance the contact area; or (iii) the presence of an unknown component in the resin (which may have also been responsible for the reduction in the resistance of H20E at around 140°C described in Chapter 3) which may enhance the contact between the contact track and silver flakes/particle, thereby reducing the contact resistance. The lower resistance of H20E than other formulated ICAs shows that the components of adhesive matrix also

have an impact on the contact resistance as well as the filler particle type. The effect of matrix type is also presented in Section 7.2.3.

7.2.2 Effect of Coating Thickness and Morphology

Figure 7.3 presents the contact resistances of the ICAs filled with 30_13A, 30_20B and 30_20C with one standard deviation error bars. These MPS have the same core diameter, but different coating thickness and are coated using three different processes. These ICAs were all prepared using the type I polymer matrix and cured at 150°C for 15mins.

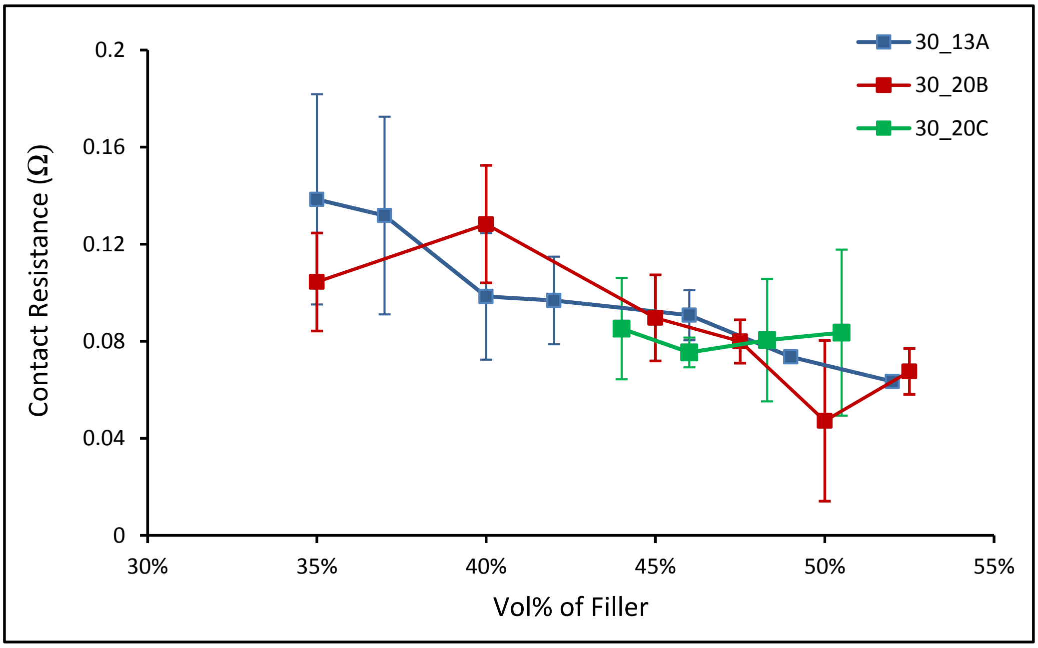

Figure 7.3 Contact resistance variation with Ag coating thickness/type

The results presented in Figure 7.3 show large variations in the contact resistance values for all of the formulated ICAs, which makes it difficult to evaluate the effect of coating thickness on contact resistance. The SEM images in Figure 5.9 show that Ag-MPS plated with processes B and C have better coating morphology/quality than those coated with process A, and ICA volume resistivity has been found to decrease for better coating quality, as discussed in Section 6.1.4.3. From the results presented in Figures 7.2 and 7.3, it can be summarised that the large MPS with thin Ag coating offers nearly the same contact resistance as the small MPS with thick Ag coating. Therefore using the larger MPS with a thin Ag coating may offer greater cost benefits. However, large deviations in the contact resistance measurements were observed in the results plotted in Figure 7.2 and 7.3. This large variability in the measurements could obscure the actual trend for the contact resistance variation with MPS diameter, coating thickness and morphology/quality. One cause of this large variation in the resistance measurements may be a non-uniform distribution of filler in the adhesives. The Ag-MPS in the ICA are assumed to be randomly distributed, thus the number of the MPS in contact with the contact track may vary from sample to sample. However, as no surfactants were used on the Ag-MPS to ensure their uniform dispersion, there may be small clumps/aggregates. ICA samples were printed manually with no automated control over speed, force or the angle of printing. The resulting variation in the speed, force or angle of the printing from sample to sample could result in variations in the particle distribution between samples and therefore in the contact resistances. Similar deviations were also be seen in the volume resistivities of these ICAs, as shown in Appendix C.

7.2.3 Effect of Matrix Type and Curing Condition

Figure 7.4 plots the contact resistances of ICAs made using the three different matrices and cured at two different curing profiles, with one standard deviation error bars. All these ICAs were made using 30_20C Ag-MPS except for H20E.

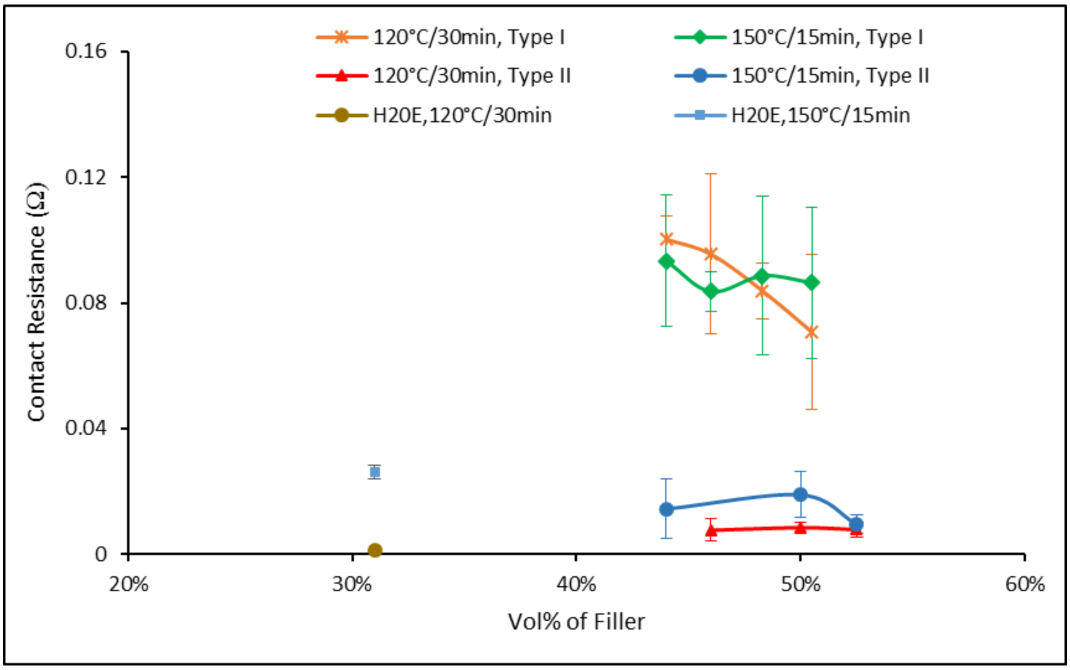

Figure 7.4 Contact resistance variation with polymer matrix and curing conditions

These results show that the type II matrix imparts significantly lower contact resistances than type I. Further, it can be seen that the contact resistances of ICAs made with type II resin are even lower than H20E cured at 150°C for 15 min, however H20E cured at 120°C for 30 min has the lowest contact resistances. One reason for the lower contact resistances for the type II matrix than type I could be its higher shrinkage than type I matrix, as was observed in Chapter 6 (Figures 6.15 and 6.16), this may enhance the contacts between filler and the substrate track lowering the contact resistance. Another reason could be its lower viscosity than the type I matrix. A lower viscosity allows the molecules to become more mobile in the early stages of cure, which results in a more reactive system (Petrie 2006) and imparts higher shrinkage. Further, H20E has the lowest contact resistances and highest shrinkage. Figure 7.4 also shows that most of the ICAs cured at 120°C for 30 min have lower contact resistances than ICAs cured at 150°C for 15 min, however they have higher shrinkage at 150°C for 15 min. One possible reason for the higher contact resistances at 150°C for 15 min could be that, samples for both the curing schedules were printed together, and while the samples were in the oven undergoing cure at 120°C for 30 min, the samples cured at 150°C for 15 min were lying at room temperature. During the delay these samples might have started to cure. This may affect the shrinkage of the matrix and hence the contact resistance.

This section presented the investigation of contact resistance of Ag-MPS filled ICAs on the PCBs with Au/Ni/Cu metallisation. The contact resistances of Ag-MPS filled ICAs on other metallisation’s, such as Cu/Ni, Ag/Sn and Ag/Pd, and on other substrates, such as glass and ceramic, needs further investigation as does their stability particularly in hot and humid conditions. This is however, out of the scope of this study.

7.3 Temperature Coefficient of Resistance Measurements

To understand the conduction mechanism within the ICAs Li et al. (1997) and Inoue et al. (2008) investigated the temperature coefficient of resistance of flake filled ICAs. Both Li and Inoue found that the TCR of an ICA is lower than that of bulk silver (3.8×10^{-3} $°C^{-1}$). Additionally, Li et al. found that the TCR of an ICA is dependent on the silver particle sizes and distributions, with small (0.5 μm), and bimodal (3–8 μm, and 1 μm) fillers imparting lower TCR (1.8×10^{-3} $°C^{-1}$ to 2.4×10^{-3} $°C^{-1}$) than larger fillers (10–15 μm) (closer to TCR for Ag). Following section presents the experiments conducted to investigate the TCR of Ag-MPS filled ICAs.

7.3.1 Materials Used

The ICAs samples manufactured for the study described in Section 6.3 were used. As the main aim was to understand the effect of Ag-MPS on TCR, only ICA samples made with type I polymer matrix were used.

7.3.2 Equipment Used

A Design Environmental climatic test chamber model Delta 190H was used to provide temperature controlled environment. The chamber has ports in the walls through which the wires attached to the ICA samples under investigation can be fed to allow resistance measurements during temperature cycling. An Agilent 34970A data acquisition system with an Agilent 34901A interface module was used to record the resistances. The data acquisition system has a 60 channel/second scan rate and can make in situ measurements of resistance and temperature simultaneously. Also, when making FWR measurements, it automatically compensates for any thermal EMFs. PET insulated wires which can withstand temperatures up to 170°C were used to connect the ICA samples to the Agilent 34901A module.

7.3.3 Methodology

The specimens used for the TCR measurements were fully cured before testing. The specimens were heated from 30°C to 120°C and kept at 120°C for 30 min, and then cooled back to 30°C while FWR measurements were made. Measurements were taken every 10 sec. To monitor the temperature in the oven during heating and cooling, a type K thermocouple was attached to one channel of the data acquisition system. A schematic of the TCR measurement set up is shown in Figure 7.5. Figure 7.6 shows a typical air temperature variation in the environmental chamber.

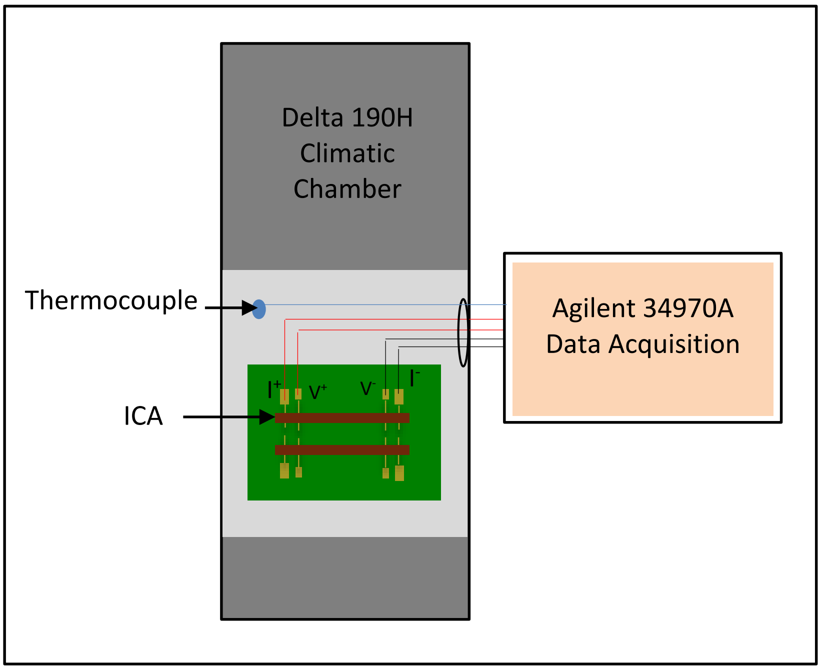

Figure 7.5 Set up for TCR measurement

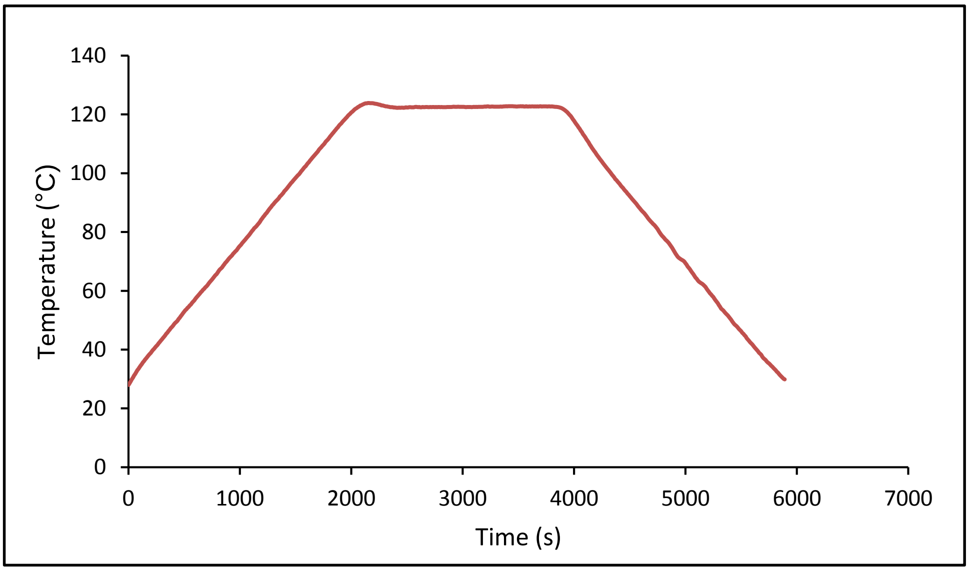

Figure 7.6 Typical time/air temperature profile observed in TCR experiments

7.4 Results and Discussions

The TCR results are presented in Figures 7.7 to 7.10. Figure 7.7 shows the resistance variation with temperature for ICAs containing 50 vol% of 30μm Ag-MPS having different Ag coating thicknesses, whereas Figure 7.8 is for ICAs having different volume fractions of 30_20B and Figure 7.9 shows the resistance variation with temperature for

ICAs containing 30µm Ag-MPS plated using different plating process (30_20B and 30_20C). All the ICAs for which data is presented in Figures 7.7 to 7.9 were cured at 150°C for 15 minutes. Figure 7.10 shows the resistance variation with temperature for ICAs cured at two different curing conditions. For comparison Figure 7.11 shows the resistance variation with temperature for Ag as given by Matula (1979). In Figures 7.7 to 7.10, the upper part of each curve corresponds to resistance variation during heating while the lower part is for cooling. It can be seen that the resistance values during cooling are lower compared to during heating. All of the curves in Figures 7.7 to 7.10 show that during heating the resistance increases linearly up to about 85°C, whereas above 90°C the rate of increase in resistance drops slightly. However, these apparent changes in TCR vary from sample to sample (and they may be due to small lag between the air and sample temperature changes).

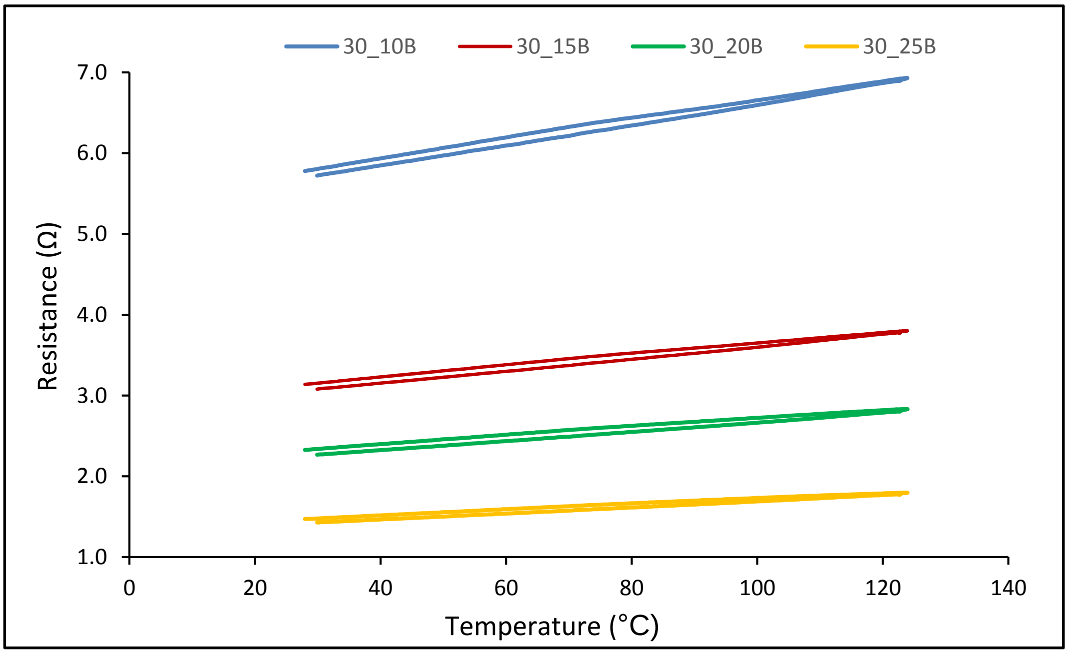

Figure 7.7 Resistance variation with temperature for ICAs filled with 30µm Ag-MPS having different coating thicknesses

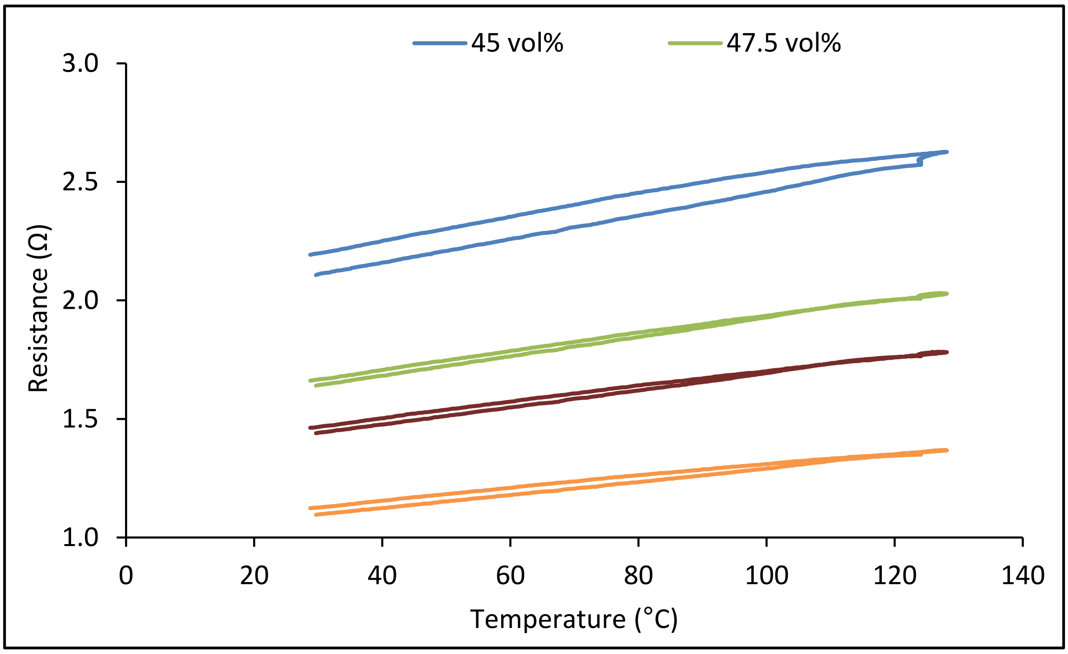

Figure 7.8 Resistance variation with temperature for ICAs having different volume fractions of 30_20B

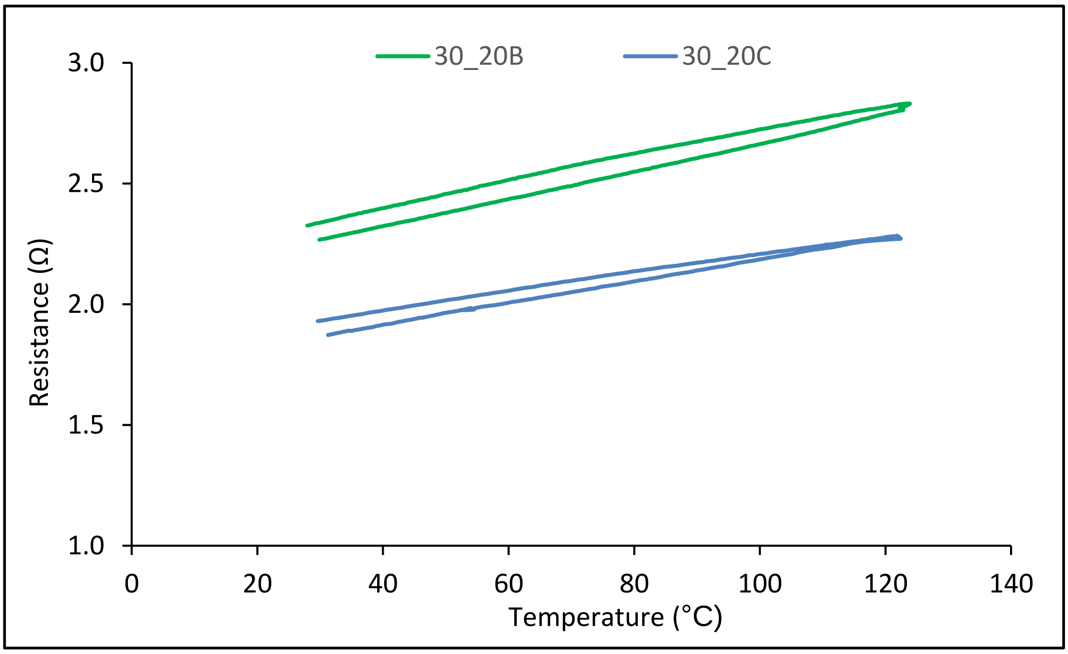

Figure 7.9 Resistance variation with temperature for ICAs made using Ag-MPS coated with different plating processes

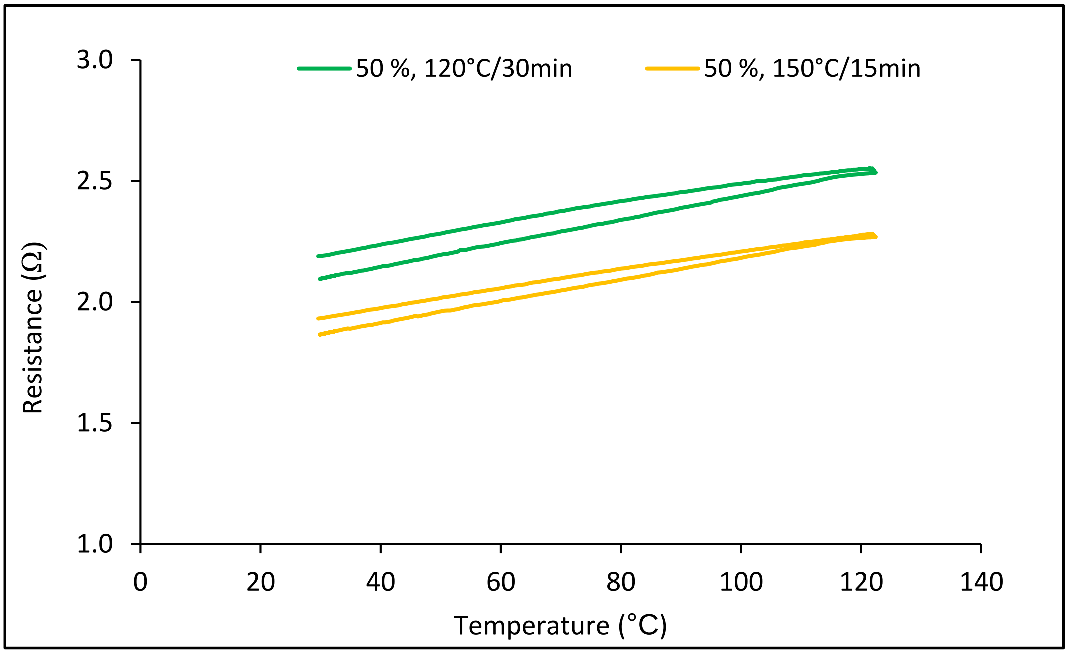

Figure 7.10 Resistance variation with temperature for ICAs filled with 30_20C and cured under different conditions

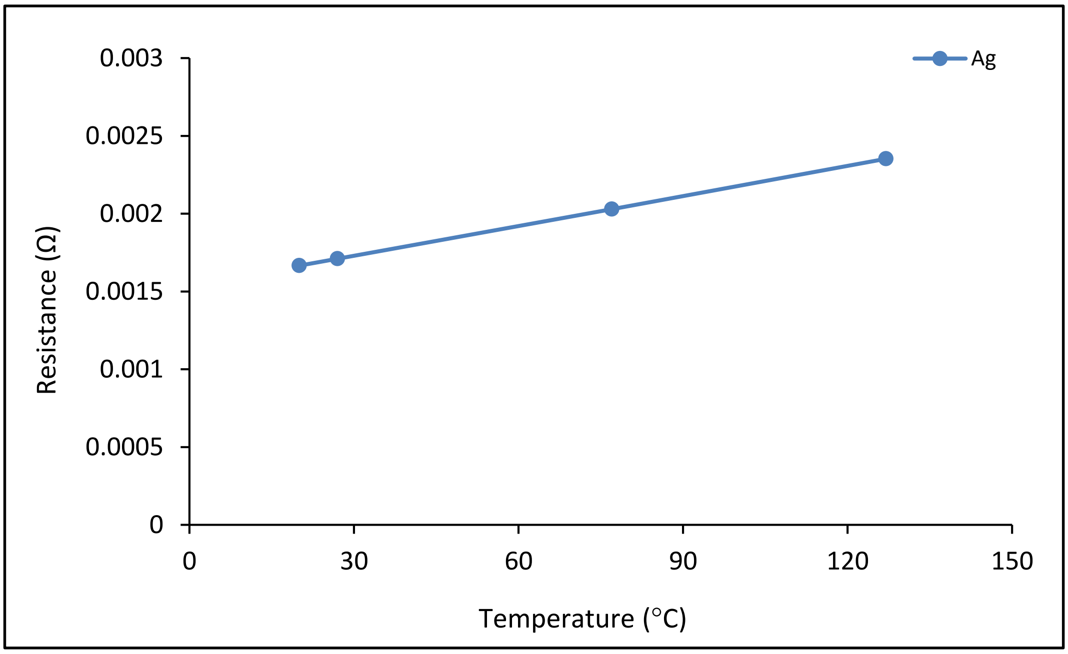

Figure 7. 11 Plot of Ag resistance variation as given by Matula (1979)

The increase in the ICA resistance with temperature is believed to be due to the combined effects of the increases in silver resistance with temperature and in the contact resistance due to expansion of the polymer matrix on heating i.e. during heating the greater expansion of the polymer matrix reduces the contact force pressing the particles together and thus decreases the contact area and increases the contact resistance. The T_g of Ag-

MPS is ~ 133°C (Nguyen et al. 2011) and the T_g of type I resin is ~ 90°C (Epotek 2010b). As the temperature increases above Tg, the resin softens. On softening, the matrix may also flow out from between two adjacent Ag-MPS, thus allowing them to be come closer and reducing their contact resistance. As the temperature is reduced contraction of the matrix will occur, pressing the particles again into the metallic contacts, which may increase the effective contact area and reduce contact resistance and could be a cause of the reduced resistance observed during cooling segment. Another reason could be post curing, as the curing profile used has been found to impart less than 100% cure (Cai 2012), the increase in the temperature would lead to further cure and may impart more shrinkage to adhesive, reducing the contact areas between filler which can ultimately reduce the resistance.

It can be seen in Figure 7.7 that the difference in the resistances during heating and cooling decreases as the coating thickness increases. With the increase in coating thickness the porosity in the coating decreases (as can be seen in Figure 5.9) and the contact area increases this may lead to differences in the mean free paths and therefore the resistance variation with temperature for different coating thickness. It can also be seen in Figure 7.8 that the difference in the resistances during heating and cooling decreases as Ag-MPS volume fraction increases. Further, sharp drop in the resistance of ICA at 45 vol% of Ag-MPS is observed during the cooling segment. Lower volume fraction of filler means higher volume fraction of resin. ICA with higher volume fraction of matrix may contract more on cooling, thus may enhance the contact areas more. And could be a cause for larger difference in resistances during heating and cooling segments for the ICAs. From Figure 7.9 the difference in the resistance values during heating and cooling is larger for 30_20B Ag-MPS than for 30_20C. The coatings on both these MPS are similar (Figures 5.9 and 6.5). Further, the difference in the resistance values during heating and cooling is also seen for ICAs cured at lower temperature. One reason may be greater increase in internal stress for ICAs cured at lower temperature during subsequent heating.

The calculated TCRs of the ICAs is presented in Tables 7.2 to 7.3. The tables show that all of the Ag-MPS filled ICAs exhibit a positive TCR, however they were all lower than the TCR for bulk Ag, which is 3.8×10^{-3} °C^{-1} at 20°C (Hyperphysics 2014). The observed TCR values are close to the TCR values observed by Li et al. (1997) and Inoue et al.

(2008) for flake filled ICAs. The lower TCR values than for Ag could be due to the following reasons. TCR of Ag in its nano form has been measured as 2.9 x 10^{-3} °C^{-1} (Qin et al. 1997), which is different from bulk silver. The Ag-MPS are coated with a thin layer of Ag which is grown by the coalescing of nano-sized Ag particles. Therefore when Ag-MPS are used TCR of the sub-micron thickness metallic layer may be lower than that of bulk Ag. This could result in lower value of TCR. Conduction in an ICA occurs by a combination of metallic conduction and the constriction and tunnelling phenomena. The constriction resistance due to the relatively small contact area imposes mean-free-path limitations on the contacts and therefore has a TCR smaller than that for bulk Ag (Qin et al. 1997). Tunnelling resistance purely depends upon the electron transmission probability through the potential barrier, which depends upon height and thickness of the barrier (which are independent of temperature) (Holm 1967). Thus tunnelling resistance is expected to have zero TCR (Morris 1999). Thus the collective contributions of metallic conduction and constriction or tunnelling may result in a lower TCR than the bulk Ag. Table 7.2 also shows that the TCR increases with coating thickness and volume fraction of Ag-MPS. The reason could be that with increasing coating thickness and volume fraction of Ag-MPS metallic contribution to the conduction increases. The grain size of the silver deposits may also be different for different coating thickness which may affect the density of grain boundaries leading to differences in the mean free paths and therefore the TCR.

Table 7.2 TCR at different (a) Ag coating thickness (b) volume fractions of Ag-MPS

(a)	
Coating Thickness	**TCR (°C^{-1})**
0.10µm	2.08 x10^{-3}
0.15µm	2.22 x10^{-3}
0.20µm	2.24 x10^{-3}
0.25µm	2.32 x10^{-3}

(b)	
Volume fraction of 30_20B	**TCR (°C^{-1})**
45.0 %	2.04 x10^{-3}
47.5%	2.19 x10^{-3}
50.0 %	2.20 x10^{-3}
52.5 %	2.21 x10^{-3}

Table 7.3 TCR for different (a) plating processes and (b) curing conditions

(a)	
Plating Process	**TCR (°C^{-1})**
Process B	2.27 x10^{-3}
Process C	1.98 x10^{-3}

(b)	
Curing Conditions	**TCR (°C^{-1})**
120°C/30min	1.83 x10^{-3}
150°C/15min	2.0 x10^{-3}

Table 7.3 shows that Ag-MPS coated with two different plating processes show different TCR. The different values of the TCR for different plating process may be due to a different grain size and therefore density of grain boundaries, which may lead to differences in the mean free paths and therefore a different TCR. Moreover, the samples (30_20B and 30_20C) were run separately in two different experiments, the small variation in temperature values or rate of change of temperature with time between these two experiments may also affect the TCR between these two MPS. Table 7.3 also shows that TCR increases with curing temperature, the reason for this may be that, for the same adhesive matrix, a higher curing temperature may induce larger shrinkage which may increase the effective areas of metallic contact and hence TCR.

7.5 Concluding Remarks

This chapter has presented an investigation of the effects of MPS diameter, Ag coating thickness, type of polymer matrix and curing conditions on the contact resistance of Ag-MPS filled ICAs. The results presented showed significant variations in the contact resistance with changing polymer matrix and curing conditions. The contact resistance was also observed to decrease with increasing filler content, but little effect of the MPS diameter and Ag coating thickness on the contact resistance was observed.

The chapter also presented a study of the TCR of Ag-MPS filled ICAs. The TCRs of the ICAs formulated with the Ag-MPS were found to be lower than that of bulk silver, and decrease slightly with temperature. The TCR of the ICA was found to increase with the coating thickness, filler content and curing conditions. This showed that both the filler and the polymer matrix affect conduction.

This chapter and the previous chapters have presented the effect of various factors on the electrical performance of the Ag-MPS filled ICAs. The next chapter will present the conclusions drawn from this research. A case study on the use of Ag-MPS filled ICAs in a novel PV module assembly application is presented in Appendix D.

CHAPTER 8

CONCLUSIONS AND RECOMMENDATIONS FOR FUTURE WORK

A summary of the progress made against the objectives set and the conclusions that can therefore be drawn from this study are presented in this chapter. During the course of this research a number of interesting areas worthy of future work have been identified. Based on these this chapter also presents recommendations for future work.

This work has resulted in a number of publications and a list of these together with further proposed publications is also included in this chapter.

8.1 Summary of Progress against Objectives

This section presents key conclusions based on how the objectives presented in Chapter 1 have been met. The objectives are repeated here for clarity.

Objective 1: To critically review the literature to gain an understanding of the factors that can affect the performance of an ICA and identify the merits and demerits of using mono-sized metal coated polymer spheres in an ICA in place of silver flakes.

To fulfill *Objective 1* a critical review of the literature was conducted. The main conclusions drawn from this review are:

- Electrical conductivity, chemical stability, nature (e.g. coated polymers vs metallic), shape, size, and size distribution of the conductive filler are the most important parameters which can affect the electrical performance of an ICA.
- Use of Ag-MPS as a conductive filler can reduce the amount of silver used in an ICA and hence help reduce its cost while achieving equivalent mechanical strength.

Objective 2: To establish the feasibility of using mono-sized metal coated polymer spheres in ICAs in place of silver flakes by benchmarking these novel ICAs against a traditional silver flake filled ICA.

To achieve *Objective 2* a feasibility study was conducted which demonstrated:

- The silver can be more efficiently used in an ICA if silver flakes are replaced with Ag-MPS
- For similar high levels of conductivity, Ag-MPS based ICAs significantly reduce the amount of silver used i.e. to approximately 7.74 vol% as compared to the commercial flake filled ICAs around 31 vol%. At such a low volume (7.74%) of silver, silver flake filled ICAs would be non-conducting.
- For moderate conductivity values of up to about 400 $(\Omega cm)^{-1}$, the volume of silver can further be reduced to less than 2 vol% with the use of 30µm Ag-MPS filler. This amounts to a reduction of 93% in the volume of silver used.
- To achieve similar conductivities a higher Ag-MPS volume fraction (around 50%) is required compared to silver flakes (around 35%). However, this is not a concern as, according to Nguyen et al (2010 and 2013), at 50 vol% of filler, Ag-MPS filled ICAs have a rheology suitable for stencil printing and dispensing.

Objective 3: To develop a theoretical model to gain an understanding of the effect of different factors such as MPS diameter (Ø), coating thickness and morphology on the electrical performance of the individual MPS.

Objective 4: To develop a theoretical model to gain an understanding of the effect of different factors such as MPS volume fraction, diameter (Ø), coating thickness and morphology, curing conditions, and curing shrinkage of the epoxy resin on the electrical performance of an ICA filled with MPS.

To accomplish *Objectives 3 and 4* theoretical models for the conductivity of both a single MPS and of an MPS filled ICA have been developed. The models show that:

- The conductivity of an individual MPS increases with increasing coating thickness and contact radius (which depends upon the inter particle forces resulting from shrinkage and the size and stiffness of the MPS core material) and decreases with increasing coating resistivity (which depends upon coating thickness and morphology) and MPS size.

- Smaller MPS with a thicker coating should offer more conductivity than larger MPS with a thin coating. However, smaller MPS with thicker coatings use more silver than larger MPS and do not give an increase in conductivity proportional to the increased amount of silver they use, indicating that larger MPS use silver more efficiently.
- Ag-MPS filled ICA conductivity increases with increasing MPS conductivity, volume fraction, coating thickness and contact area (which is believed to depend upon the matrix shrinkage and hence on the type of matrix and the curing conditions) and decreases with increasing MPS size.

Objective 5: To experimentally verify the findings of the theoretical models on the electrical performance of MPS and the novel ICAs; and

Objective 6: Based on the theoretical model and the experimental findings to establish a link between the electrical properties and different factors such as MPS volume fraction, size, coating thickness and morphology, curing conditions and epoxy shrinkage, which will help in the design of MPS filled ICAs with tailored properties for specific applications.

To accomplish *Objectives 5 and 6* the correlation between the theoretical predictions and experimental results was investigated. The main findings were:

***MPS Conductivity*:**

- With increasing deformation (contact radius) and coating thickness, the conductivity of the MPS increases, thus validating the prediction of the theoretical model.
- The measured MPS resistance is found to substantially higher than that theoretically predicted. Based on the values of the measured resistance, improvements to the theoretical model for MPS conductivity were proposed. These are: (i) that the thin film resistivity needs to be calculated using e.g. FE models and used in place of bulk metal resistivity; (ii) the actual contact geometry between MPS and between MPS and flat pads needs to be investigated

using FE models, and used in place of the assumed uniform circular contact area and; (iii) the actual contact area needs to be used in place of the apparent contact area. However, accurate predictions of the contribution of each of these factors discussed is beyond the scope of this study and needs to be addressed in future studies.

ICA Conductivity:

- The conductivity of the Ag-MPS filled ICAs increased with decreasing MPS size and increasing metal coating thickness, as predicted by the theoretical model.
- The curing schedule and type of the epoxy matrix both affect the conductivity of an Ag-MPS filled ICA, but not to as large an extent as the MPS size and coating thickness.
- Smaller MPS (4.8µm, 6µm, 10µm) do not give the increased conductivity in proportion to the extra silver they use as compared to (30µm). Larger MPS with a thicker coating use silver more efficiently and can offer more cost benefits.
- Conductivity initially increased considerably with increasing coating thickness, but only up to a thickness of 0.20µm and became nearly constant for further increases in coating thickness.
- Contact resistances for the Ag-MPS filled ICAs have been found to be higher than those of commercial silver flake filled ICAs. The contact resistances do not vary much with MPS size, coating thickness and curing schedule, however the type of matrix has been found to affect the contact resistances more than the volume fraction of filler.

To investigate the suitability of Ag-MPS filled ICA in a PV application, their performance was investigated in a novel PV module assembly application. The successful assembly of modules using Ag-MPS filled ICA proved that they could be used as an interconnection material in PV applications. However, all the assembled modules showed higher resistive losses and poorer performance than expected. Analysis identified damage and shunting of cells during the module manufacturing process, and an increase in series resistance (possibly due to oxidation of the Al metallisation and Cu tracks) to be the cause of the poor performance of the modules.

Thus further studies need to be conducted into the root causes of the shunting issues and investigate the optimum Ag-MPS filled ICA (based on MPS size, coating thickness and the adhesive matrix) for PV application as well as contact resistances, and their stability, with different conductive surfaces.

8.2 Contributions and Conclusions

Silver coated mono-sized polymer spheres have been identified as a potential conductive filler in place of traditional silver flakes/particles to improve the reliability and reduce the metal usage, and hence cost, of ICAs. However, anticipated concerns over the higher percolation threshold and lower conductivity associated with the use of Ag-MPS as conductive filler in ICA needed investigation. Further, the parameters affecting the electrical performance of Ag-MPS and ICAs based on Ag-MPS needed investigation. With the aim to address the concerns related to the use of Ag-MPS in an ICA and to gain in depth knowledge of the parameters affecting the electrical performance of Ag-MPS and ICAs based on Ag-MPS this study was undertaken. The main contributions and findings of the study are:

- This study for the first time demonstrated that the higher percolation threshold and lower electrical conductivity related to the use of Ag-MPS as a conductive filler are not significant concerns.

- This study established the use of Ag-MPS as a conductive filler, demonstrating that the silver can be much more efficiently used in an ICA if silver flakes are replaced with Ag-MPS.

- This study showed that, for similar high levels of conductivity, Ag-MPS based ICAs reduce the amount of silver required by approximately 75% as compared to commercial flake filled ICAs, while for moderate conductivities of up to 400 $(\Omega cm)^{-1}$, the silver content can be reduced by about 93 %. This study also showed that larger MPS (30µm) with a thicker coating use silver more efficiently than smaller MPS (4.8µm, 6µm, 10µm). Thus demonstrating that according to the conductivity requirement of an application, the amount of silver used can be altered. This allows tuning of the ICA properties for specific application, which is something that cannot be achieved when using silver flake filled ICAs.

- This study has indicated that when MPS are used as filler, the filler/MPS resistance is higher than that offered by bulk Ag and its contribution to ICA resistivity is significant, which is different for MPS of different size, coating thickness, and coating morphology. This is different from the case of silver flake filled IACs where the filler resistance is always taken equal to bulk silver and its contribution to ICA resistivity is negligible. In the case of flake filled ICAs the main contributions to ICA resistivity are from the contact resistances between flakes.

- This study has also indicated that the shape of the contact between MPS significantly affects the contact resistance and the MPS resistance. In the case of solid flake filler the shape of contact between two solid flakes is assumed to be circular whereas when MPS are used, the shape of contact is ring shaped instead of circular (Divigalpitiya 2008) and can affect the contact resistance and the MPS resistance significantly. However the shape of the contact between MPS and the corresponding contact resistance, needs investigation using FE models.

- In the case of ACAs, the resistance offered by MPS depends upon the degree of deformation. This study has also shown that in the case of ICAs, where the force due to adhesive shrinkage may not deform the MPS and can only force the MPS together in an electrical contact, the MPS resistance depends upon the contact radius between MPS.

- This study has revealed volume expansion of Ag-MPS filled ICA however whether the volume expansion is due to degassing/expansion of Ag-MPS or trapped air could not be confirmed in the investigation. To further investigate the possibility of this expansion being due to trapped air, volume measurements on the samples cured in vacuum compared with those, for example cured in an autoclave need to be conducted.

- The production of functional MWT (2 x 2) modules, interconnected using Ag-MPS filled ICA have demonstrated that the Ag-MPS filled ICA can be used as an interconnection material in PV module assembly. However, observed poorer performance than expected showed that the module assembly process used in this study needs improvement.

8.3 Recommendations for Future Work

This research has successfully demonstrated the use of Ag-MPS as a conductive filler and identified various factors which can affect the conductivity of an Ag-MPS and Ag-MPS filled ICAs, however further time and effort still needs to be invested in various aspects of the work. The future priorities can be summarized as follows:

MPS size distribution: This study has investigated the electrical conductivity when using mono-sized Ag-MPS. However, the effect of the Ag-MPS size distribution (bi, tri and multi modal) on the conductivity, rheology and mechanical properties of an ICA needs investigation.

Coating resistivity: The theoretical model for individual Ag-MPS conductivity predicted that Ag-MPS conductivity depends upon the metal coating resistivity. The resistivity of very thin metal coatings is different/higher than the bulk metal resistivity due to their morphology and microstructure. As the process of metallisation of the polymer spheres is typically by electroless plating, which results in the silver deposits growing from dispersed nucleation sites scattered across the surface of the particle. The discontinuities between the silver deposits on the surface can lead to a limited number of electrical pathways for conduction and many grain boundaries that scatter electrons resulting in increase in coating resistivity. Measuring or calculating coating resistivity was out of the scope of this thesis and further studies, which might include FE models to find the resistivity of coatings grown from random nucleation points followed by isotropic growth, need to be undertaken to better understand the effects of plating processes on the coating resistivity. For illustration, preliminary FE models of silver deposits in the form of random deposits is shown in Figure 8.1.

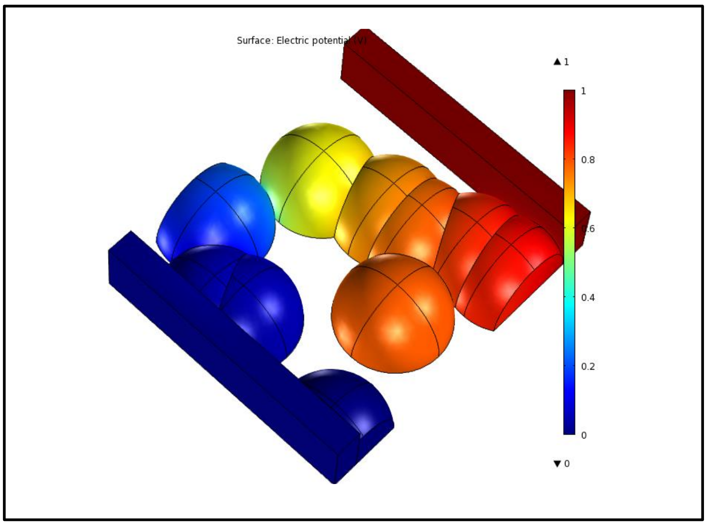

Figure 8.1 Illustrating silver coating in the form of random silver deposits (Taken from an unpublished FE modelling study by Whalley (2013))

MPS mechanical properties: The silver coating thickness can affect the mechanical properties, such as the effective Elastic modulus and Poisson's ratio, of an Ag-MPS, which in turn can affect their contact radius and hence the resulting contact resistance. The effect of silver coating thickness on these properties needs to be more thoroughly investigated.

Constriction resistance between MPS: In the case of a thin film, current lines bend sharply at the interface and current crowding occurs in a small thickness of the film, as shown in Figure 5.18. Therefore, the constriction resistance of a contact area located in a thin film may not be accurately predicted by the Hertz and Holms equations. Further, FE analysis needs to be done to predict the effective electrical contact area between two Ag-MPS taking into account the current bending at the edges of the film and current crowding in the thin film and hence more accurately predict constriction resistance.

MPS Expansion: MPS thermal expansion may affect ICA shrinkage, and therefore the contact area between adjacent particles, and hence may have an effect on ICA conductivity. Further investigation is needed to investigate MPS expansion with temperature and its effect on shrinkage the contact area and hence on ICA conductivity.

ICA mechanical strength and reliability: Reliability tests such as thermal cycling, mechanical vibration and mechanical shock (drop) need to be carried out to establish the mechanical reliability of MPS-based ICAs in comparison with conventional Ag flake filled ICAs and solders. The fracture toughness of MPS-based ICAs needs to be studied in order to understand their fracture behaviour. A study on current carrying capability of MPS-based ICAs is also crucial.

Different types of MPS with different core materials (and thus different thermo-mechanical properties), as well as coating materials, should be tested as conductive particles in ICAs in order to investigate the effect of particles on the mechanical and electrical properties of ICAs.

8.4 Publications

The study has so far resulted in three conference publications and two poster publications as listed below:

- Jain, S., Whalley, D. C., Cottrill, M., Kristiansen, H., Redford, K., Nilsen, C. B., Helland, T., Liu, C. (2011). "Electrical Properties of an Isotropic Conductive Adhesive Filled With Silver Coated Polymer Spheres", Proceedings of the IMAPS European Microelectronics and Packaging Conference (EMPC), Brighton, United Kingdom, September 12-15, pp. 240-246.
- Jain, S., Whalley, D. C., Cottrill, M., Kristiansen, H., Redford, K., Nilsen, C. B., Helland, T., Liu, C. (2013) "The Effect of Coating Thickness on the Electrical Performance of Novel Isotropic Conductive Adhesives Prepared Using Metallised Polymer Micro-Spheres", Proceedings of the 63rd Electronic Components and Technology Conference (ECTC), Las Vegas, USA, May 31-June 02, pp. 796-802.
- Jain, S., Whalley, D. C., Cottrill, M., Kristiansen, H., Redford, K., Helland, S., Helland, T., Kalland, E., Liu, C. (2013). "Factors Affecting Conduction in Novel Isotropic Conductive Adhesives Filled with Silver Coated Polymer Spheres", Proceedings of the IMAPS European Microelectronics and Packaging Conference (EMPC), Grenoble, France, September 09-12, pp. 1-7.
- Jain, S., Whalley, D. C., Cottrill, M., Kristiansen, H., Redford, K., Helland, S., Helland, T., Kalland, E., Liu, C. (2012). "Novel Isotropic Conductive Adhesives Filled with Silver Coated Polymer Spheres", Poster in IeMRC Printed & Plastic Electronics one day seminar, Loughborough, United Kingdom, March 19.

- Jain, S., Whalley, D. C., Cottrill, M., Kristiansen, H., Redford, K., Helland, S., Helland, T., Kalland, E., Liu, C. (2012). “Novel Isotropic Conductive Adhesives Filled with Silver Coated Polymer Spheres”, Poster in IeMRC Annual Conference, Loughborough, United Kingdom, September 05.

A joint journal publication with the collaborating partner has been drafted and is due to be submitted in June.

- Nguyen, H.V., Jain, S., Whalley, D.C., Aasmundtveit, K.E., Kristiansen, H., Helland, T., He, J.Y., “Electrical characterization of silver-coated mono-sized polymer spheres using a nano-indentation based flat punch method for an ICA applications’’ This publication will be partly based on the results presented in Chapter 5.

Planned future publications are:

- Jain, S., Nguyen, H.V., Whalley, D.C., Cottrill, M., Kristiansen, H., Redford, K., Helland, T., He, J.Y., “An improved MPS conductivity model based on electrical measurements on single MPS”.
- Jain, S., Nguyen, H.V., Whalley, D.C., Cottrill, M., Kristiansen, H., Redford, K., Helland, T., He, J.Y., “Correlation between MPS properties and conductivity of MPS filled ICAs”.

REFERENCES

ASTM (2004). ASTM standard D2739 “Standard Test Method for Volume Resistivity of Conductive Adhesives", *ASTM International*, United States.

ASTM (2009). ASTM standard E1171-09 "Standard Test Methods for Photovoltaic Modules in Cyclic Temperature and Humidity Environments", *ASTM International*, United States.

Barrie, J. A., Sagoo, P. S. and Johncock, P. (1985). The sorption and diffusion of water in halogen-containing epoxy resins. *Polymer*, Vol. 26(8), pp. 1167-1171.

Bjorneklett, A., Tuhus, T., Halbo, L. and Kristiansen, H. (1993). Thermal resistance, thermomechanical stress and thermal cycling endurance of silicon chips bonded with adhesives. *9th Annual IEEE Semiconductor Thermal Measurement and Management Symposium,(SEMI-THERM IX)*, Austin, TX, 2-4 Feb, pp. 136-143.

Boyle, O. (1992b). Anticipated effects of moisture on conductive adhesive joints. *Process Group Technical Report No. 92/5*. Loughborough University**,** pp. 1-5.

Boyle, O., Whalley, D. C. and Williams, D. J. (1992a). A study of process parameters involved in the manufacture of conductive adhesive joint. *ISHM Nordic*. Oslo.

Brassell, G. W. and Fancer, D. R. (n.d.). Long term strength charateristics of conductive epoxies. *Epotek Technical papers and summaries.* *http://www.epotek.com/site/technical-material/technical-material.html*, Epoxy Technology [Accessed 16 May 2011].

Bremaud, D. J. L. (2009). Investigation and development of CIGS solar cells on flexible substrates and with alternative electrical back contacts. *Doctor of Sciences Dissertation*, ETH Zurich.

Brown, R. (1999). Handbook of polymer testing: Physical methods, *CRC Press*.

Bultman, J. H., Brieko, M. W., Burgers, A. R., Hoornstra, J., Tip, A. C. and Weeber, A. W. (2001). Interconnection through vias for improved efficiency and easy module manufacturing of crystalline silicon solar cells. *Solar Energy Materials and Solar Cells,* Vol. 65(1-4), pp. 339-345.

Bultman, J. H., Eikelboom, D. W. K., Kinderman, R., Tip, A. C., Tool, C. J. J., Nieuwenhof, M. A. C. J. v. d., Schoofs, C., Schuurmans, F. M. and Weeber, A. W. (2003). Fast and easy single step module assembly for back-contacted C-Si solar cells with conductive adhesives. *Proceedings of 3rd World Conference on Photovoltaic Energy Conversion,* 11-18 May, pp. 979-982

Cai, W. (2012). Performance testing of novel conductive adhesives *Master's Dessertation,* Loughborough University.

Chen, X., Tao, B. and Yin, Z. (2011). Investigation of bulk resistance for metal-coated polymer particles used in anisotropic conductive adhesive. *12th International Conference on Electronic Packaging Technology and High Density Packaging (ICEPT-HDP),* Shanghai, 8-11 Aug, pp. 485-491.

Chin, M., Iyer, K. A. and Hu, S. J. (2004). Prediction of electrical contact resistance for anisotropic conductive adhesive assemblies. *IEEE Transactions on Components and Packaging Technologies,* Vol 27**,** pp. 317-326.

Choi, G. N. and Krieger, I. M. (1986). Rheological studies on sterically stabilized model dispersions of uniform colloidal spheres. *Journal of Colloid and Interface Science,* Vol. 113(1), pp. 101-113.

Christensen, F. M., Jorgensen, T. and Nielson, I. R. (2000). Environmental and technical characteristics of conductive adhesives versus soldering, *Danish EPA*, Denmark.

Chuang, C.-L., Liao, Q.-A., Li, H.-T., Liao, S.-J. and Huang, G.-S. (2009). Increasing the bonding strength of chips on flex substrates using thermosonic flip-chip bonding process with nonconductive paste. *Microelectronic Engineering,* Vol. 87(4), pp. 624-630.

Cognard, J. (1991). The metal polymer interphase in adhesive joints. *International Journal of Adhesion and Adhesives,* Vol. 11(2), pp. 114-116.

Cognard, P. (2005). Handbook of adhesives and sealants: basic concepts and high tech bonding. *Elsevier*, Oxford, UK,

Conpart, A. (2010). "Datasheet of Ag-MPS."

Crozier, J. L. (2012). Characterization of cell mismatch in photovoltaic modules using electroluminescence and associated electro-optic techniques. *Master's Thesis,* Nelson Mandela Metropolitan University.

Cui, X., Hutt, D. A. and Conway, P. P. (2012). Evolution of microstructure and electrical conductivity of electroless copper deposits on a glass substrate. *Thin Solid Films,* Vol. 520(19), pp. 6095-6099.

Danzl, R., F, H. and S., S. (2009). Focus variation - a new technology for high resolution optical 3D surface metrology. *Proceedings of the 10th International Conference of the Slovenian Society for Non-Destructive Testing*, Slovenia, Sep 1- Sep 3, pp.

Daoqiang, L., Wong, C. P. and Tong, Q. K. (1998). A fundamental study on silver flakes for conductive adhesives. *Proceedings of 4th International Symposium on Advanced Packaging Materials*, Braselton, GA, 15-18 Mar, pp. 256-260.

Divigalpitiya, R. (2008). Effect of insulative debris on the contact resistance of anisotropic conductive film (acf) adhesives: a comparison between a solid conducting particle and a coated insulative particle. *IEEE Transactions on components and packaging technologies,* Vol. 31(1), pp. 222-228.

Dou, G. (2007). Mechanical and electrical characterisation of anisotropic conductive adhesive particles. *Doctoral Thesis,* Loughborough University.

Dou, G., Chan, Y. C. and Liu, J. (2003). Electrical conductive characteristics of anisotropic conductive adhesive particles. *Journal of Electronic Packaging,* Vol. 125, pp. 609 - 616.

Dou, G., Whalley, D. C. and Liu, C. (2004). Electrical conduction characteristics of solid metal anisotropic conductive adhesive particles. *4th IEEE International Conference on Polymers and Adhesives in Microelectronics and Photonics*, Portland, OR, United States, 12-15 Sep, pp. 132-136.

Dou, G., Whalley, D. C. and Liu, C. (2004). Electrical conductive characteristics of ACA bonding: A review of the literature, current challenges and future prospects, *Proceeding of the 6th IEEE CPMT Conference on High Density Microsystem Design and Packaging and Component Failure Analysis*, 30 Jun -03 Jul. pp. 264-276.

Dou, G., Whalley, D. C. and Liu, C. (2006). Mechanical and electrical characterisation of individual ACA conductor particles. *International Conference on Electronic Materials and Packaging (EMAP)*, Kowloon, 11-14 Dec, pp. 1-9.

Edward, M. P. (2008). Methods for improving electrically and thermally conductive adhesives: Properties of electronic parts can be enhanced via tweaking adhesive formulations or introducing filler particles. *Metal Finishing*, Vol. 106(3), pp. 40-45.

Eerensteina, W., Bennetta, I. J., Spätha, M., Dekkera, N. J. J. and Roscaa, V. (2012). Back contact module technology. *Solar conference CPTIC China*, Shanghai, 20-22 Mar, pp.

Eikelboom, D. W. K., Bultman, J. H., Schonecker, A., Meuwissen, M. H. H., Nieuwenhof, M. A. J. C. and Meier, D. L. (2002). Conductive adhesives for low-stress interconnection of thin back-contact solar cells. *Proceedings of 29th IEEE Photovoltaic Specialists Conference (PVSC)*, May 19-24, pp. 403-406.

Eikelboom, D. W. K., Burgers, A. R., Goris, M. J. A. A., Manshanden, P., Schonecker, A. and Wyers, G. P. (2001). Conductive Adhesives for Interconnection of Busbarless Emitter Wrap-Through Solar Cells on a Sturctured Metal Foil, ECN Solar energy**:** 4.

Einstein, A. (1906). *Annalen der Physik* Vol. 19.

Epotek (2010a). Epo-Tek H20E data sheet. http://www.epotek.com/site/, [Accessed 20 June 2010].

Epotek (2010b). Epo-Tek 353ND data sheet. http://www.epotek.com/site/, [Accessed 20 June 2010].

Epotek (2010c). Epo-Tek 353ND material safety data sheet. http://www.epotek.com/site/. [Accessed 20 June 2010]

Epotek (2010d). Epo-Tek H20E material safety data sheet, http://www.epotek.com/site/. [Accessed 20 June 2010]

Epotek (2011). Epoxy Adhesive Application Guide. [Accessed 10 Feb 2011]

Epotek (2012). Personel communication.

Epotek. (n.d.). "http://www.epotek.com/site/about-us/company-history.html." [Accessed 20 June 2014]

Farnell. (2014). "Tin lead solder cost." from http://uk.farnell.com/. [Accessed 05 May 2014]

F.M.Coughlan, H. J. L. (2006). A Study of Electrically Conductive Adhesives as a Manufacturing Solder Alternative. *Journal of Electronic Materials*, Vol. 35(5).

Finkenzeller, K. (2010). RFID Handbook: Fundamentals and Applications in Contactless Smart Cards, Radio Frequency Identification and Near-Field Communication, *A John Wiley and Sons*, Ltd., UK.

Frisk, L., Lahokallio, S., Mostofizadeh, M., Kiilunen, J. and Saarinen, K. (2012). Reliability of isotropic electrically conductive adhesives under condensing humidity testing. *Proceedings of 14th Electronics Packaging Technology Conference (EPTC)*, Singapore, 5-7 Dec, pp. 174-179.

Fuyuki, T. and Kitiyanan, A. (2009). Photographic diagnosis of crystalline silicon solar cells utilizing electroluminescence. *Applied Physics A : Material science and processing*, Vol. 96, pp. 189-196.

Fuyuki, T., Kondo, H., Kaji, Y., Ogane, A. and Takahashi, Y. (2007). Analytic findings in the electroluminescence characterization of crystalline silicon solar cells. *Journal of Applied Physics*, Vol. 101, pp. 023711 (1-5).

Fuyuki, T., Kondo, H., Yamazaki, T., Takahashi, Y. and Uraoka, Y. (2005). Photographic surveying of minority carrier diffusion length in polycrystalline silicon solar cells by electroluminescence. *Applied Physics Letters,* Vol. 86, pp. 262108-262101.

Fuyuki, T., Tani, A., Tsujii, S. and Sugimura, E. (2010). Photographic distinction of defects in polycrystalline Si by spectroscopic electroluminescence. *35th IEEE Photovoltaic Specialists Conference (PVSC)*, Honolulu, HI, 20-25 Jun, pp. 001380-001382.

Gakkestad, J., Dalsjo, P., Kristiansen, H., Johannessen, R. and Taklo, M. M. V. (2010). Use of conductive adhesive for MEMS interconnection in ammunition fuze applications. *Journal of Micro/Nanolithography, MEMS, and MOEMS,* Vol. 9(4), pp. 041108-041108.

Gee, J. M., Garrett, S. E. and Morgan, W. P. (1997). Simplified module assembly using back-contact crystalline-silicon solar cells. *IEEE Photovoltaic Specialists Conference*, 29 Sep-3 Oct 1997, pp. 1085-1088.

Gelman, R. (2012). Renewable Energy Data Book, National Renewable Energy Laboratory (NREL). U.S. Department of Energy.

Genovese, D. B. (2012). Shear rheology of hard-sphere, dispersed, and aggregated suspensions,and filler-matrix composites. *Advances in Colloid and Interface Science,* Vol., pp. 1-16.

Gilleo, K. (2002). Area Array Packaging Handbook : Manufacturing and Assembly, *McGraw-Hill,* New York.

Gilleo, K. and Blumel, D. (2002). Electrically conductive adhesive for surfacemount and flip chip processes: an alternative to solder? Area Array Packaging Handbook : Manufacturing and Assembly. K. Gilleo, *McGraw-Hill,* New York.

Goobich, J. and Marom, G. (1982). Moisture absorption by tetraglycidyl 4,4′ -diaminodiphenyl methane/4,4′-diaminodiphenl sulfone epoxies containing brominated epoxy copolymers. *Polymer Engineering & Science,* Vol. 22(16), pp. 1052-1056.

Goodfellow. (2014). "CTE of PMMA." from http://www.goodfellow.com/E/Polymethylmethacrylate.html. [Accessed 26 May 2014]

Greig, W. J. (2007). Integrated Circuit Packaging, Assembly and Interconnections Springer.

Halbo, L. and Ohlckers, P. (1995). Electronic components, packaging and production, Department of Physics. Oslo, Norway, University of Oslo.

He, D., Ekere, N. N. and Cai, L. (1999). Computer simulation of random packing of unequal particles. *Physical Review E,* Vol. 60(6), pp. 7098-7104.

He, J. Y., Helland, T., Zhang, Z. L. and Kristiansen, H. (2009 b). Fracture of micrometre-sized Ni/Au coated polymer particles. *Journal of Physics D: Applied Physics,* Vol. 42(8), pp. 085405.

He, J. Y., Zhang, Z. L. and Kristiansen, H. (2007). Mechanical properties of nanostructured polymer particles for anisotropic conductive adhesives. *International Journal of Materials Research,* Vol. 98(5), pp. 389-392.

He, J. Y., Zhang, Z. L. and Kristiansen, H. (2009 a). Nanomechanical characterization of single micron-sized polymer particles. *Journal of Applied Polymer Science,* Vol. 113(3), pp. 1398-1405.

He, J. Y., Zhang, Z. L., Midttun, M., Fonnum, G., Modahl, G. I., Kristiansen, H. and Redford, K. (2008). Size effect on mechanical properties of micron-sized PS-DVB polymer particles. *Polymer,* Vol. 49(18), pp. 3993-3999.

He, J. Y., Zhang, Z. L., Midttun, M., Fonnum, G., Modahl, G. I., Kristiansen, H. and Redford, K. (2008). Size effect on mechanical properties of micron-sized PS‚ÄìDVB polymer particles. *Polymer,* Vol. 49(18), pp. 3993-3999.

Hecht, D. and Stark, D. (1994). Electrical and structural properties of thin gold films on glass substrates. *Thin Solid Films,* Vol. 238(2), pp. 258-265.

Helland, T. (2008). Experimental and numerical study on the nano-mechanical properties of polymer particles. *Masters Thesis,* Norwegian University of Science and Technology, NTNU.

Henkel. (2009). "Resistivity of gold filled adhesive ", from Technical Datasheet ABLEBOND® 85-1®.

Henkel. (2013). "http://www.photovoltaic-production.com/2012/advancing-solar-module-assembly-capability/."[Accessed 20 March 2013]

Hermann, S., Pahl, B., Ecke, R., Schulz, S. E. and Gessner, T. (2009). Carbon nanotubes for nanoscale low temperature flip chip connections. *Microelectronic Engineering,* Vol. 87(3), pp. 438-442.

Hersch, P. and Zweibel, K. (1982). Basic Photovoltaic Principles and Methods, Technical Information Office, Solar Energy Research Institute, Colarado.

Hill, R. M. (1967). Single carrier transport in thin dielectric films. *Thin Solid Films*, Vol. 1(1), pp. 39-68.

Holm, R. (1967). Electrical Contacts, Theory and Applications, *Springer-Verlag*.

Howard, J. (2009). Electroluminescence from a Solar Cell, Loughborough Unoversity.

Hu, K. X., Yeh, C. P. and Wyatt, K. W. (1997). Electro-thermo-mechanical responses of conductive adhesive materials. *IEEE Transactions on Component Packaging and Manufacturing Technology*. Vol. 20(4)**,** pp. 470-477.

Hyperphysics. (2014). "Metal resistivity." from http://hyperphysics.phy-astr.gsu.edu/hbase/tables/rstiv.html. [Accessed 26 May 2014]

Inoue, M., Muta, H., Maekawa, T., Yamanaka, S. and Suganuma, K. (2008). Temperature Dependence of Electrical and Thermal Conductivities of an Epoxy-Based Isotropic Conductive Adhesive. *Journal of Electronic Materials,* Vol. 37(4), pp. 462-468.

Instruments, N. (2012). "Part II– Photovoltaic cell I-V characterization theory and LabVIEW analysis code." from www.ni.com.

Instruments, N. (2012) "Photovoltaic cell I-V Charaterisation." Tutorial.

Ito, S., Mizutani, M., Noro, H., Kuwamura, M. and Prabhu, A. (1998). A novel flip chip technology using non-conductive resin sheet. *48th IEEE Electronic Components and Technology Conference*, Seattle, WA, 25-28 May, pp. 1047-1051.

Jagt, J. C. (1998). Reliability of electrically conductive adhesive joints for surfacemount applications : A summary of state of the art. IEEE Transactions on Components, Packaging and Manufacturing Technology. Vol. 21(2), pp. 215-225.

Jain, S., Whalley, D. C., Cottrill, M., Kristiansen, H., Redford, K., Nilsen, C. B., Helland, T. and Liu, C. (2011). Electrical properties of an isotropic conductive adhesive filled with silver coated polymer spheres. *18th European Microelectronics and Packaging Conference (EMPC)*, Brighton, UK, 12-15 Sep, pp. 1-7.

Jain, S., Whalley, D. C., Cottrill, M., Kristiansen, H., Redford, K., Nilsen, C. B., Helland, T. and Liu, C. (2013). The Effect of Coating Thickness on the Electrical Performance of Novel Isotropic Conductive Adhesives Prepared Using Metallised Polymer Micro-Spheres. *Proceedings of the 63rd Electronic Components and Technology Conference (ECTC)*, Las Vegas, USA, 31 May - 02 Jun, pp. 796-802.

Johnson, K. L. (1987). Contact Mechanics. Cambridge, U.K, *Cambridge University Press*.

Jong, P. C. d., Eikelboom, D. W. K., Wienke, J. A., Brieko, M. W. and Kloos, M. J. H. (2005). "Low-Stress Interconnections for Solar Cells." from www.ecn.nl/docs/library/report/2005/rx05006.pd. [Accessed 21 May 2011]

Kaminski, P. M. (2013). Remote plasma sputtering for silicon solar cells. *Doctoral Thesis*, Loughborough University.

Kang, S. K. and Purushothaman, S. (1998). Development of low cost, low temperature conductive adhesives. *48th IEEE Electronic Components & Technology Conference*, Seattle, WA, 25-28 May, pp. 1031-1035.

Kang, S. K., Rai, R. S. and Purushothaman, S. (1998). Development of high conductivity lead (Pb)-free conducting adhesives. *IEEE Transactions on Components Packaging and Manufacturing Technology, Part A*, Vol. 21(1), pp. 18-22.

Kay, R. and Desmulliez, M. (2012). A review of stencil printing for microelectronic packaging. *Soldering & Surface Mount Technology,* Vol. 24(1), pp. 38-50.

Kerschaver, E. V. and Beaucarne, G. (2006). Back-contact Solar Cells : A Review. *Progress in Photovoltaics: Research and Applications,* Vol. 14(2), pp. 107-123.

Kitano, T. and Kataoka, T. (1981). The rheology of suspensions of vinylon fibers in polymer liquids. II. Suspensions in polymer solutions. *Rheologica Acta,* Vol. 20(4), pp. 403-415.

Klengel, R., Petzold, M., Schade, D. and Sykes, B. (2011). Improved testing of soldered Busbar interconnects on silicon solar cells. *18th European Microelectronics and Packaging Conference (EMPC),* Brighton, UK, 12-15 Sep, pp. 1-5.

Klosterman, D., Li, L. and Morris, J. E. (1998). Materials Characterization, Conduction Development, and Curing Effects on Reliability of Isotropically Conductive Adhesives. *IEEE transactions on components, packaging, and manufacturing technology, Part A*, Vol 21(1), pp. 23-31.

Knauss, H., McCann, M., Neu, W., Fath, P., Jooss, W., Klenl, M., Keller, S., Eikelboom, D. W. K., Schoecker, A., Burto, T., Roberts, S., Earger, S., Mason, N., Dewallef, S., Lieten, K., Frisson, L., Kurth, M. and Heinzel, L. The advantage project : Development of new interconnection and encapsulation techniques for back contact cells.

Kohinata, S., Shiraki, Y., Inoue, M. and Uenishi, K. (2014). Relationship between shrinkage and conductivity properties of cured isotropic conductive adhesives. *International Conference on Electronics Packaging (ICEP),* Toyama, Japan, 23-25 Apr, pp. 316-321.

Kotthaus, S., Gunther, B. H., Hang, R. and Schafer, H. (1997). Study of isotropically conductive bondings filled with aggregates of nano-sited Ag-particles. *IEEE Transactions on Components, Packaging, and Manufacturing Technology, Part A* , Vol. 20(1), pp. 15-20.

Kreibig, U. and Fragstein, C. V. (1969). The limitation of electron mean free path in small silver particles. *Z. Phys. A,* Vol. 224(4), pp. 307-323.

Krieger, I. M. and Dougherty, T. J. (1959). A mechanism for non-Newtonian flow in suspensions of rigid spheres. *Journal of Rheology,* Vol. 3, pp. 137-152.

Kristiansen, H., Redford, K. and Helland, T. (2013). Isotropic conductive adhesive. United States, Patent No. US 2013/0323501 A1.

Kristiansen, H., Yuanliang, S. and Liu, J. (2001). Characterisation of Mechanical Properties of Metal-coated Polymer Spheres for Anisotropic Conductive Adhesive. *1st International IEEE Conference on Polymers and Adhesives in Microelectronics and Photonics,* Potsdam, Germany, 21-24 Oct., pp. 344-348.

Krupa, I., Miková, G., Novák, I., Janigová, I., Nógellová, Z., Lednický, F. and Prokes, J. (2007). Electrically conductive composites of polyethylene filled with polyamide particles coated with silver. *European Polymer Journal,* Vol. 43(6), pp. 2401-2413.

Kudtarkar, S. A. and Morris, J. E. (2002). Reliability of electrically conductive adhesives. *8th International Symposium on Advanced Packaging Materials.* Stone Mountain, GA, 03-06 Mar, pp. 144-150.

Kwon, W.-S. and Paik, K.-W. (2006). Experimental Analysis of Mechanical and Electrical Characteristics of Metal-Coated Conductive Spheres for Anisotropic Conductive Adhesives (ACAs) Interconnection. *IEEE Transactions on Components and Packaging Technologies,* Vol. 29(3), pp. 528-534.

Lewis, H. J. and Coughlan, F. M. (2008). An overview of the use of electrically conductive adhesives (ECAs) as a solder replacement. *Journal of Adhesion Science and Technology,* Vol. 22(8-9), pp. 801-813.

Li, L. and Morris, J. E. (1995). Electrical conduction models for isotropically conductive adhesives. *Journal of Electronics Manufacturing,* Vol. 5(4), pp. 289-296.

Li, L. and Morris, J. E. (1997). Electrical conduction models for isotropically conductive adhesive joints. *IEEE Transactions on Components, Packaging, and Manufacturing Technology, Part A,* Vol. 20(1), pp. 3-8.

Li, L. and Morris, J. E. (1998). An introduction to electrically conductive adhhesives. *International Journal of Microelectronics Packaging,* Vol. 1(3), pp. 159-175.

Li, Y., Daoqiang, L. and Wong, C. P. (2010). Characterizations of electrically conductive adhesives. Electrical Conductive Adhesives with Nanotechnologies. New York, USA, Springer:pp 81-117.

Li, Y. and Wong, C. P. (2006). Recent advances of conductive adhesives as a lead-free alternative in electronic packaging: Materials, processing, reliability and applications. *Materials Science and Engineering: R: Reports,* Vol. 51(1-3), pp. 1-35.

Li, Y., Yim, M. and Wong, C. P. (2007). High Performance Nonconductive Film with π-Conjugated Self-Assembled Molecular Wires for Fine Pitch Interconnect Applications. *Journal of Electronic Materials,* Vol. 36(5), pp. 549-554.

Licari, J. J. and Swanson, D. W. (2005). Adhesives technology for electronic applications : materials, processing,reliability. Adhesives Technology for Electronic Applications. Norwich, NY, William Andrew Publishing: pp 39-94.

Licari, J. J. and Swanson, D. W. (2005). Chemistry, Formulation, and Properties of Adhesives. Adhesives Technology for Electronic Applications. Norwich, NY, William Andrew Publishing: pp 95-168.

Liong, S., Wong, C. P. and Burgoyne, W. F., Jr. (2005). Adhesion improvement of thermoplastic isotropically conductive adhesive. *IEEE Transactions on Components and Packaging Technologies,,* Vol. 28(2), pp. 327-336.

Liu, J., Salmela, O., Sarkka, J., Morris, J. E., Tegehall, P. E. and Andersson, C. (2011). Conductive adhesive joint reliability. Reliability of Microtechnology : Interconnects Devices and Systems. New York, USA, Springer.

Liu, K. K., Williams, D. R. and Briscoe, B. J. (1998). The large deformation of a single micro-elastomeric sphere. *Journal of Physics D: Applied Physics,* Vol. 31(3), pp. 294- 303.

Lohokare, S. K., Lu, Z., Schuetz, C. A. and Prather, D. W. (2006). Electrical characterization of flip-chip interconnects formed using a novel conductive-adhesive-based process. *IEEE Transactions on Advanced Packaging,* Vol. 29(3), pp. 542-547.

Lu, D., Tong, Q. K. and Wong, C. P. (1999). Mechanisms underlying the unstable contact resistance of conductive adhesives. *IEEE Transactions on Electronics Components Packaging and Manufacturing,,* Vol. 22(3), pp. 228-232.

Lu, D. and Wong, C. P. (1999). Conductivity mechanisms of isotropic conductive adhesives. *IEEE Transactions on Electronics Packaging and Manufacturing,* Vol. 22(3), pp. 223 - 227.

Lu, D. and Wong, C. P. (2000). Characterization of Silver Flake Lubricants. *Journal of Thermal Analysis and Calorimetry,* Vol. 59(3), pp. 729-740.

Lu, D. and Wong, C. P. (2000). Development of conductive adhesives for solder replacement. *IEEE Transactions on Components and Packaging Technologies,,* Vol. 23(4), pp. 620-626.

Lu, D. and Wong, C. P. (2000). Effects of shrinkage on conductivity of isotropic conductive adhesives. *International Journal of Adhesion and Adhesives,* Vol. 20(3), pp. 189-193.

Lu, D., Wong, C. P., Tong, Q. K. and Zhang, E. (2000). Development of high performance surface mount conductive adhesives. *Proceedings of 50th Electronic Components and Technology Conference, (ECTC)*, Las Vegas, NV, 21-24 May, pp. 892-898.

Luoma, S. N. (2008). Silver nanotechnoogies and the environment: old problems or new challenges. PEN 15, The PEW Charitable Trusts.

Määttänen, J. (2003). Contact resistance of metal coated polymer particles used in anisotropically conductive adhesives. *Soldering & Surface Mount Technology,* Vol. 15(1), pp. 12-15.

Masterbond. (2013). "Resistivity of nickel filled adhesive ", from http://www.masterbond.com/tds/ep76m. [Accessed 21 May 2013]

Matsunaga, K., Komaru, T., Nakayama, Y., Kume, T. and Suzuki, Y. (2009). Mass-production technology for CIGS modules. *Solar Energy Materials and Solar Cells,* Vol. 93(6-7), pp. 1134-1138.

Matthey, J. (2010). FS34 Silver flakes data sheet. http://www.jmsilver.co.uk, Johnson Matthey. [Accessed 21 Aug 2010]

Matthey, J. (2012). Personal commuication.

Matula, R. A. (1979). Electrical resistivity of copper, gold, palladium and silver. *Journal of Physical Chemistry Reference Data,* Vol. 8(4).

Metalprices. (2012). "Metal costs." from www.metalprices.com [Accessed 11 Nov 2012]

Meyer, E. L. and van Dyk, E. E. (2004). Assessing the reliability and degradation of photovoltaic module performance parameters., *IEEE Transactions on Reliability,* Vol. 53(1), pp. 83-92.

Mir, I. and Kumar, D. (2008). Recent advances in isotropic conductive adhesives for electronics packaging applications. *International Journal of Adhesion and Adhesives,* Vol. 28(7), pp. 362-371.

Mir, I. A. and Kumar, D. (2010). Development of polypyrrole/ epoxy composites as isotropically conductive adhesives. *The Journal of Adhesion,* Vol. 86(4), pp. 447-462.

Moore , D. S. (2004). The basic practice of statistics. New York, W.H. Freeman.

Morris, J. E. (1999). Conduction mechanisms and microsturcture development in isotropic electrically conductive adhesives. Conductive Adhesves for Electronics Packaging. J. Liu, *Electrochemical Publications*.

Morris, J. E. (2006). Isotropic Conductive Adhesives: Future Trends, Possibilities and Risks. *Microelectronics Reliability,* Vol. 47(2-3), pp. 328-330.

Morris, J. E. (2008). Nanopackaging: Nanotechnologies and Electronics Packaging, Springer.

Morris, J. E., Anderssohn, F., Kudtarkar, S. and Loos, E. (2001). Reliability studies of an isotropic electrically conductive adhesive. *International IEEE Conference on Polymers and Adhesives in Microelectronics and Photonics*, 21-24 Oct, pp. 61-69.

Morris, J. E., Jeahuck, L. and Liu, J. (2005). Isotropic conductive adhesive interconnect technology in electronics packaging applications. *International Conference on Polymers and Adhesives in Microelectronics and Photonics, Polytronic*, 23-26 Oct, pp. 45-52.

Morris, J. E. and Liu, J. (1999). Conductive Adhesves for Electronics Packaging, *Electrochemical Publications*.

Morris, J. E. and Liu, J. (2007). Electrically conductive adhesives: A research status review. Micro- and Opto-Electronic Materials and Structures: Physics, Mechanics, Design, Reliability, Packaging: Volume II, Springer US. pp B527-B570.

Nelson, J. (2003). Introduction. The Physics of solar cells, *Imperial College Press.*

Nguyen, H. V. (2012). Interconnection technologies based on metal-coated polymer spheres. *Doctoral Thesis*, University of Oslo.

Nguyen, H. V., Andreassen, E., Kristiansen, H., Johannessen, R., Hoivik, N. and Aasmundtveit, K. E. (2013). Rheological Characterization of a Novel Isotropic Conductive Adhesive: Epoxy Filled with Metal-Coated Polymer Spheres. *Materials & Design,* Vol. 46, pp. 784-793.

Nguyen, H. V., Kristiansen, H., Gakkestad, J., Johannessen, J., Hoivik, N. and Aasmundtveit, K. E. (2010). Spherical Polymer Particles in Isotropic Conductive Adhesives: A Study on Rheology and Mechanical Aspects. *Proceedings of 3rd Electronic System-Integration Technology Conference (ESTC),* Berlin, 13-16 Sep, pp. 1-6.

Nguyen, H. V., Kristiansen, H., Johannessen, R., Andreassen, E., Larsson, A., Hoivik, N. and Aasmundtveit, K. E. (2011). Temperature Dependence of Mechanical Properties of Isotropic Conductive Adhesive Filled with Metal Coated Polymer Spheres. *Proceedings of 61st Electronic Components and Technology Conference (ECTC)*, Lake Buena Vista, FL, 31 May - 3 Jun, pp. 639-644.

Nicodemo, L., Nicolais, L., Romeo, G. and Scafora, E. (1978). Temperature effect on the electrical resistivity of metal/polymer composites. *Polymer Engineering & Science,* Vol. 18(4), pp. 293-298.

Oguibe, C. N., Mannan, S. H., Whalley, D. C. and Williams, D. J. (1998). Conduction mechanisms in anisotropic conducting adhesive assembly. *IEEE Transactions on Component Packaging and Manufacturing Technology,* Vol. 21, pp. 235-242.

Ogunjimi, A. O. and Whalley, D. C. (1992a). The effect of thermal stress on the reliability of conductive adhesive joints. Loughborough University, Loughborough University. 92/6.

Ogunjimi, A. O., Whalley, D. C. and Williams, D. J. (1992b). The influenec of adhesive matrix and curing temperature on residual stress in conductive adhesive joints. *AEI/IEEE Conference on Intercnnection Technologies for Extereme Integaration: Fine Pitch and Beyond*.

Petrie, E. M. (2006). Epoxy Adhesive Formulations, McGraw-Hill.

Puttlitz, K. J. and A. Stalter, K. (2004). Electrically conductive adhesives. Handbook of Lead Free Solder Technology for Microelectronics Assemblies. New York ,USA, Marcel Dekker.

Qi, S., Robert, L., Hutt, D. A., Vaidhyanathan, B., Liu, C., Webb, P. and Ebbens, S. (2012). Copper conductive adhesives for printed circuit interconnects. *Proceedings of 62nd Electronic Components and Technology Conference (ECTC)*, San Diego, CA, 29 May - 1 Jun, pp. 1651-1655.

Qin, X. Y., Zhang , W., Zhang, L. D., Jiang, L. D., Liu, X. J. and Jin, D. (1997). Low-temperature resistance and its temperature dependence in nanostructured silver. *Physics Review B,* Vol. 56 (16), pp. 10596-10604.

R.Zallen (1998). The Percolation Model. New York, A Wiley- Interscience Publication.

Rabilloud, G. and Philippe, C. (2005). Adhesives in electronics. Handbook of Adhesives and Sealants, Elsevier Science Ltd.

Rao, Y., Lu, D. and Wong, C. P. (2004). A study of impact performance of conductive adhesives. *International Journal of Adhesion and Adhesives,* Vol. 24(5), pp. 449-453.

Reddy, P. N., Reddy, M. H. P., Pierson, J. F. and Uthanna, S. (2014). Characterization of Silver Oxide Films Formed by Reactive RF Sputtering at Different Substrate Temperatures. *ISRN Optics*, Vol. 2014, pp. 1-7.

Redei, R. (2014). Personal Communication.

Redford, K. (2010). Personal communication.

Redford, K. (2011). Personal Communication.

RoHS (2008). Directive on the Restriction of the Use of Certain Hazardous Substances in Electrical and Electronic Equipment, RoHS.

Ruschau, G. R. and Newnham, R. E. (1992b). Critical volume fractions in conductive composites. *Journal of Composite Materials,* Vol. 26(18), pp. 2727-2735.

Ruschau, G. R., Yoshikawa, S. and Newnham, R. E. (1992a). Percolation constraints in the use of conductor-filled polymers for interconnects. Proceedings of 42nd Electronic Components and Technology Conference (ECTC). San Diego, CA, 18-20 May, pp. 841-486.

Sabayev, V., Croitoru, N., Inberg, A. and Shacham-Diamand, Y. (2011). The evolution and analysis of electrical percolation threshold in nanometers cale thin films deposited by electroless plating. *Materials Chemistry and Physics*, Vol.127(1-2), pp. 214-217

Sancaktar, E. and Bai, L. (2011). Electrically conductive epoxy adhesives. *Polymers,* Vol. 3(1), pp. 427-466.

Sander, M., Henke, B., Schweizer, S., Ebert, M. and Bagdahn, J. (2010). PV module defect detection by combination of mechanical and electrical analysis methods. *35th IEEE Photovoltaic Specialists Conference (PVSC)*, Honolulu, HI, 20-25 Jun, pp. 001765-001769.

Schonecker, A., Eikelboom, D., Manshanden, P., Goris, M., Wyers, P., Roberts, S., Bruton, T., Jooss, W., Faika, K., Kress, A., Kuhn, R., Neu, W., Knauss, H., Fath, P., Ferrazza, F., Nacci, R. V., Van Kerschaver, E., De Wolf, S., Szlufcik, J., Leistiko, O., Jorgensen, A., Glunz, S. W., Dicker, J., Kray, D., Solter, J. and Schfer, S. (2002). ACE Designs: The Beauty of Rear Contact Solar Cells. *Conference Record of the 29th IEEE Photovoltaic Specialists Conference*, 19-24 May 2002, pp. 106-109.

Schuh, C. A. (2006). Nanoindentation studies of materials. *Materials Today,* Vol. 9(5), pp. 32-40.

Schwertheim, S., Schreff, M., T.Muller, M.leinhos, W.R.Fahrner and C.Neitzert, H. (2008). Lead-free electrically conductive adhesives for solar cell interconnectors. *IEEE Photovoltaic Specialists Conference (PVSC)* San Diego, CA, USA, 11-16 May, pp. 1-6, IEEE.

Scott, G. D. and Kilgour, D. M. (1969). The density of random close packing of spheres. *British Journal of Applied Physics,* Vol. 2(2), pp. 863-866.

Shaw, S. J. and Tod, D. A. (1994). Adhesive bonding in severe environments. *Materials World,* Vol. 2(10), pp. 523-525.

Shi, F. G., Abdullah, M., Chungpaiboonpatana, S., Okuyama, K., Davidson, C. and Adams, J. M. (1999). Electrical conduction of anisotropic conductive adhesives: effect of size distribution of conducting filler particles. *Material Science and Semicondor Processing,* Vol. 2(3), pp. 263-269.

Shimada, Y., Lu, D. and Wong, C. P. (2000). Electrical characterizations and considerations of electrically conductive adhesives (ECAs). *Proceedings of International Symposium on Advanced Packaging Materials: Processes, Properties and Interfaces,* Braselton, GA, 6-8 Mar, pp. 336-342.

Shuangyan, X. and Dillard, D. A. (2003). Determining the impact resistance of electrically conductive adhesives using a falling wedge test. *IEEE Transactions on Components and Packaging Technologies,* Vol. 26(3), pp. 554-562.

Simmons, J. G. (1963). Generalized formula for the electric tunnel effect between similar electrodes separated by a thin insulating film. *Journal of Applied Physics,* Vol. 34(6), pp. 1793-1803.

Solmetric (2011) "Guide To Interpreting I-V Curve Measurements of PV Arrays: Application Note PVA-600-1."

Spath, M., Jong, P. C. d., Bennett, I. J., Visser, T. P. and Bakker, J. (2008). A novel Module Assembly Using Back Contact Solar Cells IEEE Photovoltaic Specialists Conference San Diego, USA,.

Stickel, J. J. and Powell, R. L. (2005). Fluid mechanics and rheology of dense suspensions. *Annual Rev Fluid Mechanics,* Vol. 37, pp. 129-149.

Su, B. (2006). Electrical thermomechanical and reliability modelling of electrically conductive adhesives. *Doctor of Philosophy Dissertation*, Georgia Institute of Technology.

Su, B. and J, Q. (2004). A Micromechanics model for electrical conduction in isotropically conductive adhesives during curing. *54th Electronic Components and Technology Conference (ECTC),* pp. 1766-1771.

Suhir, E., Lee, Y. C. and Wong, C. P. (2007). Micro and Opto-Electronics Materials and Structures: Physics, Mechanics, Design, Reliability, Packaging. USA, Springer.

Szlufcik, J., Agostinelli, G., Duerinckx, F., Kerschaver, E. V., Beaucarne, G., Tom, M. and Luis, C. (2005). Low cost industrial technologies of crystalline silicon solar cells. Solar Cells. Oxford, Elsevier Science.

Timsit, R. S. (2008). Constriction Resistance of Thin-Film Contacts. *Proceedings of the 54th IEEE Holm Conference on Electrical Contacts,* Orlando, FL, 27-29 Oct., pp. 332-336.

Tong, Q. K., Markley, D. L., Frederickson, G., Kuder, R. and Lu, D. (1999). Conductive adhesives with stable contact resistance and superior impact performance. *Proceedings of 49th Electronic Components and Technology Conference (EPTC)*, San Diego, CA, 1- 4 Jun, pp. 347-352.

Tummala, R. R. (2000 a). Introduction to Microsystems Packaging. Fundamentals of Microsystems Packaging. R. R. Tummala, *McGraw-Hill*, USA pp 2-41.

Ulrich, R. K. and Brown, W. D. (2006). Advanced Electronic Packaging. USA, IEEE, Wiley-Interscience, *A John Wiley and Sons*, Inc., Publication.

Usui, H., Mizutani, M., Noro, H., Kuwamura, M. and Ito, S. (1999). High reliable and mass production-able flip chip package using non conductive film resin. *Proceedings 49th Electronic Components and Technology Conference*, San Diego, CA, 01-04 Jun, pp. 415-418.

Vanlandingham, M. R. (2003). Review of Instrumented Indentation. *Journal of Research of the National Institute of Standards and Technology*, Vol. 108, pp. 249-265.

Vons, S. A., Jr., Tong, Q. K., Kuder, R. and Shenfield, D. (1998). Surface mount conductive adhesives with superior impact resistance. *4th International Symposium on Advanced Packaging Materials*, Braselton, GA, 15-18 Mar, pp. 261-267.

Wang, X., Wang, Y., Chen, G., Liu, J. and Lai, Z. (1998). Quantitative estimate of the characteristics of conductive particles in ACA by using nano-indenter. *IEEE Transactions on Components, Packaging, and Manufacturing Technology, Part A*, Vol. 21(2), pp. 248-251.

Ward, I. M. and W., H. D. (1993). An Introduction to the Mechanical Properties of Solid Polymers, *John Wiley & Sons Ltd*, Chichester.

Whalley, D. C. (1988). An Investigation of Environmental Testsing of Surface Mount Components. *Master of Philosophy Thesis*, Loughborough University of Technology.

Whalley, D. C. (2013). Personal Communication.

Wiese, S. and Kraemer, F. (2012). Analysis of thermo-mechanical stresses in novel back contact solar modules. *4th Electronic System-Integration Technology Conference (ESTC)*, Amsterdam, Netherlands, 17-20 Sep, pp. 1-6.

Wiese, S., Kraemer, F., Betzl, N. and Wald, D. (2010). Interconnection technologies for photovoltaic modules - analysis of technological and mechanical problems. *11th International Conference on Thermal, Mechanical & Multi-Physics Simulation and*

Experiments in Microelectronics and Microsystems (EuroSimE), Bordeaux, 26-28 Apr, pp. 1-6.

Williams, D. J. and Whalley, D. C. (1993). The effects of conducting particle distribution on the behaviour of anisotropic conducting adhesives: non-uniform conductivity and shorting between connections. *Journal of Electronics Manufacturing,* Vol. 3(2), pp. 85-94.

Williams, D. J., Whalley, D. C., Boyle, O. and Ogunjimi, A. O. (1993). Anisotropic conductive adhesives for electronic interconnection. *Solder Surface Mount Technology,* Vol. 5(2), pp. 4-8.

Wohlgemuth, J. H. (2003) "Long Term Photovoltaic Module Reliability."

Woods, M. E. and Krieger, I. M. (1970). Rheological studies on dispersions of uniform colloidal spheres, I. Aqueous dispersions in steady shear flow. *Journal of Colloid and Interface Science,* Vol. 34(1), pp. 91-99.

Wu, H. P., Wu, X. J., Ge, M. Y., Zhang, G. Q., Wang, Y. W. and Jiang, J. (2007). Properties investigation on isotropical conductive adhesives filled with silver coated carbon nanotubes. *Composites Science and Technology,* Vol. 67(6), pp. 1182-1186.

Xu, S., Dillard, D. A. and Dillard, J. G. (2003). Environmental aging effects on the durability of electrically conductive adhesive joints. *International Journal of Adhesion and Adhesives,* Vol. 23(3), pp. 235-250.

Yamashita, M. and Suganuma, K. (2005). Improvement in high-temperature degradation by isotropic conductive adhesives including Ag-Sn alloy fillers. *Microelectronics and Reliability,* Vol. 46(5-6), pp. 850-858.

Yamashita, M. and Suganuma, K. (2006). Degradation by Sn diffusion applied to surface mounting with Ag-epoxy conductive adhesive with joining pressure. *Microelectronics and Reliability,* Vol. 46(7), pp. 1113-1118.

Yamashita, M., Suganuma, K., Komagata, M. and Shirai, Y. (2001). An improvement of conductive adhesives on high temperature endurance by using Ag-Sn alloy powder. *First International IEEE Conference on Polymers and Adhesives in Microelectronics and Photonics*, Potsdam, Germany, 21-24 Oct, pp. 265-269.

Yi Li, Daniel Lu and Wong, C. P. (2010). Non-conductive adhesives. Eletrical conductive adhesives with nanotechnologies, *Springe*r, New York, USA,

Yi. Li, Daniel. Lu and Wong, C. P. (2010). Electrical Conductive Adhesives ith Nanotechnologies. *Springer*, New York, USA.

Yim, M. J., Li, Y., Moon, K. S. and Wong, C. P. (2007). Oxidation prevention and electrical property enhancement of copper-filled isotropically conductive adhesives. *Journal of Electronic Materials,* Vol. 36(10), pp. 1341-1347.

Yim, M. J. and Paik, K. W. (2006). Recent advances on anisotropic conductive adhesives (ACAs) for flat panel displays and semiconductor packaging applications. *International Journal of Adhesion and Adhesives,* Vol. 26(5), pp. 304-313.

Yongqing, W., Haipeng, Z., Dengyuan, S. and Ailing, C. (2013). Research to the typical defects of crystalline silicon photovoltaic cells based on EL images. *International Journal of Energy Science (IJES),* Vol. 3(3), pp. 200-204.

Yu, H., Mhaisalkar, S. G. and Wong, E. H. (2007). Evolution of Contact Resistance during the Bonding Process of NCA Flip-Chip Interconnections. *Journal of Electronic Materials,* Vol. 36(12), pp. 1719-1723.

Zhang, R. W., Lin, W., Lawrence, K. and Wong, C. P. (2010). Highly reliable, low cost, isotropically conductive adhesives filled with Ag-coated Cu flakes for electronic packaging applications. *International Journal of Adhesion and Adhesives,* Vol. 30(6), pp. 403-407

Zhang, Z. L., Kristiansen, H. and Liu, J. (2007). A method for determining elastic properties of micron-sized polymer particles by using flat punch test. *Computational Materials Science,* Vol. 39(2), pp. 305-314.

Zwolinski, M., Hickman, J., Rubin, H., Zaks, Y., McCarthy, S., Hanlon, T., Arrowsmith, P., Chaudhuri, A., Hermansen, R., Lan, S. and Napp, D. (1996). Electrically conductive adhesives for surface mount solder replacement. *IEEE*

Transactions on Components Packaging and Manufacturing Technology, Part C., Vol. 19(4), pp. 241-250.

APPENDIX A

MPS DENSITY MEASUREMENT

Aim

The aim of this experiment is to measure the density of 30μm Ag-MPS.

Material used

30μm Ag-MPS with a narrow size distribution were supplied by Conpart As, Norway.

Equipment used

Weighing Machine, Micromeritics Multivolume Pycnometer 1305

Figure A.1 Micromeritics Multivolume Pycnometer 1305

Method used

The Micromeritics pycnometer operates by detecting the pressure change resulting from displacement of Helium by a solid object.

A sample of unknown volume, V_{samp}, was placed into a sealed sample chamber of known volume, V_{cell}. After sealing, the pressure P1 within the sample chamber was measured. Then, an isolated reference chamber of known volume, V_{exp}, was charged to a pressure P2, which was greater than that of the sample chamber. A valve isolating the two chambers was opened and the pressure of the system was allowed to equilibrate. It was assumed that the system is maintained at a constant temperature and there is no net loss or gain of Helium i.e. the number of Helium molecules n is constant throughout the experiment. Applying the gas law the volume of the sample is calculated by the pycnometer software as follows:

$$\boldsymbol{V_{samp} = V_{cell} - \frac{V_{exp}}{\frac{(P1-Pa)}{(P2-Pa)}-1}} \qquad \boldsymbol{A}.1$$

where V_{samp} is the volume of sample under measurement

V_{cell} is the volume of sealed chamber

V_{exp} is the volume of reference chamber

P_1 is the pressure of sealed chamber

P_2 is the pressure of reference chamber

P_a is the pressure at equilibrium

Dividing this volume by the mass of the sample, the density is obtained

Results

V_{cell} = 36.19169 cc, V_{exp} = 20.86496 cc, Pa = 14.695949 Psi,

Mass of the sample = 7.6933g

Five sets of measurements of P1and P2 were taken for the same sample was noted. These values and the software calculated the density are shown in Table A.1

Table A.1 Density Measurement

	P1 (Psi)	**P2 (Psi)**	**P1/P2**	**Density (g/cc)**
1	19.565	11.672	1.6762	1.441
2	19.562	11.670	1.6763	1.441
3	19.563	11.670	1.6764	1.440
4	19.561	11.667	1.6766	1.437
5	19.561	11.666	1.6768	1.435
			Average	**1.438**

APPENDIX B

ADDITIONAL SCANNING ELECTRON MICROSCOPY IMAGES OF Ag-MPS

This appendix contains some additional FEGSEM images of Ag-MPS showing examples of poor plating quality.

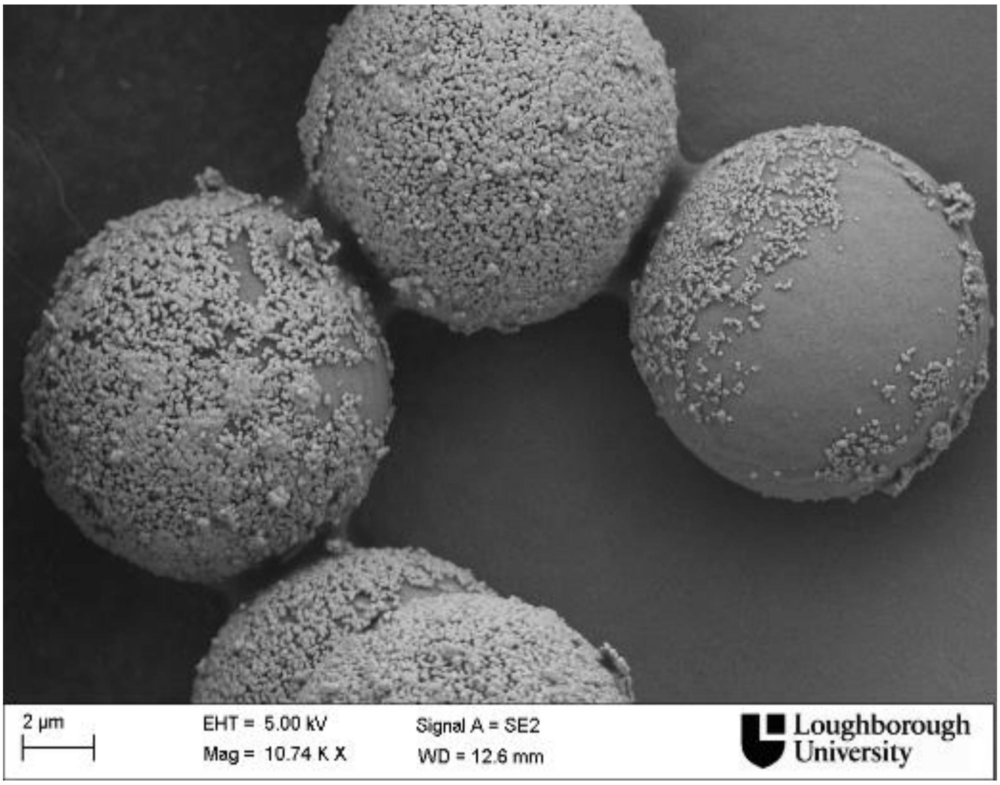

Figure B.1 10µm Ag-MPS

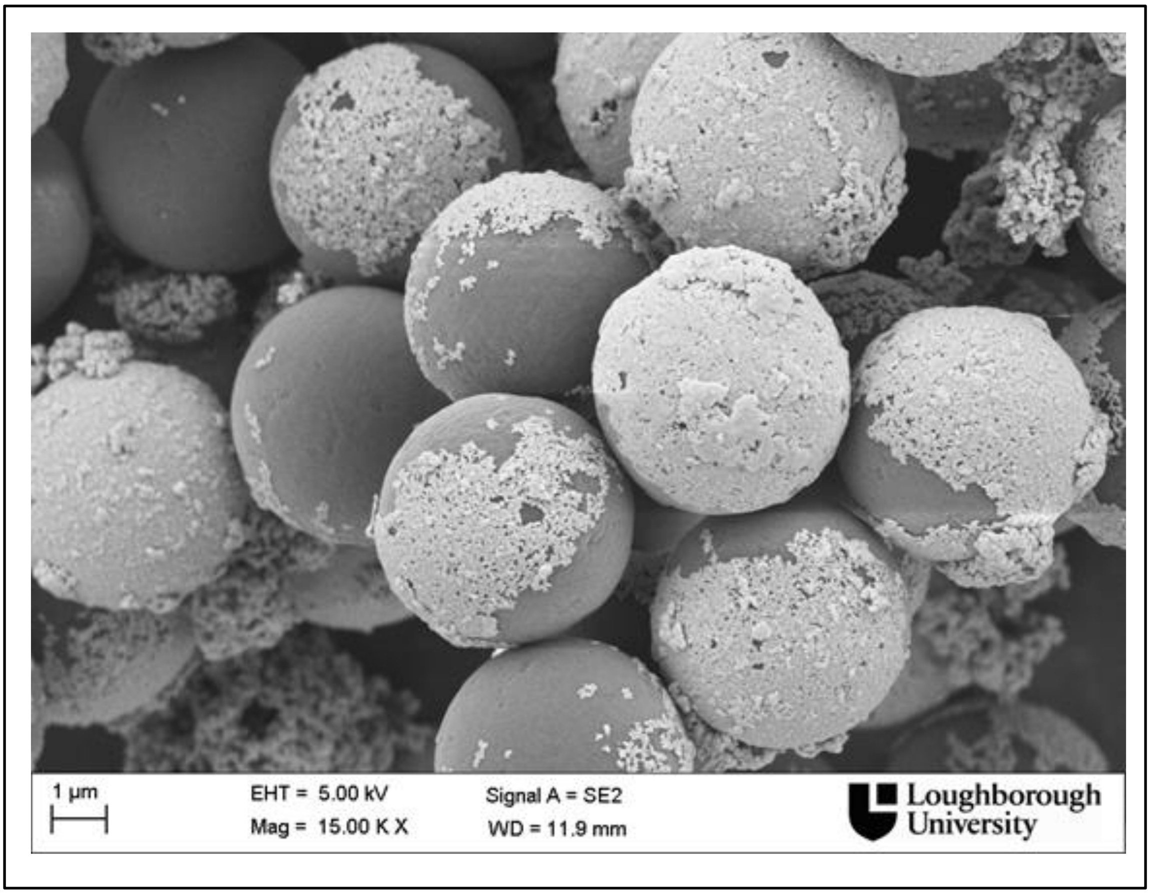

Figure B.2 4.77 µm Ag-MPS

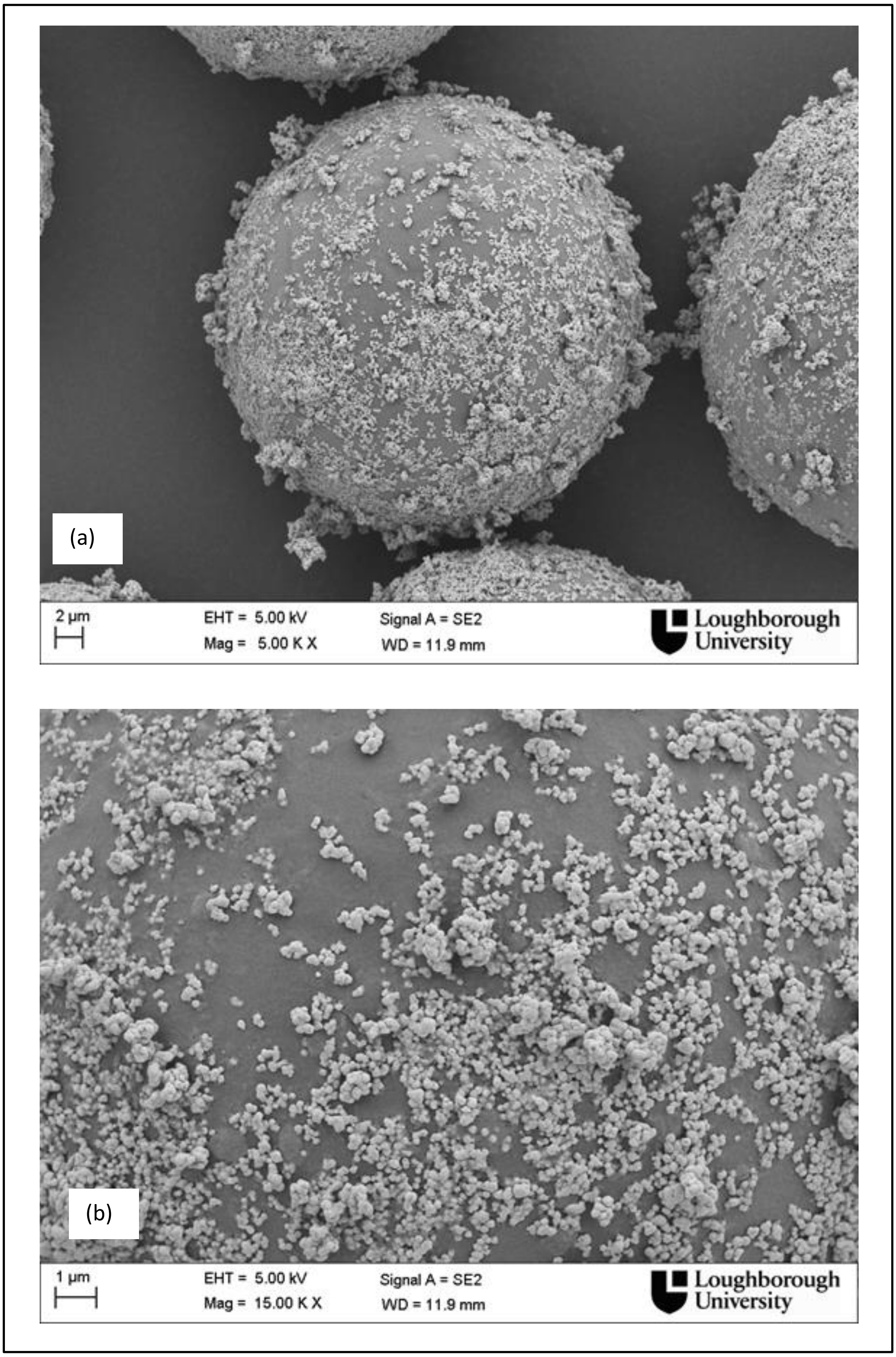

Figure B.3 (a) 30µm Ag-MPS (b) magnified image showing poor Ag coating quality

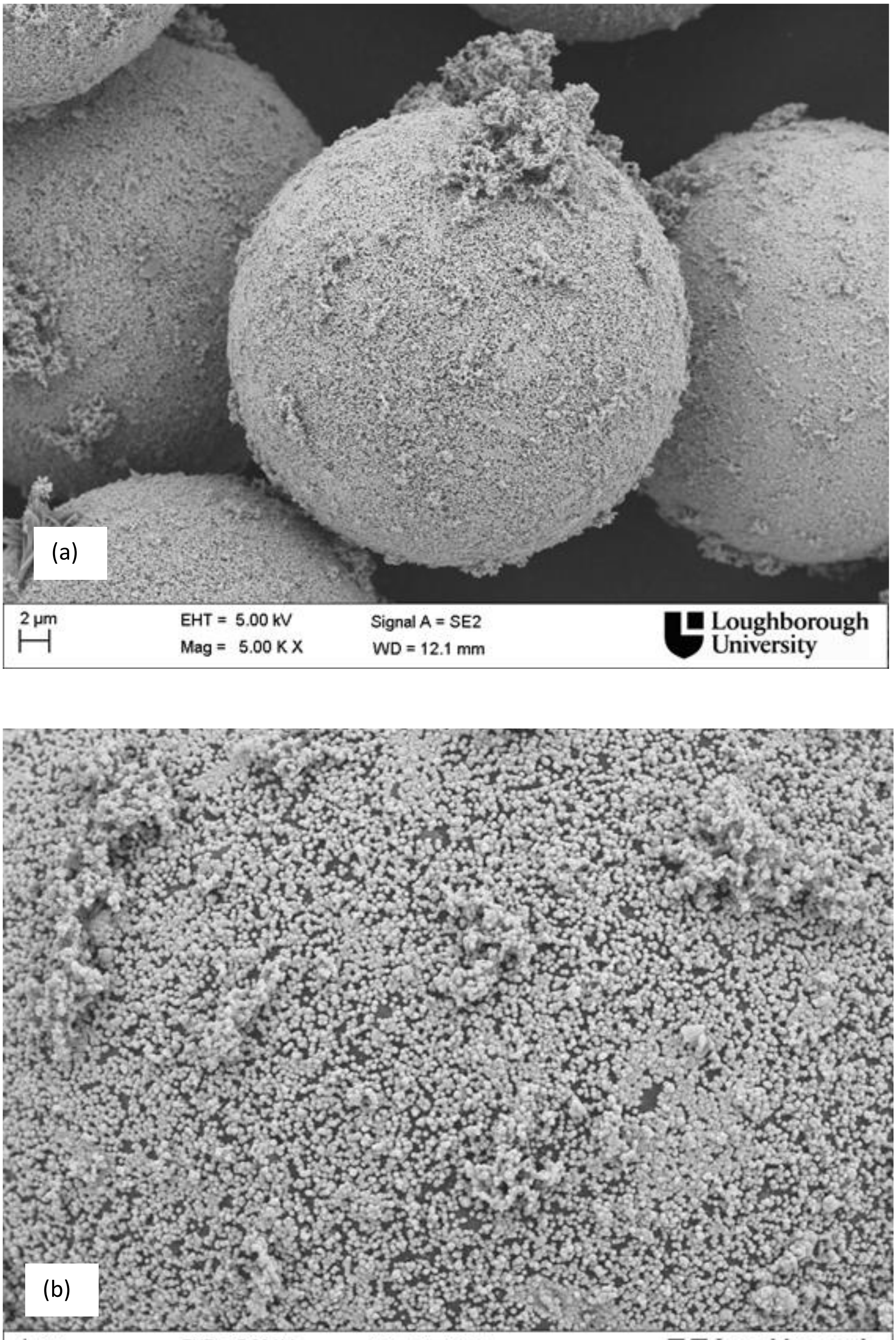

Figure B.4 (a) 30µm Ag-MPS (b) magnified image showing poor Ag coating quality

APPENDIX C

RESULTS AND CALCULATIONS USED IN CHAPTERS 6, 7 AND 8

C.1 Results and Calculations Used in Chapter 6

Volume fraction % of silver in Ag-MPS:

The formula used to calculate the % volume fraction of silver in Ag-MPS is:

$$\%\,volume\ fraction\ of\ silver\ in\ Ag-MPS = \frac{(\boldsymbol{volume\ of\ MPS - volume\ of\ PS})}{\boldsymbol{volume\ of\ MPS}} \qquad \textbf{C.1}$$

Table C.1 Volume fraction of silver in various Ag-MPS used in Chapter 6

Ag-MPS	PS Volume (cm³)	Ag-MPS Volume (cm³)	Ag Volume (cm³)	% Vol Fraction of Silver in Ag-MPS
30_10B	$1.413\text{x}10^{-08}$	$1.442\text{x}10^{-08}$	$2.846\text{x}10^{-10}$	1.97%
30_15B	$1.413\text{x}10^{-08}$	$1.456\text{x}10^{-08}$	$4.283\text{x}10^{-10}$	2.94%
30_20B	$1.413\text{x}10^{-08}$	$1.471\text{x}10^{-08}$	$5.730\text{x}10^{-10}$	3.89%
30_25B	$1.413\text{x}10^{-08}$	$1.485\text{x}10^{-08}$	$7.187\text{x}10^{-10}$	4.83%
30_22D	$1.413\text{x}10^{-08}$	$1.478\text{x}10^{-08}$	$6.457\text{x}10^{-10}$	4.36%
10_15B	$5.235\text{x}10^{-10}$	$5.721\ \text{x}10^{-10}$	$4.855\ \text{x}10^{-11}$	8.48%
10_20C	$5.235\text{x}10^{-10}$	$5.889\ \text{x}10^{-10}$	$6.537\ \text{x}10^{-11}$	11.10%
10_21D	$5.235\text{x}10^{-10}$	$5.923\ \text{x}10^{-10}$	$6.878\ \text{x}10^{-11}$	11.61%
6_10B	$1.130\text{x}10^{-10}$	$1.247\ \text{x}10^{-10}$	$1.169\ \text{x}10^{-11}$	9.36%

Volume fraction % of silver in an Ag-MPS filled ICA:

The formula used to calculate the % volume fraction of silver in Ag-MPS is:

$$\%\ vol\ fraction\ of\ silver\ in\ ICA = \left(\left(\boldsymbol{vol.of\ MPS - vol.of\ PS}\right)\middle|\boldsymbol{vol.of\ MPS}\right) * \boldsymbol{vol\%\ of\ MPS} \qquad \textbf{C.2}$$

Table C.2 Volume measurement to determine sample size

Volume Measurement (mm^3)					
No. of Measurements	**1st Dataset**	**2nd Dataset**	**3rd Dataset**	**4th Dataset**	**5th Dataset**
1	0.2722	0.2759	0.2758	0.2762	0.2781
2	0.2714	0.2756	0.2767	0.2762	0.2776
3	0.2720	0.2759	0.2758	0.2762	0.2775
4	0.2715	0.2770	0.2758	0.2770	0.2777
5	0.2747	0.2769	0.2765	0.2772	0.2779
6	0.2726	0.2760	0.2773	0.2773	0.2778
7	0.2726	0.2771	0.2766	0.2773	0.2776
8	0.2719	0.2769	0.2754	0.2770	0.2766
9	0.2720	0.2769	0.2761	0.2773	0.2759
10	0.2715	0.2766	0.2755	0.2772	0.2759
Average	0.2722	0.2764	0.2761	0.2768	0.2772
Standard Deviation	0.000913	0.000536	0.000574	0.000463	0.000776

Table C.3 Averaged volume measurements for uncured and cured ICAs using 30_20B

	Uncured Sample		**Cured Sample**		**Volume Change**	
Vol % of 30_20B	**Avg. Volume (mm^3)**	**Standard Deviation**	**Avg. Volume (mm^3)**	**Standard Deviation**	**(mm^3)**	**% Volume change**
40%	0.3025	0.000424	0.3045	0.0010	0.0020	0.5
47%	0.2519	0.00077	0.2614	0.00077	0.0095	3.7
50%	0.2912	0.00044	0.3044	0.00054	0.0132	4.5
52%	0.2312	0.0013	0.2362	0.00044	0.005	2.1

Table C.4 Comparing volume change of uncured and cured ICA for FS-34

Cure Schedule	Vol %	Uncured Sample		Cured Sample		Volume Change (mm^3)	% Volume Change
		Avg. Volume (mm^3)	Standard Deviation	Avg. Volume (mm^3)	Standard Deviation		
Type I							
150°C, 15min	21%	0.2728	0.00072	0.2631	0.0012	-0.0097	- 3.5%
Type II							
120°C, 30min	21%	0.0587	0.00076	0.0517	0.00071	- 0.0070	- 11.9%
	23%	0.0513	0.00013	0.0466	0.00058	- 0.0047	- 9.1%
150°C, 15min	21%	0.0710	0.00062	0.0596	0.00039	- 0.0113	-15.9%
	23%	0.0396	0.00020	0.0364	0.00077	- 0.0032	- 8.3%

Table C.5 Average volume of uncured and cured ICA with standard deviation for 30_20C

		Uncured Sample		Cured Sample			
	Vol %	Avg. Volume (mm^3)	Standard Deviation	Avg. Volume (mm^3)	Standard Deviation	Volume Change (mm^3)	% Volume Change
Type I							
150°C, 15min	44%	0.2547	0.0010	0.2546	0.00064	- 0.0001	0.02%
Type II							
120°C, 30min	46%	0.4212	0.000349	0.4323	0.0003898	0.0111	2.8%
	50%	0.2566	0.000644	0.2573	0.00109	0.0007	0.01%
	52%	0.333	0.000962	0.3455	0.00078	0.0125	3.75%
150°C, 15min	46%	0.2529	0.00064	0.2592	0.00071	0.0063	2.5%
	50%	0.3349	0.000571	0.3364	0.000691	0.0015	0.01%
	52%	0.3151	0.000749	0.29812	0.00058	- 0.01698	-5.3%

Table C.6 Average volume and standard deviation of cured and uncured H20E

H20E	Uncured		Cu			
	Average Volume (mm^3)	Standard Deviation	Average Volume (mm^3)	Standard Deviation	Volume Change (mm^3)	% Volume Change
120°C/30min	0.0865	0.00061	0.0715	0.0001	0.150	-17.3%
150°C/15min	0.0741	0.0004	0.0582	0.0001	0.159	-21.4%

C.2 Results and Calculations Used in Chapter 7

Resistance of Au/Ni/Cu track on PCB:

The formula used to calculate Au/Ni/Cu track resistance that need to be subtracted from TWR measurements is:

$$\frac{\mathbf{1}}{\boldsymbol{R}_{\,(\boldsymbol{Au,Ni,Cu})\boldsymbol{Track}}} = \frac{\mathbf{1}}{\boldsymbol{R}_{\boldsymbol{Au-track}}} + \frac{\mathbf{1}}{\boldsymbol{R}_{\boldsymbol{Ni-Track}}} + \frac{\mathbf{1}}{\boldsymbol{R}_{\boldsymbol{Cu-Track}}} \qquad \textbf{C.3}$$

where

$$R_{Au-Track} = \rho_{Au} \frac{Length\ of\ \ Track}{Width\ of\ \ Track\ x\ Thickness\ of\ Au\ coating}$$

$$R_{Ni-Track} = \rho_{Ni} \frac{Length\ of\ Track}{Width\ of\ \ Track\ x\ Thickness\ of\ Ni\ Coating}$$

$$R_{Cu-Track} = \rho_{Cu} \frac{Length\ of\ \ Track}{Width\ of\ Track\ x\ Thickness\ of\ Cu\ Coating}$$

Using values: $\rho_{Au} = 2.40 \times 10^{-8}$ Ωm, $\rho_{Ni} = 6.99 \times 10^{-8}$ Ωm, $\rho_{Cu} = 1.68 \times 10^{-8}$ Ωm. Length and width of track as 3.5×10^{-3} m and 0.20×10^{-3} m respectively. And Au coating thickness as 200×10^{-9}m, Ni coating thickness as 8µm and Cu coating thickness as 35µm. The track resistance is calculated as: 0.0079Ω.

Table C.7 Contact resistance and resistivity of 4.8 µm MPS filled ICA

4.8_15A						
Vol% of Filler	35%	39%	40%	42%	44%	46%
Average Contact Resistance (Ω)	0.083	0.043	0.061	0.072	0.066	0.059
Standard Deviation	0.023	0.088	0.041	0.039	0.023	0.003
% Standard Deviation	25	88	59	48	31	4
Average Resistivity (Ωcm)	0.0093	0.0047	0.0074	0.0049	0.0009	0.0004
Standard Deviation	0.0018	0.0015	0.0010	0.0011	0.0003	0.00005
% Standard Deviation	19	33	13	24	33	13

Table C.8 Contact resistance and resistivity of 6 µm MPS filled ICA

06_10B					
Vol% of Filler	35%	40%	45%	48%	50%
Average contact resistance (Ω)	0.071	0.072	0.087	0.059	0.029
Standard Deviation	0.014	0.005	0.008	0.003	0.021
% Standard Deviation	17	6	8	4	33
Average Resistivity (Ωcm)	13.90	0.0044	0.0012	0.0012	0.0011
Standard Deviation	22.31	0.0005	0.0002	0.00014	0.0001
% Standard Deviation	160	11	17	11	14

Table C.9 Contact resistance and resistivity of 30 µm MPS filled ICA

30_13A							
Vol% of Filler	35%	37%	40%	42%	46%	49%	52%
Average contact resistance (Ω)	0.138	0.131	0.098	0.096	0.090	0.073	0.063
Standard Deviation	0.043	0.040	0.026	0.018	0.010	0.002	0.002
% Standard Deviation	31	28	24	17	11	2.5	3
Average Resistivity (Ωcm)	0.029	0.0200	0.0097	0.0081	0.0068	0.0051	0.0031
Standard Deviation	0.0029	0.0046	0.0009	0.00097	0.0007	0.0001	0.0004
% Standard Deviation	9	23	9	11	11	3	16

Table C.10 Contact resistance and resistivity of silver flake filled and commercial ICA

	FS-34			H20E
Vol% of Filler	18%	20%	22%	31%
Average contact resistance (Ω)	0.090	0.068	0.062	0.034
Standard Deviation	0.026	0.006	0.004	0.002
% Standard Deviation	26	8	4	6
Average Resistivity (Ωcm)	0.006726	0.001245	0.000596	0.443
Standard Deviation	0.000575	0.00016	0.000079	0.017
% Standard Deviation	8	12	13	4

Table C.11 Contact resistance for ICAs containing 30 µm MPS plated using method B

	30_20B					
Vol% of Filler	35%	40%	45%	48%	50%	52.5%
Average contact resistance (Ω)	0.104	0.128	0.089	0.079	0.047	0.067
Standard Deviation	0.020	0.0242	0.017	0.008	0.036	0.009
% Standard Deviation	19	18	19	11	70	13
Average Resistivity (Ωcm)	11.73	0.0109	0.0038	0.0026	0.0018	0.0013
Standard Deviation	9.161	0.0117	0.0023	0.0006	0.0006	0.0003
% Standard Deviation	64	26	10	16	36	23

Table C.12 Contact resistances for ICAs containing 30µm MPS plated using method C

	30_20C			
Vol% of Filler	44%	46%	48%	51%
Average contact resistance (Ω)	0.085	0.075	0.080	0.083
Standard Deviation	0.020	0.006	0.025	0.034
% Standard Deviation	24	08	31	40
Average Resistivity (Ωcm)	0.0040	0.0030	0.0021	0.0014
Standard Deviation	0.0003	0.00006	0.0001	0.0002
% Standard Deviation	7	2	4	13

Table C.13 Contact resistances for ICAs formulated using type I matrix and different curing conditions

	120°C /30min				150°C /15min			
Vol% of Filler	44%	46%	48%	51%	44%	46%	48%	51%
Average contact resistance (Ω)	0.100	0.095	0.083	0.070	0.093	0.083	0.088	0.086
Standard Deviation	0.007	0.025	0.008	0.024	0.020	0.006	0.025	0.024
% Standard Deviation	7	26	9	34	21	7	28	27
Average Resistivity (Ωcm)	0.003	0.003	0.002	0.001	0.004	0.003	0.002	0.001
Standard Deviation	0.0002	0.0002	0.0002	0.0003	0.0003	0.00006	0.0001	0.0002
% Standard Deviation	7	7	10	18	7	2	4	13

Table C.14 Contact resistances for ICAs formulated using type II matrix

	120°C /30min			150°C /15min		
Vol% of Filler	46%	50%	53%	46%	50%	53%
Average contact resistance (Ω)	0.007	0.008	0.007	0.014	0.018	0.009
Standard Deviation	0.003	0.001	0.002	0.009	0.007	0.002
% Standard Deviation	42	12	28	64	38	22
Average resistance (Ω)	0.0018	0.0012	0.0009	0.0014	0.0014	0.0011
Standard Deviation	0.0001	0.00009	0.0001	0.00009	0.0001	0.00007
% Standard Deviation	6	9	6	6	7	11

C.3 Formulas Used in Chapter 8

Copper track resistance in MWT module:

The resistance offered by copper track for making back and front contact is calculated using formula:

$$\boldsymbol{R_{Cu-Track} = No\ of\ tracks\ x\ \rho_{Cu} \frac{Length\ of\ track}{Width\ of\ track\ x\ Thickness\ of\ track}} \qquad \textbf{C.4}$$

Using the values of ρ_{Cu} as 1.68 x 10^{-8} Ωm, length, width and thickness of Cu track as 1.6 x 10^{-2} m, 0.8 x 10^{-2} m and 35 x 10^{-6} m respectively.

ICA resistance in MWT module

$$\boldsymbol{R_{ICA} = No\ of\ ICA\ dots\ x\ \rho_{ICA} \frac{Length\ of\ Dot}{Area\ of\ ICA\ dot}} \qquad \textbf{C.5}$$

APPENDIX D

CASE STUDY: USE OF Ag-MPS FILLED ICA IN A PV APPLICATION

As discussed Chapter 1 photovoltaics are a fast growing sector among the various renewable energy sources. Back contact cells, with large cell area and made using thin Si wafers are an upcoming type of PV cell which offer many benefits such as lower cost, lower shading losses, lower series resistance and higher module packing densities and thus have a higher power output for a given area compared to modules utilising conventional H-pattern cells assembled using tab string assembly (Spath et al. 2008; Eerensteina et al. 2012). Additionally, isotropic conductive adhesives have recently emerged as an important material in photovoltaic (PV) module interconnections, especially for these large area back contact cells where the high process temperatures of soldering induces larger stresses in the cells which may lead to their degradation and poor reliability (Eikelboom et al. 2002; Bultman et al. 2003). As there is a great potential for significant growth in ICA usage in PV, the performance of ICA interconnections in a novel design of back contact PV module has been investigated and is presented in this chapter.

In this investigation metallisation wrap through (MWT) cells, a type of back contact PV cell, were used to make modules. MWT cells use the same materials as the process for standard H-Pattern cells with the only major difference being the laser drilling of vias in the wafer which are then filled with silver paste for carrying current to front contact on rear side of the cell. Therefore, the methods used to assess the performance of standard Si cells/modules were used to assess the performance of the MWT cells/modules. One of the ways in which the performance of a PV cell/module can be assessed is in terms of performance parameters deduced from current verses voltage (I-V) curves such as open circuit voltage (V_{OC}), short circuit current (I_{SC}), maximum power (P_{MAX}), fill factor (FF), efficiency (η), and series (R_S) and shunt resistances (R_{SH}), obtained at standard conditions of temperature and illumination. This chapter first briefly explain the performance of modules assembled using Ag-MPS filled ICA.

D.1 Electrical Performance of PV Modules: A Theoretical Overview

PV cells are made of semiconducting materials, most commonly silicon, arranged in the form of a p-n junction that can convert incident radiation in the solar spectrum to an electrical current. When there is no light present to generate any current, the PV cell behaves like a junction diode. A cross-section of a basic PV cell is shown in Figure D.1

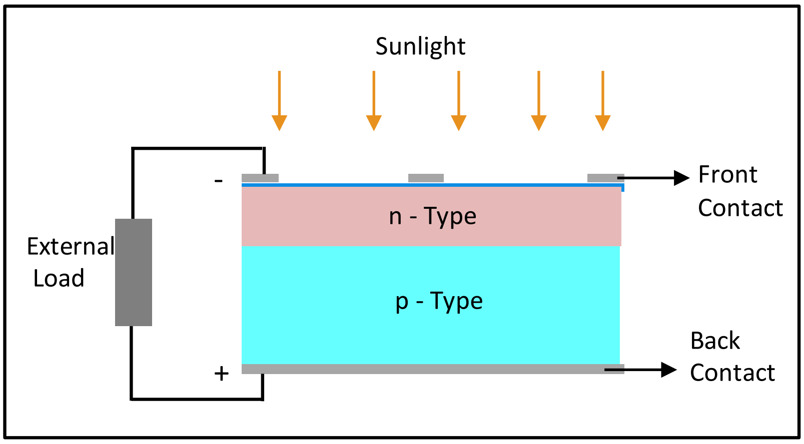

Figure D. 1 Cross-section of a PV cell after (Nelson 2003)

The idealised electronic behaviour of a PV cell can be modelled as a current source in parallel with a diode (Hersch et al. 1982; Meyer et al. 2004). In practice however no PV cell is ideal, power is dissipated through the resistance of the contacts and through the leakage currents around the sides of the device, so a shunt resistance, R_{SH}, and a series resistance, R_S, are added to the model (Nelson 2003). This equivalent circuit model for a photovoltaic cell is illustrated in Figure D.2.

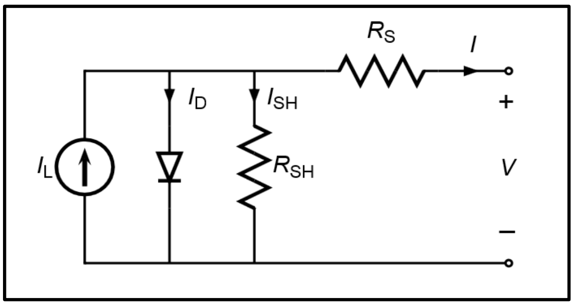

Figure D.2 Equivalent circuit model for a photovoltaic cell

From the equivalent circuit it is evident that the current produced by the PV cell is equal to that produced by the current source, minus that which flows through the diode, minus that which flows through the shunt resistor.

$$I = I_L - I_D - I_{SH} \tag{D.1}$$

where I is the output current (A);

I_L is the photo generated current (A);

I_D is the diode current (A);

I_{SH} is the shunt current (A);

By Ohm's law the current diverted through the shunt resistor is:

$$I_{SH} = \frac{V+IR_S}{R_{SH}} \qquad \text{D.2}$$

where V is the voltage (V) that is either produced or applied (voltage bias)

The Shockley diode equation gives the current diverted through the diode (Nelson 2003):

$$I_D = I_0\left(e^{\frac{q(V+IR_S)}{NkT}} - 1\right) \qquad \text{D.3}$$

where I_0 is the saturation current of the diode (A);

N is the diode ideality factor (1 for an ideal diode but typically between 1 and 2);

q is the elementary charge (C);

k is the Boltzmann constant (J/K); and

T is the cell temperature (K).

Substituting equations 8.2 and 8.3 into equation 8.1 produces the characteristic equation of a solar cell, which relates the cell parameters to the output current and voltage:

$$I = I_L - I_0\left(e^{\frac{q(V+IR_S)}{NkT}} - 1\right) - \frac{V+IR_S}{R_{SH}} \qquad \text{D.4}$$

As the forward bias voltage is swept from zero to V_{OC} (the open circuit voltage), the current verses voltage (I-V) characteristics of the PV cell can be obtained. An ideal I-V curve for an illuminated PV cell/module as the voltage is swept from zero to V_{OC}, has the shape shown in Figure D.3

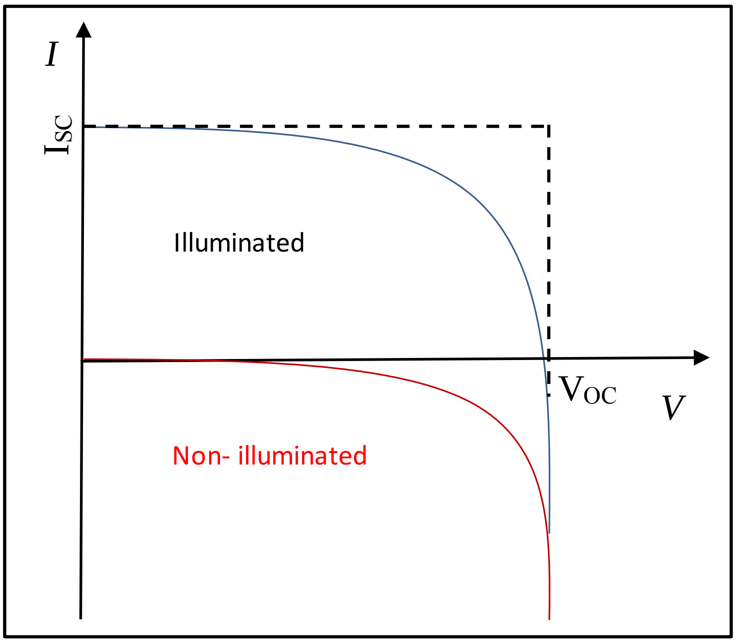

Figure D.3 I-V curves for non-illuminated and illuminated PV cells/modules

The I-V characteristics are generally used to extract useful information about the electrical performance parameters of a PV cell, or group of cells assembled into a module, such as open circuit voltage (V_{OC}), short circuit current (I_{SC}), maximum power (P_{MAX}), fill factor (FF), efficiency (η), and series and shunt resistance. The performance parameters that can be extracted from an I-V curve are described below (Instruments 2012).

D.1.1 Short Circuit Current (I_{SC})

The short circuit current is the current through the PV cell when the voltage across the cell is zero, i.e. $I = I_{SC}$ at $V = 0$. The short-circuit current is due to the generation and collection of light-generated carriers. Thus for forward-bias $I_{SC} = I_{MAX} \approx I_L$.

D.1.2 Open Circuit Voltage (V_{OC})

The open circuit voltage is the voltage across a PV cell when no external current passes through it i.e. $V = V_{OC}$ at $I = 0$. The open-circuit voltage corresponds to the amount of forward bias on the PV cell due to the bias of the cell junction with the light-generated current. It is the maximum voltage available from a cell. Thus for forward bias $V_{OC} = V_{MAX}$.

D.1.3 Maximum Power (P_{MAX}), Current at P_{MAX} (I_{MP}), Voltage at P_{MAX} (V_{MP})

The short-circuit current and the open-circuit voltage are the maximum current and voltage respectively from a PV cell. However, at both of these operating points, the power from the cell is zero. The point at which the array generates maximum electrical power output for a given illumination level is called maximum power point, P_{MAX}, as shown in Figure D.4 and lies within the knee region of the I-V curve and is sometimes also called the knee point. The voltage and current at the maximum power point are denoted as V_{MP} and I_{MP} respectively and are shown in Figure D.4.

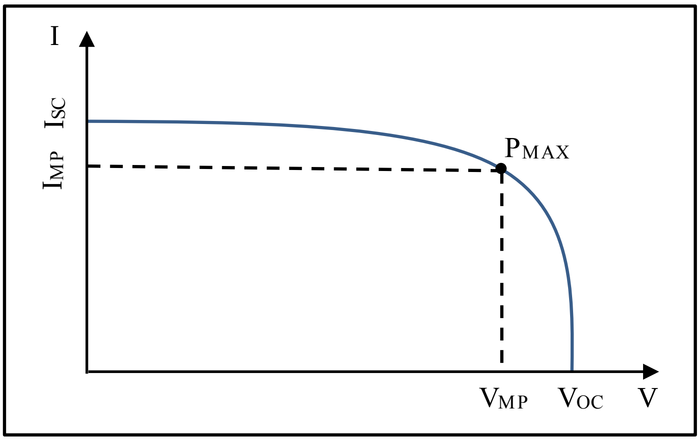

Figure D.4 Maximum power transfer point on an I-V curve

At voltages well below V_{MP}, the solar-generated electrical current to the external load is relatively independent of output voltage. Near the knee of the curve, this behaviour starts to change. As the voltage increases further, an increasing percentage of the charges recombine within the cell rather than delivering energy to the load. At V_{OC}, all of the charges recombine internally.

D.1.4 The Fill Factor (*FF*)

The fill factor is a measure of quality of the solar cell. It is defined as the ratio of the maximum power from the solar cell to the theoretical power (P_T) that would be output at both the open circuit voltage and short circuit current together as shown in Figure D.5:

$$FF = \frac{P_{MAX}}{P_T} = \frac{I_{MP} \cdot V_{MP}}{I_{SC} \cdot V_{OC}} \qquad \textbf{D.5}$$

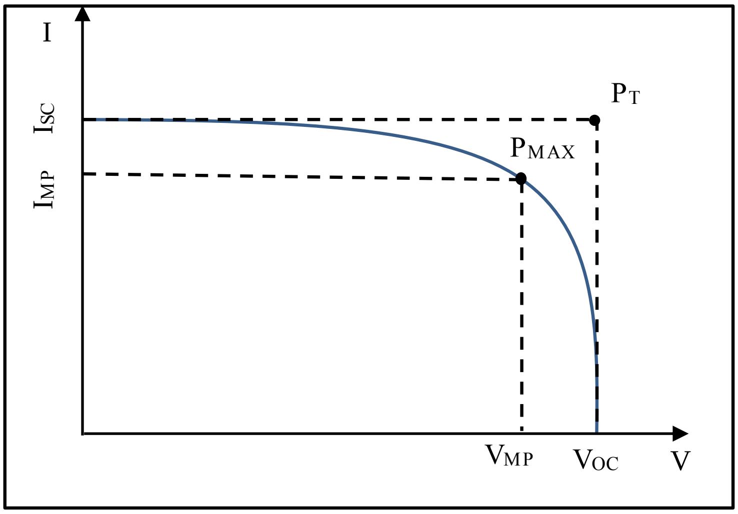

Figure D.5 Fill factor from IV curve

If the I-V curves of two individual PV modules have the same values of I_{SC} and V_{OC}, the module with the higher fill factor will be capable of producing more power. Any impairment that reduces the fill factor also reduces the output power by reducing I_{MP} or V_{MP} or both and an I-V curve helps to identify the nature of such impairments.

D.1.5 Efficiency (η)

The efficiency is the most commonly used parameter to compare the performance of one solar cell to another. The efficiency of a solar cell is the fraction of incident optical power which is converted to usable electricity and is defined as the ratio of the electrical power output P_{OUT}, to the solar power input, P_{IN}.

$$\eta = \frac{P_{OUT}}{P_{IN}} = \frac{P_{MAX}}{P_{IN}} \qquad \text{D.6}$$

P_{OUT} can be taken to be P_{MAX} since the solar cell can be operated at its maximum power output point to get the maximum efficiency.

D.1.6 Shunt Resistance (R_{SH}) and Series Resistance (R_S)

During operation, the efficiency of a solar cell/module is reduced by the dissipation of power within the parasitic series and the shunt resistances, as depicted in Figure D.6. For an ideal cell, R_S would be zero, resulting in no further voltage drop before the load, while R_{SH} would be infinite and would not provide an alternate path for current to flow. Increasing R_S and decreasing R_{SH} will decrease the fill factor (FF) and efficiency, as shown in Figure D.6. If R_{SH} is too low, V_{OC} will drop, while an excessive R_S can cause I_{SC} to drop.

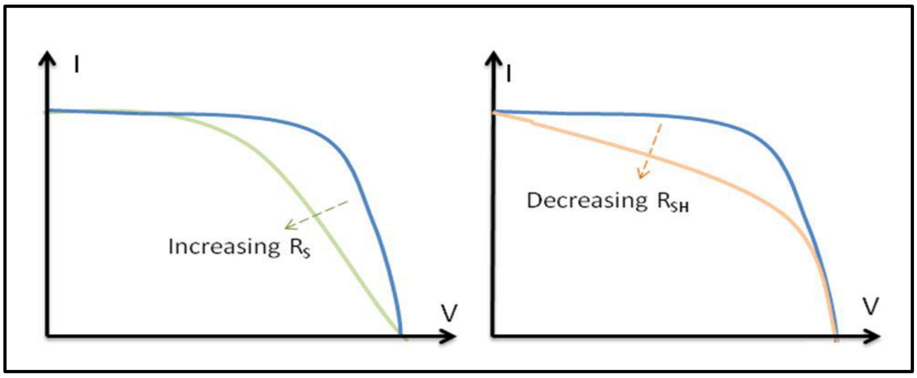

Figure D.6 Effects of R_S & R_{SH} diverging from ideality (Instruments 2012)

Experimentally the I-V curve and the performance parameters of a PV cell can be acquired using a solar simulator. Solar simulators consist of a calibrated light source, contacting system and I-V measurement system. They measure I-V characteristics under precisely specified temperature environmental conditions (Kaminski 2013). The detail of experiments conducted to test the I-V characteristics of PV module, assembled using an Ag-MPS filled ICA, are presented in the following section.

D.2 Experimental Investigation of the Electrical Performance of PV Modules Assembled Using Ag-MPS Filled ICA

Two sizes of PV modules i.e. with 36 cells and with 4 cells were made for evaluation using I-V measurements. Five samples of 36 cell module and six samples the 4 cell module were made. In the 36 cell module the cells were arranged in six rows and six columns and in 4 cell module the cells were arranged in two rows and two columns (as shown in Figure D.9 and 8.11). In real applications PV modules have to survive extreme of temperature and therefore in this study the I-V characteristics were measured before and after temperature cycling. A schematic cross-section of these MWT modules is shown in Figure D.7.

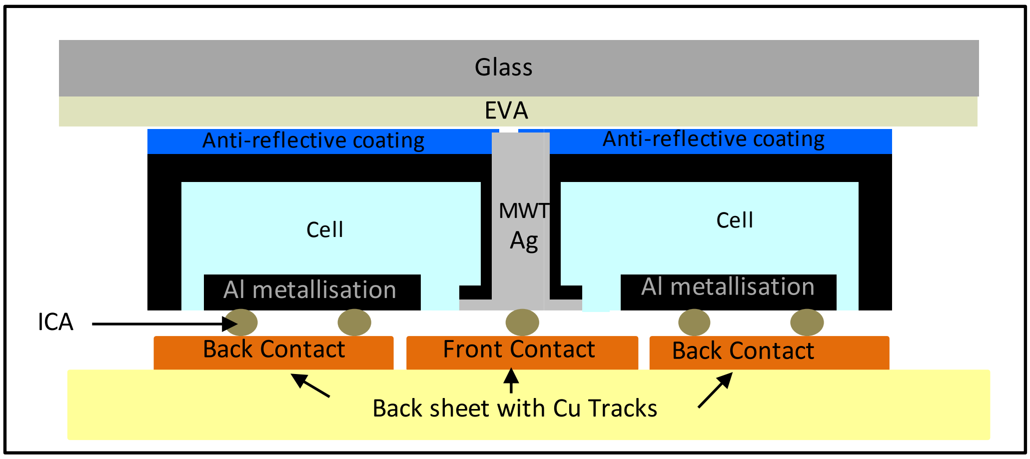

Figure D.7 Cross-section of MWT module showing only one cell (not to scale)

D.2.1 Materials Used

2.5 cm x 2.5 cm MWT cells made using 180µm thick polycrystalline Si wafers and with 150 µm Ø metallisation filled vias were used for these tests. These MWT cells were designed and produced by the Institute for Energy Technology, IFE, Norway and were performance tested before supply. Table D.1 lists the performance parameters of these MWT cells. Figure D.8 shows front and rear images and a schematic cross-section of the cell.

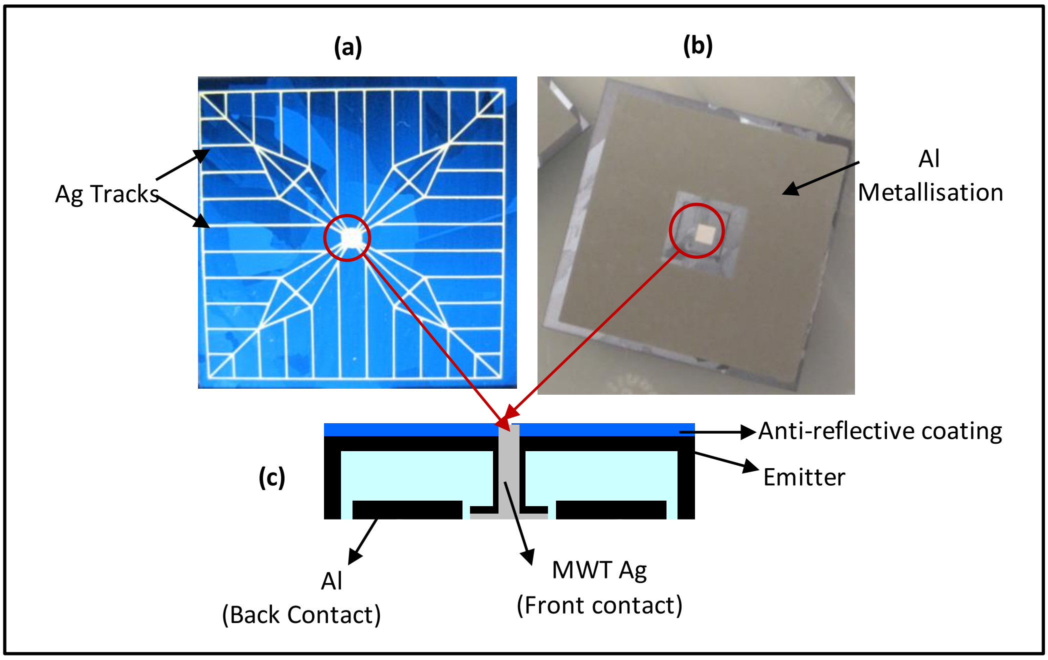

Figure D.8 Views of MWT cell used (a) front, (b) back and (c) cross-section

Table D.1 Performance parameters of MWT cells used in the study

	I_{sc} (A)	V_{oc} (V)	R_S (Ω)	R_{SH} (Ω)	Fill Factor (%)	Efficiency (%)
Average	0.223	0.618	0.615	228	63.19	13.99
Standard Deviation	0.00040	0.014	0.028	152	0.025	0.28

A specially designed back sheet was used to provide back contacts to the MWT cells. Back sheets for the 2 x 2 cells were prepared using conventional etched copper PCB processes on 1.6mm thick FR4 rigid laminate. Back sheets for the 6 x 6 cells were manufactured by In2Connect, using 125µm thick PET (polyethylene terephthalate) with etched copper tracks 35µm thick. A 200µm thick stencil with 1.5 mm diameter openings were used to print the ICA. The pattern of the back sheet and stencil was also designed by IFE, Norway as shown in Figure D.10(a). The ICA used was 45 vol% Ag-MPS 30_20B (refer to Table 3.2) in the two component epoxy matrix, type II (refer to Table 6.2). At the time of these experiments, plating process C and D were not sufficiently developed and Ag-MPS 30_20B provided the lowest resistivity among the MPS available. The type II epoxy matrix was chosen as it has a longer pot life than type I and ICAs made using type II have achieved slightly lower resistivity than those using type I. Glass and EVA from Vistasolar was used to laminate the modules. This EVA has a similar cure schedule, i.e. 150°C and 10-20 min, to that of the ICA used.

D.2.2 Methodology

D.2.2.1 Module Preparation

An automatic printer was used to print the ICA onto the pre-patterned back sheets (Figure D.9 (b)). The automatic pick and place machine was then used to place MWT cells onto the back sheet (Figure D.9 (c)). The benefit of using automatic printing and pick and place machines is that they can be programmed to accurately and quickly print the ICA and place the cells at the required locations on the pre-patterned back sheet, with controlled pressure to handle the fragile cells. The pick and place machine locates centre of the required ICA dot on the back sheet and places the MWT cell so that the centre of the backside metallisation coincides with it, as shown in Figure D.10. As the machine parameters were fixed for preparing all the modules, any variation due to the manufacturing process was minimised significantly. After placing the cells at the specified place Sn coated Cu strings were then attached to the modules for electrical connection as shown in Figure D.9 (d). The module was then heated at 150°C for 15 min. This cures the adhesive and make the interconnection permanent. This assembly process was performed at the Norwegian Defence Research Establishment, FFI, Norway. Ideally the modules would have been cured during lamination, but due to the laminator being at a different location and to prevent the movement of the cells during transfer the modules were cured before lamination. A P. Energy L036 A laminator with 610 mm x 610 mm useable heating plate area was used to laminate the assembled mini modules with glass and EVA sheets, at 1bar and 135-140°C. A complete module is shown in Figure D.9 (e). Before and after lamination I-V measurements were made on the modules at IFE, Norway[1]. The results of these I-V measurements are presented in Section 8.3.

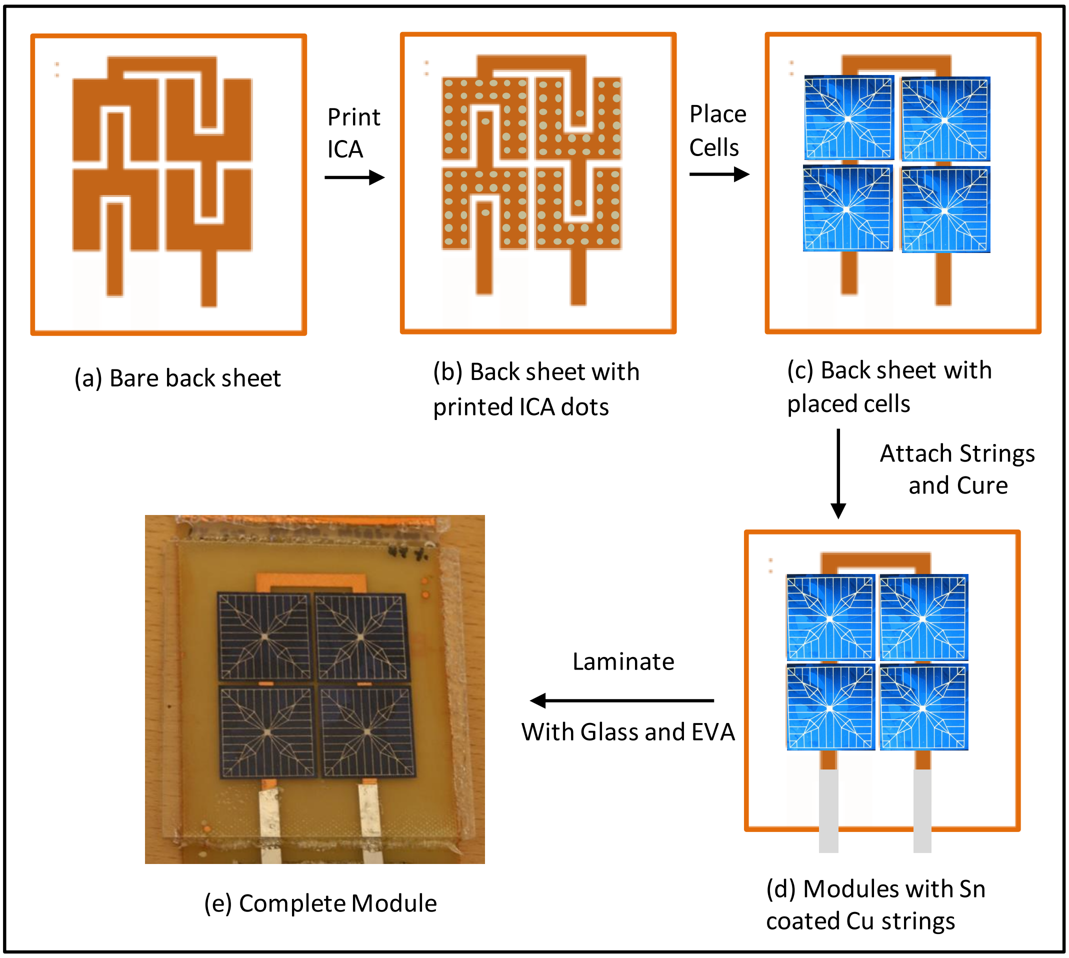

Figure D.9 Schematic of MWT module assembly processes (not to scale)

---

[1] These measurements were made by the collaborators Erik Foss and Junjie Zhu at IFE, Oslo, Norway.

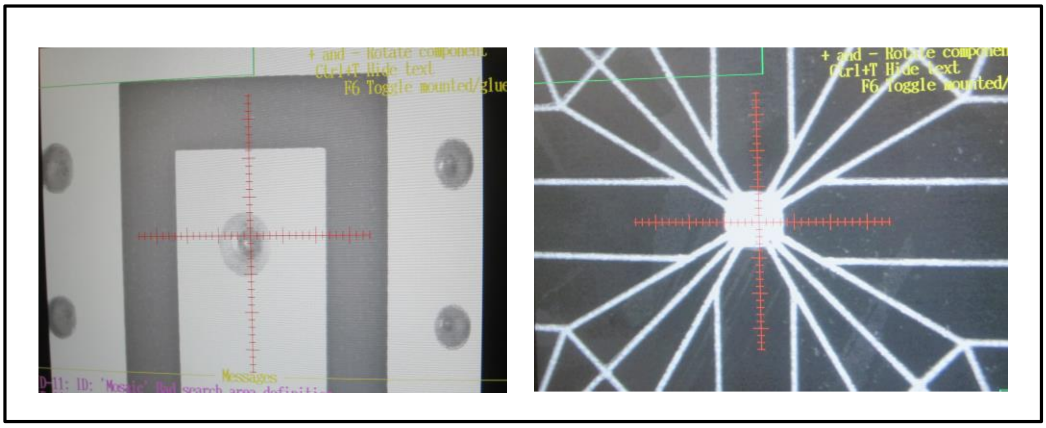

Figure D.10 Placement machine camera images showing its identification of (a) the centre of a ICA dot on the back pattern sheet and (b) the centre of a through metallisation via

D.2.2.2 I-V Measurements

Once laminated, the modules were transferred to Loughborough University where a more extensive full set of measurements were made. I-V measurements on the modules were first made using the PASAN Sun Simulator 3b. This is a large area (3m x 3m) flash simulator. The I-V characteristics of a module can be affected by ambient conditions such as temperature and the intensity and spectrum of the incident light. Thus all of the measurements were conducted under standard test conditions (STC) i.e. at a temperature of 25°C, irradiance of 1000W/m^2 and air mass AM1.5 spectrum (Hersch et al. 1982). To check the repeatability, three I-V measurements were taken for each module. The measurement system schematic is presented in Figure D.11

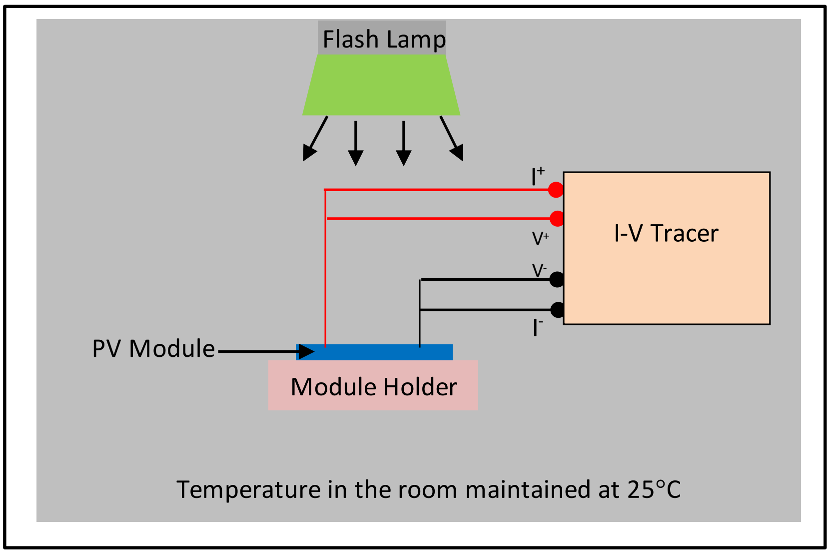

Figure D.11 Schematic for I-V measurements

D.2.2.3 Electroluminescence (EL) Imaging

After the I-V measurements, electroluminescence images were captured using a charged coupled device (CCD) camera (Atik 314E) to detect any defects in the modules. Electroluminescence (EL) is a useful solar cell and module characterisation technique as it produces images of grain boundaries and defects such as micro-cracks and broken contact fingers (Fuyuki et al. 2005; Sander et al. 2010; Yongqing et al. 2013). These defects can have a significant effect on the performance and longevity of the module. In this technique the infrared radiation emitted by a solar cell/module under forward bias is imaged in dark room conditions to produce an EL image of the cell/module (Howard 2009; Fuyuki et al. 2010; Yongqing et al. 2013). A schematic of the set up for EL imaging is shown in Figure D.12. Each MWT module was forward biased using a power supply. The maximum forward current was set at 0.2A, which corresponds to the short circuit current obtained for these modules from I-V measurements. The infrared (IR) radiation emitted by the modules was collected using a CCD camera with 1392 x 1240 pixels.

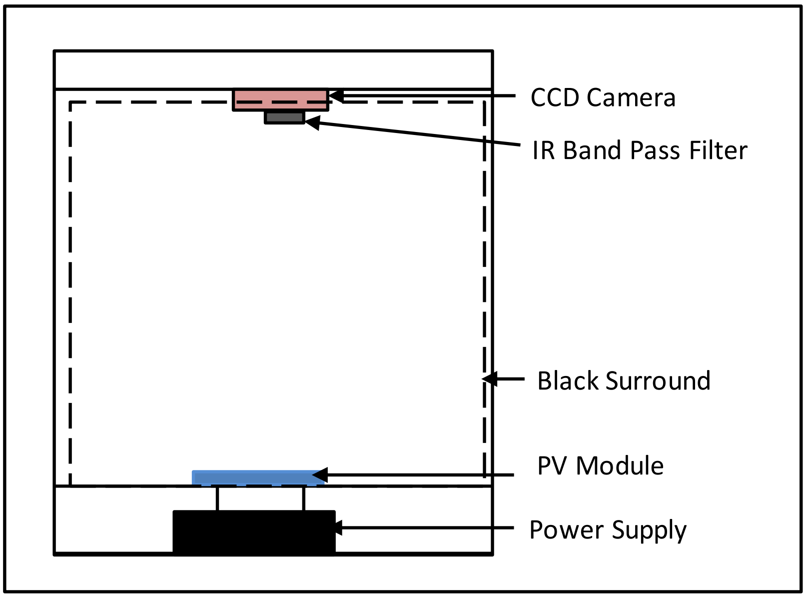

Figure D.12 Schematic of set up for EL imaging

The temperature of the camera was maintained 25°C below ambient temperature to improve accuracy and prevent noise in the image from thermally generated carriers in the detector. An IR filter that allows radiation of wavelengths of 700nm-1200nm, a range that incorporates most of the expected EL emissions from silicon cells (peak of ~ 1050 nm), was mounted in front of the camera lens. For each module it was found that after integrating radiation from the cell for 8 minutes the CCD camera produced a clear image of the module. The camera is connected to a computer for IR image capture.

D.2.2.4 Temperature Cycling (TC)

After the EL measurements the modules were put in a Delta 190H climatic test chamber for temperature cycling. The temperature cycling tests were performed according to ASTM Standard Test Methods for Photovoltaic Modules in Cyclic Temperature and Humidity Environments (ASTM 2009). The modules were subjected to 200 temperature cycles between -40°C and 85°C, at ramp rates of 100°C per hour as shown in Figure D.13. The temperature was held for 30 min at both -40°C and 85°C. After temperature cycling, the I-V measurements and EL measurements were repeated to check for any degradation of the module.

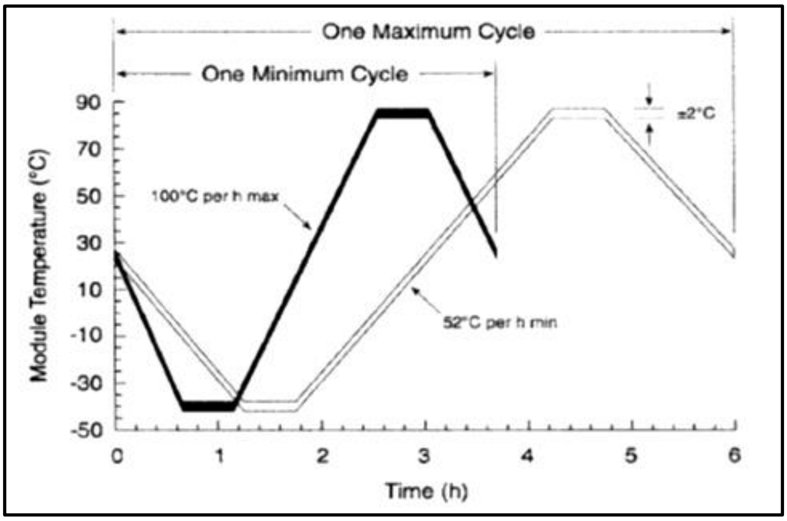

Figure D.13 Temperature variation during one cycle (ASTM 2009)

D.3 Results and Discussion

The back sheet of all five of the modules containing 6 x 6 cells warped during curing and the cells became displaced from their specified positions in the module, as shown in Figure D.14.

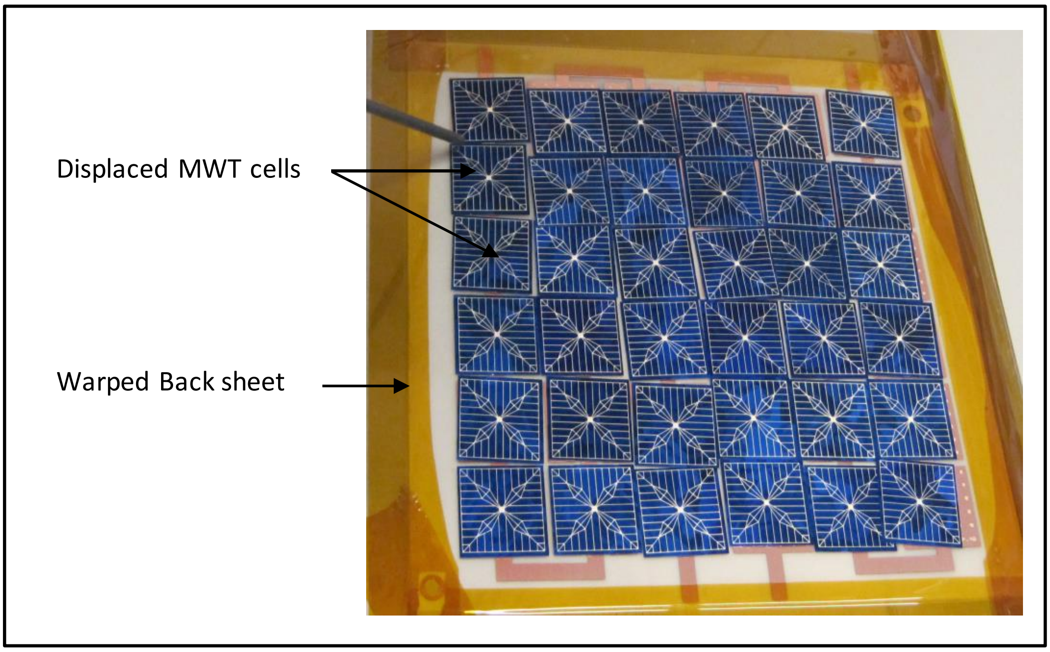

Figure D.14 Showing 6 x 6 module with warped back sheet and displaced MWT cells

These modules were therefore completely non-functional and were discarded. The back sheet for the 6 x 6 modules was a flexible PET material with copper tracks, PET has a higher CTE than copper, and as the temperature was increased for curing the flexible material expanded more than the copper inducing stresses in the sheet, which led to the warping and thus displacement of the cells. To eliminate the warping, all the 2 x 2 cell modules were made using rigid PCB laminate as the back sheet. The results of the I-V measurements for the six 2 x 2 modules assembled, before and after lamination, are presented in Tables D.2 and 8.3 respectively. These I-V measurements were made by collaborators at IFE, Norway under the same conditions as specified in Section 8.2.2.2.

Table D.2 I-V parameters measured before lamination [1]

Module No.	I_{sc} (A)	V_{oc} (V)	R_S (Ω)	R_{SH} (Ω)	Fill Factor (%)	Efficiency (%)
1	0.20	2.36	5.33	134	48	9.5
2	0.02	2.13	70.4	78.08	24	0.6
3	0.05	2.29	46.4	38.4	23	1.2
4	0.20	2.29	4.8	91.2	51	9.7
5	0.20	2.38	5.3	58.4	61	12.1
6	0.03	2.10	73.6	52.8	24	0.6

Table D.3 I-V parameters measured after lamination [1]

Module No.	I_{sc} (A)	V_{oc} (V)	R_S (Ω)	R_{SH}(Ω)	Fill Factor (%)	Efficiency (%)
1	0.22	1.28	2.13	44.8	62	7.0
2	--	--	-	-	--	--
3	0.01	0.72	20.57	54.4	35	0.2
4	0.21	1.76	1.6	80	66	10.2
5	0.22	1.24	1.6	54.4	67	7.5
6	0.20	0.57	1.6	8	44	2.7

For a (2 x 2) module containing four MWT cells arranged in series if the assembly process do not affect the all performance, I_{SC} should remain same as that of the individual MWT cells whereas the V_{OC} and R_S of the four cells would sum to give a value of 2.4V and 2.46 Ω respectively (Solmetric 2011). The total series resistance R_S, is the sum of cell internal resistances R_{cell}, contact resistances between Cu of front and back contacts and ICA, $R_{CR(Cu,ICA)}$, contact resistances between Al metallisation on the back of cell and ICA, $R_{CR(Al,\ ICA)}$, Cu track resistance $R_{Cu\text{-}Track}$, contact resistance between the Ag metallisation and ICA, $R_{CR(Ag,\ ICA)}$. These resistances can be seen in Figure D.15. The calculated combined contribution of all of these resistances for 2 x 2 module sum up to ~3.45 Ω (Appendix C, Section C.3). Table D.2 shows that before lamination all the modules have lower I_{SC}, R_{SH}, FF and efficiency than the individual MWT cells, with modules 2, 3 and 6 showing the lowest values. Table D.2 also show that all the modules had an $R_{S,}$ higher than the calculated, with module 2, 3 and 6 showing significantly higher values. The main reason for the observed reductions in $I_{SC,}$ fill factor and the efficiency of modules 2, 3 and 6 is believed to be their very high interconnection series resistances, and low shunt resistances.

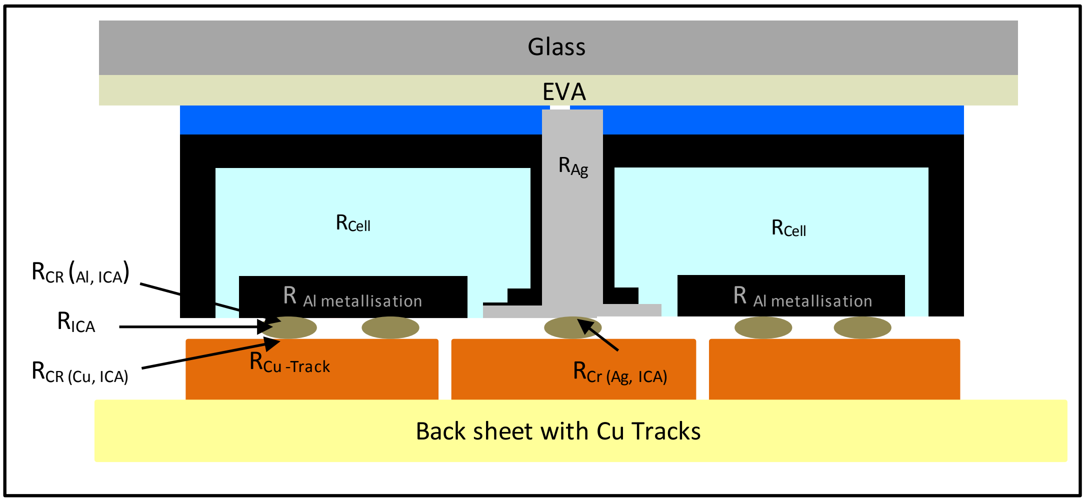

Figure D.15 Resistances contributing to the series resistance and possible flattening of ICA dots on lamination

Table D.3 shows that after lamination R_S and R_{SH} of all the modules had decreased. The fill factor of all the modules improved after lamination, but their efficiency decreased drastically with the exception of modules 4 and 6 whose efficiency improved slightly. Module 2 had stopped functioning totally and no I-V parameters could be obtained. I_{SC} had further deteriorated for module 3 but had improved slightly for modules 1, 4, and 5 whereas it had improved greatly for module 6. V_{OC} had dropped for all the modules, but more significantly for 2, 3 and 6. Module 6, which had I-V parameters similar to module 2 before lamination saw marginal improvement in the parameters after lamination. The reduction in V_{OC} for all modules could be a significant increase in the leakage current i.e. flowing through the shunt resistance. As no insulation was used to prevent any direct contact between the Al metallisation (back contact) on the cell and the Cu trace connecting to the front contact of back sheet, as can be seen in Figure D.10. Under the high pressures of lamination the Al metallisation can come into direct contact with the front contact resulting in a short circuit between the front and back contacts, and could be the reason for the decrease in Rs, V_{OC} and hence the efficiency of the modules. The reduction in R_S may also be the reason for increase in I_{SC} and FF.

The performance parameters of the modules (as shown in Tables D.2 and 8.3) show that none was perfect, however to test their robustness they were subjected to temperature cycling. To detect defects such as micro-cracks and broken contacts in PV cells EL images of the modules were also taken. Temperature cycling, EL imaging and the I-V measurements presented hereafter were all carried out at Loughborough University. For each module I-V measurements and EL images were taken before and after temperature cycling. There was a time gap of nearly six months between the I-V measurements made at IFE Norway and those at Loughborough University. This was mainly due to limited availability of the equipment. For each module three I-V measurements were taken to verify the repeatability of the test method. As all three of these measurements produced identical I-V curves only one I-V curve is presented for each module in Figure D.16. The I-V parameters measured for the modules before and after temperature cycling are summarised in Tables D.4 and D.5 respectively.

Tables D.3 and D.4 compare the I-V parameters measured after a gap of nearly six months. The comparison shows that the R_S and V_{OC} increased whereas I_{SC}, fill factor and efficiency of all the modules decreased with time. The increases in R_S are believed to be due to the formation of insulating oxide films on the bare Cu track and the Al metallisation, leading to increased contact resistances. Module 2 was again found to be non-functional in these measurements. It has to be taken into consideration that measurements listed in Table D.3 and Table D.4 were taken at two different places, at two different times of year and by two different instruments thus a small variation in them is expected. However, as both sets of measurements were taken under the same standard test conditions, the large improvements in V_{OC} for the modules was not expected. The reason for improvement in V_{OC} could be that over a period of time, possibly by expansion/oxidation of the adhesive, contact between the cell and back sheet decreased, removing the short between front and back contact thus improving their V_{OC}.

Table D.4 I-V parameters measured before temperature cycling

Module No.	I_{sc} (A)	V_{oc} (V)	R_s (Ω)	R_{sh}(Ω)	Fill Factor	Efficiency %
1	0.05	1.87	59.11	31.30	21	1.0
2	-	-	-	-	-	-
3	0.04	1.75	23.45	42.07	26	1.0
4	0.20	2.40	7.86	37.84	35	7.0
5	0.20	2.40	5.44	68.96	43	8.0
6	0.03	2.14	64.62	66.36	24	1.0

Table D.5 I-V parameters measured after temperature cycling

Module No.	I_{sc} (A)	V_{oc} (V)	R_s (Ω)	R_{sh}(Ω)	Fill Factor	Efficiency %
1	0.20	2.44	9.97	20.92	28	5.0
2	--	-	-	-	-	-
3	0.04	2.35	31.77	44.74	23	1.0
4	0.20	2.40	6.85	45.95	38	7.0
5	0.20	2.44	15.04	26.81	28	5.0
6	0.02	1.75	68.58	71.79	0.25	1.0

Further, on comparing the I-V performance parameters before and after temperature cycling in Tables D.4 and D.5 it was found that for module 1 and 3 the value of V_{OC} is further improved by nearly 0.6V, the efficiency of the modules 4 and 5 reduced and, the series resistances of module 3, 5 and 6 increased, while those of modules 1 and 4 decreased. A large reduction in the series resistance and slight improvement in the efficiency of module 1 was seen. Further, before temperature cycling modules 1, 3 and 4 had low shunt resistance compared to modules 5 and 6 but after temperature cycling the shunt resistance of modules 1 and 5 decreased whereas those for modules 3, 4 and 6 increased slightly. The values of the performance parameters were found to vary significantly from module to module, but are much lower than those expected from these modules.

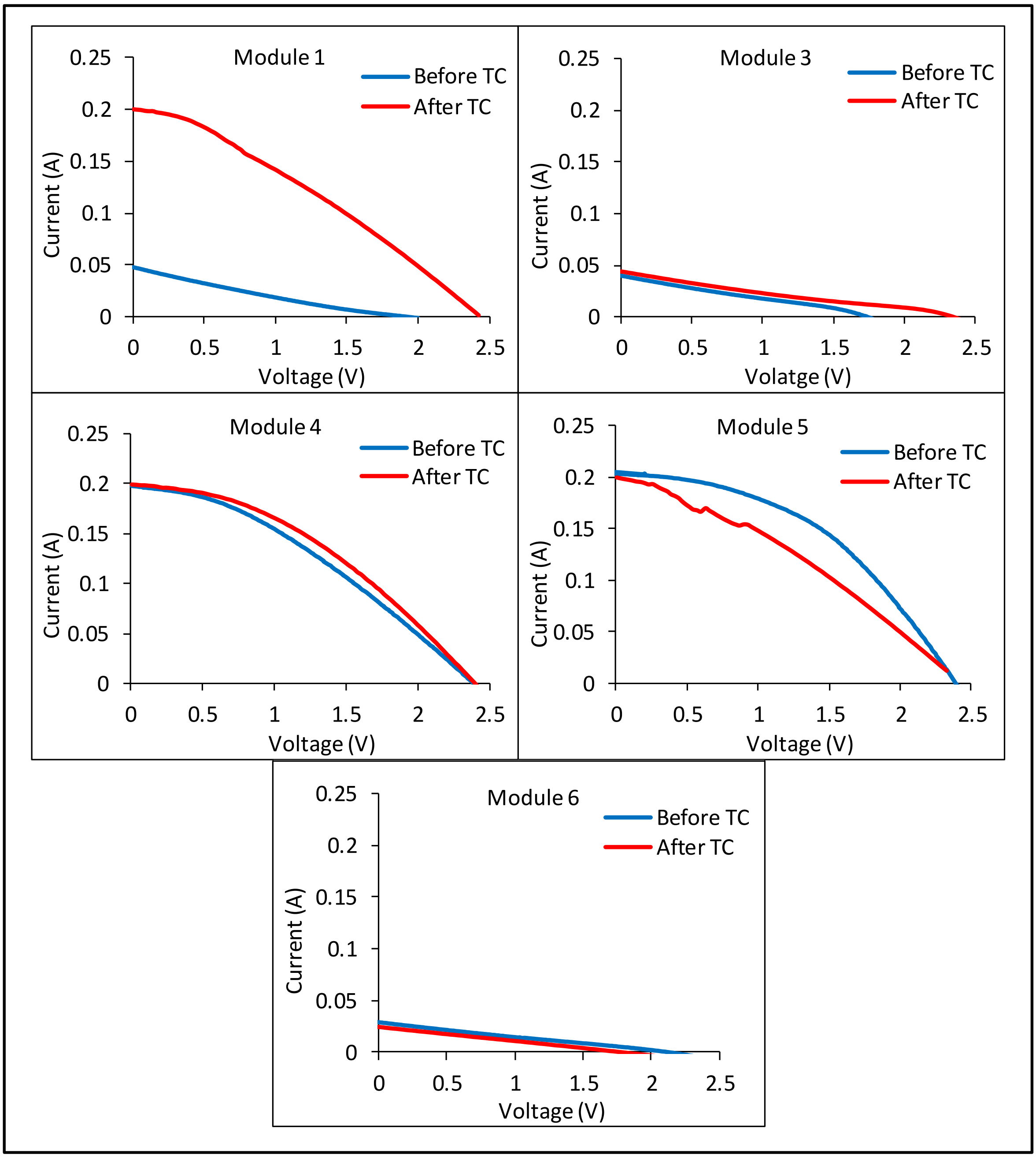

Figure D.16 I-V curves for the five functioning PV modules

The variable reduction in the I_{SC} for all modules could be due to variation in contact resistances from contact to contact within the cell and between cells, depending upon the contact area and the extent of oxidation. The reason for lower value of I_{SC} after temperature cycling could be damage to the cell during assembly, which prevent it from generating current equal to the other cells in the string. This limits the current output from the string to the current generated by the weakest cell (Solmetric 2011). This however, would only have a small effect on V_{OC} but does result in a lower power output from all the cells and hence the module. It can also lead to hot spot formation, which causes further degradation to the cell (Solmetric 2011). The large drop in I_{SC} for modules 2, 3 and 6 but only small drop in their V_{OC} may therefore be due to a damaged cell in the circuit.

The I-V measurements of the modules before and after temperature cycling were also compared with the EL images to detect any defects in the cells. The EL imaging does not give quantitative results, but only produces qualitative images utilising the radiative-recombination phenomenon (Fuyuki et al. 2007; Fuyuki et al. 2009). Broadly, an EL image is distinguished in two types of variation from the typical image intensity luminescence i.e. dark spots/regions of decreased luminescence and bright spots/regions where luminescence is higher. In an EL image, dark spots/regions are the inactive areas where no electron hole recombination is taking place. They correspond to defects or inhomogeneities that are inherent in the cell materials or result from the cell or the module fabrication process which do not produce any recombination current and are one of the regions of high resistive losses seen in I-V measurements (Fuyuki et al. 2005; Crozier 2012). Bright spots/regions usually correspond to an increase in radiative emission, such as from hot spots. The EL images of the modules taken before and after temperature cycling are shown in Figure D.17. No image was obtained for module 2. The cells are numbered clockwise within the module starting at the top right.

Four distinct type of regions can be distinguished in the EL images shown in Figure D.17:

(i) Slightly dark regions marked by black rectangles in the images: these may be due to inherent discontinuities in the cell structure;
(ii) Dark regions marked by light blue rectangles in the images: these are the regions around the through via metallisation, and as it is free from any aluminium metallisation negligible recombination is expected to in this region (Fuyuki et al. 2010);

(iii) Dark regions marked by red rectangles in the images: these are the regions showing breakage or degradation of the cells; and

(iv) Bright spots as marked by green rectangles in the images: which are the regions where non-EL emission occurs, which may be because of hot spots.

Not all the regions seen are marked with the rectangles as then the image would look cluttered. As an example only one type of each region is shown on the images. The presence of the large number of dark spots marked with red rectangles on each module indicate that cell damage or degradation is the main cause of the highly reduced $I_{SC,}$ fill factor and efficiency. The damage could be due to stresses involved during assembling and handling or due to shunting of the cells which cause large currents to deviate from their paths. EL images shows that cell nos 1 and 2 in module 1, cell no 1 in module 3 cell no 2 in module 4, and cell nos 2 and 4 in module 6 were not conducting before temperature cycling, indicating they had poor back or front contacts or shunts (a short circuit between the front and back contacts) which is also reflected in their lower V_{OC} values. However, after temperature cycling these cells started to conduct except for cell no 1 in module 1 and cell no 4 in module 6. This is indicated in the improvement of V_{OC} for modules 1, 3 and 5. However, V_{OC} for module 6 reduced. Bright spots are also observed in the centre of cell no 2 in module 3 and cell nos 3 and 4 in module 6. These bright spots show high radiative emissions and could be due to hot spots. The IR filter used for imaging allows wavelength in the range 700-1200nm because high radiative emissions of the Si normally occur around 1050nm. However, this range also includes thermal radiation emitted by hot bodies and any thermal radiation emitted by the cells in this range would be picked up by the CCD camera. The presence of hot spots could be due to damage or cracks in the cells and could further damage the cell. No EL image could be obtained for module 5 after temperature cycling although I-V measurements could still be obtained. As I-V parameters could be obtained this indicates that the module is working thus no possible reason could be assigned for not able to capture any EL image.

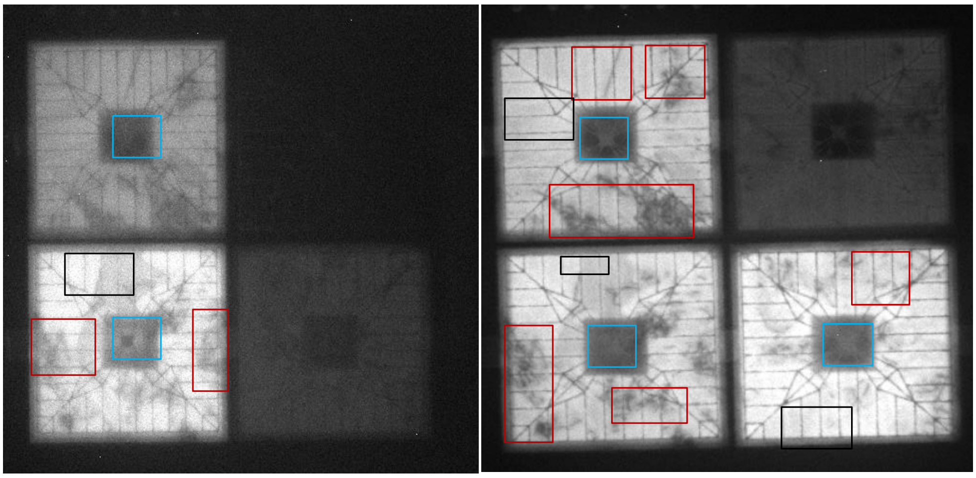

(a) Module 1

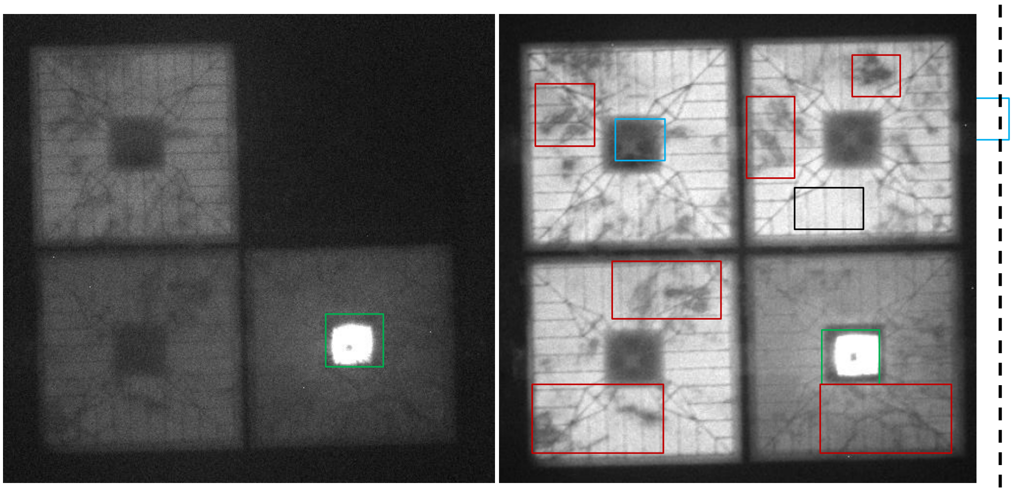

(b) Module 3

Figure D.17 Electroluminescence (EL) images of (a) module 1, (b) module 3(c) module 4, (d) module 5 and (e) module 6 (contd………)

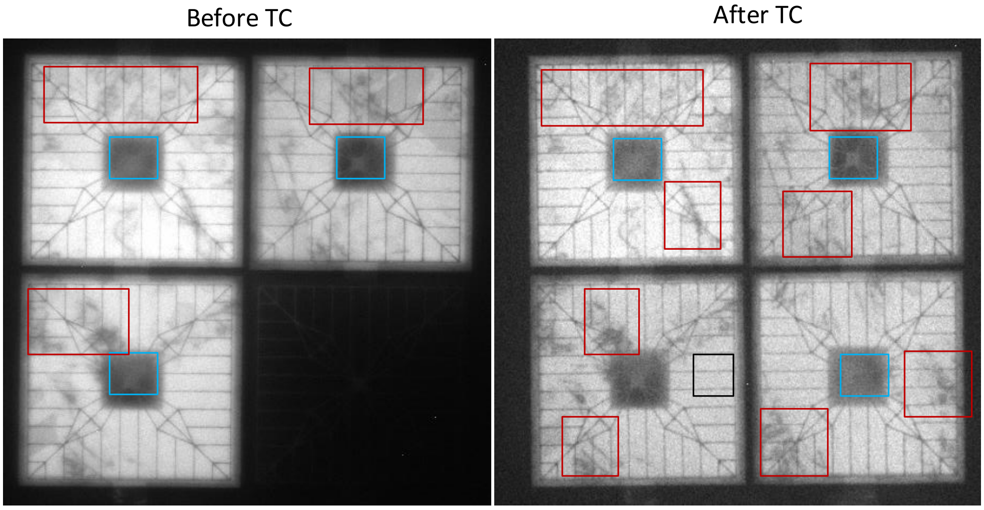
Before TC

After TC

(c) Module 4

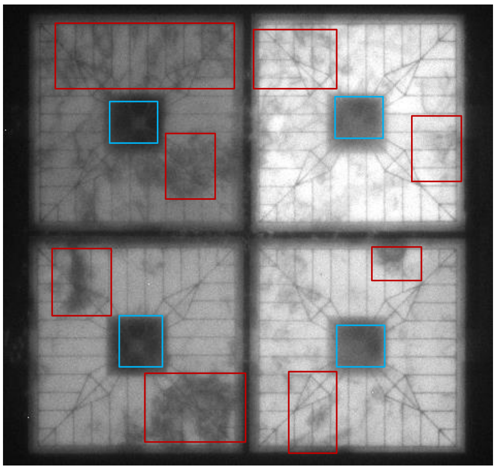
Before TC

After TC

No image

(d) Module 5

Figure D.17 Electroluminescence (EL) images of (a) module 1, (b) module 3(c) module 4, (d) module 5 and (e) module 6 (contd.........)

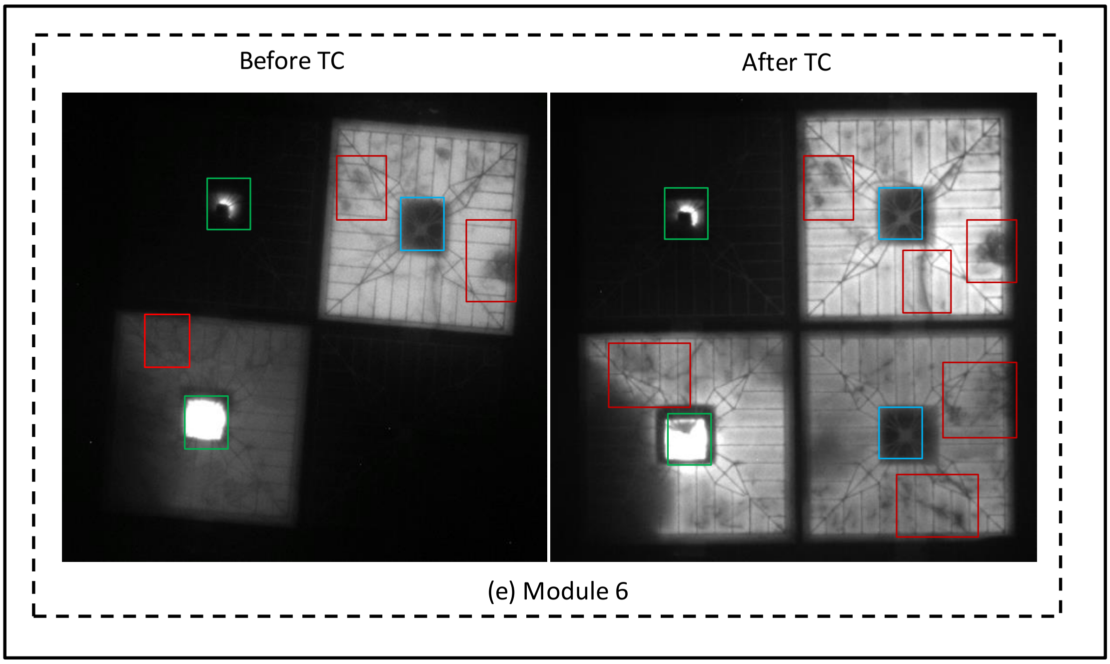

(e) Module 6

Figure D.17 Electroluminescence (EL) images of (a) module 1, (b) module 3(c) module 4, (d) module 5 and (e) module 6

All the modules tested show poor performance due to high resistive losses, shunting and cell damage thus the performance of the ICA in the assembly could not be accessed. More tests are required on single cell modules to test the performance of ICA interconnections in this type of assembly.

D.4 Concluding Remarks

This chapter investigated the electrical performance of MWT PV modules assembled using Ag-MPS filled ICA. I-V curves show poor module performance with heavy series and shunt resistive losses and defects in manufacturing which were aggravated during lamination. EL investigation before and after temperature cycling have indicated short circuits between front and back contact, degradation or breakage of the cells or manufacturing defects such as poor interconnections between cells could be the reason for the failure of the PV modules. Thus with the inherent assembly defects these experiments could not provide information about the performance of the Ag-MPS filled

ICA in PV applications. Further studies after eliminating the manufacturing defects are needed to allow analysis of the performance of the Ag-MPS filled ICAs in this application.